Experimental and Numerical Study on Hydrodynamics of Coupled FPSO and Mooring/Riser Systems in Deepwater GOM

By

©2015 Jaime Jose Torres Lopez

A Thesis submitted for the degree of Doctor of Philosophy (Integrated)

School of Marine Science and Technology

Newcastle University

United Kingdom

February, 2016

Abstract

Floating production storage and offloading (FPSO) systems have been proposed for the development of recent oil discoveries in the southern region of the Gulf of Mexico (GOM) in water depths ranging from 1000 to 2000 metres. It is increasingly challenging to predict the environmental forces and the global responses of FPSO systems and the associated dynamic behaviour of their mooring lines and risers at these depths. The combination of an appropriate FPSO scale model with a suitable level of equivalent effect reduced depth for the mooring lines and risers using a hybrid passive truncated experimental methodology is a feasible approach.

This thesis provides an effective technique to study the equivalent hydrodynamic behaviour of floating systems to validate numerical models and to predict full water depth behaviour, based on a hybrid passive truncated experimental method and a non-linear time domain coupled numerical analysis. The extreme motion response of an FPSO and the dynamics of the mooring lines and risers in the context of prevailing environmental conditions are investigated.

Several important findings are obtained based on the present experimental and the numerical study: The linear motion transfer functions are sensitive to the direction of the incident waves, and the differences between the Full and the Ballast load conditions were found to be insignificant, except for the roll motion, which showed slight differences in resonant frequency responses and the maximum peak motion amplitudes. Further, the spectra analysis revealed that the risers have a great influence on low-frequency damping, particularly in the surge direction, whereas the damping mainly contributes to roll in the wave frequency motion response. The main horizontal motion response of the FPSO (surge) under the non-collinear environmental loading condition was found to be slightly higher than that obtained for the collinear loading condition and the numerical simulation identified that the Newman's approximation is reliable to predict the extreme motion response. The dynamic tension responses of the risers are sensitive to the environment force directions and the mooring lines/risers dynamics do not affect significantly the wave frequency motion responses in heave and pitch. Additionally, the mean motion of the FPSO and the mean tensions in the mooring lines are dominant in deep-water and ultra-deepwater installations and conversely the dynamic components of the tension responses of the mooring lines decreases as the water depth increases. The findings are not only improve the understanding of the complex hydrodynamics, the extensive experimental and numerical results will also provide welcome benchmarks for

future study of the FPSO with its mooring lines and risers under both collinear and non-collinear environment loading conditions.

Acknowledgements

I would to like to thank to my supervisor Prof. Longbin Tao for his academic support and guidance throughout of the research and also for helping me to join in the six month exchange program for carrying out experiment model test in the deepwater basin at Shanghai Jiao Tong University, China. I also would like to thank my co-supervisors Dr. Yongchang Pu and Dr. Nianzhong Chen who have always been accessible to advise and support me. I like to thank Prof. Longfei Xiao for his support and sharing his experience about deepwater experimental model test and Prof. Zhiqiang Hu and the PhD student team and the staff of the offshore basin for their support during the execution of my experimental model test at Shanghai Jiao Tong University, China. I would also like to thank Prof. Grant Burgess for his help and encouragement during my thesis writing.

I would like to extend my appreciation to my friend Mr. John Garside who has helped me with his experience to understand difficult topics related to hydrodynamics and naval architecture from the beginning of my research program, and to enhance my thesis with his valuable comments. I also like to thank my friends in Offshore Engineering Research Group at Newcastle University who directly support me with their valuable advice and comments to my thesis and they also helped me to enjoy my PhD program at Newcastle University: Serena Lim, Martin Nurnberg, Maria Syrigou, Arriya Leelachai, Ralitsa Miaylova, Ayman Al-Fudhaili, Ikenna Okaro, Sudheesh Ramadasan, Yibo Liang, Zhenhua Zhang, Ralitsa Mihaylova, Ankang Cheng, Junyi Wu and Xutian Xue. My gratefulness also goes to the PhD students at Shanghai Jiao Tong University: Wenyue Lu, Rongheng Yin, Yanfei Deng, Quan Wang and Mingyue Liu for supporting me in setting up my experiment and facilitating my stay in Shanghai during my exchange program funded by British Council and Chinese Scholarship Commission. I would like to extend my gratitude to PhD Faustino Fuentes Nucamendi who has supported the deepwater professional development program at Pemex Company and has always believed in me to undertake a PhD research program. I would like to thank Pemex and Conacyt-Sener for the financial support during my PhD program.

Finally, my deepest gratitude goes to my family, my wife Alexandra Malagon Trujillo, my Son Jaime Alejandro Torres Malagon and my Daughter Sofia Montserrat Torres Malagon for accompanying me in this adventure. Without their encouragement and support, I would not have the inspiration and motivation to overcome the challenges in my life, and my Parents,

Evelio Torres Amador and Maria Elena Lopez Baños for giving me the foundations and the example of the continuous improvement.

Table of contents

List of Figures

List of Tables

Nomenclature

$\boldsymbol{A}$	Wave Amplitude of the incoming waves
$\boldsymbol{A_T}$	Transversal Projected Area
$\boldsymbol{A_L}$	Longitudinal Projected Area
$\boldsymbol{A_{11}}$	Surge added mass
$\boldsymbol{A_{22}}$	Sway added mass
$\boldsymbol{A_{33}}$	Heave added mass
$\boldsymbol{A_{44}}$	Roll added moment
$\boldsymbol{A_{55}}$	Pitch added moment
$\boldsymbol{A_{66}}$	Yaw added moment
$\boldsymbol{B}$	Spread Length on the Seabed
$\boldsymbol{BIEM}$	Boundary Integrated Element Method
$\boldsymbol{BVP}$	Boundary Value Problem
$\boldsymbol{B_{d11}}$	Surge drift damping
$\boldsymbol{B_{d22}}$	Sway drift damping
$\boldsymbol{B_{d66}}$	Yaw drift damping
$\boldsymbol{B_{11}}$	Surge radiation damping
$\boldsymbol{B_{22}}$	Sway radiation damping
$\boldsymbol{B_{33}}$	Heave radiation damping
$\boldsymbol{B_{44}}$	Roll radiation damping
$\boldsymbol{B_{55}}$	Pitch radiation damping

B_{66}	Yaw radiation damping
CFD	Computation Fluid Dynamic
C	Linear damping coefficient
C_c	Critical damping coefficient
C_h	Hydrodynamic damping
C_s	Structural damping
C_a	Added mass coefficient
c	Slope of the catenary of the mooring line
DOF	Degrees of Freedom
DWT	Deadweight Tonnage
d	Vertical Distance from the Fairlead to the seabed
EA	Axial Stiffness
$FPSO$	Floating Production Storage Offloading
FPS	Floating Production System
FEM	Finite Element Model
$F(t)$	Excitation forces
F_d	Dynamic Factor
F^{FK}	Froude-Krylov Forces (including buoyancy forces)
F^S	Diffraction Forces,
F^R	Added Mass and Damping Forces
F^D	Drag Forces
F_{kD}	Total Diffraction Force
F_{kR}	Total Radiation Force

$\boldsymbol{F_{11}}$	Surge drift force
$\boldsymbol{F_{22}}$	Sway drift force
$\boldsymbol{F_{33}}$	Heave drift force
$\boldsymbol{F_{44}}$	Roll drift moment
$\boldsymbol{F_{55}}$	Pitch drift moment
$\boldsymbol{F_{66}}$	Yaw drift moment
$\boldsymbol{GOM}$	Gulf of Mexico
$\boldsymbol{g}$	Gravity constant
$\boldsymbol{H_s}$	Significant Wave Height
$\boldsymbol{HF}$	High Frequency
$\boldsymbol{K_h}$	Hydrodynamic restoring force
$\boldsymbol{K_m}$	Mooring lines restoring force
$\boldsymbol{k}$	Degree of freedom (surge, sway, yaw)
$\boldsymbol{\delta}$	Logarithmic Decrement
$\boldsymbol{\zeta}$	Damping Ratio
$\boldsymbol{LF}$	Low Frequency
$\boldsymbol{LTF}$	Linear Transfer Function
$\boldsymbol{L}$	Mooring Line
$\boldsymbol{L_{total}}$	Total length of the mooring line
$\boldsymbol{L_W}$	Instantaneous wetted part of the cross section
$\boldsymbol{L_{BP}}$	Length Between Perpendiculars of the FPSO
$\boldsymbol{MEL}$	Mixed Eulerian-Lagragian
$\boldsymbol{M}$	Mass of the structure

$\boldsymbol{M_a}$	Added mass
$\boldsymbol{NWT}$	Numerical Wave Tank
$\boldsymbol{P^{(0)}, P^{(1)}, P^{(2)}}$	Hydrostatic Water Pressure
$\boldsymbol{QTF}$	Quadratic Transfer Function
$\boldsymbol{RAOs}$	Motion Transfer Functions
$\boldsymbol{R}$	Riser
$\boldsymbol{SCR}$	Steel Catenary Risers
$\boldsymbol{T}$	Tension
$\boldsymbol{T_H}$	Horizontal Tension
$\boldsymbol{T_V}$	Vertical Tension
$\boldsymbol{T_n}$	Natural Period
$\boldsymbol{\mu}$	Submerged Mass per Unit Length
$\boldsymbol{u_c}$	Current Velocity
$\boldsymbol{u_w}$	Wave Particle Velocity
$\boldsymbol{w}$	Submerged Weight per Unit Length
$\boldsymbol{WF}$	Wave Frequency
$\boldsymbol{\omega}$	Angular Frequency
$\boldsymbol{\Phi}$	Velocity Potential
$\boldsymbol{\Phi_0}$	Incident Potential
$\boldsymbol{\Phi_s}$	Scattering Potential or Diffraction Potential
$\boldsymbol{\Phi_R}$	Radiated Potential
$\boldsymbol{\Phi_2}$	Second-order Velocity Potential
$\boldsymbol{\eta}$	Free-Surface Elevation

$\boldsymbol{\eta_n}$	Profile of the First-order Waves
$\boldsymbol{\gamma}$	Truncation factor
$\boldsymbol{V}$	Fluid velocity
$\boldsymbol{V_w}$	Wind Velocity
$\boldsymbol{V_c}$	Current Velocity
$\boldsymbol{VIV}$	Vortices-Induced Vibrations
$\boldsymbol{VLCC's}$	Very Large Crude Carriers
$\boldsymbol{\nabla}$	Displacement volume of the model
$\boldsymbol{X}$	Displacement
$\boldsymbol{\dot{X}}$	Velocity
$\boldsymbol{\ddot{X}}$	Acceleration
$\boldsymbol{X_k}$	Amplitude of Oscillation of the Platform
$\boldsymbol{\overline{X}}$	Normalized Quantity
$\boldsymbol{X_{WF\ or\ LF}}$	Statistic Values (WF or LF component**)**
$\boldsymbol{X_{total}}$	Total motion response or Total tension response

Chapter 1

Introduction

1.1 Background and motivation

The demand for energy resources, such as oil and gas is steadily growing. This has necessitated and motivated the continuous evolution and development of new technology, crucial for both the exploration and exploitation phases of the oil and gas industries. A significant challenge has been offshore activities in deep-water and ultra-deepwater locations which has encouraged the development and installation of floating production, drilling and storage systems (see Figure 1.1). The analysis and design of floating production, drilling and storage systems under different environmental conditions have been vital in order to have reliable and safe systems and cost effective solutions for exploration and activities in deep-water.

Typically, the floating drilling and production systems are the integration of a floating structure with a system of risers and mooring lines of which the main objective is to be a stable and reliable base for drilling activities and production operations in the oil and gas fields (Figure. 1.2).

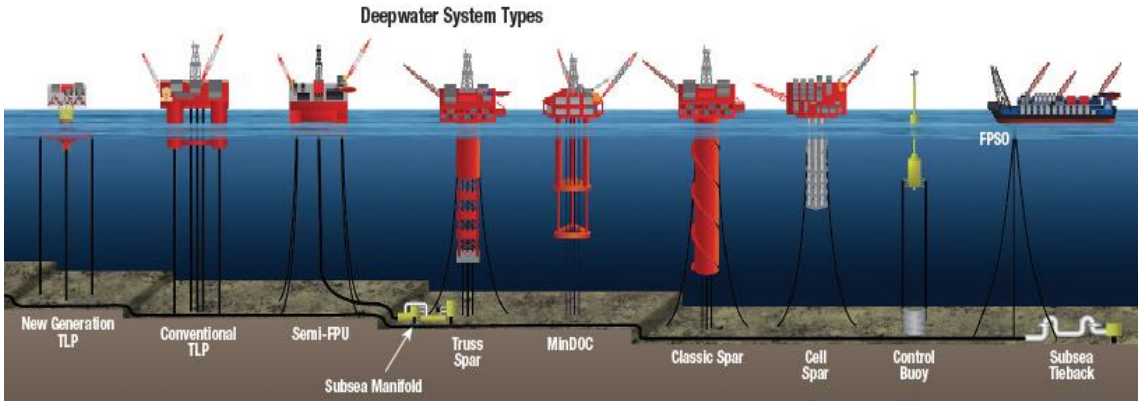

Figure 1.1 Floating drilling and production systems for deepwater and ultra-deepwater installations (Barton, 2015)

For the offshore industry, the development and deployment of floating production storage and offloading (FPSO) vessels has been very successful across different regions (Figure 1.3). One of the advantages of an FPSO, which are often made from converted bulk carriers or large tankers, compared to other forms of floating structures, is mainly in its large oil storage capacity. This is useful for remote offshore marginal fields where an infrastructure of export pipelines does not exist or where it is not technically feasible to transport the oil or gas due to limitations in outlet pressure and flow assurance concerns (waxes and hydrates) and which is a typical case in deep-water and ultra-deepwater locations (Nutter, 2014; Chakrabarti, 2005).

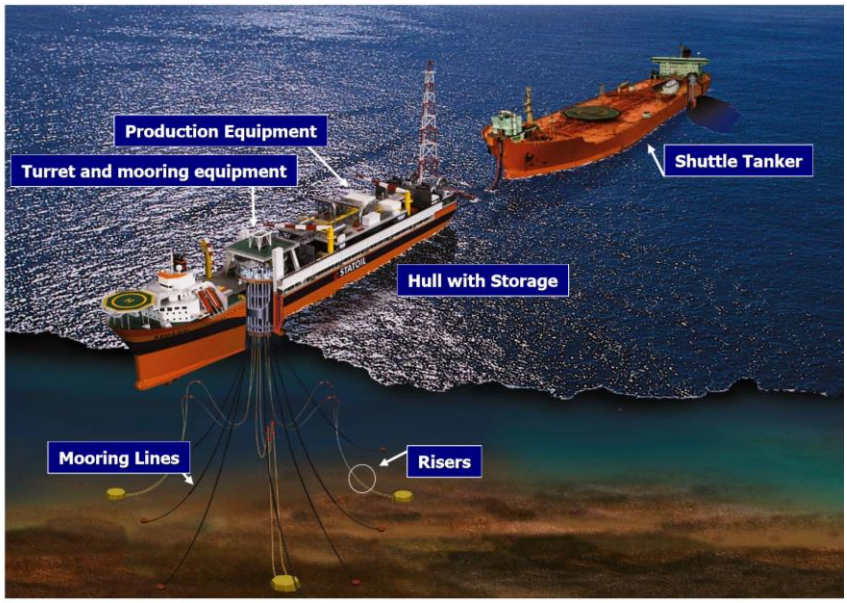

Figure 1.2 FPSO with mooring lines and risers (Statoil, 2008)

Currently, more than 151 FPSOs have been installed at sites around the word in geographically different locations and at various water depths. To date only one FPSO has been installed in a deep-water region of the GOM (Nutter, 2014; Barton and Heather, 2015). The PEMEX Oil Company is currently planning a number of projects in deep-water and ultra-deepwater regions in the south and also in the North of the GOM, where commercially viable discoveries have been made (CNH, 2010; CNH 2012a; CNH 2012b). The FPSO is thus a viable candidate for the exploitation in these marginal fields (Figure 1.4). Thus, a comprehensive understanding of the hydrodynamic behaviour of FPSOs is of great importance in order to achieve the required levels of reliability and safety.

Figure 1.3 FPSO installed in the south GOM in about 100 m of water depth. (BW offshore, 2014)

In deep-water and ultra-deepwater locations, the FPSO's with their mooring lines and risers are continuously exposed to environmental impacts such as waves, winds and currents in collinear and non-collinear conditions. The complex environmental conditions when combined with the increase of the water depth, at installation sites can impose considerable challenges in the analysis and design of the systems in order to ensure their integrity and reliability. In harsh metocean conditions, which is the case in the GOM, the internal turret mooring systems are often the preferred choice to be installed in FPSOs since they permit the FPSO to weathervane in order to reduce the wave frequency (WF) and low frequency (LF) motions and the loads on the mooring line and riser systems. The accurate prediction of the global dynamic response of an FPSO and the associated dynamics of its mooring lines and risers due to these environmental forces are required in order to enable the suitable design, adequate reliability and acceptable cost in the installed system.

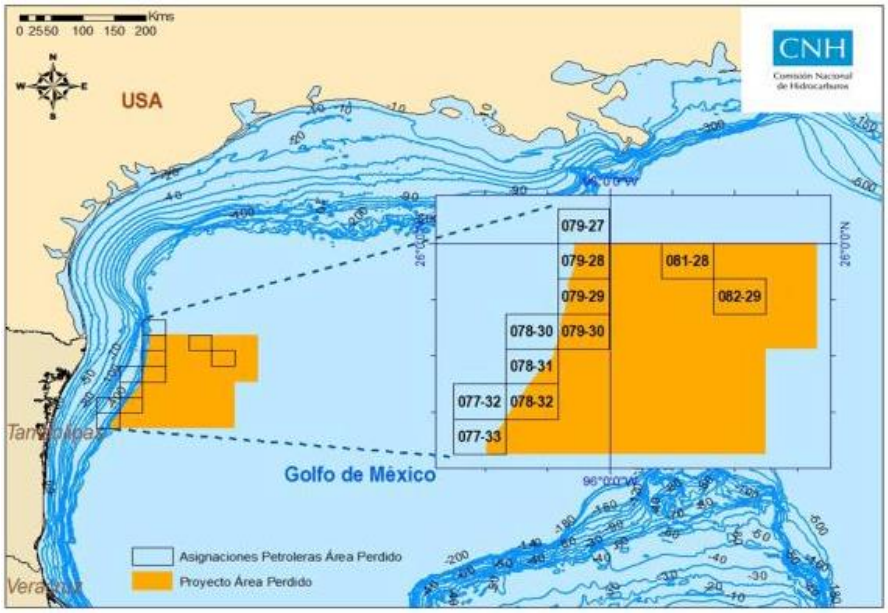

Figure 1.4 Trion and Supremus fields indicative location in the GOM (Comisión Nacional de Hidrocarburos, 2012a)

Environmental forces are usually classified as being either steady or unsteady loads. Steady loads are typically defined by the mean wind speed, the water current and the mean wave induced drift forces, while unsteady loads are produced by complex waves (varying in amplitude and period) and winds occurring in different frequency ranges, such as the wave frequency loads (first-order forces), low frequency wave loads (second-order forces), low frequency wind loads (second-order forces), and high frequency wave load (second-order forces) and even higher order wave loads. Figure 1.5 shows a brief summary of the steady and unsteady environmental loads.

The FPSO with its integral turret component to which the mooring lines and risers are connected will respond to the unsteady loads in 6 degrees of freedom (6DOF) on two different time scales namely the wave frequency (WF) motions, the low frequency (LF) motions, where the WF motions are mainly governed by potential fluid effects, and the viscous fluid effects which are important for the slower LF motions (DNV-RP- F205, 2010).

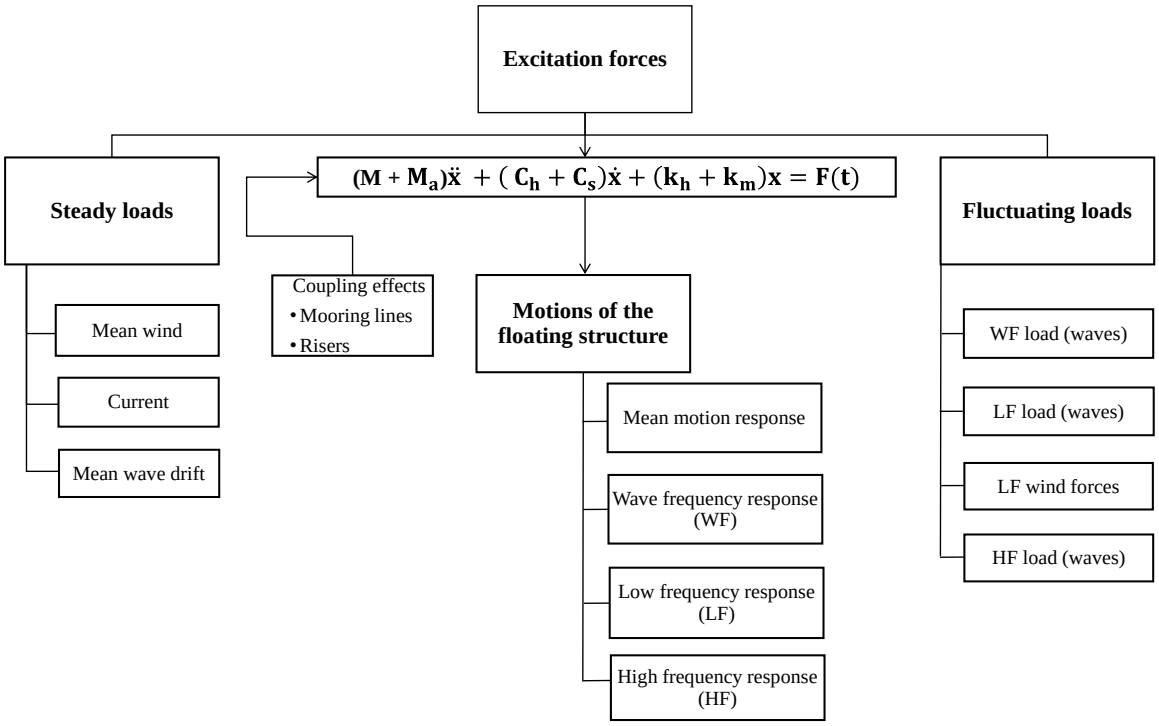

Figure 1.5 Generalized diagram of the environment excitation forces and motion responses of the floating structures

Hydrodynamic analysis of an FPSO with its mooring lines and risers can be carried out through numerical simulation or by experimental model tests. However, there are several difficult challenges that need to be overcome in a suitable way for both the numerical simulation and the experimental model tests in order to produce reliable results. For an FPSO installation in deep-water or in ultra-deepwater locations, both experimental and numerical methodologies need to be used for a better understanding and validation of the complex linear and non-linear hydrodynamics and aerodynamic phenomena and their combinations.

For example, the complex interactions between waves, current and wind on floating structures with their full mooring lines and risers will generate hydrodynamic nonlinearities that can be significant and must be taken into account. Good understanding of such nonlinearities often play an important role in order to achieve an accurate prediction of the overall response and wave drift forces, oscillation drift forces on the FPSO vessel, and the effects of the damping on the mooring lines and risers. This also includes vortex-induced-vibration (VIV) in the mooring lines and risers, geometric nonlinearities owing to deflections in the mooring lines and risers, viscous damping on the floater body itself, green water on the deck, slamming and wave run up (Faltinsen, 1990; Tahar and Kim, 2003; Luo et al., 2004; Chakrabarti, 2005; Chakrabarti, 2008).

Additionally, even though considerable studies have been undertaken on the hydrodynamic behaviour of FPSOs, uncertainties still exist due to the complexity of the hydrodynamics and the lack of experimental data for prototype verification and validation of complex numerical models (Stansberg et al., 2002; Chakrabarti, 2008). Experimental testing in particular is restricted by physical limits of the test facilities since it is not feasible to install the equivalent full scale mooring lines and riser systems and select an appropriate scale model for reducing the uncertainties in the experimental test programme in an offshore wave basin for deepwater and ultra-deepwater locations (Buchner et al., 1999; Stansberg et al., 2002, Chakrabarti, 2005).

This research project has used an effective technique to study the equivalent hydrodynamic behaviour of floating systems to validate numerical models and predict hydrodynamics of the complete system in full water depth. The research includes two parts: a) physical modelling based on a scale model and hybrid passive truncated experimental method for mooring lines and risers; and b) numerical simulation using a non-linear time domain coupled analysis. The extreme motion response of an FPSO and the dynamics of mooring lines and risers are investigated in the context of prevailing environmental conditions for field development in a specific deepwater location in the GOM.

1.2 Literature review

This section summarises the state-of-the-art of research and engineering practice related to the hydrodynamics of FPSOs with mooring lines and riser systems. Different methodologies such as numerical and experimental approaches, that have been proposed to predict the extreme motion responses of the FPSO vessel and the dynamics of the mooring lines and risers, are discussed.

1.2.1 Numerical methodologies

Floating production storage and offloading (FPSO)

The hydrodynamic problem of an FPSO is focussed on the linear and nonlinear wave interactions with the structure in which both the shape of the hull envelope and the mass distribution of the FPSO model structure are involved. The fluid-structure interactions involve linear (first-order force) and nonlinear (both second-order force and higher order forces)

hydrodynamic problems, the higher order forces are not a concern for a moored FPSO since it has a low natural frequency response (DNV-RP-F205, 2010). The rigid body motions of the FPSO can be handled through either frequency or time domain analyses (Low and Langley, 2006).

In a frequency domain analysis the output is normally in the form of transfer functions such as excitation forces/moments, and platform motions per unit wave amplitude at a range of wave frequencies. From this a linear response with wave amplitude is then assumed. The first-order wave excitation forces are thus usually expressed as being linear transfer functions (LTF) while the second-order wave loads are expressed as being quadratic transfer functions (QTF). Some of the nonlinear aspects of the motions of a floating body are well established, including steady drift force, second-order low frequency (slow drift) and high frequency loads (Chakrabarti, 2008; Low and Langley, 2008). In a frequency domain analysis, the process computations are relatively simple and computationally efficient when compared to approaches employing time domain analysis methods (DNV-RP-F205, 2010). However, in the frequency domain analysis procedure it is necessary to establish linear equations to represent the motions, because a linear assumption is employed in the random process theory in order to interpret the required solution. Thus, this approach is not convenient for considering the potential nonlinear effects such as the drag loads, time varying geometry changes (e.g., mooring lines and risers), horizontal restoring forces and variable water free surface elevation (waves). However, when the level of these nonlinearities is low, some cases can be satisfactorily approximated to a linearized formulation (DNV-RP-F-205, 2010).

Low and Langley (2008) reported that the frequency domain approach for a coupled analysis is significantly less accurate when the geometric nonlinearity resulting from the displaced response of the mooring lines and risers is important. In fact, this aspect has motivated the development of a hybrid domain analysis procedure combining both frequency and time domain aspects. However its implementation requires a relatively sophisticated method and a longer computational development phase.

On the other hand, the determination of the maximum motion responses of an FPSO typically involves site specific environment statistics for a 100 years return period of waves, currents and winds and therefore a highly non-linear behaviour is to be expected and thus a time domain analysis process is required. A time domain analysis can handle the nonlinearities that are present in the environmental excitation forces, thus the waves can be, and indeed will

be, regular or irregular with multiple frequencies and amplitudes and even with the non-linearity. However, the effects of the nonlinearities in the water free surface forces related to the wave profiles are generally only approximated by empirical methods (Faltinsen, 1990; Lee, 1991a; Chakrabarti, 2008).

The complete nonlinear wave-structure interaction boundary value problem may be resolved by the employment of a Mixed Eulerian-Lagrangian (MEL) approach. In the MEL approach the Eulerian field equations are solved in order to obtain the local fluid velocity distributions in space and time and this velocity is used to represent the flow of fluid particles on the water free surface in the Langrangian way. This method solves the full nonlinear boundary value problem without making any analytical approximations. However, it requires a large computation time and thus is not a practical methodology for general use in the offshore industry where many studies may be undertaken during the normal iterative development process (Longuet and Cokelet, 1976; Beck et al., 1993; Beck, 1994; Kim, 1995; Chakrabarti 2008;).

Several other time domain methods have been proposed in order to avoid excessive computation time but also to account for the nonlinearities in an approximate way (De-Kat and Pauling 1989; Chitrapu and Ertekin 1995). The geometric nonlinearities that are associated with hydrostatic restoring forces and the Froude-Krilov forces are normally considered, however the hydrodynamic interactions due to radiation and diffraction effects are linearized. Thus, it has allowed the typical application of 2-D or 3-D linear diffraction/radiation theory to be employed in a frequency domain analysis.

Sen (2002) developed a time domain motion simulation approach through the use of a simplified numerical wave tank that is based upon a BIEM (Boundary Integrated Element Method) approach and time integration of the boundary conditions. The simplifications employed include linearization in the radiation and diffraction hydrodynamics effects whereas the incident wave effects were considered to be complete and other nonlinearities effects associated with slender elements, representing the lines and risers, were integrated in the process. However the main inconvenience in this approach is in the way that the exterior boundary is treated which limits the length of the computer-based simulation time.

Special numerical techniques are necessary in order to evaluate the complexity of the resulting second-order forces. In particular the component that is associated with the boundary

condition on the water free surface requires an evaluation of slowly-convergent oscillatory integrals over the free surface (Lee and Newman, 1991a, Lee and Newman, 1991b).

At the present time, several different methodologies are being used for motion analysis of floating structures. However there is, unfortunately a numeric difference in the results that have been obtained among the many methodologies. A comparison of the results of first and second-order motions analyses of two specific FPSO's were obtained from calculations made by 23 different organizations and which showed that the results of the first-order motion response did not vary much from the different providers. However the second-order motion response showed a large discrepancy. The different results were mainly attributed to inaccurate modelling (FPS, 2000).

Standing (1988) studied the numerical uncertainties that are involved in estimating the second-order LF wave forces and FPSO body responses and observed that many uncertainties may arise from the hull surface and lines mesh discretisation errors or fineness or in the procedures that are used to treat the local individual source strength distributions.

Wichers (1988) studied the viscous damping component for an FPSO complete with mooring lines. The motions of the FPSO due to the current, winds and long-crested irregular waves, were analysed by employing a non-linear time domain uncoupled analysis, which calculated the motion response for the FPSO separate from the mooring lines. It was reported that the approach gives reasonable results and identified that viscosity plays a major role in producing a good estimation of the LF motion response while the drift damping was observed to be negligible under moderate sea states (Wichers, 1988).

The LF motion response and the coupled effects of the mooring lines on an FPSO were studied through a series of experimental model tests that were undertaken by Wichers and Qun (1997). It was found that the viscous contribution in a normal direction has a significant contribution to the corresponding motion responses as well. It is clear that viscous contribution plays an important role in the accurate estimation of the LF motion of the moored FPSO.

Numerical simulation of the wave-structure interactions for an FPSO hull in deep-water is conventionally solved using potential flow theory in order to handle the linear and nonlinear wave loads (first and second-order forces). The first-order wave forces on the vessel, the wave diffraction and motion induced radiation effects from the submerged portion of the vessel, can

be calculated from programs based on BIEM, and by using free surface Green functions (Faltinsen, 1990; Lee, 1991b; Chakrabarti, 2008; Kim, 2008).

The solutions of the second-order wave problem are expressed as the mean drift force and the oscillating force with low frequency ranges for which the two nonlinear solutions are resolved in terms of a quadratic transfer function (QTF) that typically requires a considerable amount of computational time when the full matrix of the QTF is being solved. This is the main obstacle for it to be applied routinely in a design process (Lee and Newman, 1991a).

For the mean wave drift forces, it is not necessary to solve the complete second-order equations due to observation that the oscillation of the pressure response of the structures over one period tends to be zero in time dependence. This means that the mean wave drift force can be calculated from the first-order velocity potential (DNV-RP-F-205, 2010). There are two main methods to solve the problem of the mean wave drift forces: The far field method or momentum method and the near field method or pressure integration method. Newman (1967) and Maruo (1960) presented the far field method in which the hydrodynamic properties of the body are evaluated through the use of a control surface that is mathematically taken as being far away from the body in order to predict the components of the wave forces on the structure. The far field method is relatively faster compared to the near field method, however, the far field method is limited to predicting the horizontal component of the mean drift forces and the moment in 3 DOF (surge, sway and yaw). A further integration step on the mean free surface defining the wetted surface of the hull body is needed if the heave, roll and pitch mean drift force and moments respectively are also required. However, these components are not normally calculated (DNV-RP-F205, 2010). This may be a limitation if the requirement is to estimate the extreme values of the motion responses in some types of floating productions systems where the full 6 DOF motions are important in the design of the mooring line and riser systems, such as in the case of Semi-submersibles (Atlar, 1986).

Pinkster (1975) introduced the near field method, which is based on direct pressure integration of the total contributions to the second–order mean wave pressure over the instantaneous wetted surface of the structure. One of the advantages of the near field method is that it can solve the 6 DOF motions.

On the other hand, Newman's approximation is normally used in frequency domain analysis for the prediction of the second-order oscillation wave forces in LF range on the vessel, due to the advantages in reduced computational time. This approximation takes into account the observation that the natural frequency of a moored floating vessel is generally very low, which is generally the case for the horizontal motions of an FPSO. Newman's approach assumes that the effects of the off-diagonal elements in the full QTF matrix can be reasonably approximated by considering only the diagonal elements (Newman, 1974). However, some limitations have been observed in Newman's approach. It underestimates the magnitude of the drift forces in shallow water, (Hauteclocque et al., 2012; Newman, 2004; Xiong et al., 2015) and that the validity may be questionable when the input sea spectrum is not narrow-banded or when the wave spectrum is double-peaked (Tahar and Kim, 2003; Pinkster 1980). However, the Newman's approach has been reported to work well in deepwater installations (Hauteclocque et al., 2012; Tahar and Kim, 2003).

Therefore, the hydrodynamic characteristics of the FPSO in this work are studied through both the Newman's approach and the full QTF approach using the direct 2nd-order pressure integration method in order to predict the extreme motion responses in 6 DOF.

The collinear and non-collinear environmental condition of waves, wind and current often occur in deepwater regions of the GOM. (Baar et al., 2000) observed that the extreme response of a turret-moored FPSO is sensitive to the non-collinear environmental conditions and the location of the internal turret has influence on the motion response and tension of the mooring lines. Irani et al., (2001) and Ward et al., (2001) showed that the response of moored FPSO is more severe in non-collinear environmental conditions, but non-collinear conditions have less influence on the tensions of the mooring lines. Faltinsen (1994) found that wave-current interaction increases the mean motions and slow-drift oscillation due to the fluid flow pattern around of the structure and the mean wave loads according to potential theory are connected with the structure's ability to create waves.

Mooring lines and risers systems

Most FPSOs generally use either a catenary or a taut mooring line system connected to an internal turret such that there is no restraint on vessel yawing motions (see Figure 1.6). In a catenary mooring system, the WF motions produce dynamic mooring forces that are caused

mainly by the transverse drag forces on the lines, which tend to increase in deep water (Chakrabarti, 2005). In contrast, a taut mooring system experiences less transverse motions and the dynamics decrease as the water depth increases. Therefore taut system tends to work in a more elastic, spring-like, manner.

The hydrodynamic analysis of mooring lines includes directional current loading throughout the water depth, and vessel motions at the top-end of the individual lines, taking into account both the wave frequency and low frequency motions. It is also important to ensure that the dynamic tension components in the lines are not underestimated, as well as the advantages of the line viscous damping contributions (Ormberg and Larsen, 1998; Chakrabarti, 2005).

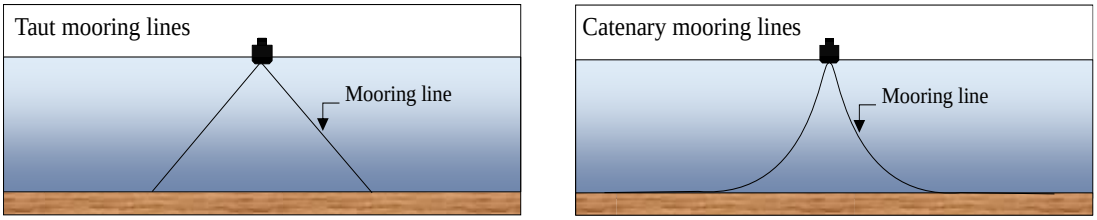

Figure 1.6 Illustrations of taut mooring lines (left side) and catenary mooring lines (right side)

Ormberg and Larsen (1998) observed that the damping contribution of the mooring lines and risers are sensitive to the environmental loading conditions and concluded that the use of damping for other environmental conditions should be avoided.

For the riser systems in deep-water, flexible risers and the compliant catenary risers are usually employed due to the possibility of significant WF motions of the FPSO. The engineering solution for the more flexible riser systems are normally obtained by configurations such as steep S, lazy S, steep wave, lazy wave, free hanging catenary (with supporting buoyancy chambers, etc.) due to the significant WF motions that may be present in deepwater (DNV-RP-F205, 2010).

The hydrodynamic behaviours of risers are readily predicted by a decoupled analysis because the dynamic loads in risers mainly depend on the WF motions of the vessel and on an estimation of the total allowable offset (Ormberg and Larsen, 1998).

However, the dynamics for mooring lines and risers is largely based on empirical design procedures. The environment-induced forces are determined in terms of established hydrodynamic coefficients applying the Morison formulation and which, in most cases it is

taken to be linearized. However, the drag force and the lift force have a strong nonlinear dependence since the calculation of these components is dependent on the local flow velocity squared (Chakrabarti, 2008).

Another point to be observed and appreciated is that the fluid dynamic drag force is the main source of damping in the mooring lines and risers. The accurate prediction of this is very important for an accurate estimation of the overall low frequency motions of the overall system in deep-water. For the mooring lines the inertial effects between the mooring lines and the surrounding fluid are normally included in the analysis. However their influence is usually relatively small. In comparison, the inertia effect is more important in the case of the risers than it is for the mooring lines (Chakrabarti, 2008). Another important aspect is the sea bed soil-structure interaction. This is also attributed as being a source of damping in the mooring line and riser systems and which reduces the local horizontal tensions over them (Chakrabarti, 2005). Moreover, Sarpkaya (1978) discussed that the drag and inertia coefficients that are used by mooring lines and risers analyses are often only an average coefficient value of the drag and inertia coefficients. These coefficients are used over the entire length of the mooring line or riser components, irrespective of its physical orientation, location and different velocity of the fluid on them. These uncertainties are added to by the possible formation of biological marine growth or fouling which produces additional uncertainties in the calculation of the local and overall inertia and drag forces.

Therefore, it is important to investigate the individual hydrodynamic contributions of the mooring lines and risers in terms of inertia, drag forces, restoring force and nonlinear geometric behaviours in order to examine their effects on the LF and WF motions of an FPSO.

Chakrabarti, (2005) observed that the contributions of the restoring forces, and the hydrodynamic drag and damping of the mooring lines and risers when calculating the horizontal plane excursions of the floating vessel may result in a conservative estimate of the maximum excursion and which may thus not be found to be acceptable. On the other hand, increased levels of floating excursions being experienced in service may produce riser fatigue damage. Thus the first-order effects may be spread over a greater length of the riser rather than being localised.

Zhen and Kim (2010) discussed the possibility that the more flexible riser systems attached to a moored vessel could experience flow related vortex shedding induced vibrations (VIV)

with relatively high frequencies (and possibly amplitudes), in addition to the other forces that are induced by the WF and LF vessel floating motions.

Chakrabarti, (2008) commented that riser technology is continuously advancing with the sophisticated coupled riser FE/CFD numerical analysis processes, in parallel with both small scale laboratory and large scale or full scale in-situ testing. However, the limitations are those still associated with large computation time, fundamental capabilities and limitations in flow solver methods (including convergence) and high Reynolds number effects.

Damping contribution to the FPSO with mooring lines and risers

The inclusion of the damping contribution is important in order to have an accurate prediction of the motions of the FPSO and tensions in the mooring lines and the risers. Previous research works have identified several different damping mechanisms.

Brown and Fang (1996) and Chakrabarti (2005) described different damping contributions that can affect the 6 DOF of motions of a moored floating system such as motion-induced radiation damping, viscous damping, wave drift damping, mooring line damping and wind drift damping.

Motion radiation damping is very important in WF motion responses since the damping contribution is linearly proportional to the wave amplitude and dependent of the WF, however for the LF motion responses the effect is insignificant (Faltinsen, 1998). The hull damping is produced by the skin friction damping, eddy-making and wave drift damping (Faltinsen, 1998). Viscous forces owing to the pressure distribution on the hull or also called eddy-making damping is important to the sway and yaw motions while the skin or friction damping is the largest contribution to the hull viscous damping.

On the other hand the floater's motions with small forward speed waves will be also experiencing an increasing in the second-order wave forces in differences frequency due to the drift damping forces. For high sea states the wave drift damping may be dominant hull damping (Faltinsen, 1998) and for the FPSO with large slow drift yaw motion the wave drift damping in three main horizontal motion surge, sway and yaw is important (DNV-RP-F205). The wind-caused damping on a floater structure due to the frictional drag between the air and the structure

has been, in most cases, identified to be relatively much smaller when compared with the other damping contributions (Chakrabarti, 2005).

Additionally, from the mooring and risers, there has been observed to have high contribution of the viscous damping in particular for deepwater installation. Three sources of damping have been identified for platforms such as FPSOs: fluid induced loads (drag forces), internal frictional forces and seabed interaction. Parametric studies have indicated that mooring line damping from the drag forces is sensitive to the level of the pretension and stiffness of the mooring line and risers. The damping from the seabed interaction has been observed that reduce the tension and increase the line stiffness (Brown and Fang, 1995, Chakrabarti, 2005).

Integration of the total system FPSO with mooring lines and risers

In practical analysis two methodologies are mainly used in the industry in order to predict and analyse the overall global response of a floating production system with mooring lines and risers: de-coupled analysis and coupled analysis. In a de-coupled analysis the 6 DOF motion equations of the rigid body (floater system) are solved traditionally in time domain, but the restoring based coupled effects (i.e. stiffness) from the mooring lines and risers are included in a quasi-statical form using non-linear springs (see Figure 1.7). The other coupled effects such as damping contribution and current loading on the mooring lines and risers are estimated through separate assessments and they need to be given as input to the analysis (DNV-RP-F205, 2010). Conversely, the coupled analysis takes into account the complete system of 6 DOF motion equations of the floater system and the slender body model for the risers and mooring lines. Floater, mooring line and riser system equations are solved simultaneously using a non-linear time domain dynamic analysis. The coupled effects (restoring forces, current load, damping and inertia contribution) from the mooring lines and the risers are automatically included in the analyses for the dynamic equilibrium (Figure 1.8).

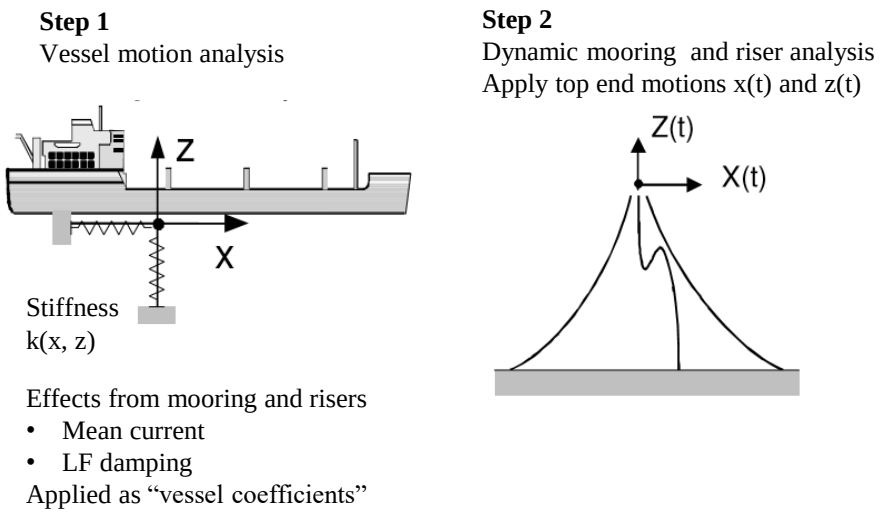

Figure 1.7 Schematic diagram of the de-coupled analysis process (Ormberg and Larsen, 1998)

Several studies have been undertaken concerning the importance of the coupled effects of the mooring lines and risers on the dynamic response of the floating body of FPSOs particularly when the installation sites are in deepwater and ultra-deepwater locations (Ormberg and Larsen, 1998; Chakrabarti, 2008; Senra et al., 2002). Ormberg and Larsen (1998) observed that the mean horizontal plane translation offset of the FPSO along with the additional LF motions typically represent approximately 95% of the total maximum excursions in deep-water (Figure 1.9).

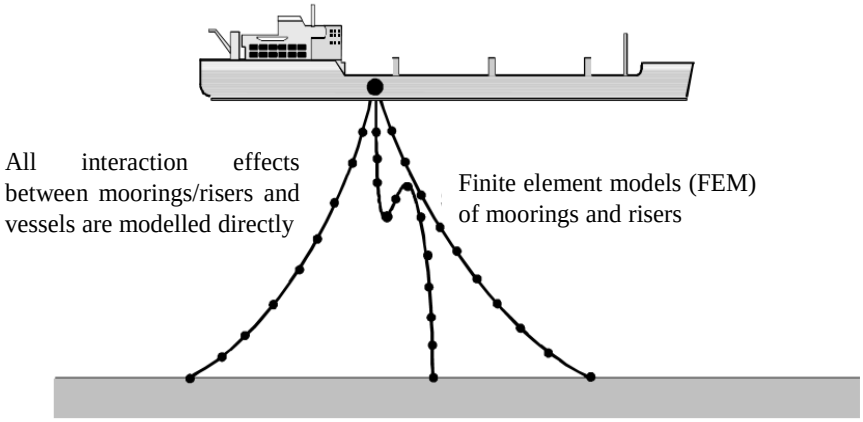

Figure 1.8 Schematic diagram of the coupled analysis process (Ormberg and Larsen, 1998)

Fully coupled analysis has long been recognized as being the most accurate design methodology that can be used to estimate the overall global response since it considers the complete integrated full system of equations, involving the calculations of the behaviour of the rigid body of the floating vessel and also those of the slender flexible mooring lines and risers elements, and which are solved simultaneously using a large displacement non-linear time

domain approach with the dynamic equilibrium being obtained at each incremented time step. In the fully coupled analysis all the coupling effects from mooring lines and risers are calculated automatically (Ormberg and Larsen, 1998; Heurtier et al., 2001; Kim et al., 2001; Correa et al., 2002; Chakrabarti, 2008).

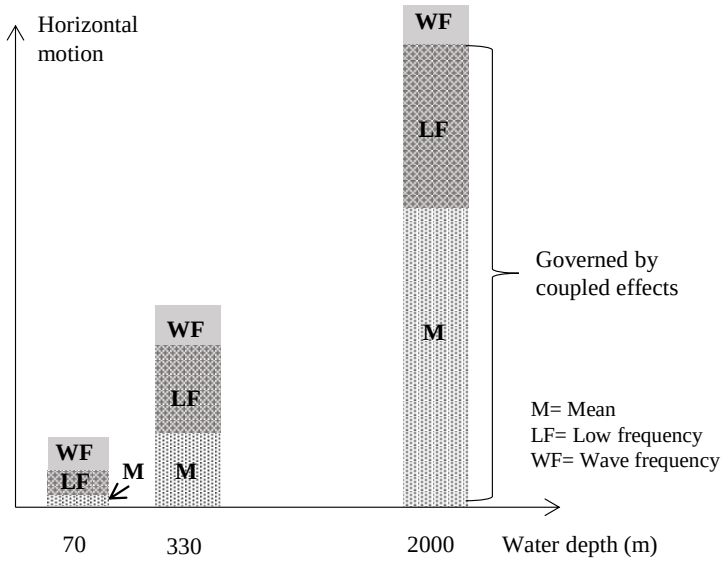

Figure 1.9 Typical characteristics of motions response for moored FPSO (Ormberg and Larsen, 1998)

Chakrabarti (2008) discussed that the global response of the FPS may be calculated through a total system analysis approach where the analysis considers the complex fluid-structure interactions of the various components of the total system and interactions of the mooring lines and risers with both the FPS and the seabed. The fluid field may be represented by a 3-D computational fluid dynamics simulation (CFD) whereas the interaction of all components and elements with the surrounding fluid could also be solved in terms of the Navier Stokes equation, with the FPSO being represented as a rigid three dimensional, surface faceted body while the mooring lines and risers represented by slender flexible elements defined by bar and beam finite elements. However, this is not a practical method for use within the design process approach at the present moment, as it requires prohibitively large computation times. Thus, normally the total analysis is typically simplified through a degree of levels of empiricism in order to produce a more practical cost effective method as illustrated in Figure 1.10.

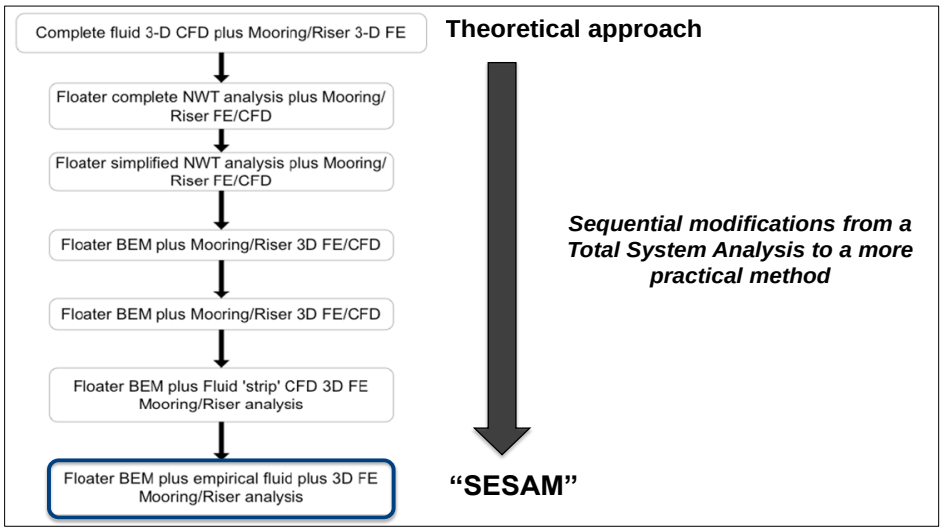

Figure 1.10 Sequential modifications from the complete total system analysis level to a more practical method (Chakrabarti, 2008)

The most common analysis approach that is currently used today in the design of an FPSO considers the fluid load forces to be represented by various empirical formulae (Potential theory) (Chakrabarti, 2005). The 3D boundary integrated element method (BIEM) is generally used for the representation of the floater and the still water free surface, while the coupled 3D finite element model is used to solve the non-linear hydrodynamic behaviour of the various mooring lines and risers (Newman, 1977; Lee and Newman, 1991b; Faltinsen, 1990; SIMO-SESAM, 2015; RIFLEX-SESAM, 2013).

1.2.2 Physical modelling

Scaled model tests of a ship-shaped FPSO, complete with turret mooring lines and risers in deepwater or ultra-deepwater locations, are considered to be the most reliable way to study the complex hydrodynamics and aerodynamics of the complete system (BMT, 2000; Stansberg et al., 2002; Stansberg et al., 2004). Using facilities fitted with advanced equipment, dedicated model tests can closely represent the motion response to realistic environmental conditions and dynamic interactions between waves, current, winds and the total floating system, including mooring and riser systems.

The experimental tests help to provide crucial information about the complex linear and nonlinear hydrodynamic behaviour of the total system, such as the total viscous damping contributions of the system, the coupled effects of the FPSO vessel with the mooring lines and risers, and the transient green water and slamming forces and wave run-up effects that are

difficult to evaluate through numerical simulation alone, without any simplifying assumptions (Faltinsen, 1990; Chakrabarti, 1998; Luo, et al., 2004). Thus, a model test is often used to validate designs throughout a complex iterative design process, typically using numerical tools.

However, when conducting model tests of offshore structures for deepwater and ultra-deepwater installations, scale effects become a major issue, and they are very difficult to handle due to the limited physical dimensions of the offshore basins (Stansberg et al., 2002; Chakrabarti, 2005). To limit the scale effect, a scale ratio of 1:50-1:70 has been recommended for model tests of FPSO systems and has been found to be reliable for predicting full-scale behaviour (ITTC, 2008). However, this range of scale ratios is unable to represent a full-scale water depth when it is equal or greater than 1000 m, and the experiments involve testing the mooring arrangement and riser system behaviour (ITTC, 2008).

Continued efforts have been made to overcome the test basin limitations by using relatively small models. A scale ratio of 1:170 is considered to be close to the practical limit, particularly for examining the hull behaviour, based on existing model basin facilities and limitations such as model accuracy, instrumentation accuracy and environment loading generation (Moxnes and Larsen, 1998). Small-scale testing at scales of 1:150-1:170 have been undertaken, and studies on reliability at this scale have been suggested to evaluate and quantify the uncertainties and to keep them within acceptable levels of accuracy (Stansberg, et al., 2004). An alternative procedure, called the hybrid passive methodology, has been explored. It combines an appropriate scale model for the FPSO hull with a depth truncation to yield equivalent quasi-static horizontal restoring force-excursion effects from mooring lines and risers in responding to the test basin limitations. However the dynamics from the mooring lines and risers on the motions of the vessel must be found through numerical simulation procedures by extrapolation of the motion responses of the design prototype system in full water depth (Chakrabarti, 1998; Tahar and Kim, 2003; Luo, et al., 2004; Fylling and Stansberg, 2005; Baarholm, et al., 2006; ITTC, 2008; Su, et al., 2009).

Stansberg, et al., (2000) investigated the hybrid passive methodology and made a comparison for a moderate water depth using both the hybrid passive methodology and a full depth model with a conventional scale model. The results showed that the truncated mooring and riser model approach is technically feasible Figure 1.11.

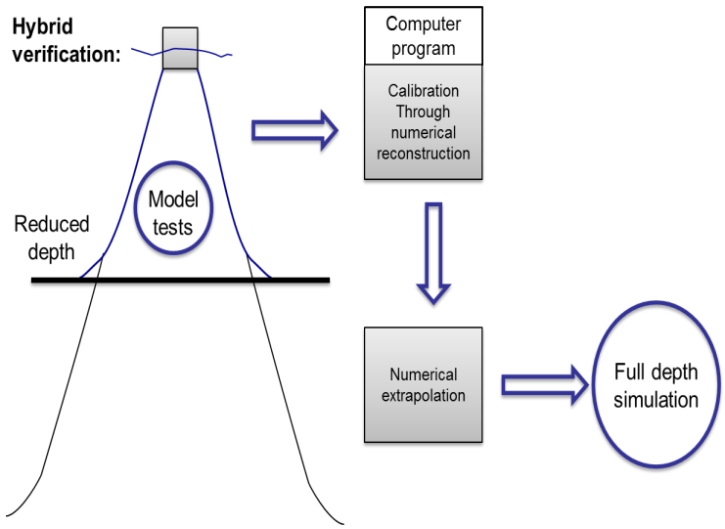

Figure 1.11 Sketch of hybrid passive methodology for the truncation of the mooring lines and risers (Stansberg et al., 2000)

On the other hand, conceptual studies have been carried out in order to overcome the limitation of predicting the dynamics of the mooring lines and risers using model tests specific for deepwater and ultra-deepwater installations. The hybrid active truncation methodology for mooring lines and risers has been proposed to be used in the real time, where a computer system and control actuator systems are used for substitute the truncated segment of the mooring lines and risers that cannot be installed in a basin with appropriate traditional model scale (BMT, 2000; Stansberg et al., 2004).

Fryer et al., (2001) discussed that the hybrid active truncation system needs more development and that limitations such as intelligent software and powerful computers together with a control system and actuators to simulate the real time are not available and they need to be developed in the future.

Recently, Cao and Tahchiev (2013) investigated the hybrid active system and they concluded that active system needs to improve particularly in the controllers in order to produce a good synchronization in random environments and also overcome the effect of the time delay between the sensors installed in the mooring lines or risers and the controller and the actuator system. Chabaud et al., (2013) studied a simple case based on a linearized one degree of freedom for representing a floating wind turbine using a real-time hybrid testing (RTHT). They found that a linear system may give acceptable results but the coupled experimental model and numerical model involved a time delay that must be reduced. This represent the central problem of the active truncated procedure.

As a result the hybrid active truncation methodology for mooring lines and risers has been established and developed up to a conceptual stage. However, this methodology needs additional hardware development in order to be accepted as an accurate and technically feasible methodology.

1.3 Aims and Objectives

Based on the background and the previous work carried out, the aim of this research is to contribute to the understanding of the hydrodynamics and to the prediction of the extreme motion response of an FPSO vessel as well as the dynamics of the mooring lines and risers in deepwater locations. Thus a comprehensive experimental and numerical study is carried out to investigate the motion dynamics of surface FPSO vessel and dynamics of mooring line and riser systems at a specific deepwater field location (GOM) under a full dynamic collinear and non-collinear environment loading conditions.

The experimental study applied the hybrid passive truncation methodology for the mooring lines and risers in order to overcome the limitations of the offshore basin. In addition, the motion dynamics of the surface FPSO vessel and line dynamics of mooring and riser systems was investigated. The comprehensive experimental results also provide a benchmark for validation of the numerical model. The numerical modelling is conducted using a nonlinear time domain coupled analysis methodology. The complex dynamics of the mooring lines and risers are studied through an extrapolation method from the test results obtained from the truncated model (also involving an associated analytical model) of the mooring lines and risers to the original full depth prototype model using a coupled analysis.

The specific objectives of this thesis are summarized as follows:

1. To develop an experimental model test using hybrid passive technique for mooring lines and the risers.
    a. To design the model FPSO including internal turret for connection of mooring and riser systems.
    b. To design the mooring line system and select the riser system.
    c. To design the truncated mooring line and riser systems.
    d. To define the experimental setup, testing matrix and environment conditions.

e. To process the experimental results (viscous damping of the FPSO model in 6 DOF, damping contribution of the mooring lines and the risers and extreme motion response of the FPSO model and dynamics of the mooring lines and the risers).

2. To develop a numerical model using a non-linear time domain coupled analysis methodology.
    a. To validate the numerical model with the experimental results for mean motion and dynamic motion response of the FPSO model and dynamic tension response of the mooring lines and risers under collinear and non-collinear environment loading condition.
    b. To evaluate the accuracy of two different numerical methodologies in order to predict the LF motion response (Newman's approximation and the full QTF).
    c. To extrapolate the truncate numerical model to full depth model in order to study the dynamics of the mooring lines and the risers and their influence on the LF and WF motion responses. Additionally to examine the reliability of the passive truncated methodology through the coupled analysis.
3. To investigate the coupled effects of the FPSO and the mooring lines in two different water depths and how they affect the extreme motion responses, in terms of the mean, LF and WF motions, of the FPSO and the dynamics of the mooring lines.

1.4 Thesis Outline

The thesis is organised and presented in five chapters which describe the activities and results obtained.

Chapter 1 provides the background and the motivation to the chosen research topic and a review of state-of-the-art research and methodologies related to the topic as well as the aims and objectives of the thesis are presented.

Chapter 2 describes the hybrid passive truncated experimental methodology and the particular FPSO model, with mooring lines and risers selected. This chapter also describes the design procedure of the truncated mooring and riser systems, the experimental set-up and the complete test matrix to evaluate the system under the collinear and non-collinear environment loading condition directions. The spectral response and statistical analysis of the results of the FPSO model and mooring lines and risers are discussed.

Chapter 3 describes the numerical simulation used to predict the hydrodynamic responses of FPSO model and the mooring line and the riser systems. Also, the calibration and validation of numerical models for various cases studies through use of the experimental data that have been obtained (Model to Model) are presented. Two different numerical methodologies are used to predict the extreme motion response of the FPSO model (Newman's approximation and the full QTF). The validity of the hybrid passive truncated experimental methodology approach for evaluating the dynamics of the mooring lines and risers is examined through an extrapolation process from the truncated model to the full depth prototype model.

Chapter 4 presents the results of the decoupled and coupled analyses through a sensitivity analysis for a collinear environment condition. Two different installation water depths (1000 m and 2000 m) are considered, the LF and WF motion responses and the coupled effects such as damping and restoring forces contribution and the dynamic tension force response of the mooring lines and risers are evaluated.

Chapter 5 provides an overall synthesis and summary of the project with the major findings and their importance highlighted. Potential future research studies are suggested.

Chapter 2

Experimental Study

2.1 Design of FPSO system with mooring lines and risers

This chapter describes the experimental study that was carried out in order to examine the dynamics of the complete FPSO vessel, together with its mooring line and riser systems. The experimental tests were undertaken in a Deepwater Offshore Basin with 10 m of water depth at Shanghai Jiao Tong University in China (SJTU). A hybrid passive truncated methodology is applied for representing the full-length design of the mooring lines and risers. The FPSO global response for both the Full and Ballast loading conditions and the associated dynamics of the mooring lines and risers were investigated for both collinear and non-collinear environmental conditions.

The FPSO vessel used in this study is designed with a maximum storage capacity of 1,000,000 bbls and a 180,000 DWT based on the typical daily production rate of the field in the region of Southern GOM. The FPSO hull is 300 m in length between perpendiculars, a breadth of 46.20 m and a depth at the side of 26.20 m in prototype. The hull has a simple fairly high block coefficient form, and the middle cross section of the model is box-shaped (see Figure 2.1a and Figure 2.1b). Both the Full Load and Ballast Load conditions were tested. The Full Load condition is associated with a level keel draught equal to 16.5 m with a corresponding displacement of 218,876 tonnes, and in the Ballast Load condition, the average draught was 9 m with a corresponding displacement of 122,530 tonnes. A crude representative topside arrangement was used with a beam area on the deck of 5190 m^2, and a bow projected area on the deck of 1448 m^2, sufficient to allow for an evaluation of the wind loading on a typical topside area on the FPSO model. The details of the estimation of the wind area from two

directions can be seen in Appendix B. The hull of the FPSO includes a bilge keel of 1.00 m width and 120 m length centrally positioned about amidships (Figure 2.2).

Figure 2.1a FPSO model, scale 1/64th

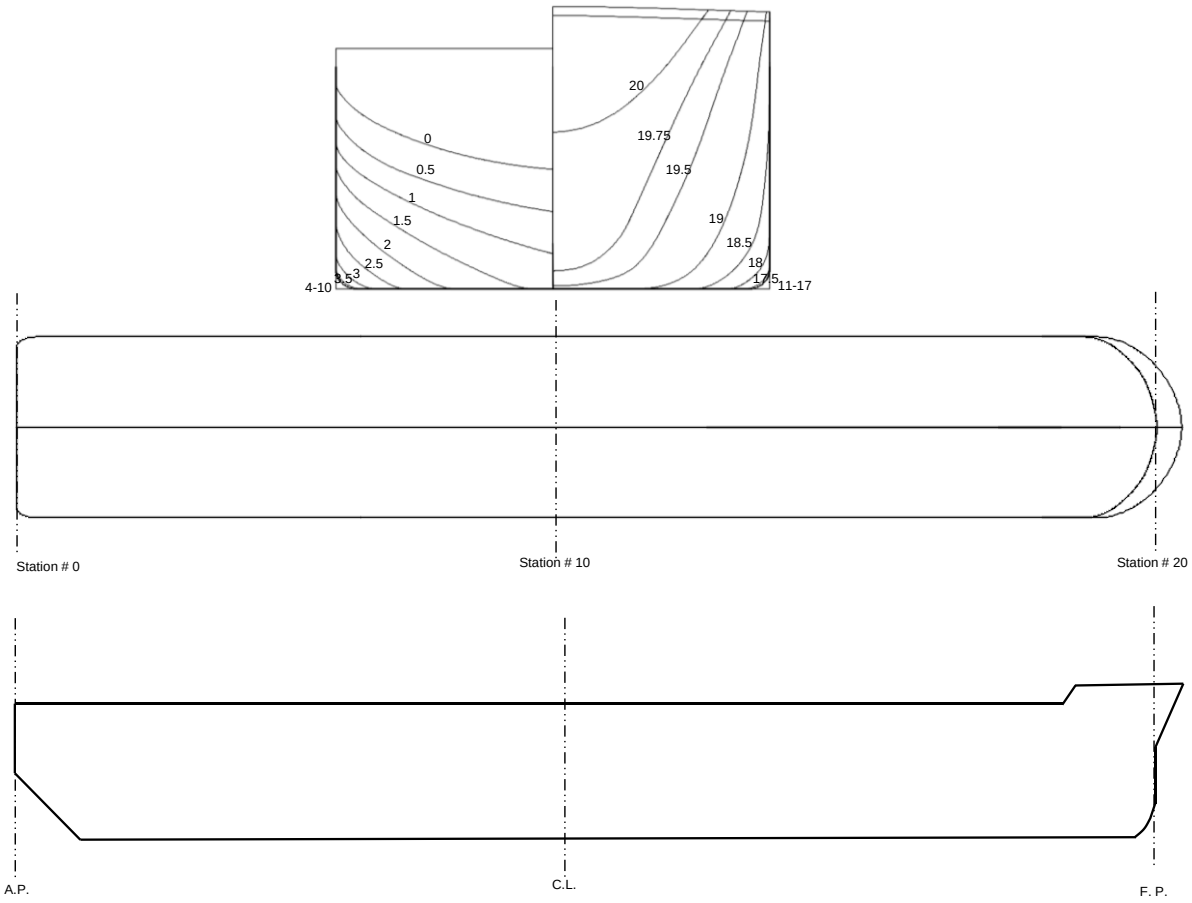

Fig. 2.1b Body plan and outline form of the FPSO model

The FPSO model was fitted with an internal turret mooring lines and risers connection system, which has a diameter of 12 m in the prototype. Its vertical centre line was located 30

m from the forward perpendicular of the FPSO vessel. The function of the turret was to provide a tie-in mechanism for the FPSO, with 9 mooring lines and 6 risers thus enabling the hull to freely yaw relative to the mooring lines and risers.

Figure 2.2 Bilge keel

In the experimental tests, the Froude and Strouhal numbers of the model and prototype were kept the same making the gravitational and inertial forces similar. The main particulars of the FPSO vessel in both prototype and the corresponding model scale dimensions are summarized in Table 2.1.

Table 2.1 Prototype and model scale dimensions and characteristics of the FPSO

	Full Load Condition		**Ballast Load Condition**	
Description	Prototype	Model Scale	Prototype	Model Scale
Length LPP (m)	300	4.69	300	4.69
Breadth, B (m)	46.20	0.72	46.20	0.72
Depth, H (m)	26.20	0.41	26.20	0.41
Draught, T (m)	16.50	0.26	9.00	0.14
Ta (m)	16.50	0.26	9.50	0.15
Tf (m)	16.50	0.26	8.50	0.13
Length/Beam ratio (L/B)	6.49	0.10	6.49	0.10
Beam/Draught ratio (B/T)	2.80	0.04	5.13	0.08
Displacement (tonnes)	218876	0.82	122530	0.46
XB, XG (m)	2.43	0.04	3.08	0.05
ZG (m)	11.43	0.18	7.87	0.12`
Kxx (m)	16.17	0.25	20.79	0.33
Kyy (m)	86.72	1.36	86.72	1.36

A permanent mooring system was designed to allow for the expected extreme horizontal motions values of the FPSO vessel and the maximum tensions of the lines. A coupled non-linear time domain analysis was carried out for the mooring system using SESAM software

(SIMO-SESAM, 2015; RIFLEX-SESAM, 2013) where both collinear and non-collinear environmental loading conditions were independently exposed to the total system. The mooring lines were designed for restraining and covering the maximum horizontal offset 100 m that is equivalent to 10 % of the water depth and the required strength of the mooring lines according to the API 2SK (2005). The mooring system was reviewed for both intact and single line damaged conditions of one significant event in a three hour stationary storm and hurricane conditions for a 100-year return period (short term analysis), together with both a current and wind environment condition typical of the installation location in the GOM. The configuration of 3x3 mooring lines each with chain specification of the R4S studless (fairlead chain and chain ground sections) and a length of wire to specification of spiral strand (wire mid-section) was found to be sufficient for meeting the safety factor of the axial strength of the mooring lines and the target offsets limits of the FPSO vessel according to API-RP-2SK (2005) and Wichers (2011) respectively. A minimum strength safety factor of the most loaded mooring line (L-2) of the mooring system was 1.55 compared to 1.25 of API-RP-2SK (2005) for the single line damaged condition when the FPSO vessel overall system is exposed to non-collinear environment loading. The mooring system leads to the maximum offset of the FPSO vessel being 88.39 m in the collinear environment loading condition which was found to be inside of the limit of 10% of the full water depth installation (i.e. 100 m at 1000 m depth) (Wichers, 2011) (for details see Appendix A)**.** The mooring system has 9 lines with a symmetric configuration arranged in three groups, each group having 3 lines. The groups were 120 degrees apart, as shown in Figure 2.3. The individual lines are identical with three integrated chain-spiral and strand-chain segments. Each line in a group is separated by 5 degrees from the adjacent lines. The mooring system was established with each line being defined to be semi-taut but have a simple catenary mechanism that was subsequently verified through the slightly non-linear behaviour of the restoring force curves and offsets as shown in Figure 2.4**.** Comprehensive details and characteristics of the mooring lines are given in Table 2.2.

Further, six steel catenary risers (SCR) for oil production and potential injection were assumed with a simple symmetric configuration. SCR risers with 273 mm outside diameter and 235 mm inside diameter were selected in accordance with specification API-5L-X-65. The risers were selected only for the purpose of including and evaluating their typical static and coupled dynamic effects on the vessel. The riser arrangement in three groups is shown in Figure 2.3, in which each of the groups are separated by 120 degrees. The main riser characteristics are detailed in Table 2.3.

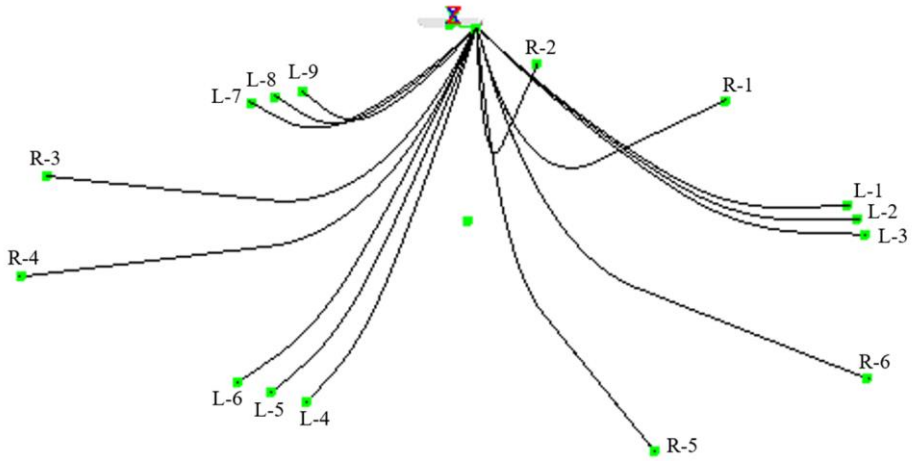

L= mooring line
R= riser

Figure 2.3 Total system of the FPSO model and the mooring lines and risers

Table 2.2 Prototype mooring line characteristics

Description	Prototype
Number of mooring lines	9
Pretension (kN)	2025
Total length of mooring line (m)	2185
Segment 1: Fairlead chain	R4S Studless
Length (m)	50
Diameter (mm)	90
Mass in water (tonnes/m)	0.146
EA (kN)	691740
Breaking strength (kN)	8167
Segment 2: Mid-section	Spiral Strand
Length (m)	1200
Diameter (mm)	90
Mass in water (tonnes/m)	0.0336
EA (kN)	766000
Breaking strength (kN)	7938
Segment 3: Chain ground section	R4S Studless
Length (m)	935
Diameter (mm)	90
Mass in water (tonnes/m)	0.146
EA (kN)	691740
Breaking strength (kN)	8167

Table 2.3 Prototype riser characteristics

Description	Prototype
Number of risers	6 symmetric
Pretension (kN)	1500
Total length of riser (m)	2650
Outside diameter (mm)	273
Inside diameter (mm)	235
Mass in water (tonnes/m)	0.096
EA (kN)	3039364
Specification	API-5L-X-65

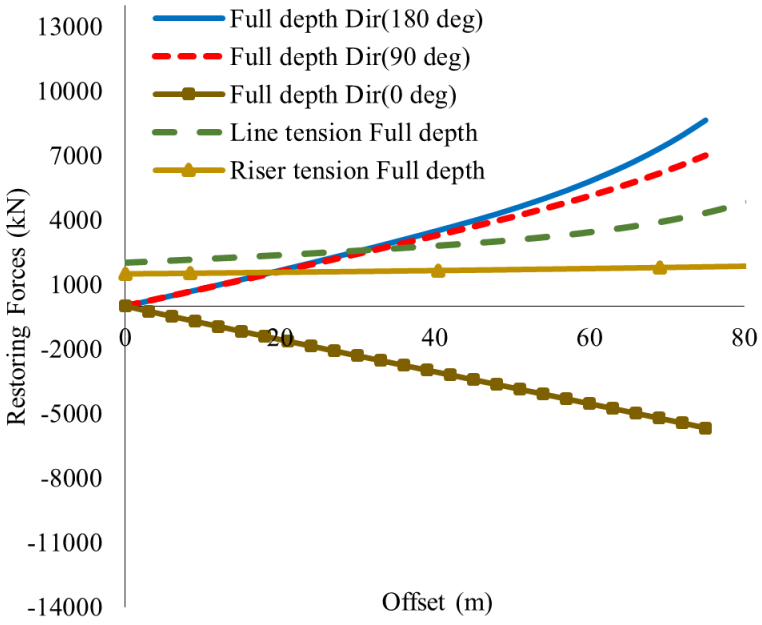

Figure 2.4 Restoring forces characteristics of the mooring line system

2.2 Experimental methodology

The experiments followed the strategy of employing the passive truncated methodology for representing full sized mooring lines and the risers. A suitable model scale for the total system was selected following Froude's law. The inertia to gravity force ratio (v^2/gD), which is described by Froude Number, was kept similar where v = fluid velocity, g = gravitational acceleration and D = element characteristic dimension (Chakrabarti, 2005).

On the other hand, the truncated methodology for the mooring lines and risers is based on the static catenary formulations for solving the static equilibrium of the total system of the FPSO model with fully connected mooring lines and risers, for a different range of horizontal offsets defined and the corresponding instantaneous total horizontal restoring force characteristics of the mooring lines and risers. Figure 2.5 and Figure 2.6 show the catenary shape for a single cable line and a diagram of the forces acting on the cable line. The computer program ORCAFLEX (2014) was used for quasi-static analysis through an iterative numerical simulation process with the following general formulations.

The local axis system of the line (cable) is defined in which the cable is fully presented in a simple two-dimensional plane (Figure 2.5). The relationship between this local axis system and that of the global system is subsequently defined in Figure 2.6.

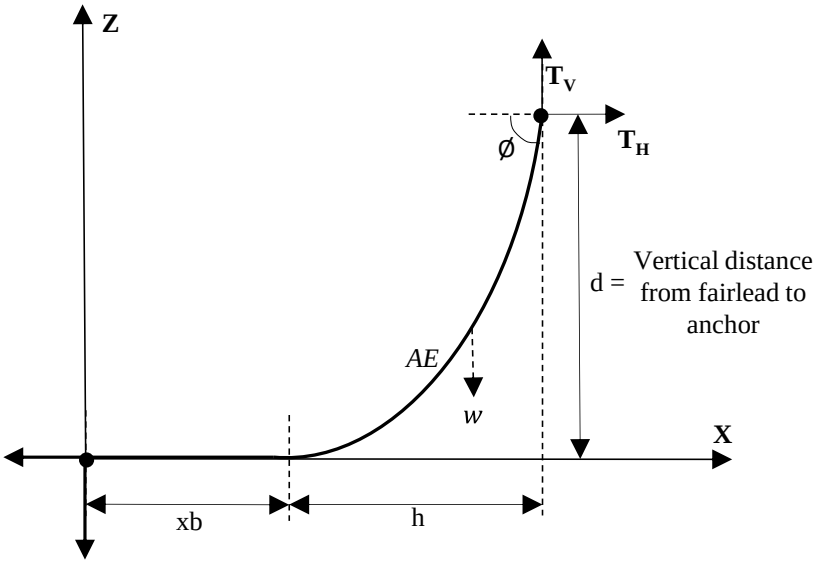

Figure 2.5 Single catenary cable line adapted from (Barltrop, 1998)

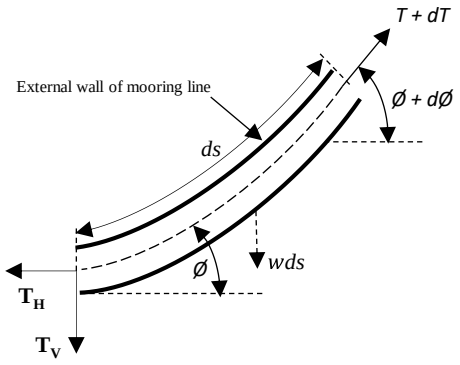

Figure 2.6 Diagram of static forces acting on the cable line (Barltrop, 1998)

2.2.1 Catenary Formulations

Figure 2.6 shows the static equilibrium equations for mooring lines and risers in 2D. The solution can be expressed by resolving the tangential and the normal forces.

$$\frac{d\emptyset}{ds} = \frac{w}{T} \cos \emptyset \tag{2.1}$$

$$\frac{dT}{ds} = w \sin \emptyset \tag{2.2}$$

Where T is the axial local tension in the mooring line, s is the length of the curved line, w is the submerged weight per unit length and $\emptyset$ is the fairlead angle between the line and the horizontal projection. The fairlead is at the attached point of the mooring lines to the turret.

$$T_H = T \cos \emptyset \tag{2.3}$$

$$T_V = T \sin \emptyset \tag{2.4}$$

$$T_V = T \sin \emptyset = \mu g s \tag{2.5}$$

$$w = \mu g \tag{2.6}$$

Resolving forces at the upper end of the line:

$$T^2 = T_V^2 + T_H^2 \tag{2.7}$$

$$\tan \emptyset = \frac{ws}{T_H} \tag{2.8}$$

$$c = \frac{T_H}{W} \tag{2.9}$$

$$h = c \cosh ((d+c)/c) \tag{2.10}$$

$$s = c \sin h (h/c) \tag{2.11}$$

$$L_{total} = s + xb \tag{2.12}$$

$$B = h + xb \tag{2.13}$$

Where T_H is the local horizontal tension, T_V is the local vertical tension, w is the submerged weight per unit length (the actual dry weight less the buoyancy due to the volume) of the chain or wire, μ is the sumerged mass per unit length, g is the gravity, c is the local slope of the catenary, L_{total} is the total length of the mooring line, h is the horizontal scope, B is the spread

length on the seabed and *d* is the vertical distance from the fairlead to the seabed (Chakrabarti, 1987; Barltrop, 1998; Faltinsen, 1998).

The following relationship can be established according to the static equilibrium:

$$dx = ds\cos\emptyset \tag{2.14}$$

$$dz = ds\sin\emptyset \tag{2.15}$$

The following equation can then be obtained:

$$\frac{d^2z}{dx^2} = \frac{d\emptyset}{dx}\sec^2\emptyset \tag{2.16}$$

Using equation (2.1) the classic catenary can be derived:

$$\frac{d^2z}{dx^2} = \frac{w}{T_H}\sqrt{1+\left(\frac{dz}{dx}\right)^2} \tag{2.17}$$

The non-linear differential equation can be solved:

$$z = \frac{T_H}{w}\left(\cosh\left(\frac{wx}{T_H}\right)-1\right) \tag{2.18}$$

The elasticity can be included through axial stretch from the element extending (*dx)*, where *AE* is the axial stiffness per unit length. Then the equations 2.14 and 2.15 are modified:

$$dx = ds\left[1+\frac{T}{AE}\right]cos\,\emptyset \tag{2.19}$$

$$dz = ds\left[1+\frac{T}{AE}\right]\sin\emptyset \tag{2.20}$$

The solution for a catenary line including the elasticity effects can be obtained as:

$$T_H = AE\sqrt{\left[\frac{T}{AE}+1\right]^2-\frac{2wh}{AE}}-AE \tag{2.21}$$

$$T_V = wL \tag{2.22}$$

$$h = \frac{T_H}{w}\sinh^{-1}\left[\frac{wL}{T_H}\right]+\frac{T_HL}{AE} \tag{2.23}$$

$$L_{total} = \frac{1}{w}\sqrt{T^2-T_H^2} \tag{2.24}$$

2.2.2 Truncation process for the mooring lines and the risers

The truncated design of the mooring lines and risers followed the requirements for them having closely similar static characteristics in the full depth prototype. Therefore, an iterative process for adjusting the static response was carried out based on the following parameters: length of the mooring lines or length of the risers, their axial stiffness (AE) and their submerged weight per unit length (W_{sub}) and keeping the same design pretension.

The initial process established the basis of the concept of geometric scaling shapes according to Waals et al., (2004). The truncation factor (γ) was then calculated as being the ratio between the length of the truncated system and the length of the full depth prototype system.

$$\gamma = \frac{WD\ truncated}{WD\ full} \tag{2.25}$$

Thus:

$$L_{trunc} = \gamma * L_{full} \tag{2.26}$$

$$EA_{trunc} = \gamma * AE \tag{2.27}$$

$$W_{sub\_trunc} = \frac{W_{sub\ full}}{\gamma} \tag{2.28}$$

Where:

WD truncated = Truncated water depth

WD full = Full prototype water depth

L_{trunc} = Truncated length of the mooring line or riser

AE_{trunc} = Axial stiffness of the truncated mooring line or riser

W_{sub_trunc} = Submerge weight of the truncated mooring line or riser

W_{sub_full} = Submerge weight of the prototype full depth mooring line or riser

After establishing an initial condition to define the truncated system, an iterative empirical process was implemented. Figure 2.7 illustrates the process of the design for the truncated mooring lines and risers which was adopted.

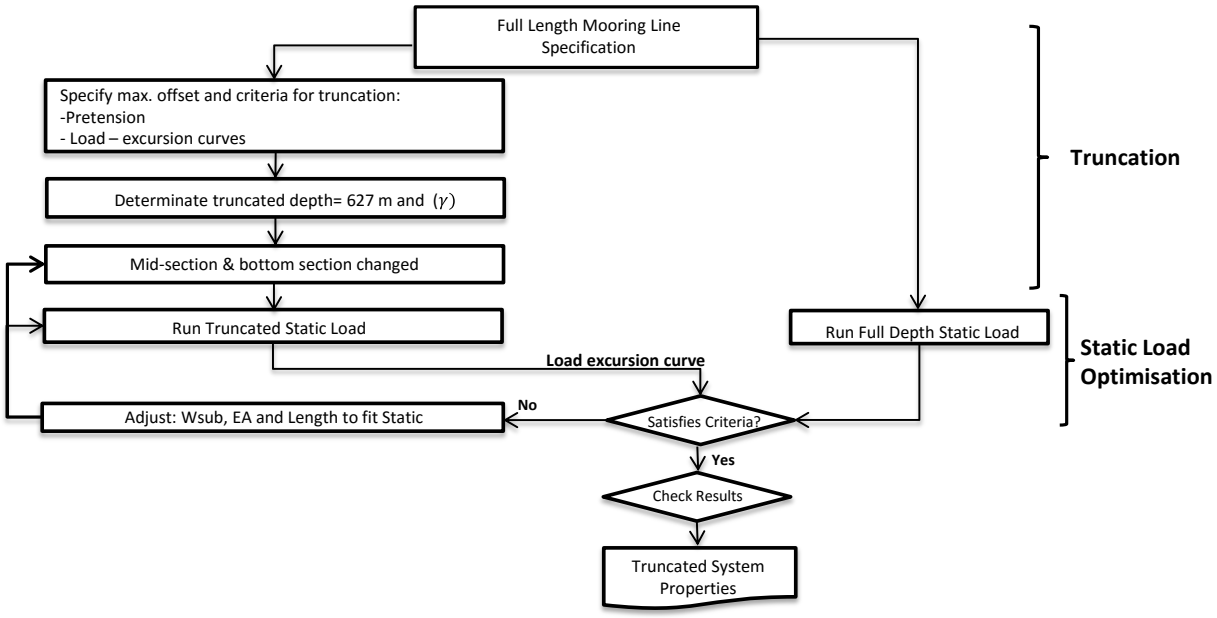

Figure 2.7 Iterative design processes for the truncated mooring lines and risers adapted from (Waals et al., 2004)

2.3 Test facilities and model description

The model tests were performed in the Deepwater Offshore Basin at Shanghai Jiao Tong University (SJTU) in China. The dimensions of the basin are 50 m by 40 m, with a maximum available water depth of 10 m. A large-area movable floor allows flexible modelling of water depths between 0 m and 10 m. A secondary movable floor in the deep pit, which has a diameter of 5 m, further enables the modelling of water depths of 10-40 m. various environments can be modelled, including collinear and non-collinear waves, currents and winds, which are simulated using two multi-flap wave generators, a deepwater global current generation system, and an axial wind fan matrix, respectively. The capabilities of the facility include the generation of significant wave heights of up to 0.3 m, surface current velocities of up to 0.4 m/s, and wind speeds of up to 10 m/s (Figure 2.8).

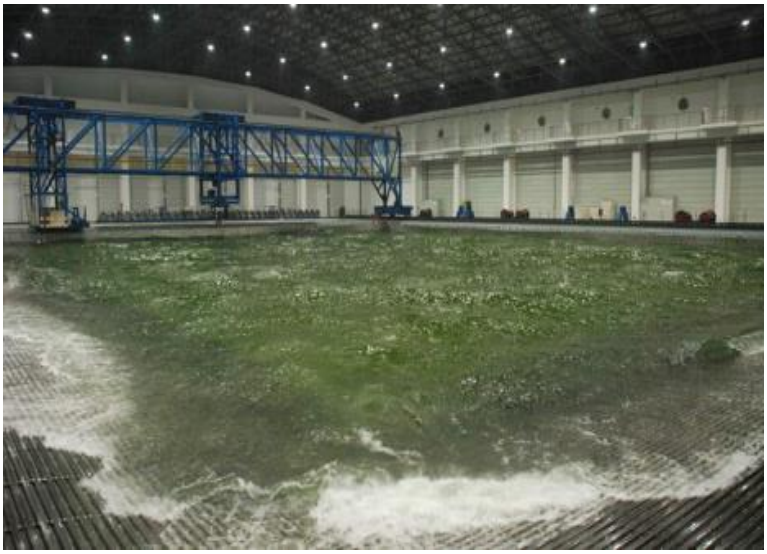

Figure. 2.8 View of the deep water offshore test basin at SJTU

2.4 Truncated mooring lines and risers

Considering the offshore basin dimensions and the instrumentation capacity that was available for environments and measurements, a model scale of 1:64 was chosen for the experiments in order to minimize any adverse scaling effects. The passive hybrid method was used to design the truncated mooring lines and risers with an equivalent effect to the FPSO to represent an installation in 1000 m water depth. The complete FPSO with truncated mooring and riser system was tested in the Deepwater Offshore Basin at Shanghai Jiao Tong University (SJTU).

The mooring lines and the risers were thus truncated to the equivalent of 627 m depth in the full-scale. The choice of the model scale and level of truncation were thus selected in order to minimize the potential uncertainties related to scaling effects on all of the system components and meet the depth limitation in the test facility.

The criteria for the design of the truncated mooring and riser systems seek to model as closely as possible the following parameters of the full prototype system:

- Total mass and its distribution in the FPSO vessel
- Total horizontal stiffness-offset response of the system
- Representative single line and riser tensions
- The number of components and the overall layout of the mooring lines and risers

A quasi-static analysis was performed in order to design a system of truncated mooring lines and risers that satisfies the horizontal restoring forces characteristics of the full depth prototype system for the three principal horizontal directions (180 degrees, 90 degrees, and 0 degrees) in the hull axis system. A procedure similar to that presented by Waals et al. (2004) and ITTC (2008) was used to evolve and evaluate the design of the truncated mooring line and riser systems**.**

The truncation methodology was based on the geometric scaling of the mooring line shapes. The maximum water depth in the basin as installed was 9.8 m, thus the equivalent full water depth prototype available in the basin was defined of 627.2 m according to model scale selected (1:64). The initial step was to establish the truncation factor ($\gamma = 0.627$) according to Equation 2.25. After that the appropriate truncation factor was established. The truncation factor was used to make a length reduction to the spiral strand mid-section (truncated mid-section length = 752 m) and also to the studless chain of the bottom section (truncated bottom section length = 586 m) for each of the prototype mooring lines. The studless chain arrangement of the top section was kept unchanged (top section length = 50 m).

After that the initial overall truncated mooring line length was established and a quasi-static analysis was carried out using the computer program ORCAFLEX (2014) in order to know the differences between the horizontal restoring forces and pretension of the initial truncated mooring line system when compared to the full depth prototype mooring line system. Subsequently an iterative process continued progressively reducing the length of the truncated mid-section and the length of the truncated bottom section of the mooring lines only and correspondingly modifying the submerged weight and the axial stiffness of each line element in order to reach a suitable degree of similarities in the main three horizontal water plane movement directions (surge 180 degrees, surge 0 degrees and sway 90 degrees) with the full depth prototype system, together with the corresponding pretension, the restoring forces of the total system and the critical line tensions at each of the mooring lines.

The truncation of the riser system also considered to establish an initial truncated riser length (1662 m) and subsequently an iterative process in parallel continued aimed at reducing the length of the truncated riser and modifying the submerged weight and axial stiffness up to a level to reach similar quasi-static behaviour that the full depth prototype riser system, the process is illustrated in Figure 2.7.

A comparison of the restoring forces of the mooring line and riser between full depth prototype systems and the truncation design is shown in Figure 2.9.

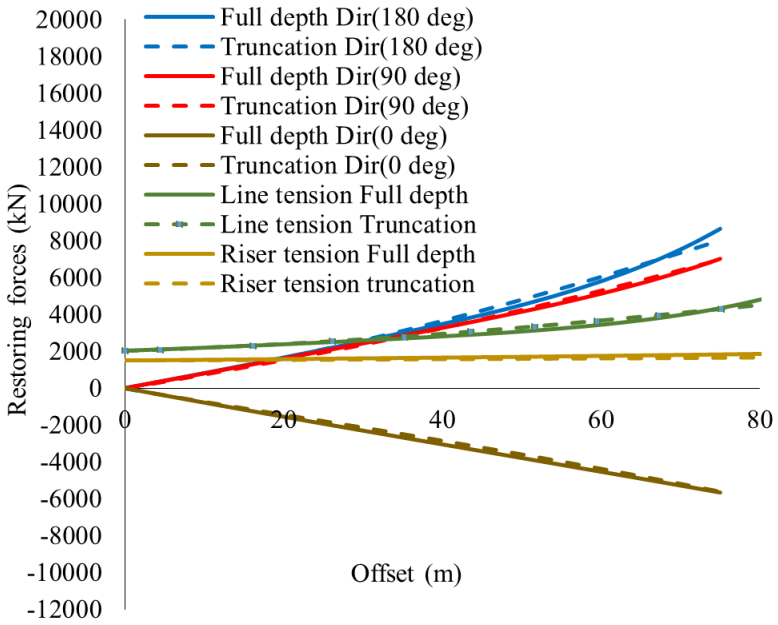

Figure 2.9 Mooring line and riser restoring forces of the truncated model and the full depth prototype model

Maximum differences of approximately 8% were observed in the general restoring forces between the truncated version and the prototype in the horizontal plane aftwards direction of 0 degrees, which were considered to be acceptable. In the other directions, 180 degrees and 90 degrees, smaller differences were observed. A similar discrepancy was observed for the most critical line tension and the most critical riser tension, demonstrating that a good agreement was achieved between the truncated model and the full depth model. The maximum horizontal spread length in the model scale was 15.48 m for the mooring lines and 13.79 m for the risers, which could fit within the length and width dimensions of the measuring area in the basin. The main characteristics of the prototype and the corresponding truncated mooring line and riser systems are shown in the Table 2.4 and Table 2.5, respectively.

Table 2.4 Mooring line characteristics

Description	Prototype	Truncate Specification
Number of mooring lines	9	9
Pretension (kN)	2025	2025
Total Length of mooring line (m)	2185	1160
Segment 1: Fairlead chain	R4S Studless	
Length (m)	50	50
Diameter (mm)	90	90
Mass in water (tonnes/m)	0.146	0.146
EA (kN)	691740	691740
Breaking strength (kN)	8167	-
Segment 2: Mid-section	Spiral Strand	
Length (m)	1200	580
Diameter (mm)	90	90
Mass in water (tonnes/m)	0.0336	0.116
EA (kN)	766000	68000
Breaking strength (kN)	7938	-
Segment 3: Chain ground section	R4S Studless	
Length (m)	935	530
Diameter (mm)	90	90
Mass in water (tonnes/m)	0.146	0.133
EA (kN)	691740	60000
Breaking strength (kN)	8167	-

The truncated mooring system was built for the actual in-basin tests using combined chain and spring segments to provide the appropriate submerged weight, axial stiffness (AE), pre-tension and restoring force contributions for each of the mooring lines (Figure 2.10).

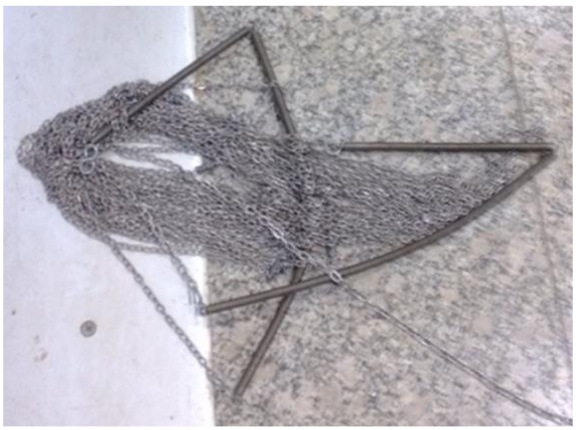

Figure 2.10 Mooring lines model, scale 1:64

Table 2.5 Riser characteristics

Description	Prototype	Truncate Specification
Number of risers	6 symmetric	6 symmetric
Pretension (kN)	1500	1500
Total length of riser (m)	2650	1400
Outside diameter (mm)	273	273
Inside diameter (mm)	235	235
Mass in water (tonnes/m)	0.096	0.234
EA (kN)	3039364	85000
Specification	API-5L-X-65	

For the model tests, the six risers were also built of wire and spring segments to satisfy the main requirements of the truncation design, such as the submerged weight, axial stiffness (AE), pretension, and restoring force characteristics. The bending moment capabilities of the riser section were not taken into account in the design (Figure 2.11).

Figure 2.11 Riser model, scale 1:64

2.5 Experimental set up

2.5.1 Model setup

A schematic plan view of the basin is given in Figure 2.12**.** The basin is fitted and equipped with environment simulation equipment, including two fixed multi-flap wave generation systems disposed along two adjacent edges, a deepwater global current generation system and a local moveable wind generation system and is thus capable of creating both collinear and non-collinear directional environment loading conditions relative to the mooring lines arrangement.

The six-degrees-of-freedom motion of the FPSO model were captured through a contactless optical motion tracking system, in which four passive tracking targets were installed on the stern of the FPSO model vessel. The conversion of the tracking target positions to rigid body motions at desired reference point is achieved through proprietary software licensed by Qualisys (2010). The signal captured can then be converted to give the motion values measured at the centre of the internal turret of the FPSO model. The tensions in the mooring lines and risers were measured using fifteen tension transducers installed individually at the fairlead connection points at the base of the turret of each lines and risers.

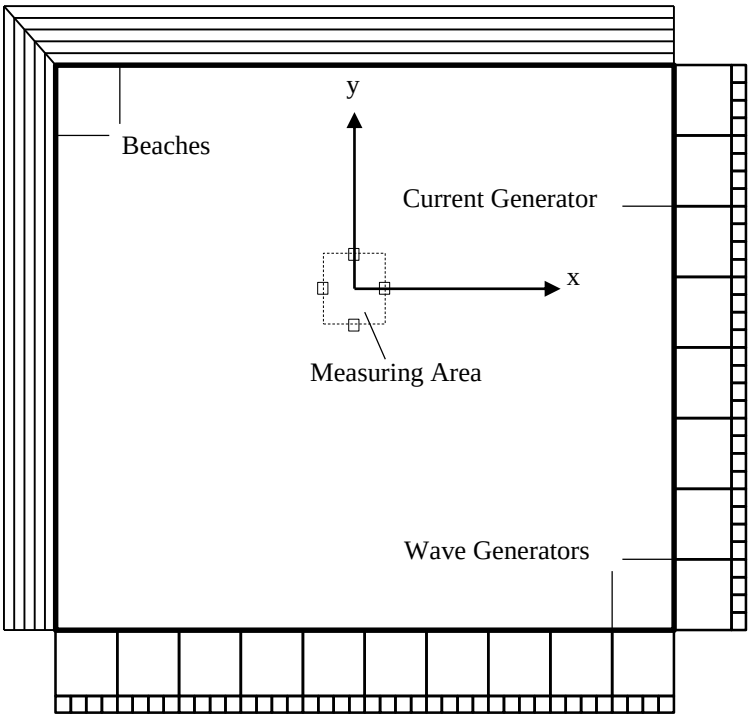

Figure 2.12 Plan view of the deep water offshore test basin SJTU

2.5.2 Environmental loading conditions

Both collinear and non-collinear environmental conditions are often observed in the specific locations in the GOM. In this study, the cases include both collinear and non-collinear environmental conditions with defined storm conditions of a 100 year return period. Figure 2.13 shows the three situations considered, namely collinear (2 cases) and non-collinear (1 case), the latter with a wind direction of 60 degrees and current direction of 90 degrees with respect to the wave direction. The irregular waves combined with current and wind governed the main part of the test programme, and the test duration for each run corresponded to three hours of continuous exposure in the prototype.

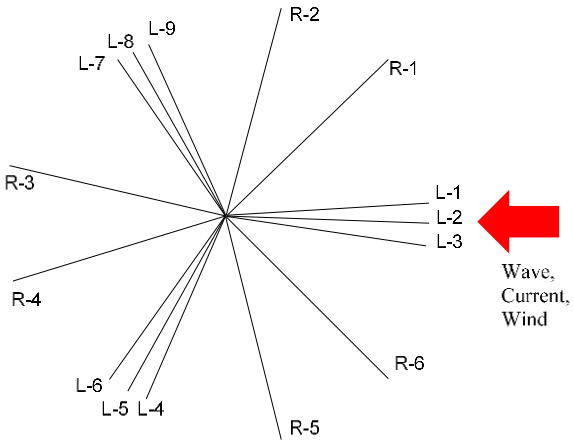

(a) Collinear 'In-line'

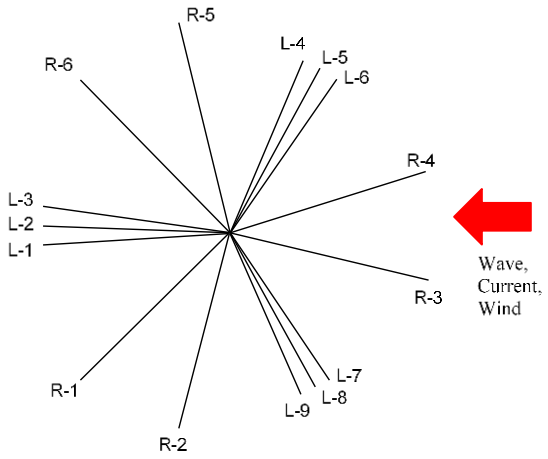

(b) Collinear 'Between-lines'

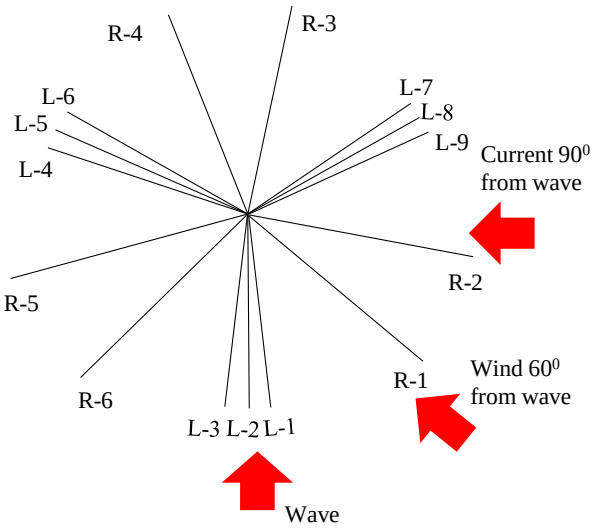

(c) Non-collinear

Note: L- Mooring lines
R-Risers

Figure 2.13 (a) Collinear 'In-line' and (b) 'Between-lines' and (c) Non-collinear (relative to the mooring lines) environment loading conditions

2.5.3 Testing matrix

The experimental test programme consists of the following main components:

- Calm water decay tests in the 6 DOF of the freely floating FPSO model for Full and Ballast Load conditions
- Calm water decay tests of the floating FPSO model with mooring lines only, and with mooring lines and risers for Full and Ballast Load conditions
- Horizontal stiffness (restoring forces) of the mooring lines and risers
- White noise wave tests (head, beam and bow quartering directions)
- FPSO motions in six DOF at the turret and tension force components at the turret fairleads for the 9 mooring lines and 6 risers under the following environmental loading conditions:
    - Collinear 'In-lines' loading condition of irregular waves only
    - Collinear 'In-line' and 'Between-lines' loading conditions of the combined irregular waves, current and wind for the Full Load conditions
    - A single typical non-collinear combination of environment loading condition of irregular waves, current and wind for Full Load and Ballast Load conditions

Three configurations were considered as the basis to study the hydrodynamic behaviour of the FPSO itself and the complete system of the FPSO together with mooring lines and risers. The particular arrangement for "Case A" only considers the FPSO model held in the basin with temporary horizontal restraining lines fitted above of the water. "Case B" is the FPSO model with mooring lines only, and the arrangement for "Case C" is the FPSO model fitted with full mooring lines and risers (see Figure 2.14). The comprehensive details of the experimental test matrix are given in Table 2.6.

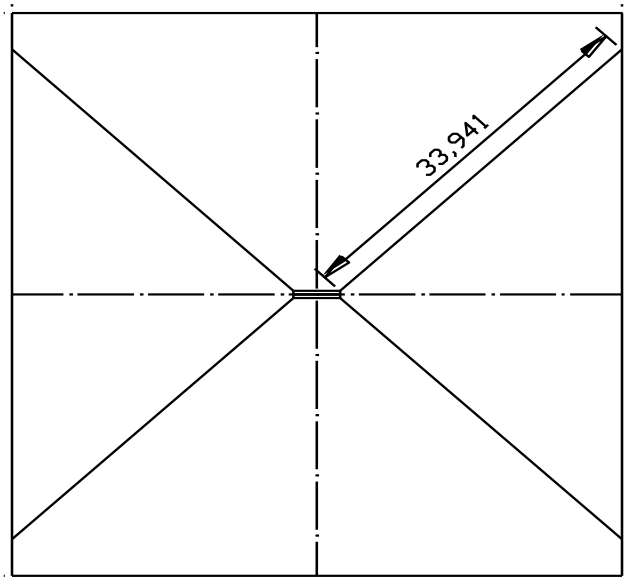

"Case A" (FPSO motions test light restrains)

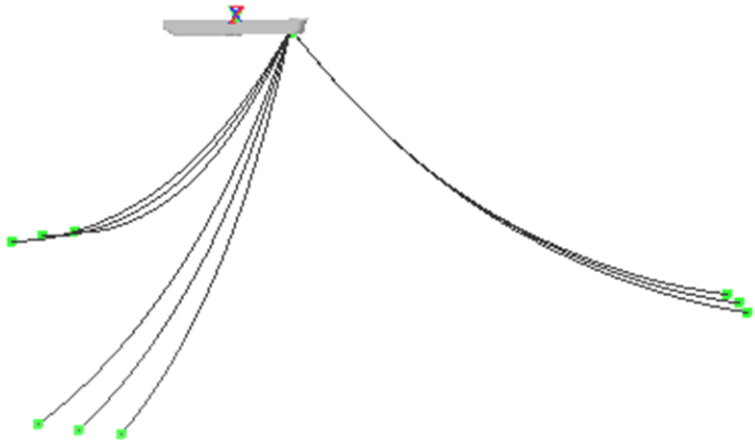

"Case B" Mooring Lines Arrangement

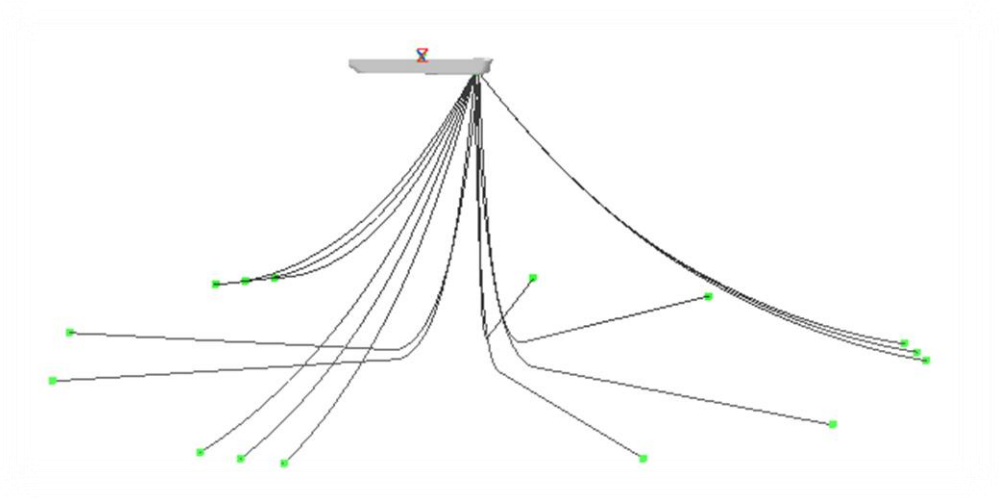

“Case C” Full Mooring Lines and Risers

Figure 2.14 Experimental test configurations, “Case A”, “Case B” and “Case C”

Table 2.6 Complete experimental test matrix

Full Load Condition				
Test No.	**Description of Test**	**Environ No.**	**Wave heading**	**Comment**
FA1-1, FA1-2, FA1-3, FA1-4, FA1-5, FA1-6	Case A: Decay test in still water	Calm	-	FA1-1= Surge, FA1-2 =Heave, FA1-3 =Roll, FA1-4 =Pitch, FA1-5 =Sway, FA1-6 =Yaw
FA2	Case A: White noise wave test	3	Head	
FA3	Case A: Current	1	Head	
FA6	Case A: Current	1	Bow Quartering	
FA7	Case A: White noise wave test	3	Bow Quartering	
FA4	Case A: Current	1	Beam	
FA5	Case A: White noise wave test	3	Beam	
FA8	Case A: Wind	1	Head	
FA10	Case A: Wind	1	Bow Quartering	
FA9	Case A: Wind	1	Beam	
FB11	Case B: Decay test in still water	Calm	Collinear 'In-line'	Mooring lines Only
FB12	Case B: Horizontal stiffness (180^0)	Calm		
FB13	Case B: Decay test in still water	Calm	Collinear 'Between lines'	
FB14	Case B: Horizontal stiffness (0^0)	Calm		
FB16	Case B: Irregular wave	1	Head	
FB17	Case B: Current	1	Head	
FB18	Case B: Wind	1	Head	
FB19	Case B: Irregular Wave-Current-Wind	1	Collinear 'In-line'	Mooring lines only
FB20	Case B: Irregular Wave-Current-Wind	1	Collinear 'Between lines'	Mooring lines only
FB21	Case B: Irregular Wave-Current-Wind	2	Non-Collinear	Mooring lines only, Current 90^0 to wave and Wind 60^0 to wave
FB24	Case B:Horizontal stiffness (900^0)	Calm		Mooring lines only
FC22	Case C: Horizontal stiffness (180^0)	Calm		Mooring lines and risers
FC23	Case C: Horizontal stiffness (0^0)	Calm		Mooring lines and risers
FC25	Case C: Horizontal stiffness(90^0)	Calm		Mooring lines and risers
FC31	Case C: Decay test in still water	Calm	Collinear 'In-line'	Mooring lines and risers
FC32	Case C: Decay test in still water	Calm	Collinear 'Between line'	
FC34	Case C: Irregular wave	1	Head	Mooring lines and risers
FC35	Case C: Current	1	Head	Mooring lines and risers
FC36	Case C: Wind	1	Head	Mooring lines and risers
FC37	Case C: Irregular Wave-Current-Wind	1	Collinear 'In-line'	Mooring lines and risers
FC38	Case C: Irregular Wave-Current-Wind	1	Collinear 'Between lines'	Mooring lines and risers
FC39	Case C: Irregular Wave-Current-Wind	2	Non-Collinear	Mooring lines and risers, current 90^0 to wave and Wind 60^0 to wave
Ballast Load Condition				
BA-40-1, BA-40-2, BA-40-3, BA-40-4, BA-40-5 and BA-40-6	Case A: Decay test in still water	Calm	-	BA-40-1=Surge, BA-40-2= Heave, BA-40-3=Roll BA-40-4=Pitch, BA-40-5=Sway, BA-40-6=Yaw
BA-41	Case A: White noise wave test	3	Head	
BA-42	Case A: White noise wave test	3	Bow Quartering	
BA-43	Case A: White noise wave test	3	Beam	
BA-44	Case A: Wind	1	Head	
BA-45	Case A: Wind	1	Bow Quartering	
BA-46	Case A: Wind	1	Beam	
BB-47	Case B: Decay test in still water	Calm	Collinear 'In-line'	Mooring lines Only
BB-48	Case B: Irregular Wave-Current-Wind	2	Non-Collinear	Mooring lines only, Current 90^0 to wave and Wind 60^0 to wave
BC-49	Case C: Decay test in still water	Calm	Collinear 'In-line'	Mooring lines and risers
BC-50	Case C: Irregular Wave-Current-Wind	2	Non-collinear	Mooring lines and risers, Current 90^0 to wave and Wind 60^0 to wave
BC-51	Case C: Current	1	Collinear 'In-line'	Mooring lines and risers
BC-52	Case C: Irregular wave-current-wind		Non-collinear	Mooring lines only, Current 90^0 to wave and Wind 30^0 to wave

2.5.4 Static characteristics of the mooring line and riser systems

The static characteristics of the mooring and riser lines of the FPSO were obtained from the experiment and from the numerical calculations for the design of the truncated mooring and riser systems and their behaviour were verified. The longitudinal directions (180 degrees and 0 degrees) (corresponding to 'In-line', and 'Between-lines' conditions) and in the transverse direction (90 degrees) where the displacements corresponding to surge and sway were compared. Figures 2.15 and 2.16 show a very good agreement in the alternative fore and aft longitudinal directions (180 degrees and 0 degrees) with mooring lines with and without the risers for examination of the maximum offsets. The tensions for the most highly loaded mooring line and the riser were also examined, and the tension levels obtained in the experiment and in the numerical design for the surge direction (180 degrees) showed good agreement.

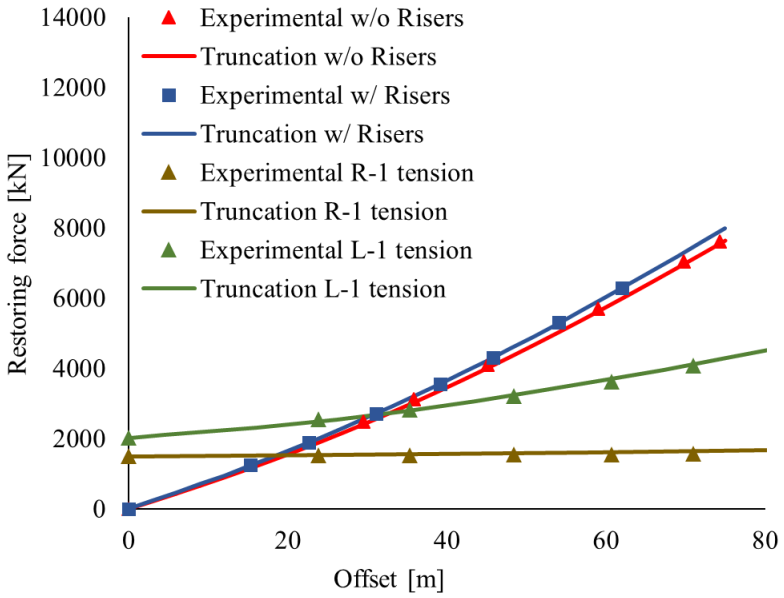

Figure 2.15 Restoring forces and offset characteristics in the forwards direction (180^0)

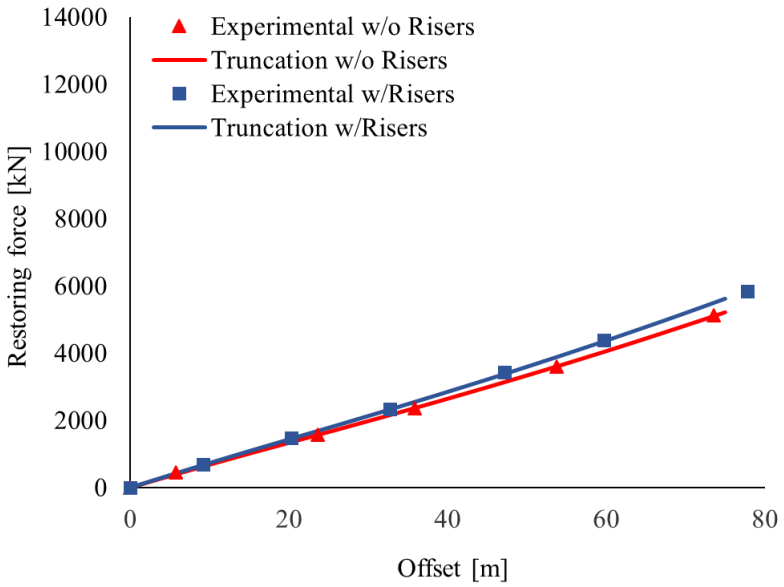

Figure 2.16 Restoring forces and offset characteristics in the aft wards direction (0^0)

Figure 2.17 provides a comparison of the restoring forces in sway, the transverse direction (90 degrees) between the theoretical numerical results obtained for the truncated mooring and riser system and those measured in the experiment. It is seen that numerical results of the truncated lines agree well with the experimental measurements up to about 60 m offset and the difference slightly increases afterward. As expected there will be a mean dynamic response in the range of 30 to 50 m in average in this direction. Thus, the similarities of the restoring force characteristics were considered to be reasonable in the sway direction. It should be noted that the contribution to the restoring forces due to the risers in this direction was found to be negligible.

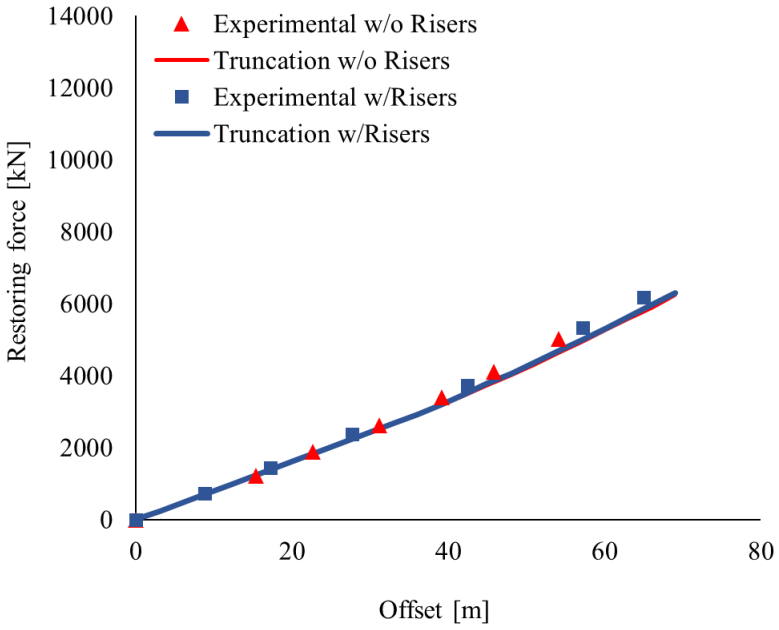

Figure 2.17 Restoring forces and offset characteristics in the transverse direction (90^0)

2.5.5 Metocean conditions

A storm condition for a 100-year return period was selected to study the hull motion responses and the associated dynamics of the mooring lines and risers. The environmental conditions are selected for the specific project location in the GOM. The JONSWAP spectrum is chosen with the characteristics of a significant wave height of 9.67 m and a wave period of 13.28 s. The sustained wind velocity at the standard 10 m reference height for one hour is 21.95 m/s. The current velocity on the surface is 1.44 m/s, varying linearly down to zero at a depth below the surface approximately of 300 m (see Table 2.7).

Table 2.7 Storm environmental conditions

Description	Unit	Storm environment condition
Waves		
Hs	m	9.67
Tp	s	13.28
Wave spectrum	Jonswap (γ=2.3)	
Wave direction	deg	180^0
Wind speed (1-hr)	m/s	21.95
Wind spectrum	API RP 2A-WSD	
Wind direction	deg	0^0 and 60^0 relative to waves
Current profile		
Surface	m/s	1.44
Current direction	deg	0^0 and 90^0 relative to waves

a. White noise wave calibration

A white noise wave environment was generated in order to represent the equivalent of the full-size and full range sea state environment with wave periods from 5 to 25 s and a significant wave height range of 0-3.25 m. This covers the range of incident wave frequencies for the operational Full Load and Ballast Load conditions of the FPSO model. Then, the white noise wave generation was calibrated with the specific parameters in the deepwater basin with the FPSO model installed ("Case A" in Figure 2.14). Figure 2.18 shows a very good agreement between the target spectrum of the waves and the actual measurements of the in-basin generated waves.

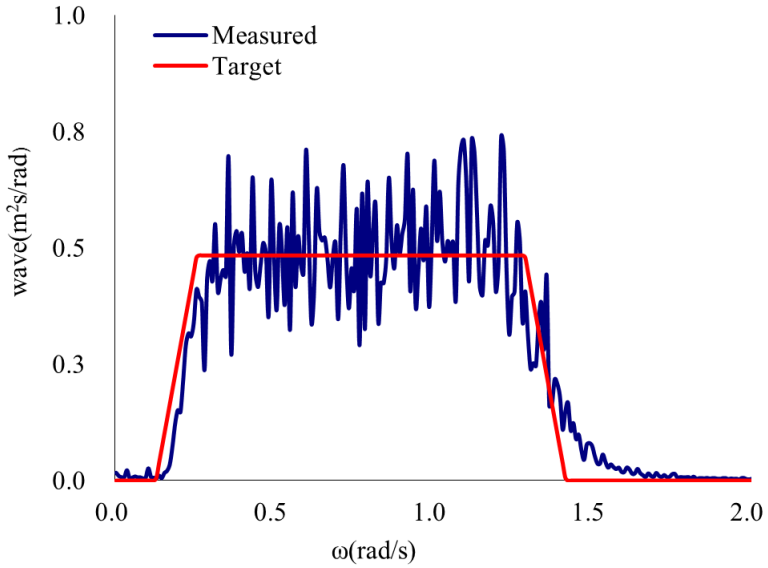

Figure 2.18 White noise wave calibration

The generated white noise wave spectrum with a near uniform energy distribution over the full range of the wave frequencies (5 to 25 s) was used in this experimental study in order to obtain the RAOs motions response, for all six-degree-of-freedoms in the head, beam and bow quartering seas conditions. The advantages of the white noise spectrum is that it allows to spectrally analyse the response signals and thus to develop response transfer functions over the given wave period range in one single run in the test basin. The method of data reduction is basically straightforward with the help of the cross-spectral technique (Bendat and Pierson, 1980; Tian et al., 2010). For these tests, the FPSO model was held in the required position and orientation in the basin with the simple elastic restraining horizontal lines held above the water surface and set-up in the required relative wave headings for the studies.

b. Irregular wave calibration

The irregular waves generated in the basin were calibrated in the directions of 180 and 90 degrees with the characteristics including the significant wave height, the mean period, gamma shape factor for the JONSWAP wave spectrum (Table 2.7). These characteristics were selected to represent the typical environment of a southern region of the Gulf of Mexico.

Figures 2.19 and 2.20 plotted the irregular wave spectrum for the actual measured and the target waves in the 180 and 90 degree directions respectively, showing that excellent agreements were achieved.

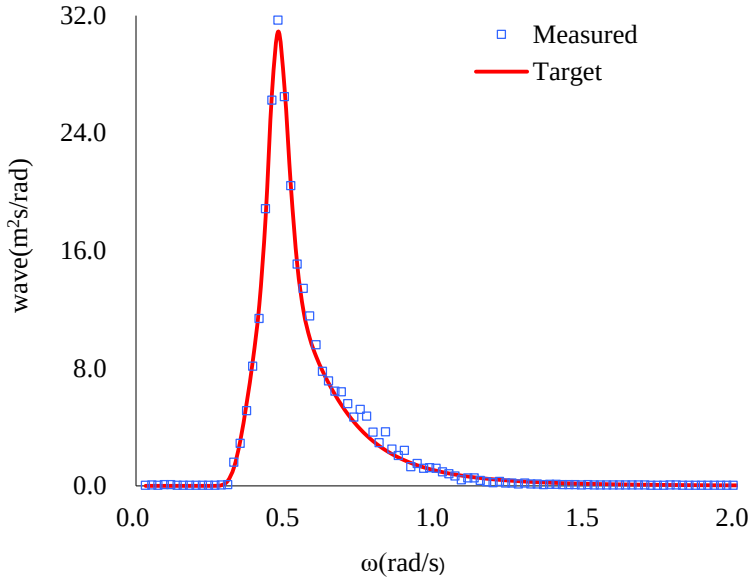

Figure 2.19 Irregular waves calibration, direction 180 degrees

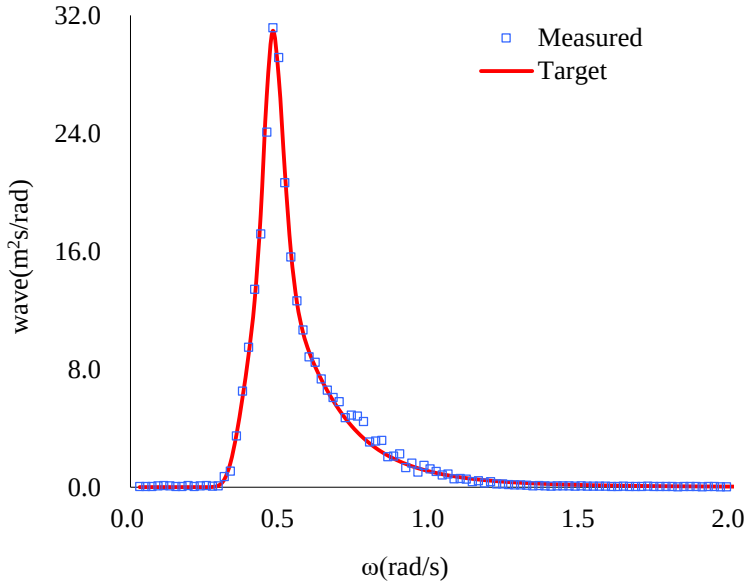

Figure 2.20 Irregular waves calibration, direction 90 degrees

The calibrated irregular waves in two different directions were used in conjunction with the current and wind generated to create the collinear and non-collinear environment loading conditions in the two directions during the experiment.

2.6 Results and discussion

This section presents the results and various analyses of the experimental measurements, and it is organized into the following sub-sections: decay tests, motion RAOs from white noise wave tests, spectrum analysis and statistical analysis of the FPSO motion response and the dynamics of the mooring lines and risers.

2.6.1 Decay tests in calm water (Natural periods and damping)

Decay tests were carried out in calm water for the six DOF of the uncoupled motions of the FPSO model for both the Full Load and the Ballast Load conditions. Additionally, surge decay tests for the 'In-line' and 'Between-lines' conditions of the FPSO model with the truncated mooring lines and risers for the Full Load condition were carried out.

The natural periods for each of the six DOF of the basic freely floating FPSO model were obtained from decay tests. The tests were conducted by manually translating or rotating the model in the directions of each of the required FPSO model DOFs and then releasing the model and allowing it to return to its initial equilibrium position. For the natural periods of the surge and sway modes, the test arrangement "Case A" shown in Figure 2.14 with the FPSO model being fitted with temporary horizontal light restraining lines, and held above the water surface, was used in order to generate a very slight restoring force to the FPSO model for it to freely return to its equilibrium position. The surge and sway decay tests were initiated by gently tugging the model with a cable for it to have a small horizontal displacement or translation and then releasing it to result in a free oscillation.

For the natural period in the heave mode, the FPSO model was simply manually pressed down symmetrically, maintaining level keel to a certain modest draught and then releasing it to perform free oscillation motions. In the case of the natural period in the pitch mode, the FPSO model was manually pressed down at the top surface of the bow of the model only up to a certain modest draught and then released to perform free oscillations. In the case of the roll mode the model similarly was heeled to one side symmetrically by applying a downward force and then released in order to perform free roll oscillations. All the natural periods of the six DOFs were determined by taking average cycle time over a number of cycles allowing for a small number of the initial oscillations to be omitted to avoid any irregularities in the releasing action.

i. FPSO model only (Full Load *vs* Ballast Load conditions)

Based on the decay tests of the FPSO model in calm water, the natural periods and damping ratios of the FPSO hull, the latter based on the logarithmic decrement method, were calculated (Chakrabarti, 1994; Journee et al., 2001). The first starting cycle of measurement for each decay test was discarded in order to allow a short period of time for the attenuation of any initial transient loads that may have been mechanically or accidentally induced during initiation, and the time series of the signals were then recorded for the decay tests.

The damping ratios are estimated in terms of the motion amplitude and one average value of damping ratio from the complete decay test can be approximated by the logarithmic decrement of amplitude and their differences logarithm values (Chakrabarti, 1994):

$$\delta = \ln|y_n| - \ln|y_{n-1}| \tag{2.29}$$

The logarithmic decrement is related to the damping ratio by the equation:

$$\zeta = \frac{C}{C_c} = \frac{\delta}{\sqrt{\pi^2+\delta^2}} \tag{2.30}$$

Where:

ζ = Damping ratio (ratio between damping and critical damping)

$\delta =$ Logarithmic decrement

C = Linear damping coefficient

$C_c =$ Critical damping coefficient

$y_n \; and \; y_{n-1} =$ Two succeeding amplitudes at a time interval of period of oscillations

The relationship between the logarithmic decrement and the peak amplitudes and the local damping ratios for two adjacent cycles can also be evaluated by the relation: (Journee et al., 2001):

$$\zeta = \frac{1}{2\pi} \ln\left\{\frac{y_n}{y_{n+1}}\right\} \quad vs \quad \bar{y} = \frac{y_n+y_{n+1}}{2} \tag{2.31}$$

Where:

ζ = Local damping ratio (ratio between damping and critical damping)

y_n and $y_{n+1} =$ Two succeeding amplitudes at a time interval of period of oscillations

Then the damping ratios can be shown from two successive positive peak amplitudes.

After the natural periods (T_n) are known, the added mass coefficients can be calculated as follows:

$$M_a = \frac{K(T_n)^2}{(2\pi)^2} - M_0 \ldots\ldots \quad (2.32)$$

$$C_a = \frac{M_a}{M_0} \quad (2.33)$$

K = restoring force or restoring moment
M_0 = mass displacement
M_a = added mass
C_a = added mass coefficient

Table 2.8 shows the results of the natural periods and one average value of the damping ratios of the FPSO from the decay tests. It can be seen that the natural periods of the FPSO model in the Full Load condition were higher than those in the Ballast Load condition indicating a strong influence of the model displacement and the draught of the submerged model and also of the hydrodynamic restoring force characteristics on the natural periods.

Table 2.8 Natural periods and damping ratio of six DOF for Full Load and Ballast Load conditions

DOF	**Full Load**			**Ballast Load**		
	T_n (s)	ζ	C_a	T_n (s)	ζ	C_a
Surge	223.58	0.015	-	168.56	0.013	-
Sway	277.39	0.030	-	184.21	0.040	-
Heave	11.55	0.130	1.06	11.15	0.120	2.11
Roll	13.21	0.020	0.17	11.23	0.030	0.14
Pitch	11.60	0.100	0.95	10.38	0.210	1.53
Yaw	166.90	0.030	-	119.66	0.013	-

The experimental measured damping ratios in the surge direction for both the Full Load and Ballast Load conditions show approximately linear trends. As can be seen in Figure 2.21, the variation for the surge damping ratios for the Full Load condition (from 0.011 to 0.017) is slightly higher than that for the Ballast Load condition (from 0.011 to 0.014). The increased viscous damping contribution is mainly due to the friction drag of the larger submerged surface area of the FPSO for the Full Load condition, whereas the dependency on the mean surge amplitude appears to be negligible, indicating that flow separation does not occur in this case under the Reynolds number at the model scale. Additionally, skin friction is dominant in the viscous damping for the surge motion.

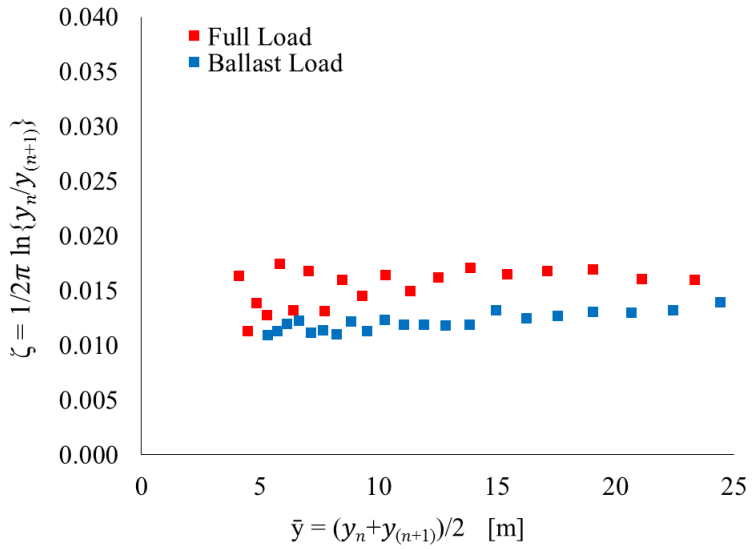

Figure 2.21 Surge damping ratios of the horizontal plane motions of the FPSO model

ii. FPSO model with mooring lines (Full Load condition)

Similarly, surge decay tests for the 'In-line' and the 'Between-lines' conditions of the FPSO model with the truncated mooring lines for the Full Load condition were carried out. The test arrangement shown in Figure 2.14 "Case B" was used for the decay test in calm water. The natural period for the 'In-line' case was found to be 353.57 s and 362.05 s for the 'Between-lines' case. The slightly higher natural period for the 'Between-lines' case was due to a reduced contribution of the horizontal restoring forces from the truncated mooring in this direction, as shown in Figures 2.15 to 2.17.

In contrast to Case A (Figure 2.14), the damping ratios obtained from the decay tests for Case B (Figure 2.14) were dependent on the amplitude of the oscillation, primarily due to the

flow separation from the interaction of the mooring lines with the calm water. Figure 2.22 shows that the estimated linear viscous damping ratios are approximately at the same level of magnitude for both collinear cases ('In-line' and 'Between-lines' cases).

iii. FPSO model with mooring lines and risers (Full Load condition)

The full arrangement of the FPSO model was also tested, together with the truncated mooring lines and risers. The two different directional arrangements ('In-line' and 'Between-lines') were also used to evaluate the additional effects of the riser system (see Figure 2.14 "Case C"). The natural period for the 'In-line' case was found to be 339.35 s, and for the 'Between lines' case, the natural period was found to be 344.18 s.

Figure 2.22 shows the trends of the viscous damping ratios of the FPSO model with the mooring lines only and the FPSO model with both mooring lines and risers, for both the 'In-line' and the 'Between-lines' cases in the surge direction, respectively. Significant contributions of the mooring lines and the risers to the total damping of the complete system are evident. Notably, the riser system makes a greater contribution to the overall damping for the 'In-line' case in the surge direction.

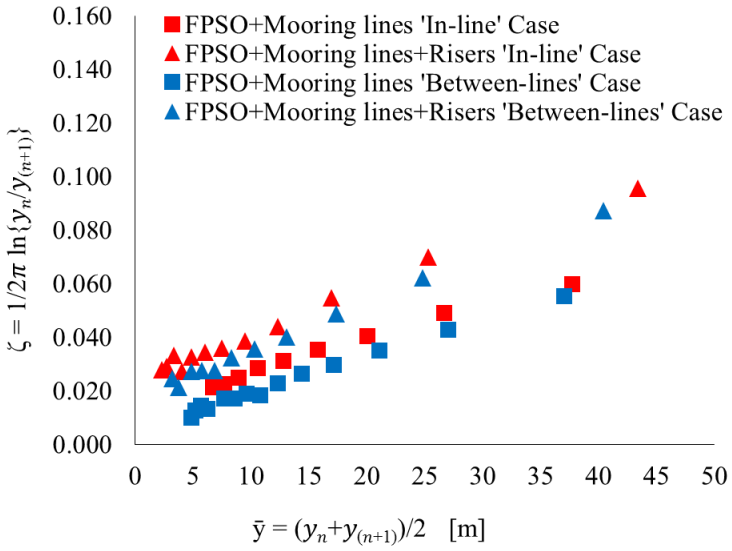

Figure 2.22 Damping ratios from surge decay test of the FPSO model, truncated mooring lines and risers for the 'In-line' and the 'Between-lines' cases for the Full Load condition

The effects of the mooring line and riser systems are expected to be even more significant in the full depth systems. The details of natural periods and the estimated damping ratios for the 'In-line' and 'Between-lines' cases are given in Table 2.9.

Table 2.9 Natural periods and total damping ratio obtained from the free decay tests of the FPSO model, mooring lines and risers for the 'In-line' and the 'Between-lines' cases in the surge direction, in the Full Load condition.

Parameters	**Only FPSO**	**FPSO+Mooring lines 'In-line' Case**	**FPSO+Mooring lines 'Between-Lines' Case A**	**FPSO+Mooring lines+Risers 'In-line' Case C**	**FPSO+Mooring lines+Risers 'Between-Lines' Case C**
Natural Period (s)	223.81 s	353.57 s	362.05 s	339.35 s	344.18 s
Damping ratio (ζ)	0.015	0.030	0.028	0.043	0.034

2.6.2 Motion response – linear transfer functions (RAOs)

The RAOs for each of the six DOF were calculated at the centre of gravity (C.G.) of the FPSO. The directions of the white noise waves for the studies were, relative to the ship, head seas (180^0), bow quartering seas (135^0) and beam seas (90^0) conditions. The RAOs were calculated according to the equation (DNV-RP-F205, 2010; Tian et al., 2010; Wichers, 2013):

$$RAO\ (\omega) = \sqrt{\frac{S_R(\omega)}{S(\omega)}} \quad \ldots\ldots\ldots \qquad (2.34)$$

$RAO\ (\omega)$ = Linear transfer function

$S_R(\omega)$ = Response spectrum

$S(\omega)$ = White noise wave spectrum

(ω) = Angular wave frequency

The motion RAOs from the model tests were obtained based on the measurements captured by the Qualisys and further analysed using a software developed in-house based on Visual Studio 2005 platform with the technique of mixed-language program. The program is an effective tool for data processing and analysis (Tian et al., 2010).

i. FPSO motion response in head seas

The surge, heave and pitch motion RAOs of the FPSO are the most important motion modes in head sea condition (Figure 2.23). Both the Full Load and Ballast Load conditions for surge RAOs show a weakly coupled effect with a slight increase around the heave natural frequency

(w = 0.54 rad/s) and with the maximum amplitude increasing at a lower frequency of 0.45 rad/s. Difference between the Full and Ballast Load conditions were found to be insignificant. However, the difference between the Full and Ballast Load conditions for the heave RAOs near the natural frequency is more pronounced, which shows that the heave RAO for Full Load condition was higher than that for the Ballast Load condition. Furthermore, the amplitude of the pitch RAO close to the natural frequency, was relatively small, which is attributed to the fact that the FPSO model's length is generally greater than the incident wave length.

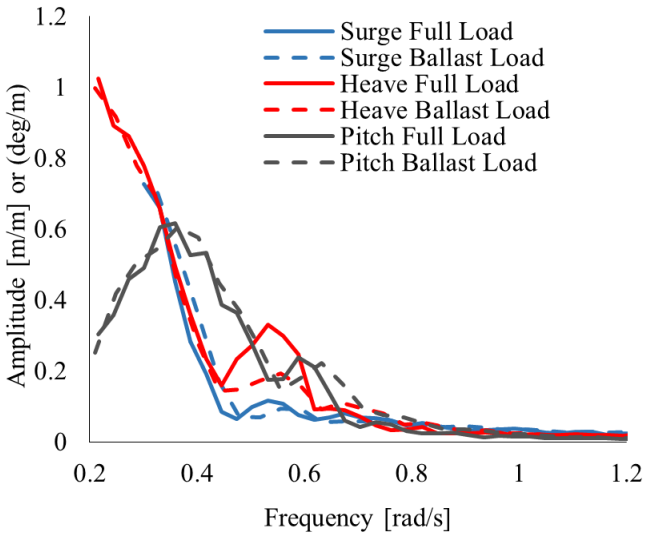

Figure 2.23 Surge, Heave and Pitch RAOs of the FPSO model for Head seas condition

ii. FPSO motion response in beam seas

For the beam seas condition, the roll, sway and yaw RAOs are the most important. Figure 2.24 shows insignificant differences in the sway and yaw RAOs between the Full and the Ballast Load conditions. However, the roll RAOs for the two load conditions show marked differences in both amplitudes and resonant frequencies. The roll RAO for the Full Load condition possesses a higher peak amplitude at a frequency equal to w = 0.47 rad/s than that for the Ballast load condition at w = 0.55 rad/s. In addition, the shape of the roll RAO for the Ballast Load condition is wider than that for the roll RAO for the Full Load condition.

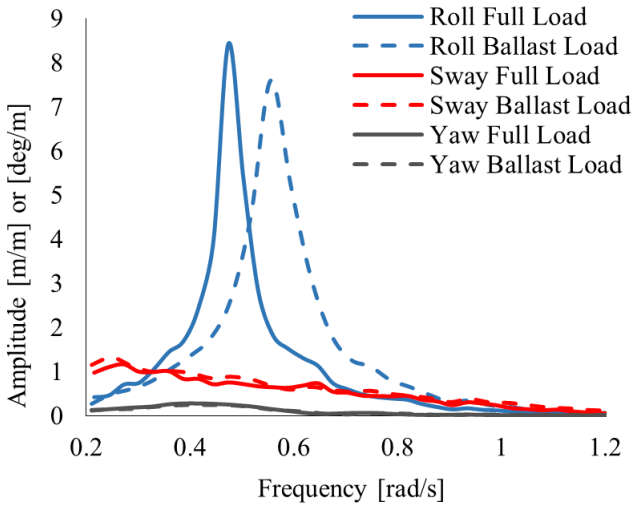

Figure 2.24 Roll, Sway and Yaw RAOs of the FPSO model for beam seas condition

iii. FPSO motion response in quartering seas

Furthermore, for the bow quartering seas, the six DOF, surge, sway, heave, roll, pitch and yaw motion RAOs are all important. All six DOF motions show coupled effects for both Full Load and Ballast Load conditions (Figure 2.25). Significant motion response is observed in the roll motion which is seen to be similar for the Full and Ballast Load conditions, whereas the resonance frequency is smaller for the Full Load (0.50 rad/s) compared to the Ballast Load condition (0.58 rad/s). Differences between the Full Load and Ballast Load conditions for the other motions were found to be insignificant.

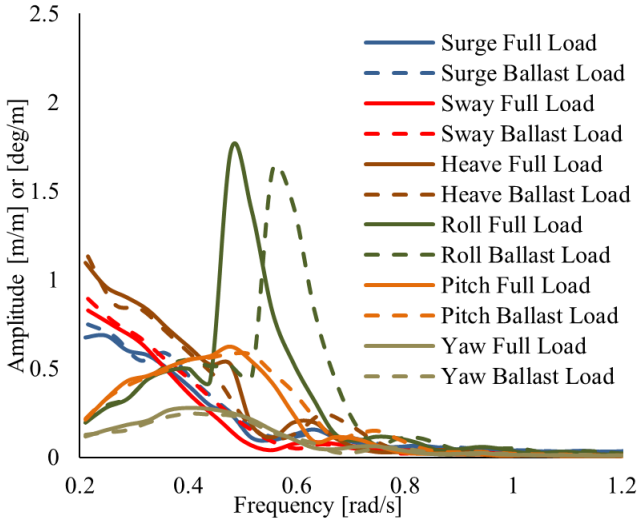

Figure 2.25 Surge, Sway, Heave, Roll, Pitch and Yaw RAOs of the FPSO model for the bow quartering seas condition

iv. Summary of RAOs

The RAOs, or linear transfer functions, of the individual 6 DOF motions for both Full and Ballast Load conditions were calculated, and the motion responses were captured well within the frequency range of the incident waves. The RAOs of the FPSO are sensitive to the direction of the incident wave, and the differences between the Full and Ballast load conditions were found to be insignificant, except for the roll motion, which showed clear differences in resonant frequencies and amplitudes.

2.6.3. Response spectra for the FPSO

The motion response spectra in the frequency domain of the six DOF motions were calculated from the time series data obtained from the experiments using Fast Fourier Transformation. A spectra smoothing coefficient equal to 4 for the low frequency range and 10 for the higher frequencies was applied in order to remove any possible noise in the initially recorded signals.

The motion response spectrum of the FPSO model was analysed, complete with the mooring lines and risers exposed to the collinear 'In-line' and Between-lines' and non-collinear environment conditions of the irregular waves, current and wind as previously defined for the Full Load and Ballast Load conditions.

i. FPSO in collinear and non-collinear environments for the Full Load condition

The motion response spectrum of the FPSO model, complete with the mooring lines and risers exposed to the collinear and non-collinear environmental load conditions of the irregular waves, current and wind were studied for the Full Load condition, as illustrated in Figure 2.13**.** The motion response spectra for surge, heave, roll and pitch were analysed. The surge motion response spectra of the FPSO model were analysed with mooring lines only, and with both mooring lines and risers.

-FPSO model with mooring lines only

The surge motion response spectra of the FPSO model in the Full Load condition for the 'Between-lines' and non-collinear cases show the same level of peak response at the resonance frequency, whereas the 'In-line' case shows a smaller peak amplitude. This, indicates that the

'In-line' case provides more damping from the mooring lines. Additionally the 'Between lines' case and non-collinear case have less restoring force contribution in the surge direction due to both show slightly lower resonance frequencies (Figure 2.26). The motion response spectra show that only energy at the low frequency range has a notable influence on the global response, whereas the wave frequency response contribution is negligible in the surge direction.

The wave frequency motions (roll, heave and pitch) were analysed for the collinear cases and the non-collinear cases (Figures 2.27 to 2.29). Roll motion for the non-collinear case was observed to have the highest peak response (Figure 2.27). The heave and pitch motion responses were also higher in the non-collinear case compared with the collinear cases (Figures 2.28 to 2.29). The coupled effect between heave and pitch motion responses was observed in both the collinear and non-collinear cases since the resonance frequencies for both pitch and heave motions responses are relatively close. In the case of the most loaded mooring line, Figure 2.30 shows that the highest peak response of the line tension spectrum is observed in the 'In-line' case (L-1) for the Full Load condition, which is associated with the higher mean load condition, compared to the other cases. The line tension response spectrum (L-1) shows that only the low frequency range energy response has a dominant influence on the global response, whereas the wave frequency response contribution is negligible.

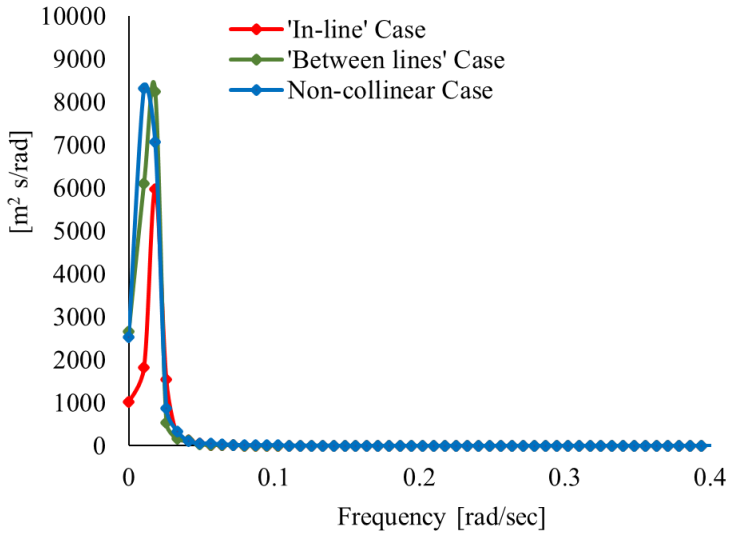

Figure 2.26 Surge motion response spectra for the Full Load condition

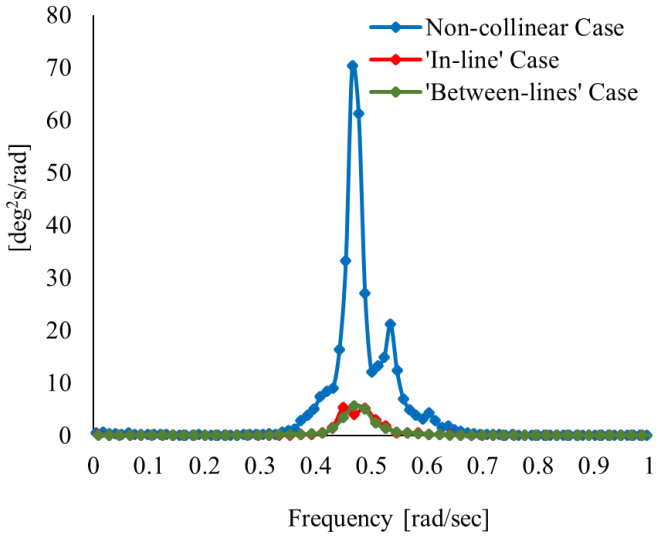

Figure 2.27 Roll motion response spectra for the Full Load condition

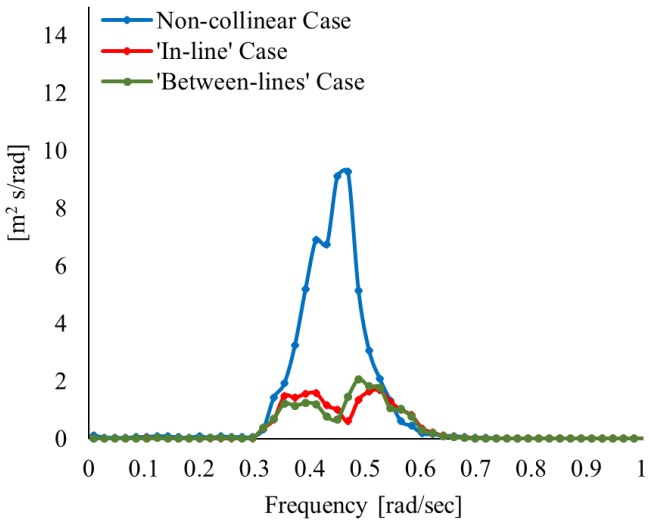

Figure 2.28 Heave motion response spectra for the Full Load condition

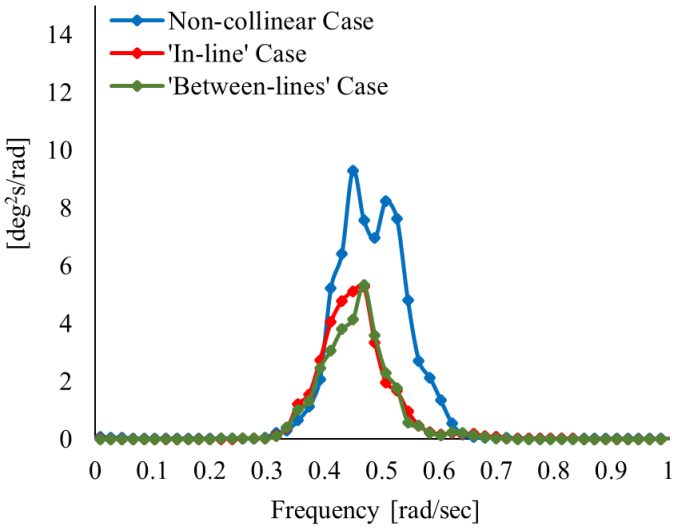

Figure 2.29 Pitch motion response spectra for the Full Load condition

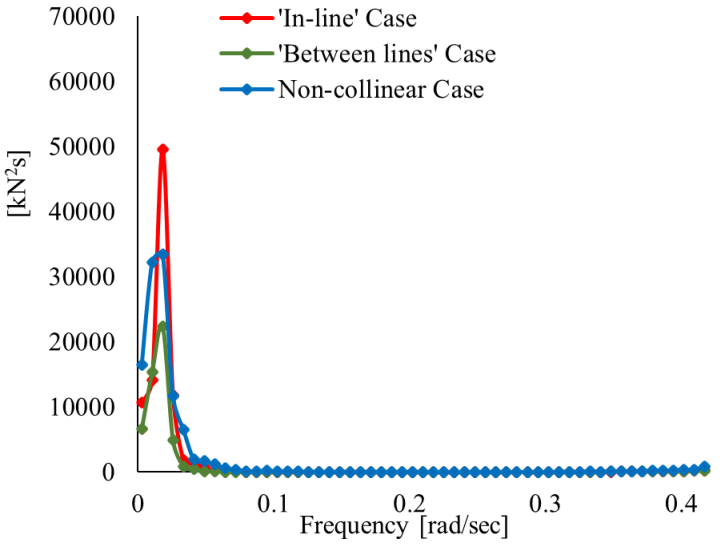

Figure 2.30 Line tension response spectra for the Full Load condition

-FPSO model with mooring lines and risers.

The motion response spectra of the FPSO model with mooring lines and risers for the Full Load condition were analysed for the environment loading case with the maximum motion responses identified previously (surge and roll motion in non-collinear cases). Figure 2.31 shows the surge motion response with a peak energy associated with a low frequency of 0.018 rad/s, which was observed for the system with mooring lines only and a frequency of 0.022 rad/s for the system with both mooring lines and risers, respectively. The peak energy at the

resonant frequency of the FPSO model with mooring lines and risers decreases by approximately 11% compared to the system with mooring lines only, due to the additional damping contribution from the risers.

In the range of the wave frequency, the roll motion spectrum was analysed to examine the influence of the risers on the roll motion response. Figure 2.32 shows that the peak response decreases by approximately 31% when the risers are included. However, the frequency associated with the peak response appears to be not affected by the risers, due to small contribution of restoring forces from the risers. Figure 2.33 shows the mooring line tension response for the maximum loaded line (L-1) observed in the 'In-line' case for the FPSO with mooring lines only, under the Full Load condition. The response spectrum for the maximum loaded riser (R-1) is presented in the non-collinear case (Figure 2.34) because the wave frequency motion response is slightly higher than the collinear cases.

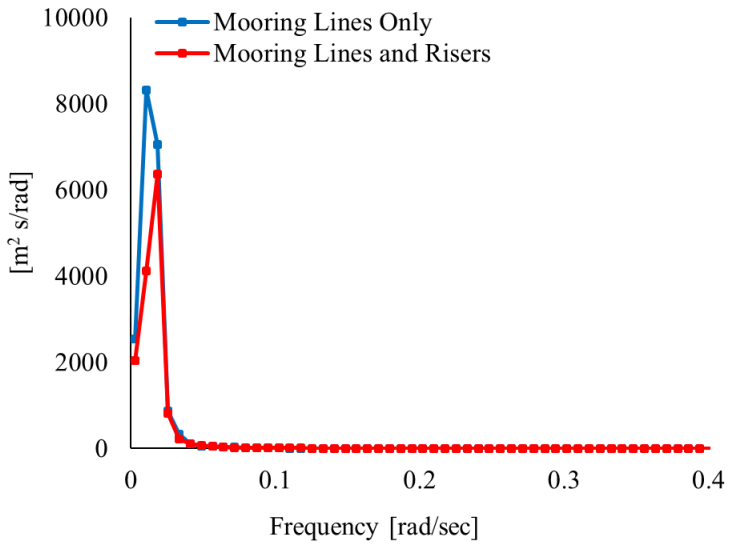

Figure 2.31 Surge motion response spectra, non-collinear Case for the Full Load condition

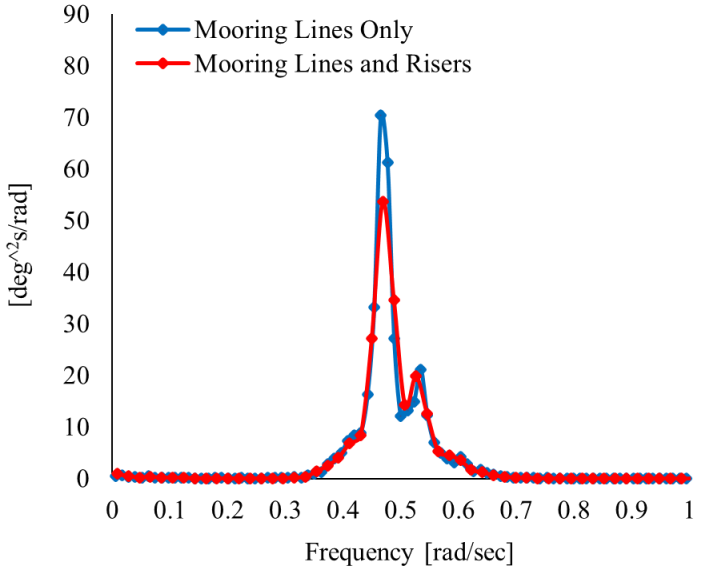

Figure 2.32 Roll motion spectra, Non-collinear case for the Full Load condition

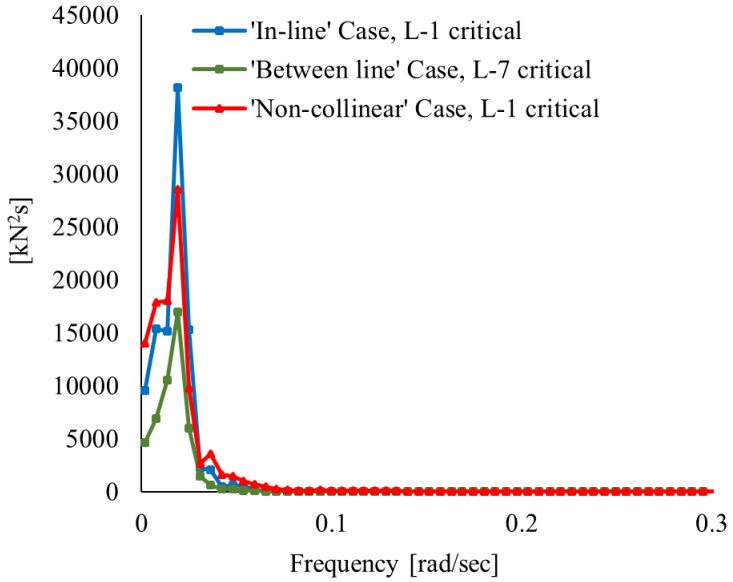

Figure 2.33 Line tension response spectra for the Full Load condition

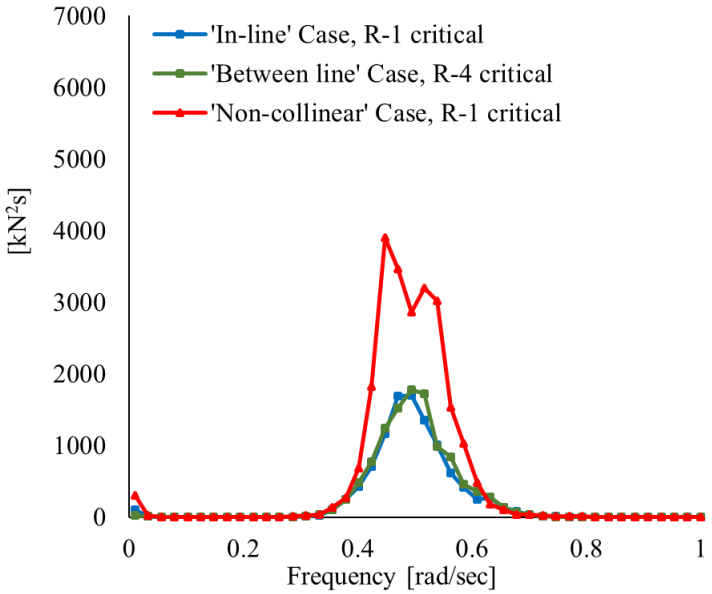

Figure 2.34 Riser tension response spectra for the Full Load condition

ii. Full *vs* Ballast Load conditions for the non-collinear environment loading case

As distinct from the other tests, the specific Ballast load condition was only included in the non-collinear set of measurements. This allowed a comparison between Full Load and Ballast Load conditions for the non-collinear case to be carried out for the maximum low frequency motion (surge motion) and of the tension in the most critical mooring line.

Figure 2.35 shows that the Full Load condition has a higher peak response compared with the Ballast Load condition. The influence of riser damping in the response is observed to be important. The highest peak of the line tension response spectrum is observed in the FPSO model with mooring lines only, for the non-collinear case in the Full Load condition (Figure 2.36). This is consistent with the observation on the motion responses of the FPSO due to the omission of the restoring force and damping contributions from the risers.

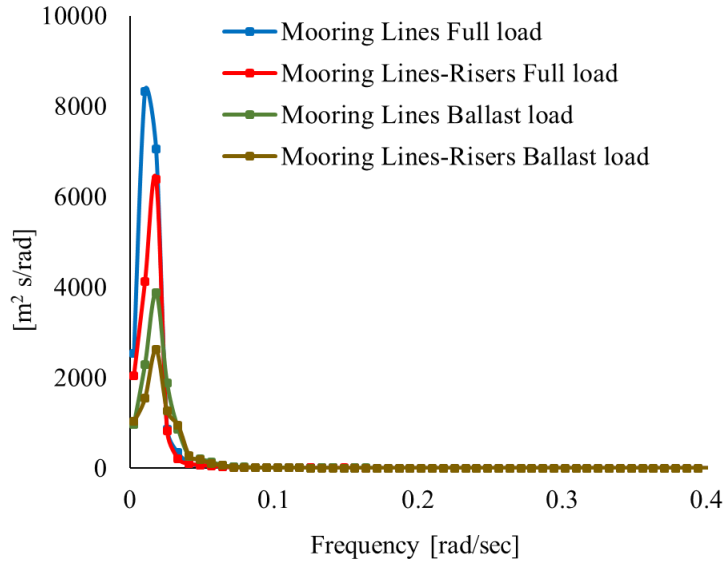

Figure 2.35 Surge motion response spectra for Full and Ballast Load condition

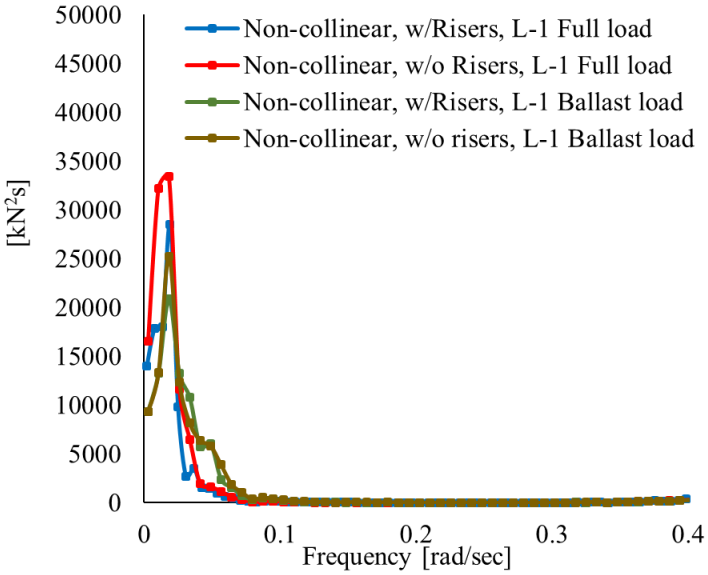

Figure 2.36 Line tension response spectra for the Full and Ballast Load condition

2.6.4 Statistical Analyses

The time series of motion responses in the six DOF of the FPSO model in the Full Load and Ballast Load conditions and of the most loaded mooring line and riser were further examined, the detailed experimental record information can to be seen in Appendix D. The collinear 'In-line', collinear 'Between-line' and Non-collinear environment conditions of the irregular waves, current and wind, as previously defined, were used in the analysis. The comparisons

were made in terms of their statistical properties such as the mean, minimum and maximum values and the associated standard deviations in full-scale.

i. Collinear *vs* non-collinear environmental loading cases for the Full Load condition

-FPSO model with mooring lines

The maximum motion responses were observed to be in the low frequency range in the surge direction for all environmental loading cases. The maximum motions occurred in the surge direction due to the mooring line/internal turret system, which allowed the FPSO to rotate freely about the moorings, similar to a weather vane and to point in the direction of least resistance against the various combined components in the environment loading conditions.

A maximum surge motion response of -86.62 m was observed in the non-collinear case for the arrangement of the FPSO model and mooring lines compared to the corresponding collinear 'In-line' condition (-56.93 m) and collinear 'Between lines' condition (-84.46 m) respectively, as shown in Table 2.10. Clearly, negative values of surge motion indicate that the vessel is moving in an aftward direction, the reciprocal to the conventional surge sense, as a result of the weather vane rotation about the turret.

This behaviour is mainly due to the non-collinear environmental loading condition, with the current at 90 degrees relative to the incident wave, which increases the energy of the incident irregular waves (Chakrabarti, 2005). Therefore, the mean and extreme surge motion responses increase in the FPSO model owing to the increase of the mean and slow-drift excitation wave (Faltinsen 1994; Stansberg, et al., 2013)). Based on the comparison was made between collinear and non-collinear environmental loading conditions, then, the mean motion response in the surge direction was observed to be higher in the non-collinear case (-43.24 m) compared with the collinear cases ('In-line' case = -28.86 m, and 'Between-lines' case = -35.67 m). The maximum values of the low frequency sway and yaw motions in the non-collinear case, in terms of absolute values, were obtained as 34.18 m and 54.53 degrees, respectively, compared to the 'In-line' condition (sway=14.88 m and yaw=17.58 degrees) and the 'Between-lines' condition (sway=18.11 m and yaw=15.03 degrees).

The coupling effects of the yaw motion in the wave frequency are observed with roll, heave and pitch. In the non-collinear case, the motions in terms of absolute values, (roll= 8.19 degree, heave = 3.99 m and pitch = 3.50 degrees) were found to be higher compared to the motions in

the collinear cases. It is worth noting that, in the non-collinear case, the incident wave length effectively increases due to the wave-current interaction, and the length ratio between the FPSO and wavelength was less than one in the present study, leading to the increased wave frequency motions.

Furthermore, the maximum tension in the most critical line (L-1) was found to be 3812.17 kN in the non-collinear case, mainly because of the higher contribution of the coupled surge-sway motion responses while the maximum mean tension was observed in the collinear 'In-line' case (L-1, 2665.07 kN), a clear indication that mooring lines in the non-collinear condition are more sensitive to the dynamic response of the FPSO vessel.

-FPSO model with mooring lines and risers

Table 2.11 shows the statistical results for the FPSO model complete with mooring lines and risers in the full operational configuration. The non-collinear case also showed slightly higher statistical values for low frequency surge motion (-76.75 m) compared to the results for the collinear 'Between-lines' case (surge = -75.53 m), whereas for the collinear 'In-line' case, the motion response (surge = -50.90 m) was observed to be smaller. The highest motion response in the non-collinear case was mainly attributed to the wave-current interaction load, which increases the mean drift force and slow-drift excitation forces on the FPSO model. For yaw motions, the non-collinear condition tends to induce the highest mean motion (-43.43 degrees) compared to the collinear conditions, as expected. In the case of the wave frequency induced motions of heave, pitch and roll, the non-collinear case also showed the highest values due to a dependency on the yaw motions.

The maximum tension in the most loaded mooring line (L-1) was 3598.29 kN, which was observed in the 'In-line' case, whereas the most critical tension in the risers for R1 was 2364.77 kN in the non-collinear case, mainly due to the increase in wave frequency motion.

The influence of the riser system on the maximum motion response and dynamic tension response of the mooring lines for the most critical case (Non-collinear) in Full Load condition was further examined, and the results are presented in Table 2.10 and Table 2.11. The motion response in surge direction was reduced by 13%, with a standard deviation of 15%. The differences in mean motion response were relatively small when the riser system was considered. The contribution of risers to the maximum response results mainly from the hydrodynamic damping, which reduces the dynamic motion response. The maximum dynamic

tension response of the most loaded mooring line (L-1) decreased by 6% and again the difference in mean tension response is negligible when the riser system was considered.

ii. Full Load condition *vs* Ballast Load condition under the non-collinear environment

-FPSO model with mooring lines

The statistical values for the Ballast Load condition of the FPSO model were studied for the non-collinear case only. Table 2.10 shows that the maximum motion response for the Ballast Load condition in the surge direction (-68.94 m) is smaller than that for the Full Load condition (-86.62 m) in the non-collinear case. The same trend is observed for the mean motion and standard deviation (Figures 2.37 to 2.39). However, the maximum sway motion response (39.57 m) for the Ballast Load condition tends to be marginally larger than that for the Full Load condition (34.18 m). This is mainly attributed to the fact that, for the Ballast Load condition, the mean, maximum and minimum values of the yaw responses, in terms of absolute values, are higher (41.73, 22.98 and 60.09 degrees, respectively) than those for the Full Load condition (39.30, 20.88 and 54.53 degrees). The increases in the yaw motions is due to the larger projected area of the FPSO model exposed to wind for the Ballast Load condition than that for the Full Load condition resulted from the differences in the draughts. The higher yaw responses also lead to slight increases of the wave frequency motion in roll, heave and pitch for the Ballast Load condition.

The maximum line tension was observed in L-1 (3999.20 kN) for the Ballast Load condition, which is slightly higher than that for Full Load condition (3812.17 kN) in the non-collinear environment. This can be attributed to the higher coupled surge and sway motion responses and the differences in the draughts of the FPSO model.

-FPSO model with mooring lines and risers

The maximum motion response for the Ballast Load condition was -63.64 m in surge, which is smaller than that (-76.75 m) for the Full Load condition, both in non-collinear environment, as shown in Table 2.11 and Figures 2.37 to 2.39. In contrast, the maximum absolute value of sway (39.61 m) for the Ballast Load condition is similar to that for the Full Load condition (39.15 m) in the same non-collinear environment.

For the wave frequency motions, the differences in heave, roll and pitch between the Ballast Load condition and Full Load condition are small. Furthermore, the maximum critical line

tension L-1 (3758.36 kN) for the Ballast Load condition is slightly higher than that for the Full Load condition (3585.89 kN), but the maximum tension in the most loaded riser (R-1) (2229.30 kN) for the Ballast Load condition is slightly lower than that for the Full Load condition (R-1) (2364.772 kN) in non-collinear environment.

Table 2.10 Statistical values of the motions in the Full Load and Ballast Load conditions for the Collinear and the Non-Collinear cases for the FPSO model with mooring lines

FPSO vessel and Mooring lines "CASE B" **Environment condition: Irregular Waves-Current-Wind**					
Description	**FPSO Full Load Condition**				**FPSO Ballast Load Condition**
	Statistical	**Collinear 'In-line' Case**	**Collinear 'Between-lines' Case**	**Non-Collinear Case**	**Non-Collinear Case**
Surge (m)	Max	-3.92	-3.02	-3.38	-10.83
	Min	-56.93	-84.46	-86.62	-68.94
	Mean	-28.86	-35.67	-43.24	-37.09
	Stdv	9.16	12.31	12.64	9.05
Sway (m)	Max	14.88	15.83	34.18	39.57
	Min	-14.48	-18.11	-16.85	-28.92
	Mean	0.33	-1.53	5.66	1.06
	Stdv	6.14	6.49	10.15	10.84
Heave (m)	Max	2.07	2.24	2.50	3.47
	Min	-2.37	-2.60	-3.99	-4.01
	Mean	-0.11	-0.102	-0.44	-0.29
	Stdv	0.60	0.60	1.00	1.06
Roll (deg)	Max	2.90	2.66	6.49	7.56
	Min	-2.83	-2.83	-8.19	-8.20
	Mean	0.09	0.02	-0.34	-0.21
	Stdv	0.70	0.65	2.01	2.06
Pitch (deg)	Max	3.09	2.87	3.50	4.12
	Min	-2.90	-2.71	-3.18	-3.73
	Mean	0.02	0.02	0.05	0.05
	Stdv	0.804	0.78	1.14	1.23
Yaw (deg)	Max	6.10	5.97	20.88	22.98
	Min	-17.58	-15.03	54.53	60.09
	Mean	-5.14	-3.47	39.30	41.73
	Stdv	4.94	3.89	5.52	5.91
Critical tension line (kN)		L-1	L-7	L-1	L-1
	Max	3729.23	3612.74	3812.17	3999.20
	Min	1915.24	1873.03	1619.00	1766.53
	Mean	2665.07	2451.97	2446.61	2467.93
	Stdv	276.84	220.48	311.49	282.00

Table 2.11 Statistical values of the motions in the Full Load and Ballast Load conditions for the Collinear and the Non-Collinear cases for the FPSO model complete with mooring lines and risers

FPSO, Mooring lines and Risers "CASE C" **Environment condition: Irregular Waves-Current-Wind**					
Description	**FPSO Full Load Condition**				**FPSO Ballast Load Condition**
	Statistical	**Collinear 'In-line' Case**	**Collinear 'Between-lines' Case**	**Non-Collinear Case**	**Non-Collinear Case**
Surge (m)	Max	1.02	-5.76	-10.43	-14.20
	Min	-50.90	-75.53	-76.75	-63.64
	Mean	-22.56	-33.28	-42.09	-33.32
	Stdv	8.49	11.40	10.97	8.12
Sway (m)	Max	25.03	5.25	22.07	39.61
	Min	-14.64	-29.10	-39.15	-19.90
	Mean	0.68	-12.29	-11.89	9.51
	Stdv	7.32	7.98	10.13	10.32
Heave (m)	Max	2.19	2.64	3.65	3.04
	Min	-2.53	-2.50	-4.27	-4.07
	Mean	-0.15	-0.10	-0.31	-0.51
	Stdv	0.59	0.60	1.09	0.84
Roll (deg)	Max	4.48	2.94	6.01	6.04
	Min	-3.93	-2.77	-7.20	-6.80
	Mean	0.06	0.03	-0.32	-0.29
	Stdv	0.71	0.70	1.95	1.66
Pitch (deg)	Max	3.11	3.13	4.11	4.17
	Min	-3.04	-2.90	-4.22	-3.84
	Mean	0.02	0.03	0.03	0.14
	Stdv	0.79	0.80	1.20	1.15
Yaw (deg)	Max	5.72	8.38	29.40	7.29
	Min	-26.45	-11.83	59.67	69.07
	Mean	-6.37	-0.748	43.43	49.68
	Stdv	4.40	4.11	5.36	5.55
Critical tension line (kN)		L-1	L-7	L-1	L-1
	Max	3598.29	3313.35	3585.89	3758.36
	Min	1802.29	1846.79	1692.26	1677.92
	Mean	2508.06	2413.59	2431.79	2485.05
	Stdv	253.64	194.85	281.88	278.24
Riser tension (kN)		R-1	R-4	R-1	R-1
	Max	2127.60	2147.79	2364.77	2229.30
	Min	943.00	978.26	806.74	905.77
	Mean	1499.15	1544.38	1542.06	1547.68
	Stdv	161.81	152.77	226.61	203.59

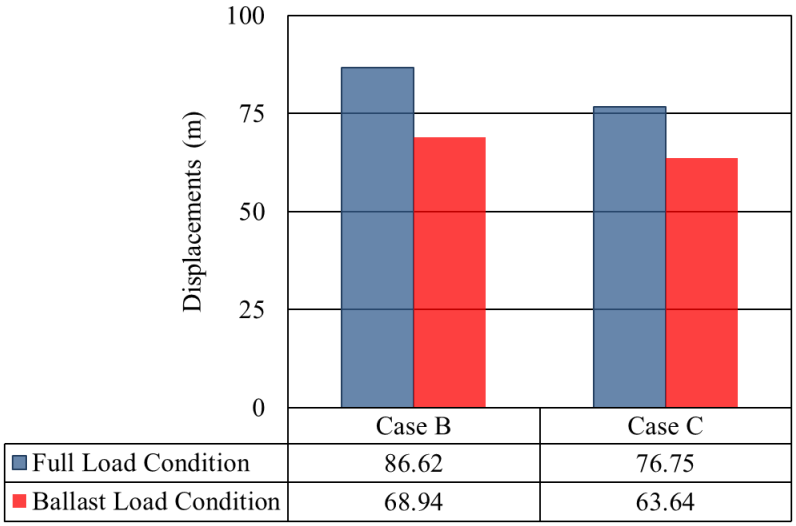

	Case B	Case C
Full Load Condition	86.62	76.75
Ballast Load Condition	68.94	63.64

Figure 2.37 Comparison of the extreme surge motion FPSO mooring lines (Case B) vs FPSO mooring lines and riser (Case C) for the Full Load and Ballast Load conditions (in terms of absolute values)

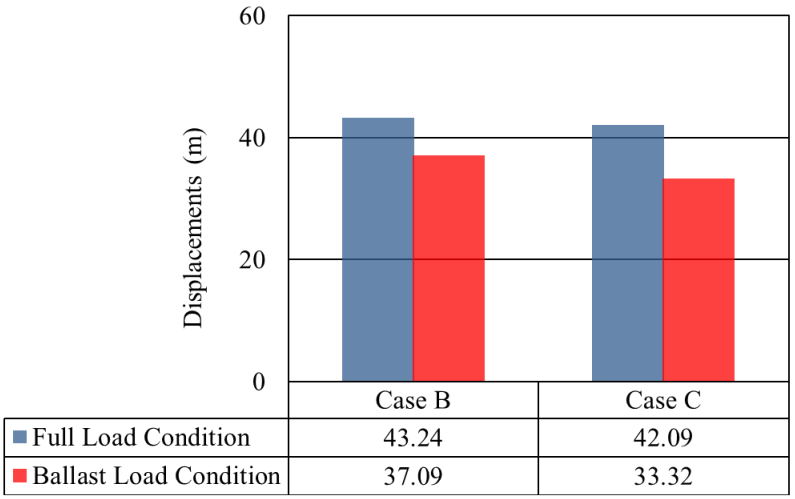

	Case B	Case C
Full Load Condition	43.24	42.09
Ballast Load Condition	37.09	33.32

Figure 2.38 Comparison of the mean surge motion FPSO mooring lines (Case B) vs FPSO mooring lines and riser (Case C) for the Full Load and Ballast Load conditions (in terms of absolute values)

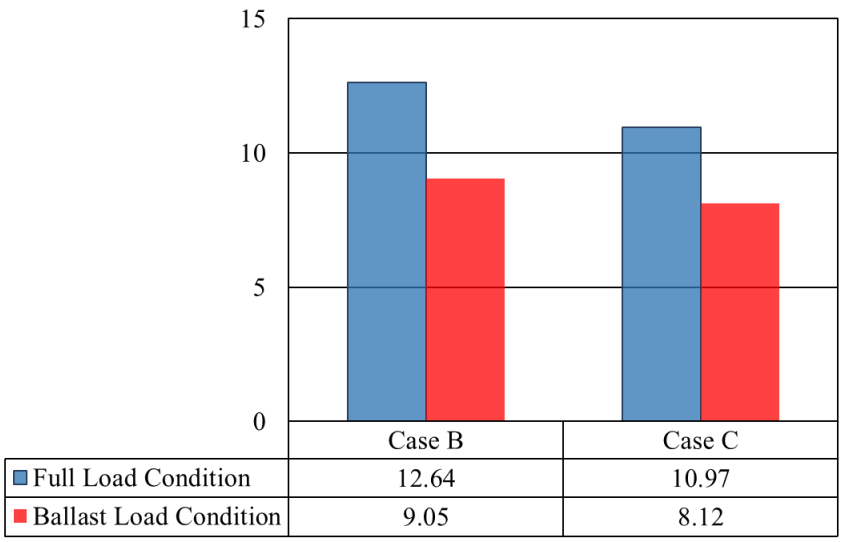

Figure 2.39 Comparison of the standard deviation of surge motion FPSO mooring lines (Case B) vs FPSO mooring lines and riser (Case C) for the Full Load and Ballast Load conditions

iii. Effects of current and wind

In order to examine the effects of current and wind on the dynamics of the coupled system, comparisons are made for the results obtained under the two collinear 'In-line' cases, i.e., one with irregular waves only and the other with irregular waves, current and wind, as shown in Figure 2.40. The statistical values for the surge motions of the FPSO model with mooring lines only were analysed. It is clear that the mean drift motion response increased two-fold for the environment with irregular waves, current and wind compared with the system under irregular waves only. Further, the mean drift motion of the FPSO model tends to govern the total motion response when the irregular waves are influenced by wind and current while the dynamic motion (slow drift motion) component decreased by an average of 18% compared to the FPSO model exposed to irregular waves only. This behaviour is mainly due to the collinear wave-current interactions which increase the drift mean forces and the wave-drift damping on the FPSO model. This is consistent with the observations of (Zhao and Faltinsen 1989; Faltinsen 1994; Monroy et al., 2012; Stansberg et al., 2013).

On the other hand, the motion response of the FPSO model due to the current load was slightly higher than the motion response due to the wind load, and a small standard deviation was observed for both motions from the current and wind loads respectively, which confirms that the FPSO system with mooring lines mainly responds to the mean motion behaviour. Oscillatory loads from the current and wind are insignificant.

Figure 2.41 shows the comparison of the line tension in the most loaded mooring line (L-1) for both collinear cases with irregular waves only and irregular waves, current and wind in combination. The mean tension response is approximately 15% higher for the system exposed to the combined effect of the irregular waves, current and wind compared to that of the system in irregular waves only. The dynamic tension response of the most loaded mooring line was observed to be similar in both collinear cases (irregular waves, current and wind, and irregular waves only). It is clear that the dynamics of the system when exposed to a collinear environment of irregular waves, current and wind, is dominated by the mean drift motion response of the FPSO and mean tension response of the mooring lines.

The statistical values for the surge motions of the FPSO with mooring lines only show that, for the non-collinear environment with the irregular waves, current and wind, the mean drift motion response increases by more than two-folds compared to the system exposed to irregular waves only (see Figure 2.42). The dynamic motion (slow-drift oscillation) is higher by 27% compared to the system under irregular waves only. The mean tension response of the most loaded mooring line (L-1) for the system exposed to irregular waves, current and wind was observed slightly higher (6%) compared to the system under irregular waves only (Figure 2.43). However, a sharp increase (approximately 21%) in the dynamic tension in the most loaded mooring line is observed for the system exposed to irregular waves, current and wind compared that for the system under irregular waves only. This is a clear indication that wave-current interaction in non-collinear environment has an important effect on both mean drift motion and the slow-drift oscillation motions of the FPSO and on the dynamic tension of the mooring lines. The reason is that wave-current interaction changes the fluid flow pattern around of the structure and subsequently impacts on the mean wave loads according to potential theory, and they are connected with the structure's ability to create waves and the wave length decreased compared with the collinear cases which increase the wave drift load on the FPSO (Faltinsen 1994).

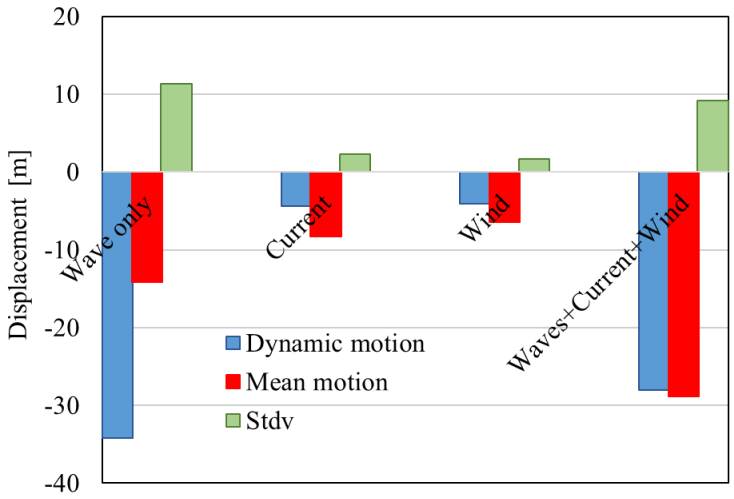

Figure 2.40 Statistical values of surge motion responses for the Collinear 'In-line' cases for the FPSO with mooring lines exposed to irregular waves only and irregular waves, current and wind

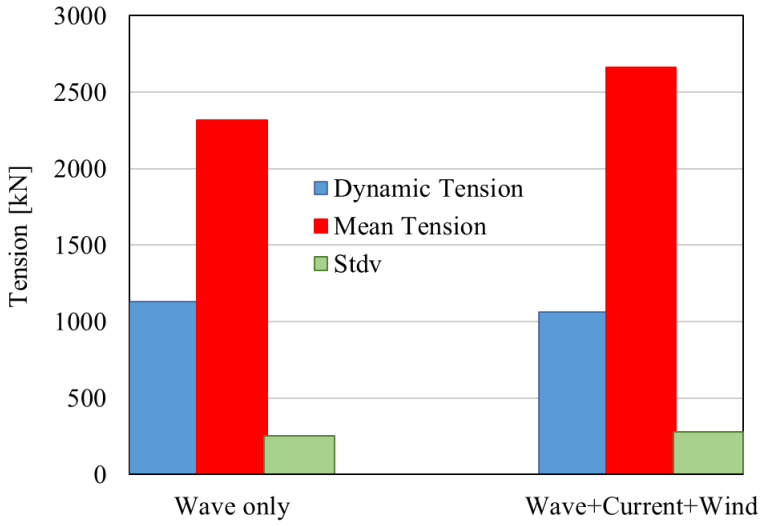

Figure 2.41 Statistical values of tension response of the loaded line (L-1) for the Collinear 'In-line' cases for the FPSO with mooring lines exposed to irregular waves only and irregular waves, current and wind.

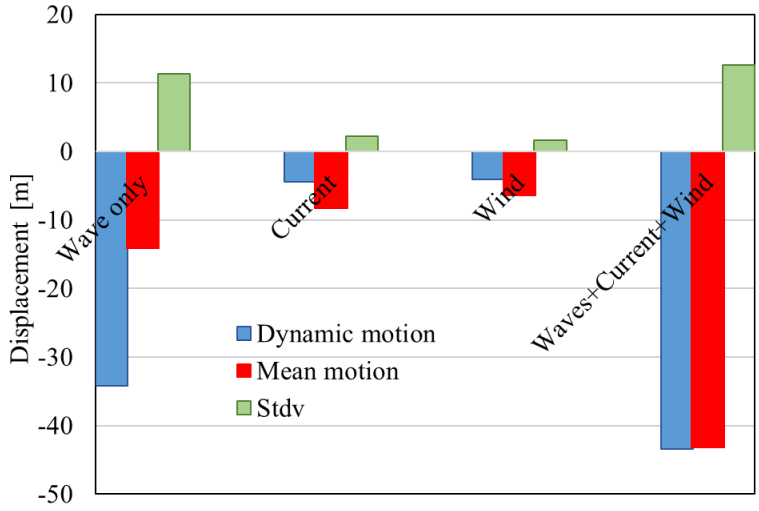

Figure 2.42 Statistical values of surge motion responses for the Collinear 'In-line' case exposed to irregular waves only and Non-Collinear cases exposed to irregular waves, current and wind, FPSO model with mooring lines

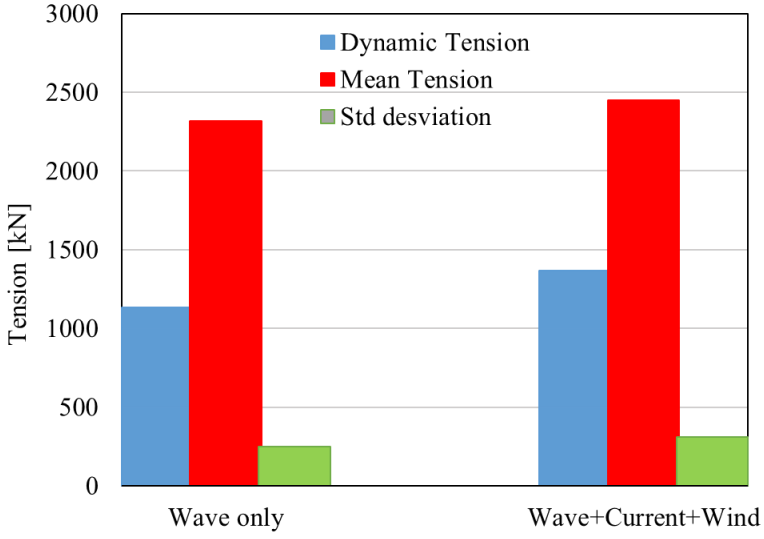

Figure 2.43 Statistical values of tension response of the loaded line (L-1) for the Collinear 'In-line' and Non-collinear cases for the FPSO with mooring lines exposed to irregular waves only and irregular waves, current and wind.

2.7 *Summary*

Based on the results of the present study, the motion response of the FPSO (RAOs) for both Full Load and Ballast Load conditions were observed to be sensitive to the direction of the incident waves. The beam and bow quartering seas incident wave conditions are the critical conditions leading to the maximum roll motion responses. The spectrum analyses revealed that risers have a significant influence on low-frequency damping, particularly in the surge direction, whereas their damping effect to the wave frequency motion response contributes mainly to the roll motion response. In the non-collinear environmental condition, the directions of the interactions between the irregular waves and the current significantly increase the steady wave drift force on the FPSO compared to the collinear cases. The yaw motion response was identified influence in the wave frequency motions (heave, roll, and pitch) for the non-collinear condition as well. The impact of the (Full/Ballast) Load condition of the FPSO model on the wave frequency motion was found to be insignificant. The highest tension in the mooring lines was observed to occur in the Ballast Load condition for the non-collinear case due to a higher coupled surge and sway motion response and the smaller draught of the FPSO hull. The tensions in the risers were observed to be slightly higher in the non-collinear case for the Full load condition. It indicated that risers are sensitive to wave frequency motions.

On the other hand, the interaction between the irregular waves, current and wind in collinear environment increases the mean drift motion of the FPSO and the drift damping contribution but decreases the slow-drift oscillation response of the FPSO compared to that of FPSO exposed in the irregular waves only. However, the interaction of waves, current and wind in non-collinear environment is more complex which tends to increase the mean drift motion, the drift damping and the slow-drift oscillation response of the FPSO compared to the system exposed to irregular waves only.

The passive truncation methodology for application to the mooring lines and risers as employed in the present study produces a correct quasi-static behaviour of the horizontal restoring forces-offset. However, for the mooring lines and risers the damping effects and the dynamics are not the case. Therefore a coupled non-linear time domain analysis is needed in order to represent the accurate damping and dynamic behaviour of the mooring lines and risers in the prototype full depth installation.

Chapter 3

Numerical Modelling

3. Introduction

This chapter provides the numerical methodology that was used for predicting the FPSO motion responses (mean, wave frequency WF and low frequency LF motions) in six DOF and the dynamic tension response of the mooring lines and the risers under both collinear and non-collinear environment conditions. The numerical model for the hydrodynamic analysis of the FPSO with its mooring lines and risers is validated (model-model) using data obtained from the experimental results. The WADAM-SESAM (2014) software is used for estimating the first-and second-order wave forces on the FPSO. Both the Newman's approximation and the full QTF are employed in order to predict the extreme motion responses of the overall system and the dynamics of the mooring lines and risers using a non-linear time domain coupled analysis RIFLEX and SIMO, SESAM computer program (RIFLEX-SESAM, 2013; SIMO-SESAM, 2015).

3.1 Numerical methodologies

3.1.1 Wind and Current loads on the FPSO hull model

The methodology used to predict the wind and current force coefficients for the FPSO is based on the studies by The Oil Companies International Marine Forum (OCIMF, 1994) which is an International Research Institute that has studied, amongst other topics, the wind and current induced loads on Very Large Crude Carriers (VLCC's).

The forces and moments from a constant velocity wind acting on a moored FPSO model, which has a general similarity with a typical VLCC, except for the additional on-deck structures and process equipment, can be calculated by (OCIMF, 1994):

-Wind forces and moments

$$F_{Xw} = \frac{1}{2} C_{Xw}\, \rho_w\, V_w^2 A_T \quad (3.1)$$

$$F_{Yw} = \frac{1}{2} C_{Yw}\, \rho_w\, V_w^2 A_L \quad (3.2)$$

$$M_{XYw} = \frac{1}{2} C_{XYw}\, \rho_w\, V_w^2 A_L L_{BP} \quad (3.3)$$

F_{Xw} and F_{Yw} are the wind forces in the surge and sway directions relative to the vessel and its defining axis system, and M_{XYw} is the wind yaw moment. The C_{Xw}, C_{Yw} and C_{XYw} are the wind force in surge, sway and yaw moment shape related coefficients, respectively, where the shape related coefficients at various heading angles are obtained from the figures given in the OCIMF (1994) and which have been validated by experimental model tests representing real structures. The ρ_w is the density of the air, and the A_T and A_L are the transversal and longitudinal projected areas, essentially the silhouettes, including the hull above the still water line and the various structures and items of equipment on the deck, and L_{BP} is the length between perpendiculars of the FPSO hull model. The mean wind velocity (V_w) is defined at the standard reference elevation of 10 m above the mean water surface for use in the wind induced forces and moment formulations.

The OCIMF (1994) established force and moment coefficients for different heading angle directions relative to the wind and for two types of bow shapes (cylindrical bows and conventional bows). The incident wind angle is from 180 degrees directly onto the bows to 0 degree directly on to the stern. In this study, the wind areas were determined through a crude topside arrangement and are given in (Appendix B). The wind force coefficients for different heading attack angles on the FPSO are calculated in order to be used in the numerical simulation and they will depend on the yaw motion related A_T and A_L values in each time step.

-Current forces and moments

Similar to wind force calculations, the steady current forces due to the constant velocity current in the surge and sway directions and the yawing moment acting on the FPSO hull at various heading angles can be calculated according to the OCIMF (1994) formulations:

$$F_{Xc} = \frac{1}{2} C_{Xc}\, \rho_c V_c^2 L_{BP} T \quad (3.4)$$

$$F_{Yc} = \frac{1}{2} C_{Yc}\, \rho_c V_c^2 L_{BP} T \quad (3.5)$$

$$M_{XYc}=\frac{1}{2}\,C_{XYc}\,\rho_c V_c^2 L_{BP}^2 T \tag{3.6}$$

F_{Xc} and F_{Yc} are the current induced forces in the surge and sway directions respectively and M_{XYc} is the current induced yaw moment. The C_{Xc}, C_{Yc} and C_{XYw} are the surge, sway and yaw force/moment coefficients respectively, and the values of these coefficients are chosen from the plots at various heading angles given in the OCIMF (1994) document. The ρ_c is the density of the sea water, V_c is the current velocity which is constant through the depth, T is the draught of the vessel, again allowing for Full Load condition and L_{BP} is the length between perpendiculars of the FPSO.

The OCIMF formulations calculate the forces and moments due to the wind and the current about the center of the vessel with the reference convention as shown in Figure 3.1. Thus the forces and moments are transferred to the vertical central axis of the internal turret according to the following expressions:

$$\begin{Bmatrix}\tilde{F}_X\\ \tilde{F}_Y\end{Bmatrix}=\begin{bmatrix}\cos\theta & -\sin\theta\\ \sin\theta & \cos\theta\end{bmatrix}\begin{Bmatrix}F_X\\ F_Y\end{Bmatrix} \tag{3.7}$$

$$\widetilde{M_{XY}} = F_Y X_{turr} + M_{XY} \tag{3.8}$$

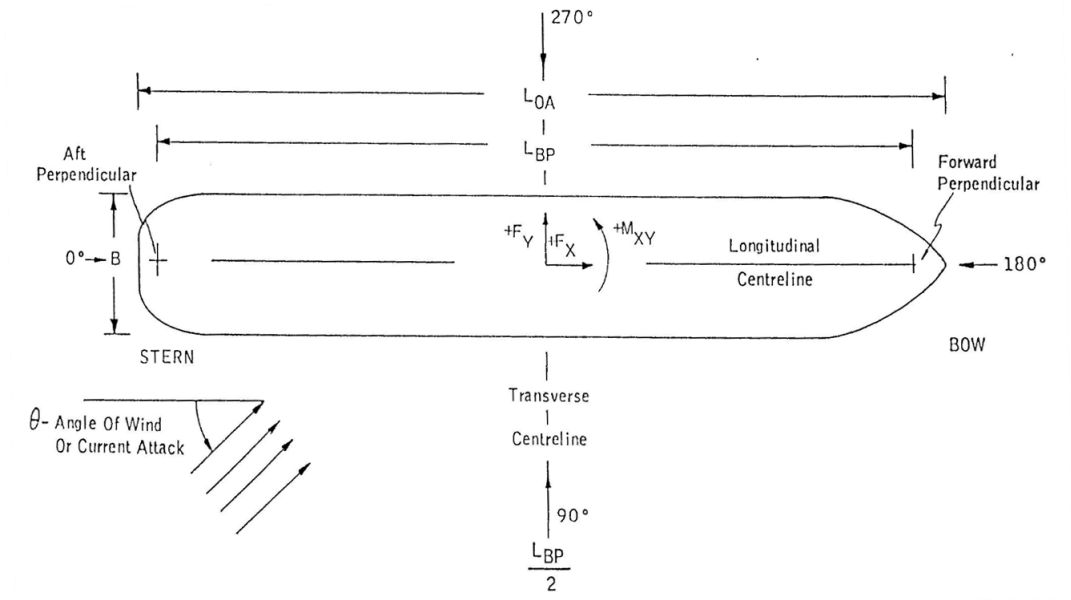

Figure 3.1 Coordinate system conventions for wind and current loads on the FPSO hull, OCIMF (1994)

After the wind and current shape coefficients have been calculated, the SIMO computer program, which is for the simulation of the motions and station-keeping behaviour of complex systems of floating vessels (SIMO-SESAM, 2015), is used to evaluate the wind loads and current loads on the FPSO. The Full Load operational condition is studied and the typical wind and current environment conditions of the selected location in the GOM were analyzed.

On the other hand, the current induced drag forces on the wetted surface area of the FPSO hull are calculated using the velocity of the current at the still water surface (Z=0). The viscous current forces in the surge and sway directions and the yaw moment are calculated from the current coefficients and the translational relative velocity between the fluid and the vessel. Then, the current drag forces are calculated by (SIMO-SESAM, 2015):

$$q_{CU}^{(k)}(\alpha, \mathrm{t}) = C_1^{(k)}(\alpha)|u(t)| + C_2^{(k)}(\alpha)\,|u(t)|^2 \quad \text{...(3.9)}$$

$$|u|^2 = (v_1 - \dot{x}_1)^2 + (v_2 - \dot{x}_2)^2 \quad \text{…(3.10)}$$

$$\alpha = \arctan \frac{v_2 - \dot{x}_2}{v_1 - \dot{x}_1} \quad \text{…(3.11)}$$

Where:

k = degree of freedom (surge, sway, yaw)

C_1 = linear current force coefficient

C_2 = quadratic current force coefficient

u = relative velocity between low-frequency body velocity and current velocity

α = relative angle between direction of low-frequency body velocity and current velocity

v_1, v_2 = current velocity components in the surface for floating bodies and at the center of gravity for submerged bodies

$\dot{x}_1,\ \dot{x}_2$ = vessel velocity components in the vessel's coordinate system

In SIMO-SESAM (2015), the numerical model account the viscous yaw moment as the sum of both the translational velocity and the yaw velocity and it is given by:

$$q^{(6)}(\alpha) = C_2^{(6)}(\alpha)\,|u|^2 + b_{66}\dot{x}_6|\dot{x}_6| \quad \text{..(3.12)}$$

Where:

$C_2^{(6)}(\alpha)$ = Current coefficient in yaw as a function of the incident heading (α).

b_{66} = Quadratic damping coefficient in yaw due to a pure yaw velocity.

$\dot{x}_6$ = Yaw velocity

3.1.2 Wave interaction with the FPSO hull model

The interaction of the waves with the FPSO hull is solved based on potential theory. The resulting local surface loads are found through the velocity potential of the fluid that is assumed to be irrotational, incompressible and inviscid conditions. The first-order and second-order hydrodynamic wave forces on the FPSO hull structure are the basis of the work carried out in this research project. The total mean motion, the wave frequency (WF) and the low frequency (LF) motion responses in six DOF are the results of the wave-structure interaction. Thus a general description is provided for both the first-order and the second-order hydrodynamic wave forces on the FPSO hull in the following sections and for a more detailed description of the complete methodology can be found in (Chakrabarti, 1987; Lee and Newman, 1991a; Lee and Newman, 1991b; Faltinsen, 1998).

-First-order hydrodynamic wave forces on the FPSO

A numerical model of the wave interaction with the FPSO was developed using the computer programs WADAM-SESAM (2014) and which are based on the linear potential theory. A 3D boundary integral equation method (BIEM), or so-called panel method, using Green's theorem with the free surface source potentials defined as the Green's functions, is used to solve numerically the wave interaction with the FPSO hull. The integral equation is discretized in algebraic equations by approximating the hull body external surface with a large number flat, quadrilateral panels. The hydrodynamic pressures and forces acting on the wetted surfaces of the FPSO are calculated using the Bernoulli's equation (Lee and Newman, 2005). The linear solution includes both the wave diffraction and the vessel rigid body motions-induced radiation effects from the submerged portion of the FPSO. In this approach, the water free surface condition and floating body boundary condition are satisfied both on the mean position of the still water free-surface and on the submerged hull surface respectively. The kinematic and dynamic boundary conditions on the water free surface are linearized based on

the assumption that potential theory is applied (irrotational motion, an inviscid and incompressible fluid) and that the motion can be expressed by a velocity potential.

The fluid motion can be represented by the Laplace equation with the assumptions of irrotational motion and an incompressible fluid. Then, the velocity potentials have to satisfy the following general boundary conditions:

$$\nabla^2\Phi = 0 \tag{3.13}$$

$$\nabla^2\Phi = \frac{\partial^2 \Phi}{\partial x^2} + \frac{\partial^2 \Phi}{\partial y^2} + \frac{\partial^2 \Phi}{\partial z^2} = 0 \tag{3.14}$$

Where $\Phi = \Phi_0 + \Phi_s + \sum_{n=1}^{6} \Phi_{Rk}$. (3.15)

Which Φ_0 is the incident potential velocity, Φ_s is the scattering potential or diffraction potential Φ_d velocity and Φ_R is the radiated potential velocity due to forced harmonic motions of unit amplitude of the floating body in the k^{th} mode of the body of the floating FPSO.

-Dynamic free surface boundary condition:

$$\frac{\partial \Phi}{\partial t} + g\eta + \frac{1}{2}\left[\left(\frac{\partial \Phi}{\partial x}\right)^2 + \left(\frac{\partial \Phi}{\partial y}\right)^2 + \left(\frac{\partial \Phi}{\partial z}\right)^2\right] = 0 \qquad \text{at } z = \eta \tag{3.16}$$

Which η is equal to free-surface elevation ($z = \eta(x, y, t)$) and g = acceleration owing to gravity.

-Kinematic free surface boundary condition:

$$\frac{\partial \eta}{\partial t} + \frac{\partial \Phi}{\partial x}\frac{\partial \eta}{\partial x} + \frac{\partial \Phi}{\partial z}\frac{\partial \eta}{\partial z} - \frac{\partial \Phi}{\partial y} = 0 \qquad \text{at } z = \eta\ (x, y, t) \tag{3.17}$$

-Sea bottom boundary condition:

The bottom boundary condition is expressed by the condition that the sea bed is impermeable:

$$\frac{\partial \Phi}{\partial z} = 0, \qquad \text{at} \qquad z = -d \tag{3.18}$$

Where *d* is the water depth.

-Body surface-boundary condition:

$$\frac{\partial \Phi}{\partial n} = 0 \qquad \text{on the body surface at } -d \leq z \leq \eta \tag{3.19}$$

-Boundary condition at infinity, for the scattered potential:

$$\lim_{R \to \infty} \sqrt{R} \left(\frac{\partial \Phi}{\partial \mathrm{R}} - i\mathrm{k}\Phi \right) = 0 \text{ at far field} \tag{3.20}$$

The incident wave velocity potential is assumed from the undisturbed wave where the shape of the waves are not affected by the structure platform.

The solution for the assumed Φ take the form of a power series considering a perturbation parameter:

$$\Phi = \sum_{n=1}^{\infty} \varepsilon^n \Phi_n \tag{3.21}$$

In the same way, the water surface elevation take also the power series form:

$$\eta = \sum_{n=1}^{\infty} \varepsilon^n \eta_n \tag{3.22}$$

Where η_n is equal to the profile of the first-order waves

Then, the incident wave potential at a point (x, y, z) in the fluid domain can be solved by Chakrabarti, (1987) and Lee et al., (1991b):

$$\Phi_0 (\mathrm{x}, \mathrm{y}, \mathrm{z}) = i \frac{ghcoshk(y+d)}{2\omega \cosh kd} \exp(ikx) \tag{3.23}$$

In which i = imaginary quantity, g= gravitational acceleration; h= wave height; ω=wave frequency; k= wave number; and d= water depth.

The scattering wave potential in the fluid is represented by that due to a continuous distribution of individual sources on the whole wetted hull surface and is given as:

$$\Phi_s(x, y, z) = \frac{1}{4\pi} \iint_S \sigma(a,b,c) G(x,y,z;a,b,c) ds \tag{3.24}$$

The σ is the local source strength, positioned at location (a, b, c) which characterizes the coordinates of the local source point on the external surface of the structure, (x, y, z) are the field point coordinates in the fluid, and *ds* is the area of the individual flat panel on the submerged hull surface. The function $G(x,y,z;a,b,c)$ represents the near-field Green's function and σ is calculated from the integral:

$$2\pi\sigma_s(x, y, z) - \iint_S \sigma_s(a,b,c) \frac{\partial G}{\partial n}(x,y,z;a,b,c) ds = -4\pi u_n(x, y, z) \tag{3.25}$$

In which u_n= the normal fluid velocity at (x, y, z) due to the incident wave. Then the integral Eq. (3.25) is solved numerically, and the individual source strength σ at the center of each elemental quadrilateral panel is obtained from the inverse of the matrix. All the velocity components in Eq. (3.15) are solved under their individual boundary conditions.

On the other hand, the radiation wave owing to the linearization motion of the floating structure is calculated by the assumption that the structure experiences one simple specific harmonic motion in calm water. In this case the boundary value problem, introduced previously, is valid except for the body surface condition which take the form:

$$\frac{\partial \Phi_k}{\partial n} = i\omega X_k n_k \qquad k = 1, 2, \ldots, 6 \tag{3.26}$$

The radiation potential is solved with the Eq. (3.25) in which the right hand side is replaced by the normal unit displacement of the floating structure at one of the 6 DOF motion. After the inverse matrix is calculated, the radiation potential is solved. The body motion is calculated by

a coupled set of equations of a linear analysis assuming 6 DOF motion. Subsequently, the added mass and potential damping due to the motions of the rigid body are calculated.

When the diffraction and radiation potentials are known at the center of each panel, plate element, defining the hull, the comprehensive external hydrodynamic forces on the submerged part of the vessel are obtained from the integrals through the Bernoulli's equation from the total diffraction and radiation potentials:

$$F_{kD} = -i\rho\omega \iint_s (\Phi_0 + \Phi_s)\, n_k ds \tag{3.27}$$

$$F_{kR} = -i\rho\omega \iint_s \Phi_{Rk}\, n_k ds \tag{3.28}$$

$$\omega M_{kR} + iC_{kR} = \frac{F_{kR}}{\omega X_k} \tag{3.29}$$

Where F_{kD} is the total diffraction force and F_{kR} is the total radiation force where k=1, 2…6 and S= total submerged surface area up to the surface still water level. The incident wave forces and moments by linear wave theory are obtained by Eq. (3.27), while the added mass and radiation damping values are calculated from Eq. (3.29). Where X_k is the amplitude of oscillation of the platform, and *M* and *C* are the added mass matrix and linear radiation damping matrix respectively. The solutions of the diffraction and radiation theories (first-order motion) are expressed in term of linear transfer functions (LTF or RAOs), where the hydrodynamic forces, moments, added mass and potential damping are considered. The details of the formulations for the linear solution procedure can be found in Chakrabarti (1987), Newman (1977), Faltinsen (1990), Lee and Newman, 1991a; and Journee and Massie (2001).

-Second-order hydrodynamic wave forces on the FPSO

In the second-order wave-structure interaction process (which is more accurate non-linear method), the approach to solve the problem is to use a perturbation technique with typically the wave steepness selected as a small parameter. Thus, based on the same potential flow theory, the problem is solved to include the second-order terms of the incident wave amplitude. The solutions of the second-order wave forces are expressed as the mean drift force and the oscillating force with either a low frequency or a high frequency of which the latter solution is

involved in terms of a quadratic transfer function (QTF) and which, for full rigorous calculations, requires a considerable amount of computer time, which is questionable if it is to be applied routinely in a design development process and particularly in the early stages where alternative configurations are being investigated. A solution is thus more efficiently obtained by using the frequency domain approach due to it being a second-order problem with a low nonlinear contribution while at the same time obtaining advantages in terms of reduced computation time as compared to an analysis that is undertaken in the time domain (Faltinsen, 1994).

The second-order theory gives:

$$\nabla^2\Phi_2 = 0 \tag{3.30}$$

Where Φ_2 is second-order velocity potential that should satisfy the following boundary conditions at free surface, sea bottom, on the boundary surface and infinity:

$$\frac{\partial^2 \Phi_2}{\partial t^2}+g\frac{\partial^2 \Phi_2}{\partial y} = \frac{1}{g}\frac{\partial^2 \Phi_1}{\partial t}\frac{\partial}{\partial y}\left(\frac{\partial^2 \Phi_1}{\partial t^2}+g\frac{\partial^2 \Phi_1}{\partial t^2}\right) - \frac{\partial}{\partial t}\left[\left(\frac{\partial^2 \Phi_1}{\partial x}\right)^2+\left(\frac{\partial^2 \Phi_1}{\partial y}\right)^2+\left(\frac{\partial^2 \Phi_1}{\partial z}\right)^2\right]$$

at $y = 0$ (3.31)

$$\frac{\partial \Phi_2}{\partial z} = 0 \quad \text{at z = -d} \tag{3.32}$$

$$\frac{\partial \Phi_2}{\partial n} = 0 \quad \text{on the body surface} \tag{3.33}$$

$$\text{Rad}\,[\Phi_2] \text{ at } R\rightarrow\infty \tag{3.34}$$

The first-order and second-order boundary value problem (BVP) are solved for Φ_1 and Φ_2 respectively. After that the pressure on the wetted surface area of the floater is calculated. The Bernoulli's equation is used and the total second-order hydrodynamic force can be written as (Lee and Newman, 1991b):

$$F^{(2)} = \iint_{S_0} P^{(1)}\,\mathbf{n}^{(1)}\,dS + \iint_{S_0} P^{(2)}\,\mathbf{n}^{(0)}\,dS + \iint_{S_0} P^{(0)}\,\mathbf{n}^{(2)}\,dS + \iint_{S-S_0} P^{(1)}\,\mathbf{n}^{(0)}dS \tag{3.35}$$

$$M^{(2)} = \iint_{S_0} P^{(1)}\,\mathbf{r}\mathbf{x}\mathbf{n}^{(1)}\,dS + \iint_{S_0} P^{(2)}\,\mathbf{r}\mathbf{x}\mathbf{n}^{(0)}\,dS + \iint_{S_0} P^{(0)}\,\mathbf{r}\mathbf{x}\mathbf{n}^{(2)}\,dS + \iint_{S-S_0} P^{(1)}\,\mathbf{r}\mathbf{x}\mathbf{n}^{(0)}dS \tag{3.36}$$

Where $P^{(0)}$, $P^{(1)}$ and $P^{(2)}$ are the hydrostatic water pressure, the first-order and the second-order hydrodynamic pressures respectively while $\mathbf{n}^{(0)}$, $\mathbf{n}^{(1)}$ and $\mathbf{n}^{(2)}$ represent the mean, the first-order and the second-order local normal vectors of the body surface expressed in the earth-fixed coordinate system. The **r** relates to the position vector. S_0 denotes the mean wetted surface. Though the second-order wave forces are relatively small, their contributions can be significant when they are close to natural frequencies of the wave-induced rigid body responses of the floater.

At the present time, there are two main methodologies used for calculating the mean drift force in the frequency domain, i.e., the far field method based on momentum conservation with which it is possible to generate the surge, sway and yaw components while the other DOF motions heave, roll and pitch components require additionally integration in the mean free surface. Therefore, these DOF motions are not calculated (Maruo, 1960; Newman, 1967). On the other hand, the near field method or direct pressure integration method calculates the six DOF motions components of the drift force (Pinkster et al.; 1977), however it is often considered to be less accurate approach and a convergence analysis process needs to be carried out carefully (FPS, 2000). In this study, the direct integration of the pressures on the FPSO vessel's wetted surface is used in order to calculate the mean wave drift forces and moments for the six DOF body motions.

For the slowly varying wave drift force, both the full QTF and the Newman's approximation, in which the latter states that the effects of the off-diagonal elements in the full QTF matrix in the bi-frequency domain can be approximated by using the diagonal elements only, are used. A comparative study was conducted to illustrate the validity of the Newman's approximation approach in a specific offshore deepwater location for an FPSO potentially experiencing large yaw motion responses due to non-collinear environment loading conditions.

The second-order force matrix diagonal elements (Newman's approximation) can be calculated by:

$$H^{(2-)}(\omega_i, \omega_j) = \tfrac{1}{2}\,[H^{(2-)}(\omega_i, \omega_j) + H^{(2-)}(\omega_i, \omega_j)] \tag{3.37}$$

Where the differences frequencies is equal to the natural frequency ω_N which is representing two lines in the $\omega_i\,\omega_j$-plane:

$$\omega_i = \omega_j \pm \omega_N \tag{3.38}$$

As the natural frequency of the FPSO is very low in this case study for the surge, sway and yaw motion (horizontal motions), the differences frequencies will tend to be equal ($\omega_i = \omega_j$). Then it is expected that the off-diagonal elements in the full QTF can be calculated well by the Newman's approximation.

As a result, the solutions for the first-order and the second-order wave forces on the vessel (i.e.; the added mass, potential damping, forces, moments, linear transfer function and QTF) are solved using the frequency domain analysis. All of these parameters or physical quantities are subsequently used as input data in the nonlinear time domain coupled analysis.
The details of the formulations for the non-linear solution procedure can be found in Faltinsen (1990), Lee and Newman (1991a), Lee and Newman (1991b), Lee (2005), Chakrabarti (2005), and Chakrabarti (2008).

3.1.3 Motion of Structure

The response motion of the FPSO to the incident waves are computed by solving the linear coupled 6 degree freedom motion equations in the frequency domain (WADAM-SESAM, 2014).

- **Linear equation of motion in frequency domain**

The general dynamic Newton's law equation is applied to calculate of motion of FPSO due to the sinusoidal wave in frequency domain:

$$\sum_{k=1}^{6}[-\omega^2\left(M_{sjk} + M_{fjk}^{"}\right) - i\omega\left(C_{sjk} + C_{fjk}\right) + \left(B_{sjk} + B_{fjk}\right)]\,u_k = F_{j,\ j=1,\ 2,\ldots,6} \tag{3.39}$$

The above equation is the linear coupled six degree of freedom motion of the structure in frequency domain. $u_k = (\xi_1, \xi_2, \xi_3, \alpha_1, \alpha_2, \alpha_3)$ and F_j indicates *j*th mode first-order wave forces and moments. M_{sjk}, C_{sjk} and B_{sjk} represent the inertial mass, damping and restoring force of the structure, whereas, $M_{fjk}^{"}$, C_{fjk} and B_{fjk} are the added mass, damping and restoring force coefficient due to fluid (Kim, 2008).

-Hydrostatic restoring force and moment

Since the FPSO vessel is symmetric about a principal vertical plane. The hydrostatic pressure below the waterline gives the buoyancy force that keep the structure in equilibrium. Then, The heave, roll and pitch motion of a floater structure in waves produces heave restoring force, roll and pitch restoring moments (Lewis, 1929):

$$\begin{aligned} B_{33} &= \rho g A_{WP} \\ B_{44} &= \rho g \nabla \overline{GM}_T \\ B_{55} &= \rho g \nabla \overline{GM}_L \end{aligned} \tag{3.40}$$

Where: A_{WP} is equal to the water plane area, ∇ is equal volume displacement, $\overline{GM}_T$ is the transverse metacentric height and $\nabla\overline{GM}_L$ is the longitudinal metacentric height.

3.1.4 Fluid Interaction with mooring lines and risers

The total hydrodynamic loads on the mooring lines and risers from the surrounding fluid are considered. The hydrodynamic forces are calculated based on two-dimensional strip theory. The wave-induced excitation forces (Froude-Krylov and diffraction forces) are computed by a relatively long wave length approximation which involves both added mass and potential damping of the actual cross sections together with the wave kinematics. The Morison formulation is used for computing the viscous loads.

The total hydrodynamic forces on the slender elements, representing segments of the mooring lines and risers, are included in the analyses (including both buoyancy and current induced forces) (RIFLEX-SESAM, 2013).

$$F^H = F^{Pot} + F^D = F^{FK} + F^S + F^R + F^D \tag{3.41}$$

Where the potential flow contributions to the hydrodynamic forces are:

F^{FK} = Froude-Kriloff forces (including buoyancy forces)

F^S = Diffraction forces

F^R = Added mass and damping forces and

F^D = Drag forces

Comprehensive details about the derivation of the equations used for the potential flow based hydrodynamic forces on slender elements (representing the mooring lines and risers) can be found in (Kaplan and Silbert, 1976; Dixon et al., 1979).

On the other hand, the Morison formulation in terms of the relative fluid-structure velocities and accelerations is used for computing the viscous forces. The contribution of the current and the wave kinematics are considered in the local fluid velocity and acceleration. The methodology of the hydrodynamic load estimation is based on the cross-flow principle first introduced by Hoerner (1965). The drag forces are calculated using the relative velocity in the local line definition system expressed by:

$$u_r = u_c + u_w - \dot{v} = u_{rx}\, i_1 + u_{ry}\, i_2 + u_{rz}\, i_3 \tag{3.42}$$

Where u_c is the current velocity, u_w is the wave particle velocity and $\dot{v}$ is the structural velocity.

-Longitudinal loads on slender elements

The longitudinal drag forces on the slender elements are calculated by:

$$f_x^D \Delta x = \frac{1}{2} \rho\, C_{Dx}\, L_W\, |u_{rx}|\, u_{rx}\, \Delta x i_1 \tag{3.43}$$

where ρ is the density of the water, C_{Dx} is the skin friction coefficient, L_W is the instantaneous wetted part of the cross section and u_{rx} is the total velocity component (combined current and wave velocity) of the particular in the local longitudinal direction of the individual slender element.

-Transverse loads on slender elements

In the case of the transverse relative velocity vector is described by:

$$u_{rn} = u_{ry}\, i_2 + u_{rz}\, i_3 \tag{3.44}$$

Thus, the transverse drag force is calculated according to:

$$f_n^D \Delta x = \frac{1}{2} \rho\, C_{Dy}\, h_{rel}\, |u_{rn}|\, u_{ry}\, \Delta x i_2 + \frac{1}{2} \rho\, C_{Dz}\, b_{rel}\, |u_{rn}|\, u_{rz}\, \Delta x i_3 \tag{3.45}$$

where $h_{rel} = \frac{A_s}{A} h$ and $b_{rel} = \frac{A_s}{A} b$

C_{Dy} and C_{Dz} are the drag coefficients in the local y and z directions respectively, A_s is the instantaneous submerged cross section area and A is the cross section area while b and h are the width and height dimensions of the section respectively.

3.1.5 Coupled analysis of the total system FPSO with mooring lines and risers

A nonlinear time domain coupled analysis was applied in order to calculate the FPSO's motion equations in the full 6 DOF taking into account the fully coupled effects of the attached mooring lines and risers. The FPSO vessel was included as a rigid body nodal component in the three dimensional finite element model, of 6-DOF, and with full arrangement of the mooring lines and risers each being represented as a line of finite elements representing slender structures Figure 3.2.

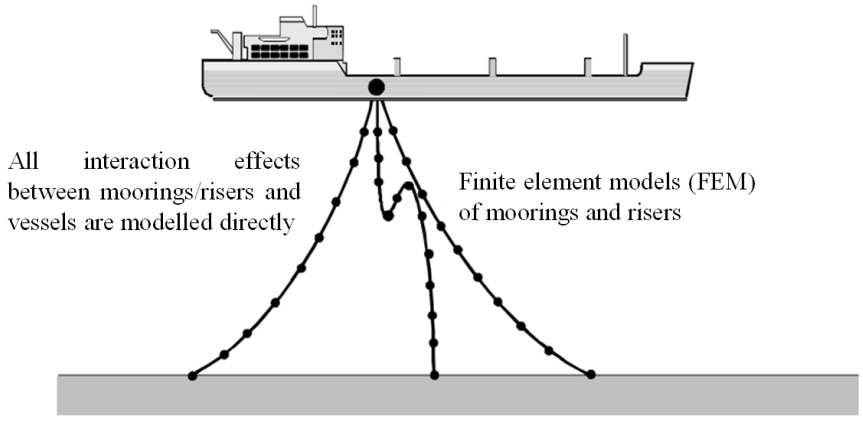

Figure 3.2 Total system FPSO with mooring lines and risers (Chakrabarti, 2008)

The dynamic equilibrium equation of the overall spatially discrete complete system model is expressed by (RIFLEX-SESAM, 2013):

$$R^I(r, \ddot{r}, t) + R^D(r, \dot{r}, t) + R^s(r, t) = R^E(r, \dot{r}, t) \quad (3.46)$$

The inertia force vector is expressed as:

$$R^I(r, \ddot{r}, t) = M(r)\,\ddot{r} \quad (3.47)$$

And the damping force vector is expressed as:

$$R^D(r, \dot{r}, t) = C(r)\,\dot{r} \quad (3.48)$$

Where C is the system damping matrix that includes contributions from internal structural damping and external hydrodynamic damping.

The internal reaction force vector R^s is calculated based on the instantaneous state of stress in each of the various elements of the whole system. The external load vector R^E considers the weight and buoyancy for each element, forced displacements, environmental forces and other specific forces. The numerical solution is then established on an incremental technique using a dynamic time integration scheme according to the Newmark β-family of methods. The Newton-Raphson iteration technique is used in order to ensure equilibrium between internal and external forces at every time step.

Introducing the tangential mass, damping and stiffness matrices at start of the next time increment, and with the implementation of the residual force vector from the previous time step, the linearized incremental equation of motion is given by:

$$M_t \Delta\ddot{r}+C_t \Delta\dot{r}+K_t \Delta r = R^E_{t+\Delta t}- (R^I_t + R^D_t +R^S_t) \quad (3.49)$$

Where Δr, $\Delta\dot{\mathbf{r}}$ and $\Delta\ddot{\mathbf{r}}$ are the incremental nodal displacements, velocities and accelerations. The forces on the vessel, represented by the large volume rigid body nodal component, are computed separately at each time step and included in the external load vector R^E. The exceptions are the vessel's inertial forces representing the vessel's mass properties, and the frequency-independent part of the added mass which are included in the hydrodynamic mass matrix of the system.

3.2 Case studied

The Full Load condition was studied for the first-order motion responses (linear transfer functions) through the numerical simulations and then compared with the experimental results. Furthermore, the Full Load condition was studied in more detail for the extreme motion responses of the FPSO and the associated dynamics of the mooring lines and risers and five (5) analyses based on the experimental test cases were considered in order to reconstruct the behaviour with the numerical simulation validated by the experimental measurements (Table 3.1). Thus, the extreme responses of the FPSO and the dynamics of the mooring lines and risers were investigated in combination with both the numerical simulations and the experimental model tests. The collinear and non-collinear environment load conditions, introduced in

Chapter 2, were used to make the comparisons between the experimental model tests, the truncated numerical model and the full depth prototype numerical model.

Table 3.1 Case studies

Test no	**Case**	**Configuration**	**Environmental loading condition**
FB-16	Collinear 'In-line'	FPSO with mooring lines	Irregular waves
FB-19	Collinear 'In-line'	FPSO with mooring lines	Irregular waves + current + wind
FC-37	Collinear 'In-line'	FPSO with mooring lines + risers	Irregular waves + current + wind
FC-38	Collinear 'Between-lines'	FPSO with mooring lines + risers	Irregular waves + current + wind
FC-39	Non-collinear	FPSO with mooring lines + risers	Irregular waves + current + wind

The general process for the calibration of the numerical model using the frequency domain analysis for the first-order motion response of the FPSO model and the non-linear time domain analysis for the extreme motions response of the FPSO and dynamic tensions in the mooring lines and risers is illustrated in Figure 3.3.

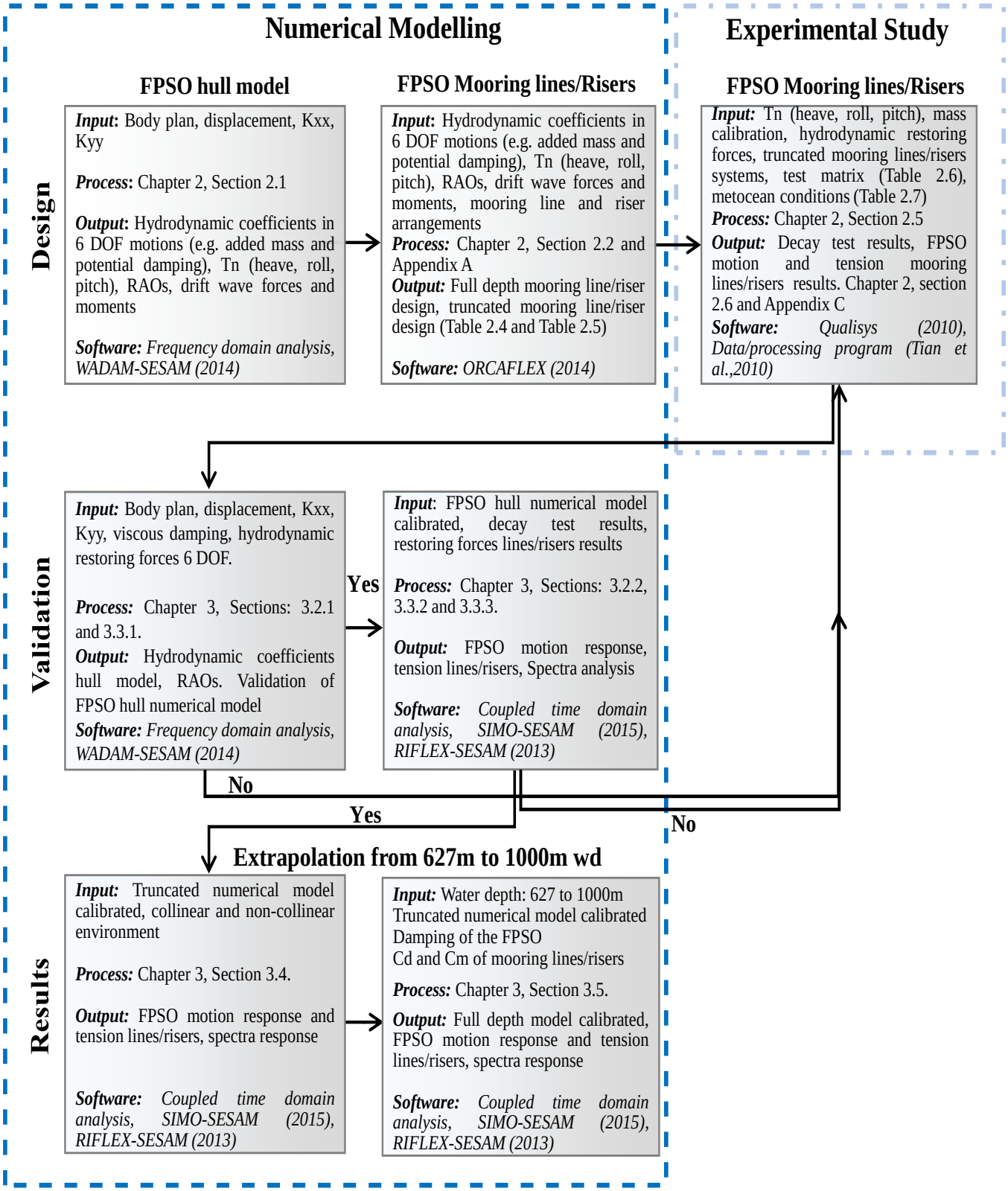

Figure 3.3 General process of the numerical validation using experimental results

3.2.1 Frequency domain analysis

- FPSO hull model

Since the FPSO hull is symmetric to the *x*-axis, only one half of the numerical model and the associated free surface domain was created in order to reduce computation time. A convergence analysis for the wave diffraction and radiation solution of the FPSO hull in the frequency domain was conducted. This convergence analyses helped to ensure the accuracy and efficiency of the calculations in order to save computation time in the subsequent analysis (Figure 3.4). Thus in model establishment, the number of quadrilateral panels was defined as 2175 panels on the submerged FPSO hull surface area and for the water free surface this was 1842 panels with a fluid domain radius equal to 5 times that of the length of the FPSO hull as show in Figures 3.5 and 3.6.

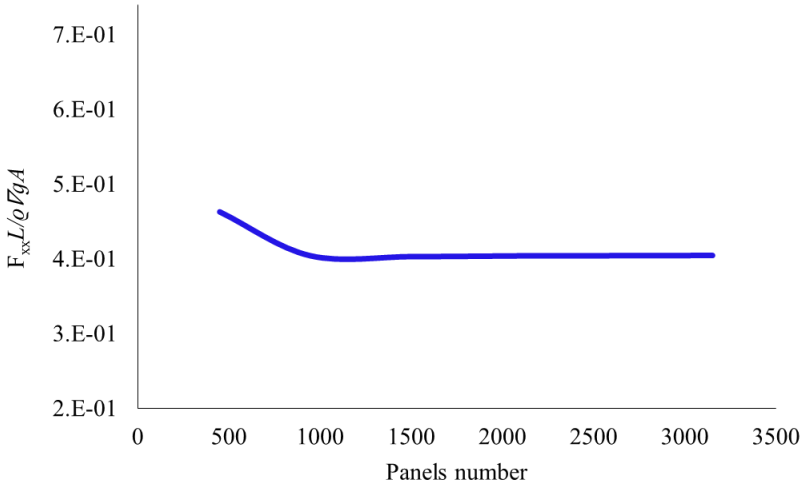

Figure 3.4 (a) Non-dimensional real part hydrodynamic exciting force on the FPSO hull model, (heading=180 degree), frequency=0.48 (rad/s)

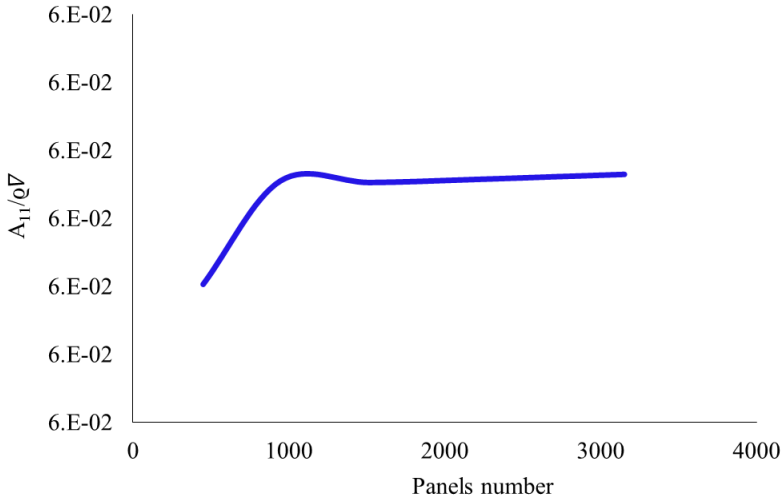

Figure 3.4 (b) Non-dimensional added mass of the FPSO hull model, frequency=0.48 (rad/s) surge direction

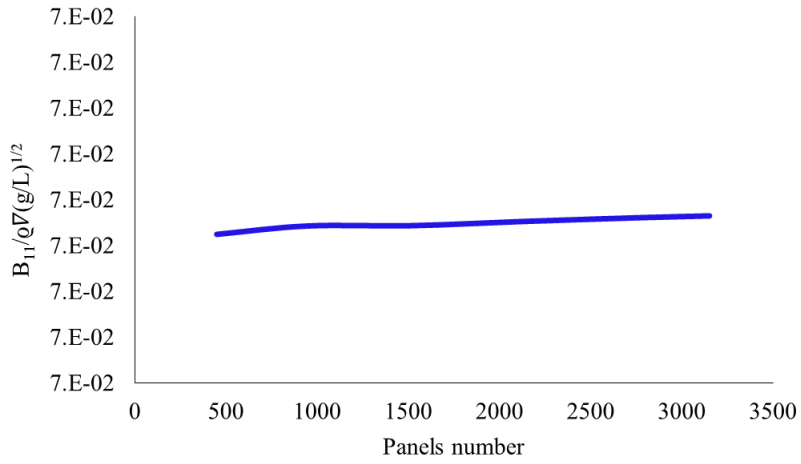

Figure 3.4 (c) Non-dimensional potential damping of the FPSO hull model, frequency=0.48 (rad/s) surge direction

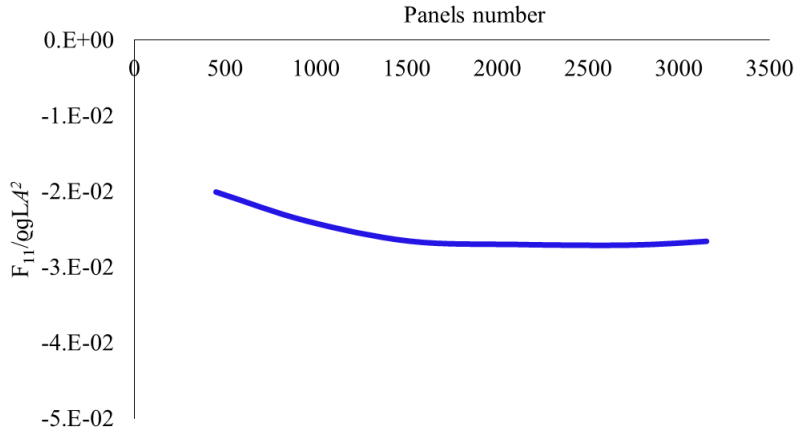

Figure 3.4 (d) Non dimensional mean wave drift force on the FPSO hull model (heading=180 degree), frequency=0.48 (rad/s)

Figure 3.4 Convergence analysis on the hull FPSO model

The second-order forces, or drift force components, with different frequencies but that are near to the floating hull's natural frequencies in surge are the most important on a moored FPSO (Tahar and Kim, 2003; Chakrabarti, 2005). Thus the range of the frequency selected for study by both the Newman's approach and the QTF was chosen between 0.2 to 1.4 rad/s. This range of frequencies covers the energy of the environment wave spectrum that was selected. The computation time required to solve the linear and the second-order forces through the full QTF and considering only one bi-directional heading (i.e. 0-180 degrees and 180-180 degrees) was 11.75 hours. Then, for the second-order wave force, the full QTF was calculated through the pressure integration method, using a bi-chromatic and bi-directional waves. The full QTF shows that the magnitude of the second-order forces (difference-frequency) are small on the diagonal and also close to the diagonal, while these increase in magnitude progressively outside of the main diagonal. The full QTF for 0-180 degrees is presented in non-dimensional form in Fig. 3.7.

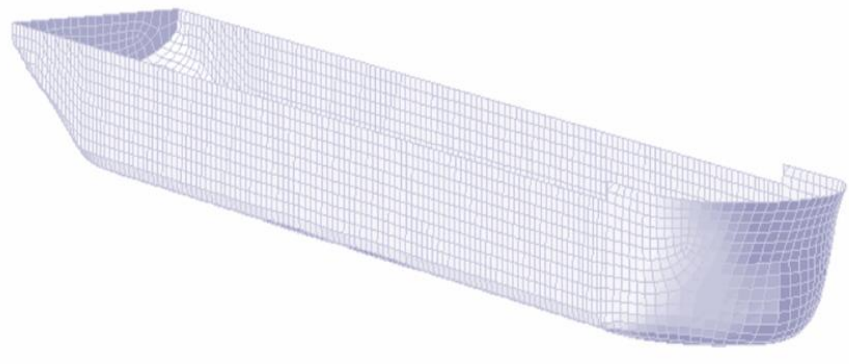

Figure 3.5 FPSO panel (full Model)

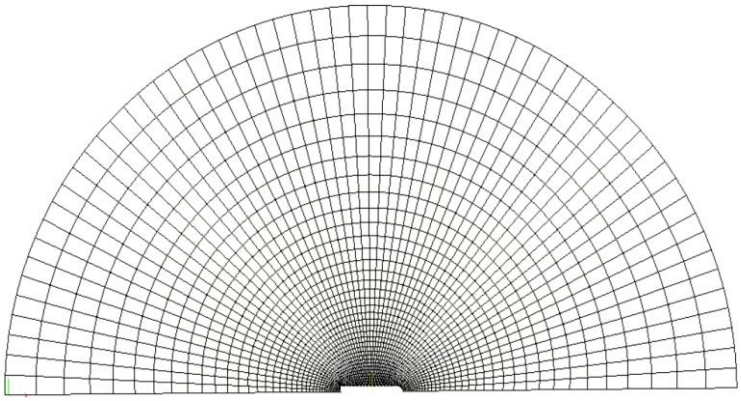

Figure 3.6 Free water surface model (half model)

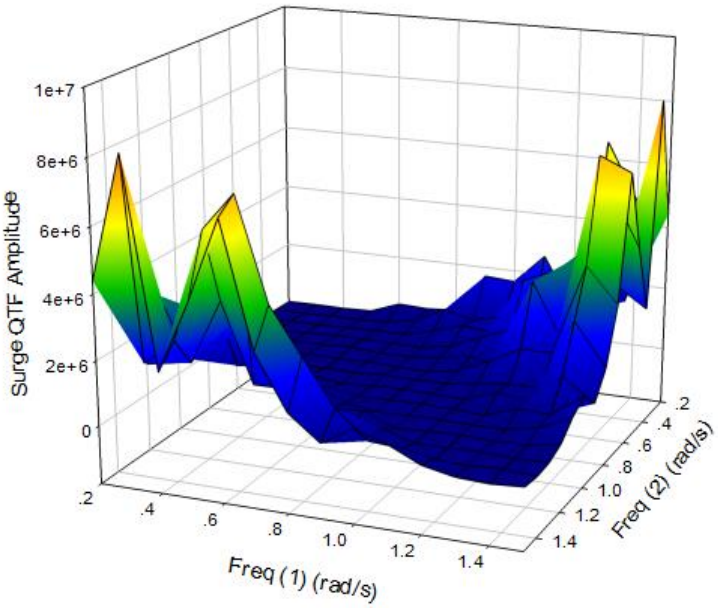

Figure 3.7 Full QTF for second-order excitation forces at differences frequencies in surge (0^0-180^0)

3.2.2. Time domain coupled analysis

A nonlinear time domain coupled analysis of the FPSO complete with mooring lines and risers was carried out using the RIFLEX and SIMO, SESAM computer program (RIFLEX-SESAM, 2013; SIMO-SESAM, 2015). The hydrodynamic coefficients of the vessel obtained from the frequency domain analysis were used in the representation of the vessel as a rigid body in the numerical simulation. Each of the mooring lines (bar elements) and risers (beam elements) were discretized in finite element form.

A convergence analysis was conducted for eventually defining a maximum acceptable mesh slender element length of 10 m for both the mooring lines and the risers. A time step (Δt) for the dynamic analysis was chosen as $\Delta t = 0.4$ s, also based on the convergence tests that were undertaken and the running length of the overall time series was defined as 3hrs. The average computation time for the coupled analysis was 47 minutes using a Desktop Intel coreli5, 3.30 Ghz and 8 GB in RAM memory. The time series of motion response in 6 DOF obtained in the center of gravity of the FPSO model for both experimental and numerical were used in the analysis.

3.3 Results and discussion

This section is organized in the following subsections:

- Calibration of the FPSO hull model for the motion response linear transfer functions RAOs
- Horizontal restoring forces verification, and
- Decay tests documentation.

-Experimental results *vs* truncated models (model to model)

- Collinear 'In-line' cases under irregular waves only (FB16)
- Collinear 'In-line' cases under irregular waves + current + wind (FB19)
    - Influences of risers (FC37)
- Collinear 'In-line'(FC37), 'Between-lines' (FC38) and Non-collinear (FC39) cases under irregular waves + current + wind

-Truncated model *vs* full depth prototype model

- Collinear 'In-line' case under irregular waves only (FB16)
- Collinear 'In-line' case under irregular waves + current + wind (FB19)
    - Influences of risers (FC37)
- Non-collinear case under irregular waves + current + wind (FC39)

The actual tests examined both the FPSO with the mooring lines only and also the full installed system which included the riser arrangement. The results of the total system FPSO with mooring lines and risers are presented in this study.

3.3.1. FPSO hull (First-order motion response)

A frequency domain analysis was undertaken in order to calibrate the FPSO hull model only (WADAM-SESAM, 2014). The natural periods, mass, added mass and restoring forces of the FPSO hull model for heave, roll and pitch motions were verified through comparison with the results of the decay tests of the experimental results (Table 3.2).

Table 3.2 Natural periods and damping ratios of six DOF for Full Load conditions

DOF	Full load		
	T_n (s)	Damping ratio (ζ)	Added mass coeff. (C_a)
Surge	223.58	0.015	-
Sway	277.39	0.030	-
Heave	11.55	0.130	1.06
Roll	13.21	0.020	0.17
Pitch	11.60	0.100	0.95
Yaw	166.90	0.030	-

The viscous damping results from the experiment decay tests were subsequently used to calibrate the FPSO numerical model in six DOF. After that, a comparison was made in terms of the added mass and the hydrodynamic restoring force characteristics for heave, pitch and roll motions between the FPSO experimental measurements and the results from the present numerical model. Then, the transfer functions, or RAOs, for the linear motions from experimental and numerical results were compared. The viscous roll damping was identified to be important to the roll RAOs while those for surge, sway, yaw, pitch and heave appeared to be relatively less important. This was attributed to that the roll motion RAO is dominated by the resonant response and which has the strong influence from the viscous effects due to the vortices that are generated by the bilge keels of the FPSO model (Avalos et al., 2014), whereas the other linear motion RAOs (surge, sway, yaw, heave and pitch) are largely governed by the inertia of the FPSO model.

Figures 3.8 to 3.13 show the RAOs for the six DOF in the Full Load condition. It is observed that the numerical analysis provides a good agreement with the experimental results.

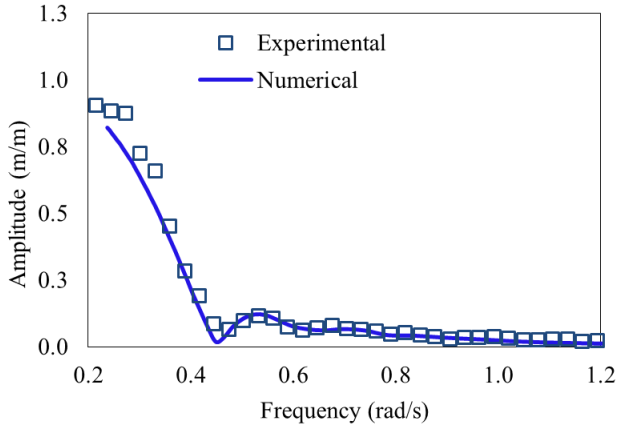

Figure 3.8 Surge RAOs for Full Load condition (Head seas condition)

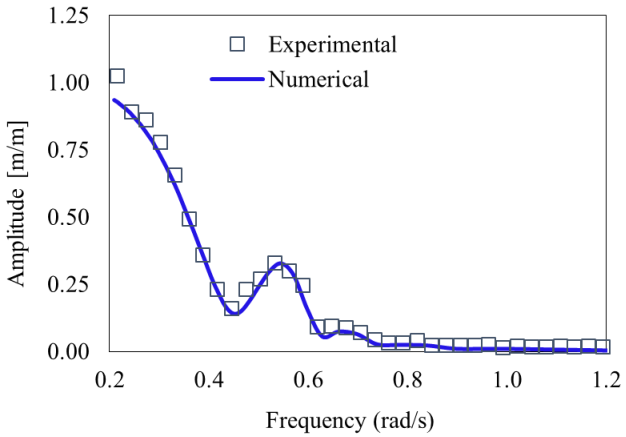

Figure 3.9 Heave RAOs for Full Load condition (Head seas condition)

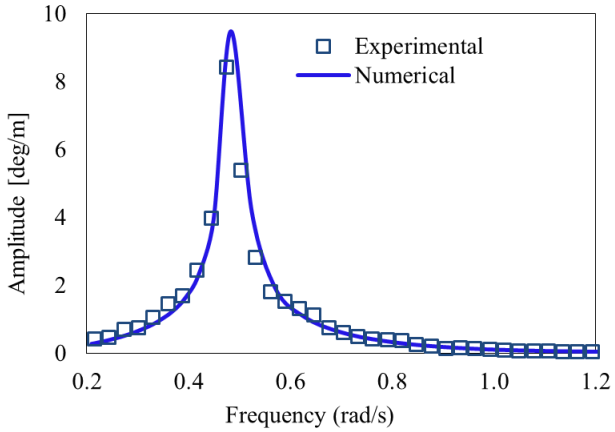

Figure 3.10 Roll RAOs for Full Load condition (Beam seas condition)

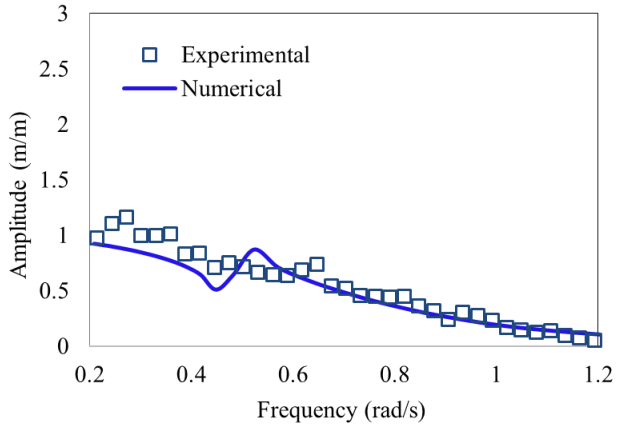

Figure 3.11 Sway RAOs for Full Load condition (Beam seas condition)

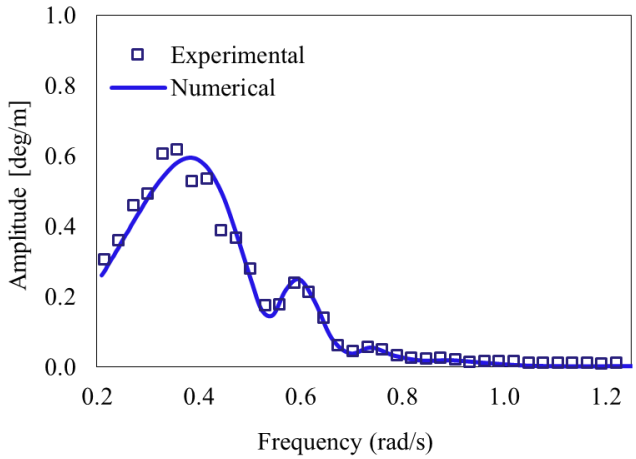

Figure 3.12 Pitch RAOs for Full Load condition (Head seas condition)

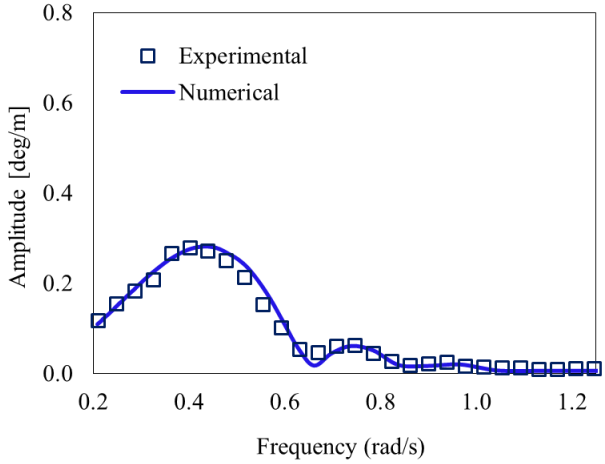

Figure 3.13 Yaw RAOs for Full Load condition (Quartering seas condition)

The added mass components for the uncoupled heave, roll and pitch motions were determined numerically for the radiation effect (Figures 3.14 to 3.16). The dimensional added mass for the pitch motion is seen to be the highest when compared to the heave and roll motions and is considered to be due to the higher hydrodynamic restoring force contribution. Moreover, the added mass values that were derived from the experimental decay tests were compared and observed to make good agreement with those numerically obtained for the associated natural frequency of the FPSO in the Full Load condition.

As a result, the RAOs and hydrodynamic coefficients of the FPSO numerical model were considered to be feasible for their use in the subsequent further stages of the numerical modelling. Additionally, the potential damping, drift damping, added mass and mean drift forces calculated numerically for the Full Load condition in the 6 DOF are presented in Appendix E.

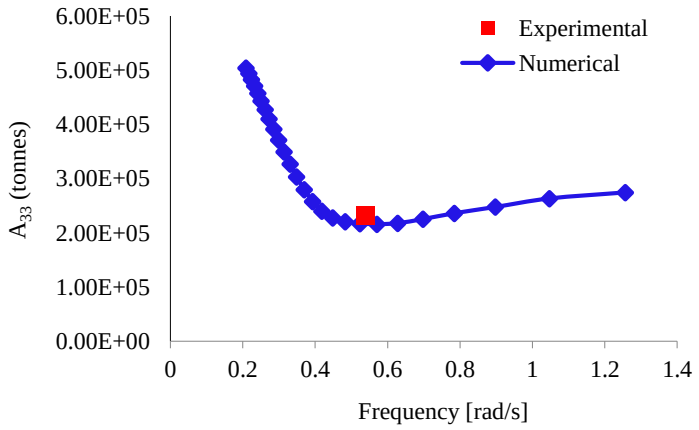

Figure 3.14 Heave added mass of the FPSO hull

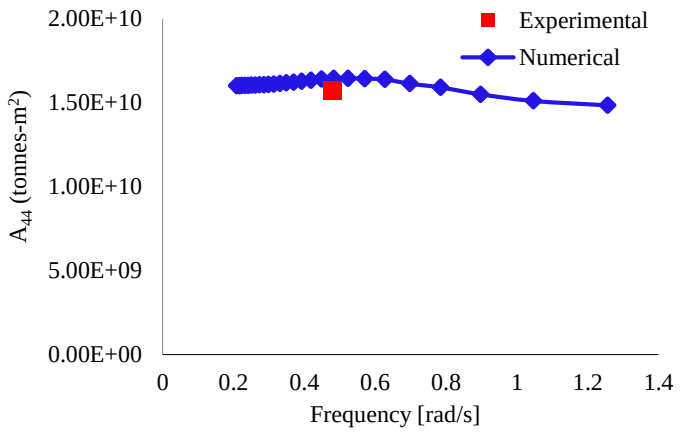

Figure 3.15 Roll added moment of the FPSO hull

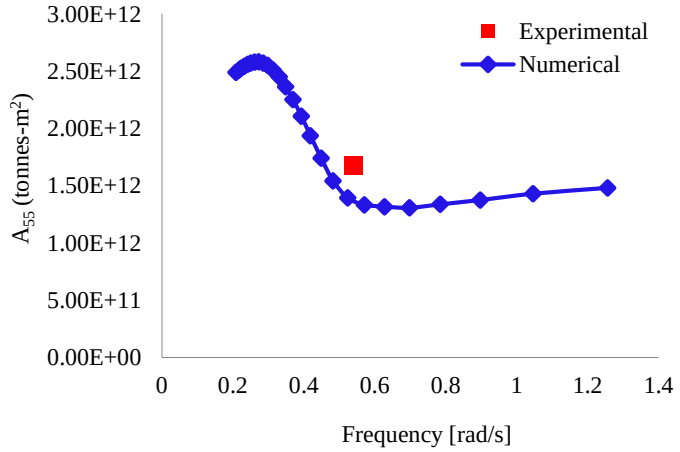

Figure 3.16 Pitch added moment of the FPSO hull

3.3.2 Restoring force/mooring/riser stiffness

A verification of the static restoring forces for the hull horizontal plane offsets obtained from the experiment results and the numerical design of the truncated mooring line and riser systems was undertaken. The two longitudinal surge directions (180-0 degrees) and the transverse sway direction (90 degrees) were compared as shown in Figures 3.17 to 3.19. The arrangements for the collinear 'In-line' and 'Between-lines' cases were used for validating the surge and sway directions. The comparisons of restoring forces *vs* offset between the experimental results and the numerical results are seen to have, in general, a good agreement in the two surge directions (0-180 degrees) while in the sway direction slight differences are

observed. In the same way, the critical mooring line tensions and critical riser tensions were compared and are also seen to be showing a good agreement. From these results, the horizontal plane restoring forces and the critical mooring line and riser tensions were considered to be reproduced satisfactorily in the FPSO numerical model for the truncated arrangement.

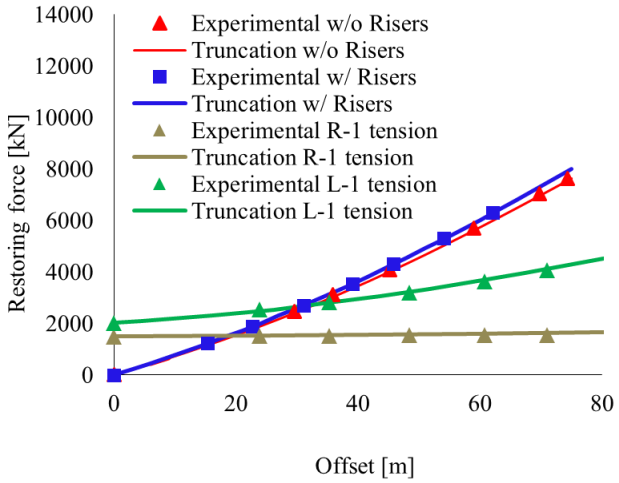

Figure 3.17 The horizontal restoring forces vs offset surge direction (180 degrees)

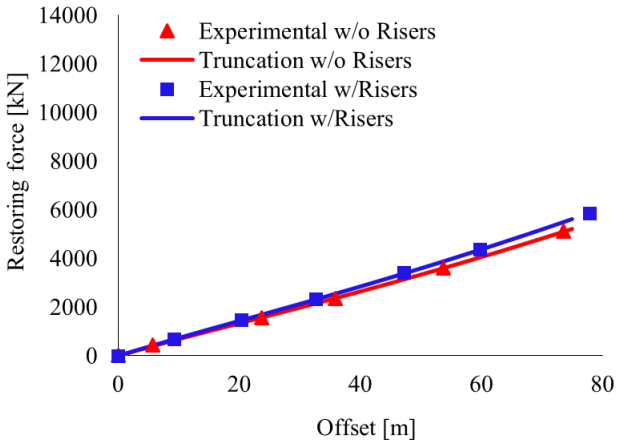

Figure 3.18 The horizontal restoring forces vs offset surge direction (0 degrees)

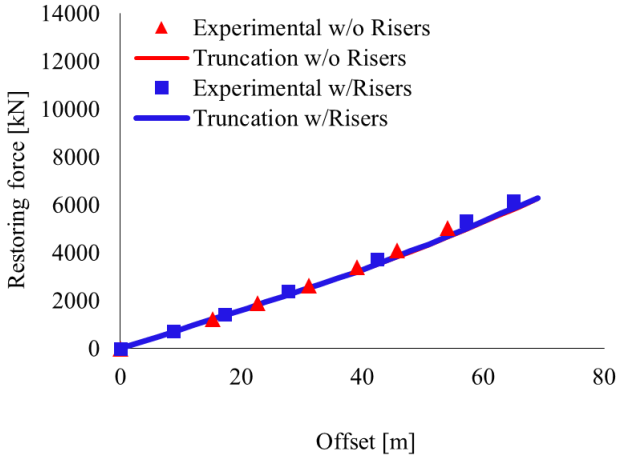

Figure 3.19 The horizontal restoring forces vs offset sway direction (90 degrees)

3.3.3 Decay tests

Eigen-periods and the damping level of the FPSO model with its mooring lines and risers for the collinear 'In-line' and the 'Between-lines' cases were calibrated through the data obtained from the experimental decay tests in calm water (Table 3.2). The normal drag and inertia coefficients for the components of the mooring lines and risers were set-up and established for the design according to their equivalent hydrodynamic diameter, Table 3.3 (DNV-RP-C205, 2007) Then, a total of four decay tests were created numerically. The source for the tuning of the viscous damping effects on the numerical model was obtained from the experimental decay tests that were undertaken in calm water for both the 'In-line' and the 'Between-lines' cases. Then, the FPSO hull numerical model on its own was calibrated using the linear damping results derived from the experimental decay tests (see i.e.: Figures 3.20 to 3.23).

Table 3.3 Hydrodynamic coefficients of the mooring lines and risers

Description	Symbol	Chain	Spiral/Strand	Riser
Drag normal	C_d	2.4	1.4	1.2
Added inertia	C_{in}	2.0	1.15	1.0

The decay time series from both experimental and numerical results indicate a good agreement for the eigen-periods and the level of damping of the system. The linear viscous damping used on the FPSO numerical model was 579 kNs/m for the surge direction derived from the experimental decay test in calm water. In the same way, the FPSO model with both

mooring lines and risers (FC-31 and FC-32) for the collinear 'In-line' and 'Between-lines' cases were also calibrated. In this case, the linear damping and quadratic damping values are used in the numerical calculations in order to reach a suitable damping level when compared with experimental model test results. It was observed that when the risers were incorporated in the calibration a non-linear damping effect should be considered. This may be partly due to that the truncated risers had a segment laying on the basin floor and which could result in an additional nonlinear damping component in the overall system. All of the decay test comparisons between the experimental results and those from the numerical model were in good agreement (see Figures 3.20 to 3.23).

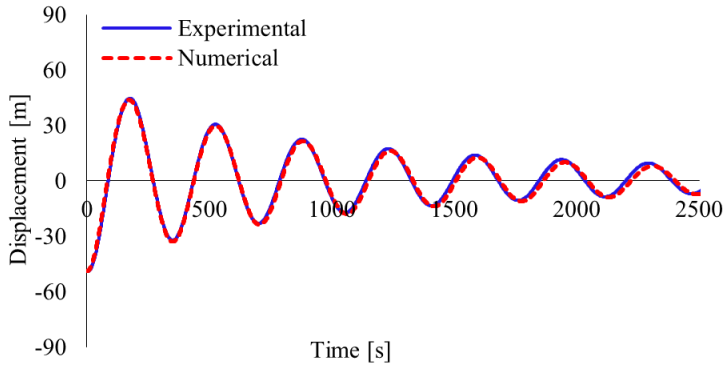

Figure 3.20 Experimental and numerical decay tests for the FPSO with mooring lines 'In-line' case, (FB11)

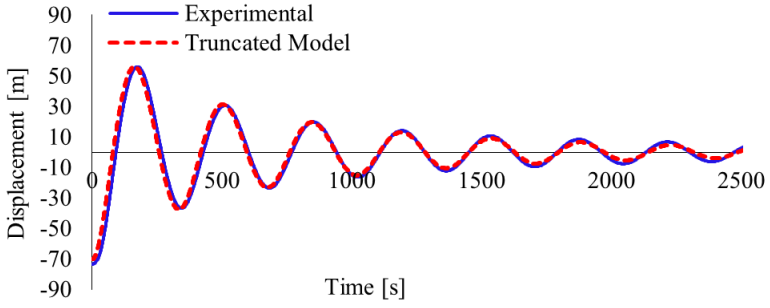

Figure 3.21 Experimental and numerical decay tests for the FPSO with mooring lines and risers 'In-line' case, (FC31)

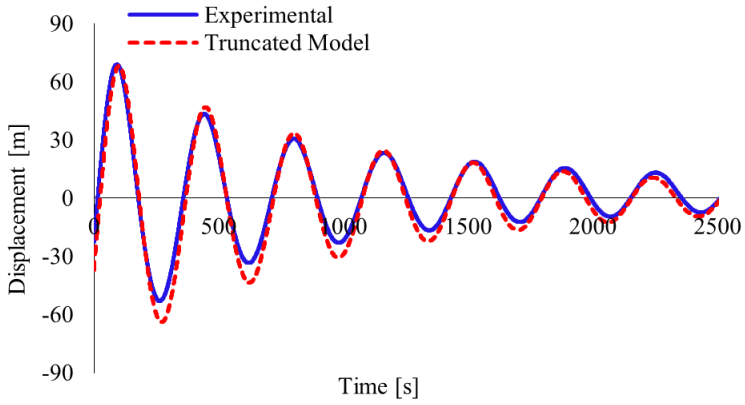

Figure 3.22 Experimental and numerical decay tests for the FPSO with mooring lines 'Between-lines' case, (FB13)

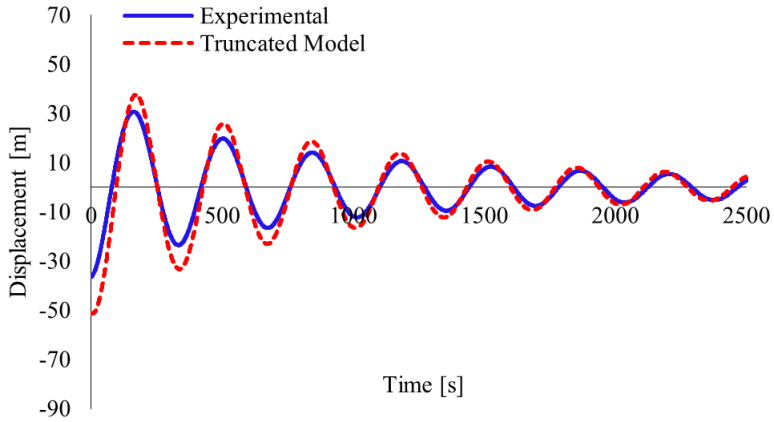

Figure 3.23 Experimental and numerical decay tests for the FPSO with mooring lines and risers 'Between-lines' case, (FC32)

3.4 Truncated modelling (Experimental results *vs* truncated models)

3.4.1 Collinear 'In-line' case, irregular waves only

A non-linear time domain coupled analysis was undertaken in order to validate the truncated numerical model in comparison with the experimental model test results. Subsequently, the surge motion responses and the dynamic response of the most loaded mooring line were both studied using both the Newman's approximation and the full QTF approach, for the collinear case. The FB16 case considered irregular waves only in the calibration process of the numerical truncated model. Then, the actual calibrated irregular waves measured in the basin were used as input in the numerical simulations. This was done in order to evaluate the numerical model

without incurring any additional uncertainties that may exist in the actual environment generation of the irregular waves in the test basin.

Newman's approach for the second-order wave forces was used for the initial calibration stage in order to save computation time. Fig. 3.24 shows the comparison between the experimental and the numerical truncated model results for the surge motion response obtained in time series method. The truncated model considered the viscous damping of the FPSO hull derived from the decay test in calm water. The drift damping was observed to be negligible which is in agreement with previous studies reported under moderate sea states in which viscous effects are dominate (Wichers, 1988). However, this assumption may only apply for deepwater FPSO installations, since in shallow waters and survival sea states the drift damping can be significant according to Luo et al., (2004) and Hermans (1999). In this study, the restoring forces from the mooring lines was considered while the effects of damping and the added mass were not taken into account. In other words, a decoupled analysis was undertaken in the first stage. The drag coefficients and the added mass coefficients affecting the mooring lines were not considered in the beginning of the analysis in order to simplify the calibration process and also to identify the level of the dynamics of the mooring lines which is mainly affected by the drag forces (Tahar and Kim, 2003). For this assumed condition, differences of a maximum of 20% were observed in the truncated model compared with the experimental results for the maximum extreme motion response identified in the low frequency (LF) motion in the surge direction.

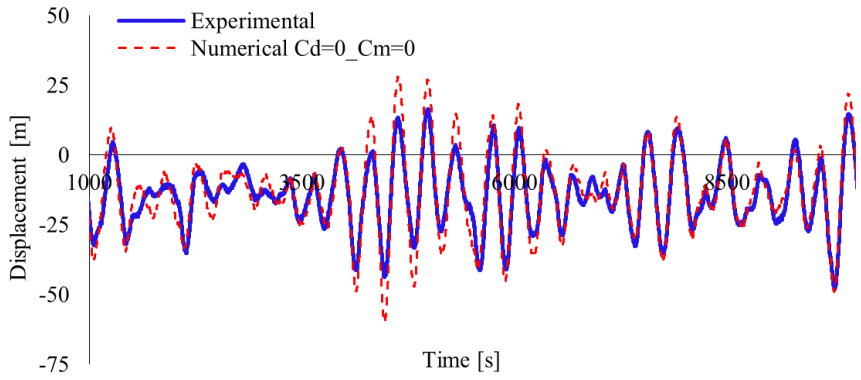

Figure 3.24 Comparison of the experimental model test vs truncated numerical model for the motion response in surge direction, excluding calculations involving Cd and Cm on the mooring lines (ie. C_d and C_m=0), (FB16)

For the tension response of the mooring lines, maximum differences of 18% were observed between the truncated model and the experimental results when the damping and added mass effects from the mooring lines are not considered (Figure 3.25). Subsequently, the main effort was to adjust empirically both the drag and the added mass coefficients in order to reach similar statistical standard deviations to those that the experimental results for tension response of the mooring lines produced. It was observed that the C_d and C_m coefficients as defined from the design for the chain and wire segments of the mooring lines (Table 3.3) showing a good agreement with the standard deviation of the experiment results for the mooring lines. Figures 3.26 to 3.28 show the comparison between the experimental results and the numerical simulation (truncated model) for the LF motion response and the response spectrum in the surge direction. It was observed that the mean drift force coefficients obtained from the Newman's approximation and those obtained from the full QTF and the damping levels in the truncated model system show a good agreement with the experimental results for the case using irregular waves. The motion response spectrum shows that only the LF range energy response has the total influence on the global response while the wave (WF) response contribution is seen to be negligible in surge direction (from 0.2-0.6 rad/s, see Figure 3.28).

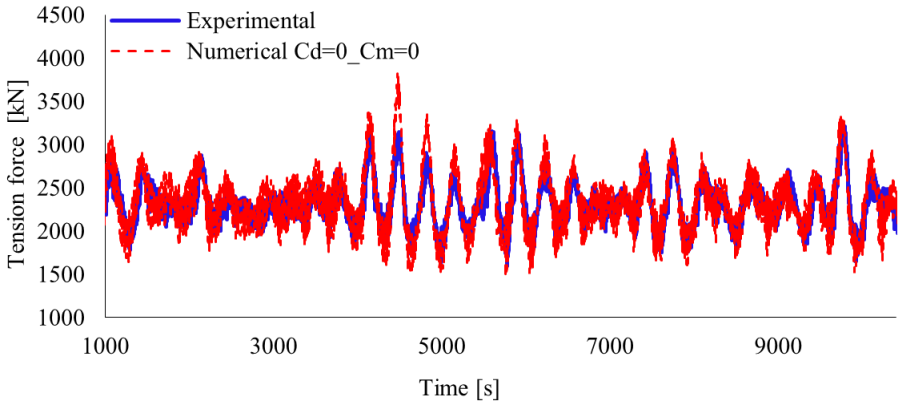

Figure 3.25 Comparison of the experimental model test vs truncated numerical model for the tension response most loaded mooring line (L-1), not including Cd and Cm on the mooring lines (ie. C_d and C_m=0), (FB16)

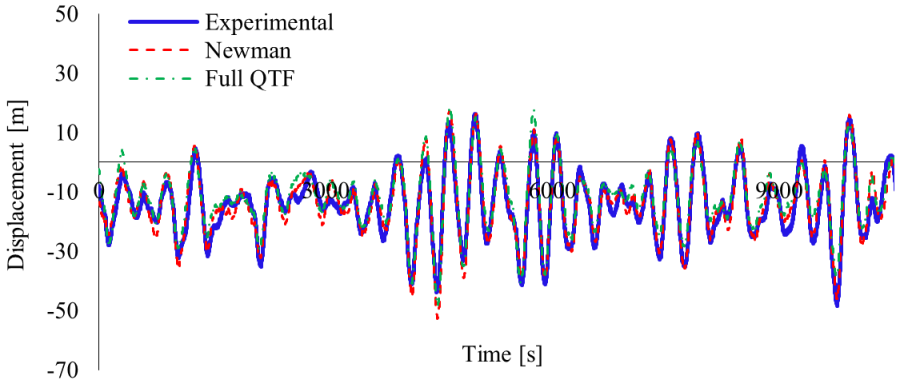

Figure 3.26 Comparison of the experimental model test vs truncated numerical model, FPSO with mooring lines, final calibration, (FB16)

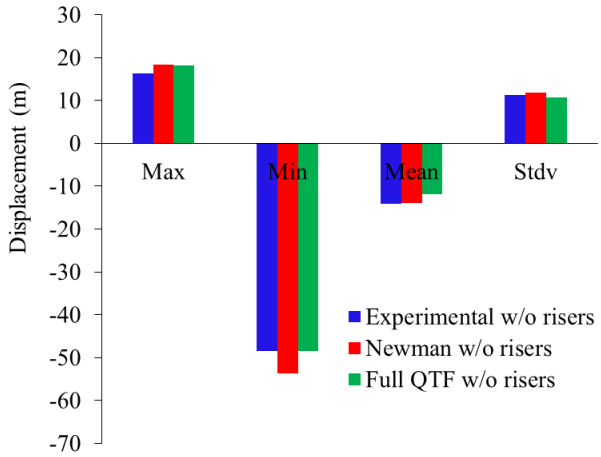

Figure 3.27 Statistics values comparisons of the surge motion response, experimental model test vs truncated numerical models, FPSO with mooring lines, final calibration, (FB16)

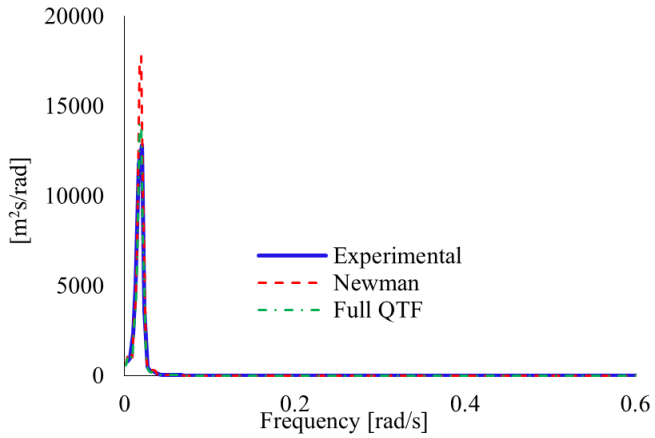

Figure 3.28 Comparison of the motion response spectra in the surge direction of the experimental model test vs truncated numerical model, FPSO with mooring lines, final calibration, (FB16)

Additionally, the most loaded mooring line (L-1) from the truncated model was also compared with the experimental results. The truncated model was observed to slightly over-predict (by 9 %) the measured maximum dynamic tension response (3541.21kN) when Newman's approximation was used compared to the experimental measurement (3242.98kN), while the full QTF results (3297.95kN) shows a good agreement with the experiment. It is also observed that the damping level is slightly under-predicted when the Newman's approach is used but it is still kept within reasonable limits as shown in Figures 3.29 to 3.30. It is to be noted that the tension response spectrum showed that the WF range energy response has not influenced on the loading in the mooring line while LF tension response governs the behaviour of the semi-taut mooring lines system (Figure 3.31).

The LF motion responses of the FPSO and maximum tensions in the most loaded line (L-1) show a good agreement (Figure 3.30) and the mean and standard deviation values also agree well. This indicates that the truncated model was calibrated successfully. Newman's approximation was observed to have handled well both the mean drift forces and the oscillation drift forces which, however, can be only for the specific environment loading condition that was used in the present study and clearly verification would need to be made for different conditions in terms of the wave H_S and T_s characteristics, (Ormberg, 1998).

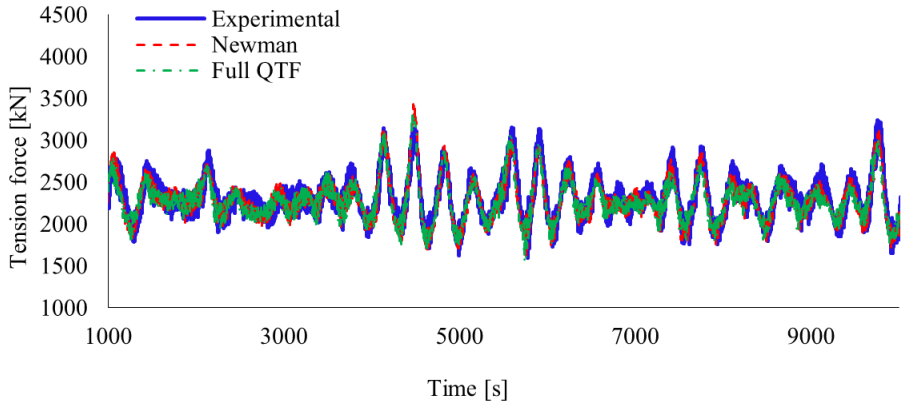

Figure 3.29 Comparison of the extreme tension response of the most loaded mooring line (L-1), experimental model test vs truncated numerical model, final calibration, (FB16)

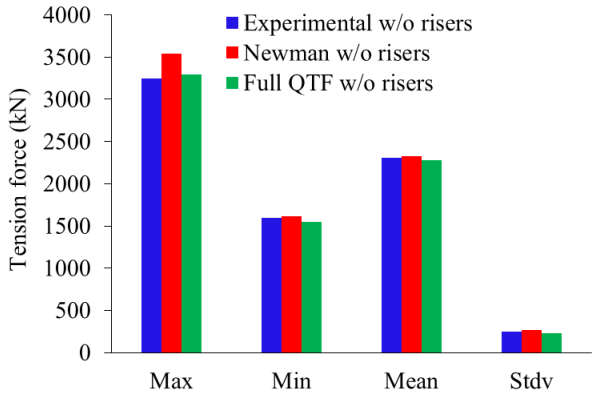

Figure 3.30 Statistics values comparison of the most loaded mooring line tension (L-1), experimental model test vs truncated numerical models, final calibration, (FB16)

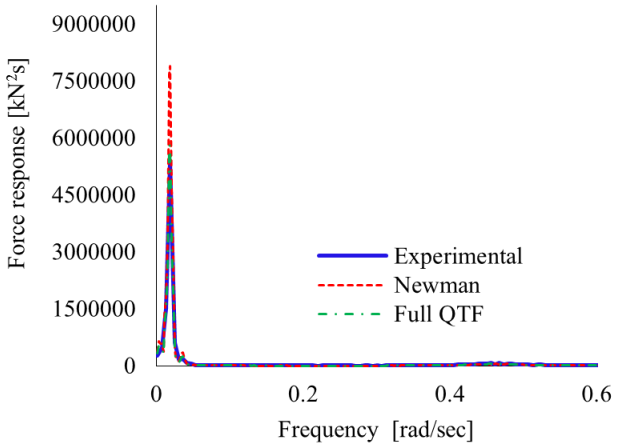

Figure 3.31 Comparison of the tension response spectrum of the most loaded mooring line (L-1) of the experimental model test vs truncated numerical model (FB16)

3.4.2 Results under collinear loading conditions: irregular waves + current + wind (FB19) (FC37)

A comparison of two collinear 'In-line' cases, specifically one with the FPSO with mooring lines only (FB19) and the other with the FPSO with both mooring lines and risers (FC37), was carried out. The statistical values for both the surge motions and the tensions of the most loaded mooring line and the most loaded riser were analysed. Both the experimental results and the numerical simulation results using the truncated numerical model were examined.

Since an in-situ test basin calibration with actually generated combined waves and current condition was not carried out, uncertainties in the estimation of the mean wave drift forces and the slow-drift forces with environmental data applied to the truncated numerical model were expected (Faltinsen, 1994; Chakrabarti, 2005). Thus, an evaluation using only the current to calibrate with the experimental results and, subsequently, repeated using the wind only was made for the various case studies. From this, it was useful to concentrate the efforts only on the mean wave drift force contribution in the estimation of the mean motion response for the head sea condition. The mean wave drift coefficients were slightly adjusted empirically according to Baarholm et al., (2004).

Moreover, the viscous damping value on the FPSO hull and the Cd values of the mooring lines and the risers were adjusted in the numeric model in order to provide a reasonable match to the standard deviations of the FPSO motions and tensions in the mooring lines and risers of the experimental results. This is due to the wave-current interaction increase the viscous damping and the drift damping contribution on the FPSO since the Reynolds number at model scale had changed.

The final calibration provided that the FPSO with mooring lines (FB16) with the Full QTF method show a good agreement for the mean and the extreme motion responses in the surge direction whilst Newman's approach predicted the mean drift forces well, but the dynamic motion (LF+WF) in surge direction was slightly over-predicted (6 %) compared with the experimental result (Figure 3.32 and Table 3.4).

In the case of the extreme tension response of the most loaded line (L-1), a good agreement in the mean and dynamic tension response for both the Full QTF and the Newman's approach has been achieved (Figure 3.33). In the same way, the numerical simulation for the wave frequency motion responses (heave and pitch) showed similar values compared with the experimental results (Table 3.4).

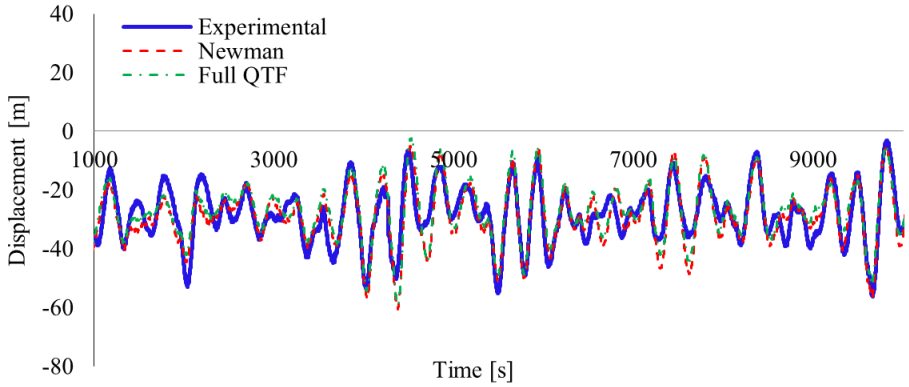

Figure 3.32 Extreme surge motion response of the FPSO with mooring lines, experimental vs numerical results (FB19)

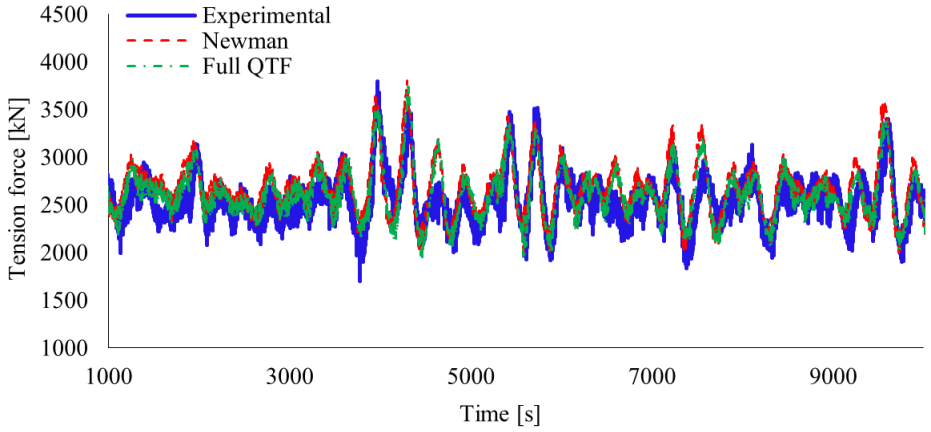

Figure 3.33 Extreme tension response of the most loaded line (L-1) for the FPSO with mooring lines (FB19), experimental vs numerical results

3.4.3. Influence of the risers (FC37)

The influence of the risers on the system dynamics of FPSO with mooring lines was also studied for the full dynamic collinear 'In-line' environment loading condition (irregular waves, current and wind). A comparison of the FPSO with mooring lines only (FB19) and the FPSO complete with mooring lines and risers (FC37) was carried out in order to determine the relative influence of the risers. For the FPSO model with mooring lines and risers, it was observed that the mean motion response decreased by approximately 28% compared to the FPSO with mooring lines only for the surge motion response. However, for the dynamic motion response (LF+WF) the differences between the two configurations were observed to be minimal (Table 3.4 and Figure 3.34).

In the case of the mooring line tension response, for the most loaded line (L-1), it was observed that there was a decrease of about 6% in the mean tension response compared with the system that did not include the risers, while the dynamic response for the full system of mooring lines and risers, it was seen that the influence of the risers was negligible (Table 3.4). This indicates that the risers influence is mainly on the mean motion response for the surge direction, while for the dynamic tension response of the most loaded line (L-1) the contribution from the risers was, again, to be relatively small when the total system is exposed to a full dynamic collinear environment loading condition (irregular waves, current and wind). The time series motion response in the surge direction and the tension response of the most loaded mooring line (L-1) were also reproduced well with the numerical simulation, as shown in Figures 3.34 and 3.35 respectively. The most loaded riser (R-1) was also examined for both experimental and numerical results and a good correlation was observed for both the statistical values and the underlying time series, the latter shown in Figure 3.36.

In the case of the most important WF motions for the collinear case, such as the heave and pitch, it was observed that the numerical results agree well with experimental data and that the risers do not affect significantly the WF motions response (Table 3.4).

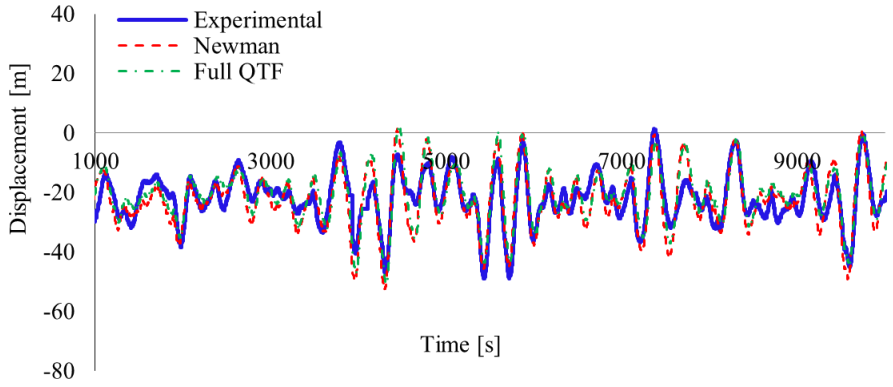

Figure 3.34 Extreme surge motion response of the FPSO with mooring lines and risers, experimental vs numerical results (FC37)

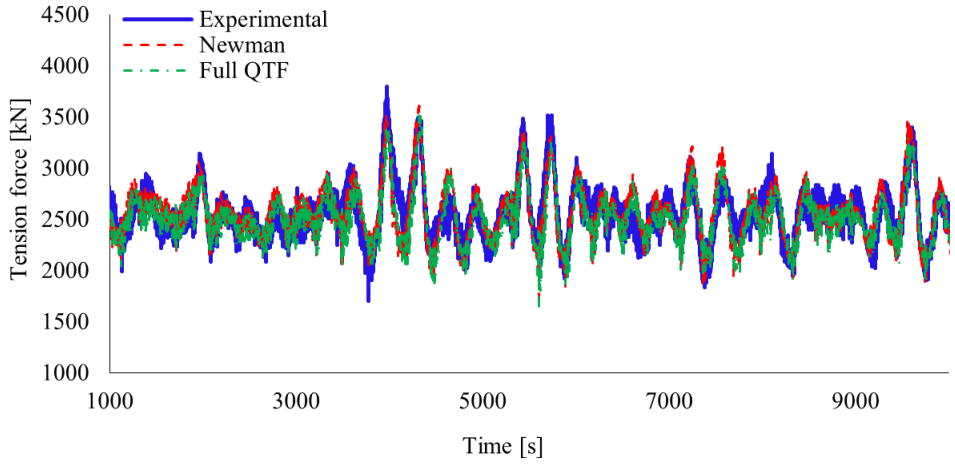

Figure 3.35 Extreme tension response of the most loaded mooring line (L-1) for the FPSO with mooring lines, experimental vs numerical results (FC37)

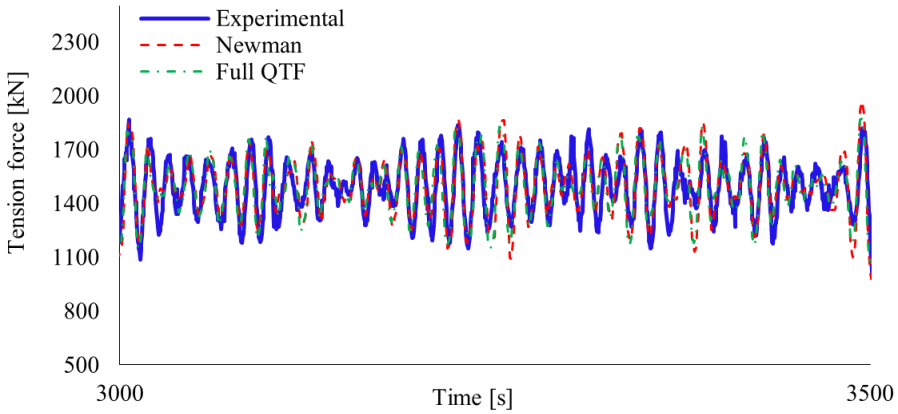

Figure 3.36 Extreme tension response of the most loaded riser (R-1) for the FPSO with mooring lines and risers, experimental vs numerical results (FC37)

Table 3.4 Comparison of experimental vs numerical results, collinear 'In-line' environment condition of irregular waves + current + wind

Experimental vs Numerical irregular waves + current + wind							
Description	'In-line' Case						
	Statistical	FPSO-mooring lines (FB-19)			FPSO-mooring lines-risers (FC-37)		
		Experimental	Newman	Full QTF	Experimental	Newman	Full QTF
Surge (m)	Max	-3.92	-4.87	-4.89	1.02	1.31	2.10
	Min	-56.93	-59.97	-58.49	-50.90	-53.01	-50.77
	Mean	-28.86	-28.74	-27.18	-22.56	-22.61	-20.89
	Stdv	9.16	9.30	8.84	8.49	10.05	9.28
Heave (m)	Max	2.07	2.01	2.18	2.19	2.07	2.22
	Min	-2.37	-2.40	-2.44	-2.53	-2.25	-2.28
	Mean	-0.11	-0.12	-0.12	-0.15	-0.01	-0.10
	Stdv	0.60	0.59	0.61	0.59	0.58	0.60
Pitch (deg)	Max	3.09	2.94	3.20	3.11	3.30	2.95
	Min	-2.90	-2.85	-2.91	-3.04	-2.76	-2.80
	Mean	0.02	0.10	0.10	0.02	-0.07	0.00
	Stdv	0.80	0.75	0.77	0.79	1.06	0.76
L1 (kN)	Max	3729.23	3812.54	3760.91	3598.29	3606.52	3520.61
	Min	1915.24	1921.86	1908.51	1802.29	1717.90	1649.24
	Mean	2665.07	2698.54	2654.31	2508.06	2561.12	2514.78
	Stdv	276.84	273.82	258.04	253.64	275.05	251.49
R1 (kN)	Max	NA	NA	NA	2127.60	2175.29	2194.6
	Min	NA	NA	NA	943.00	835.56	748.27
	Mean	NA	NA	NA	1499.15	1497.22	1494.40
	Stdv	NA	NA	NA	161.81	142.11	146.61

3.4.4 Comparison of collinear 'In-line' (FC37), 'Between-lines' (FC38) and the Non-collinear (FC39) environments

The cases of collinear and non-collinear under irregular waves, current and wind are studied to further examine the hydrodynamic behaviour of the complete FPSO system under different environments. The time series analyses are carried out in order to make comparisons in terms of the statistical properties such as the mean, minimum and maximum values and the associated standard deviation for each of the six DOF motions of the FPSO with mooring lines and risers. The surge motion is examined in particular to evaluate the results through both the experimental measurements and the corresponding numerical results using the Newman's approximation.

The maximum motion responses were observed to be in the LF range for the entire environment loading cases studied. The maximum motions occurred in the surge direction due to the mooring line/internal turret system, which allowed the FPSO to rotate freely about the moorings and riser, similar to a weather vane and point in the direction of least resistance against the various combined components in the environment loading conditions.

The highest surge motion responses of -76.75 m (experimental) and -78.45 m (numerical) occurred in the non-collinear case, even though small differences were perceived compared with the collinear 'Between-lines' condition (-75.53 m, experimental and -78.90 m, numerical) and higher differences were perceived as compared to the corresponding collinear 'In-line' condition (-50.90 m, experimental and -53.01 m, numerical) as shown Figure 3.37.

The highest mean value of the surge motion response was also observed to be higher in the non-collinear case (-42.09 m, experimental, and -45.77 m numerical). Clearly the 'negative' values in the surge motions indicate that the vessel is moving in an aft-wards direction, the reciprocal to the conventional forwards motion surge sense, as a result of the weather vane rotation about the turret. This behaviour is mainly due to the non-collinear environment loading condition, with the current at 90 degrees relative to the incident waves, which increased the energy of the incident irregular waves (Chakrabarti, 2005). The interaction of the waves-current-wind loads increase both the steady wave drift force and the slow-drift forces on the FPSO in the non-collinear case.

Moreover, the FPSO under the non-collinear environment experienced a higher hydrodynamic force occurring with the crest of the water surface since the ratio between the FPSO vessel length and the average wave length is less than one introducing an extra influence in increasing the WF motion.

The maximum mean tension was observed in the collinear 'In-line' case (L-1, 2508.06 kN, experimental and 2560.71 kN, numerical), even though, small differences were observed compared with the non-collinear and 'Between-lines' cases (Figure 3.38).

The dynamic tension response under the non-collinear environment shows the maximum tension forces approximately 6 % compared with the collinear 'In-lines' and 28 % compared with the collinear 'Between-lines' cases respectively. Furthermore, tension in the most loaded riser (R-1) (2364.77 kN, experimental and 2461.62 kN numerical) was perceived in the non-collinear case where the differences were observed mainly in the dynamic component ('In-line' (R-1) 2127.60 kN, experimental and 2178.65 kN, numerical; 'Between-lines' (R-4) 2147.79 kN, experimental and 2191.92 kN, numerical). For the mean tension response, significant differences were not perceived compared to the collinear cases (Figure 3.39). In general, the numerical results using the full dynamic loading condition (irregular waves, current and wind) for collinear cases agree well with the experimental measurements. This was evident not only in the statistics of the motions and forces, but also in the time series (Figures 3.37 to 3.42).

On the other hand, the maximum statistical values obtained from the numerical simulation for the non-collinear case showed reasonable agreement with the experimental results, but differences were observed in the underlying time series mainly for the plane horizontal motion responses (surge, sway and yaw) due to stronger non-linear behaviour compared to the collinear cases (Figures 3.43 to 3.45). It may be attributed to the following reasons: an unsteady motion behaviour of the moored FPSO especially the performance of the internal turret with the mooring system in large yaw motion response which makes difficult to predict the motion response; the non-linear behaviour due to the mechanism from the wave-current interaction, which increases both the mean wave drift forces and the slow-drift force oscillations on the FPSO compared to the collinear conditions (Wichers, 1988; Faltinsen, 1994; Stansberg, 2013; Ma et al., 2015); and additionally the lacking of the wave-current calibration, which was not used as input data in the numerical simulation increasing the uncertainties in the environment

loading condition used in the numerical simulation. However the tension force response for the most loaded mooring line (L-1) and the riser (R-1) from the numerical simulation shows a reasonable correlation to the experimental results (Figures 3.46 and 3.47).

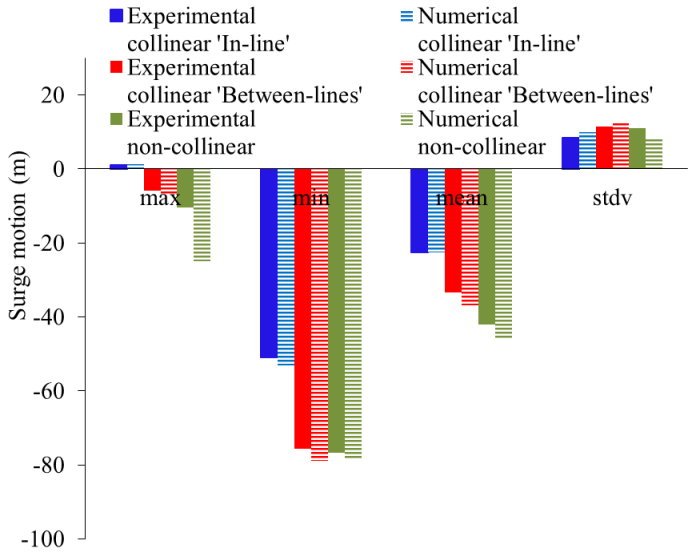

Figure 3.37 Statistics values comparison of surge motion response, experimental model test vs numerical simulation, final calibration

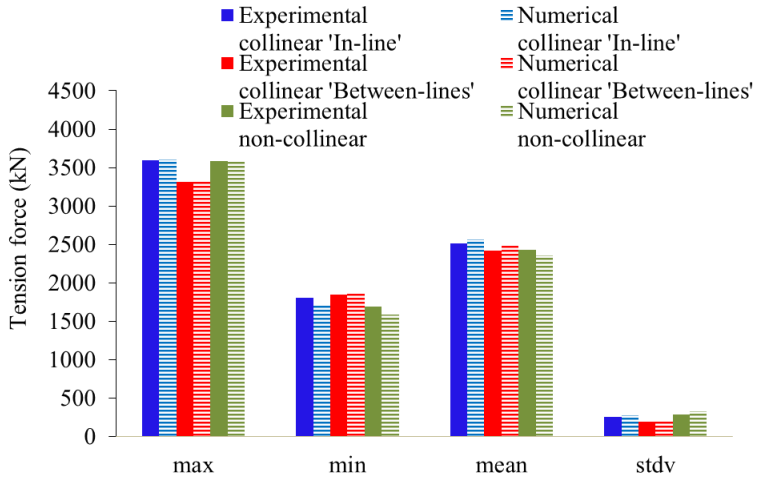

Figure 3.38 Statistical values comparison of the most loaded mooring line tension (L-1) for the 'In-line' and non-collinear cases and (L-7) for the 'Between-lines' case, experimental model test vs truncated numerical models, final calibration

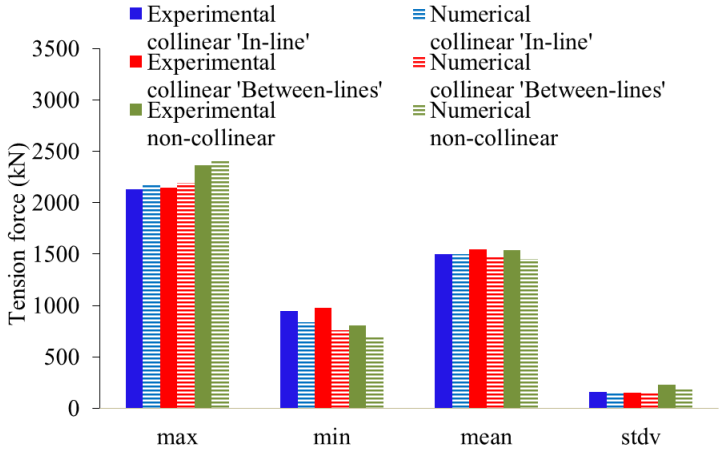

Figure 3.39 Statistical values comparison of the most loaded riser tension (R-1) for the 'In-line' and non-collinear cases and (R-4) for the 'Between-lines' case, experimental model test vs truncated numerical models, final calibration

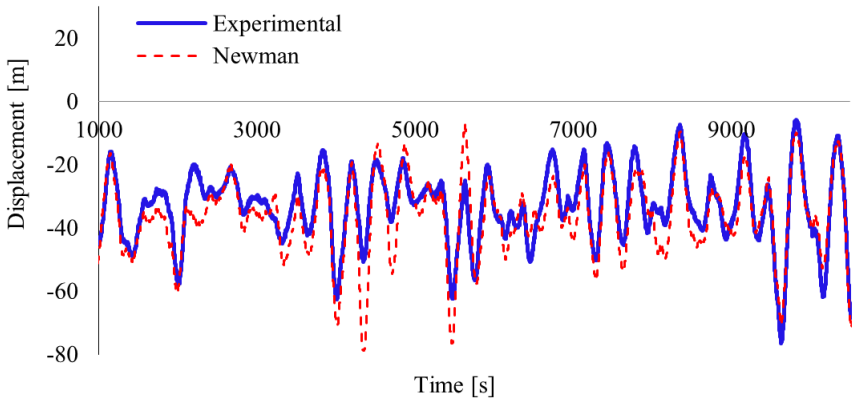

Figure 3.40 Comparison of the surge motion response, experimental vs numerical results, 'Between-lines' case, for the configuration FPSO model with mooring lines and risers, (FC38)

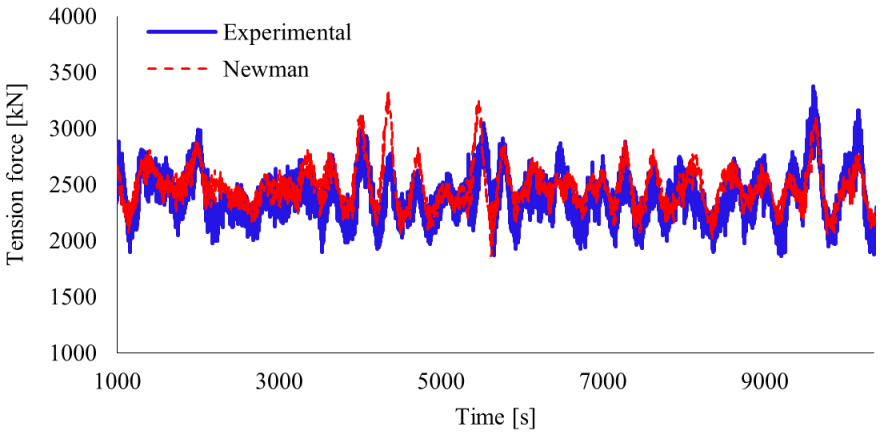

Figure 3.41 Comparison of the extreme tension response of the loaded mooring line (L-7), 'Between-lines' case, experimental vs numerical results, (FC38)

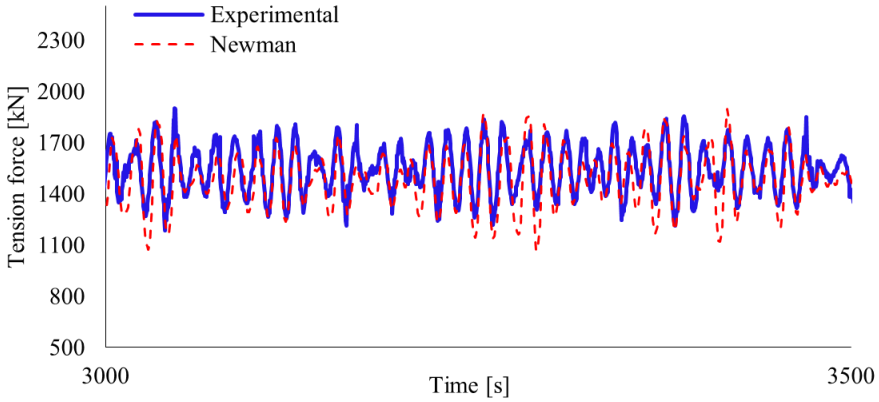

Figure 3.42 Comparison of the extreme tension response of the most loaded riser (R-4), 'Between-lines' case, experimental vs numerical most loaded riser (FC38)

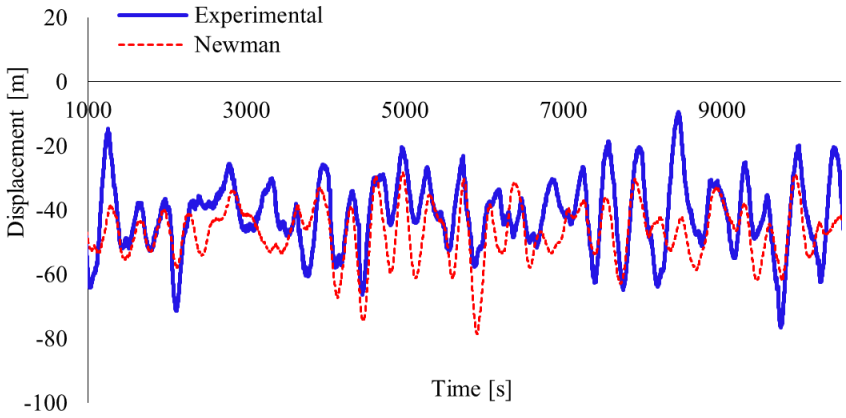

Figure 3.43 Comparison of the surge motion response, experimental vs numerical results, 'Non-collinear' case, for the configuration FPSO model with mooring lines and risers, final calibration (FC39)

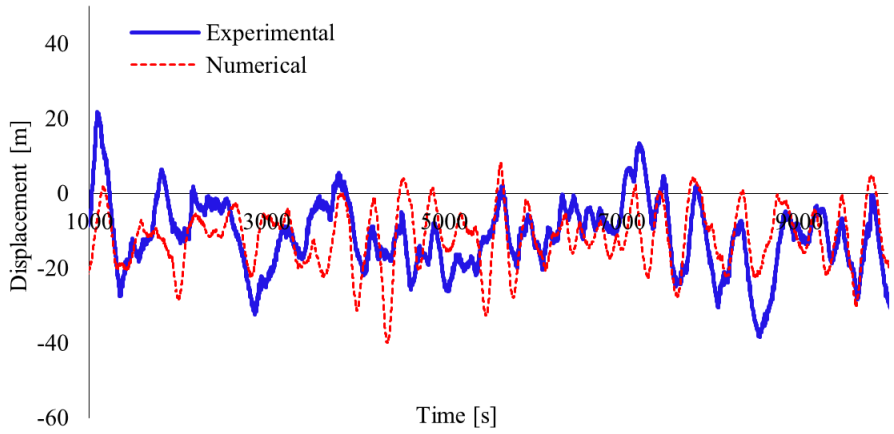

Figure 3.44 Comparison of the sway motion response, experimental vs numerical results, 'Non-collinear' case, for the configuration FPSO model with mooring lines and risers, final calibration (FC39)

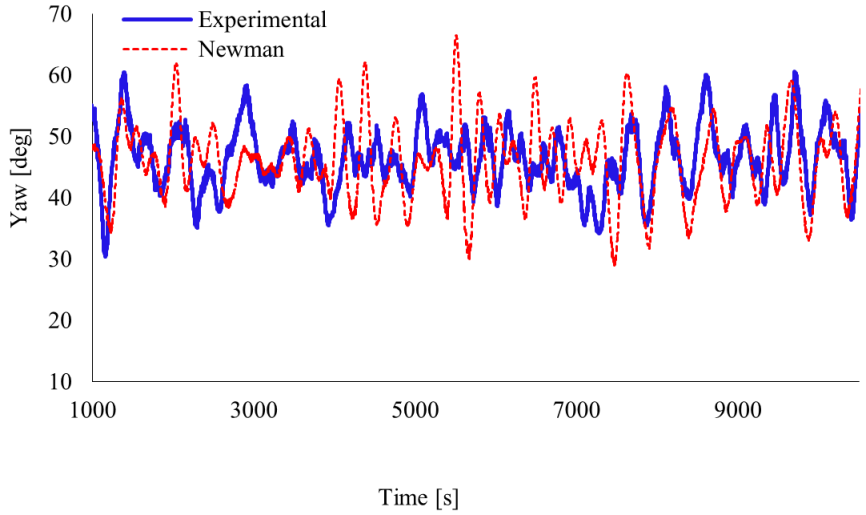

Figure 3.45 Comparison of the yaw motion response, experimental vs numerical results, 'Non-collinear' case, for the configuration FPSO model with mooring lines and risers, final calibration (FC39)

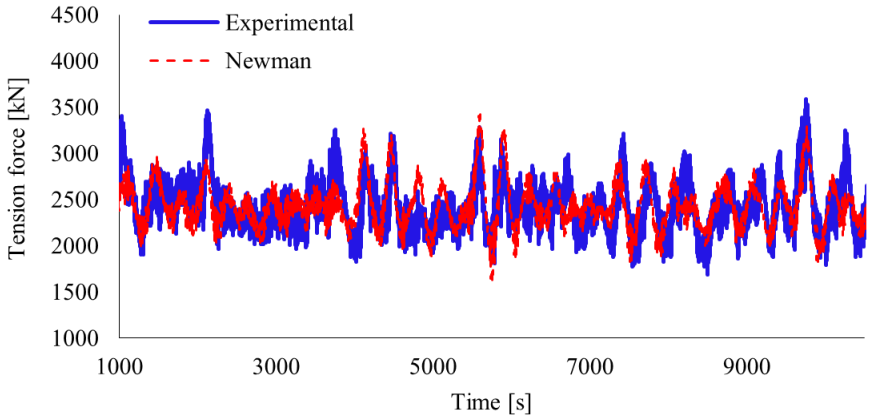

Figure 3.46 Comparison of the extreme tension response of the most loaded mooring line (L-1), for the 'Non-collinear' case, experimental vs numerical results (FC39)

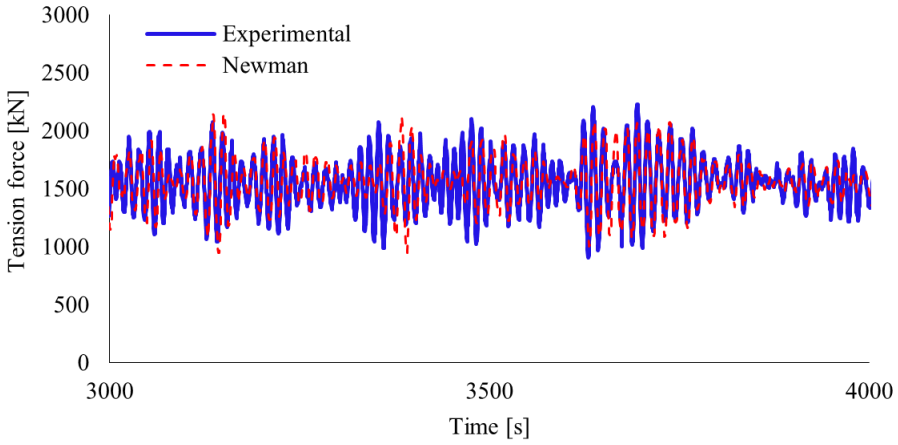

Figure 3.47 Comparison of the extreme tension response of the most loaded riser (R-1), for the 'Non-collinear' case, experimental vs numerical (FC39)

3.5. Truncated model *vs* full depth prototype model

After the rigorous validation, the truncated numerical model was then extrapolated to full depth prototype. The extrapolation of the test results of motions and loads to the full-scale is mainly on the basis of the Froude scaling law, which means the similarity of the gravitational force and inertia force was satisfied and Reynolds number effects are neglected. This was because of the dominance of these forces over the viscous force in the behaviour of large-volume structures such as FPSO in ocean waves. However, the viscous damping may be a dominant factor on particular motions, such as roll motion and low-frequency horizontal motions of the FPSO. In this situation, the viscous damping is related to the dynamic viscosity and thus had significant Reynolds number effects on the extrapolation of the test results. Owing to the limitation of the physical dimensions of testing facilities, it can be difficult to prevent the scale effect with respect to the viscosity. The realistic approach is to choose the model scale as large as possible in order to minimise Reynolds number effects which is the way that the coupled FPSO-mooring-riser system model (1:64) was designed.

The linear damping values of the FPSO and the drag coefficients of the mooring lines and risers extracted from the truncated numerical model validated were then used in a straightforward manner in the full depth numerical model in order to study the dynamics of the complete system in the full depth installation Table 3.5 and Table 3.6.

Table 3.5 Linear damping values of the truncated numerical model (FPSO hull model) for collinear and non-collinear environment loading conditions.

Condition	Surge kN/(m/s)	Sway kN/(m/s)	Heave kN/(m/s)	Roll kNm/(deg/s)	Pitch kNm/(deg/s)	Yaw kNm/(deg/s)
FPSO Collinear environment	700	0	0	190000	0	0
FPSO Non-collinear environment	579	900	0	190000	0	14000

Table 3.6 Hydrodynamic coefficients of the mooring lines and risers validated with experimental results for the collinear and non-collinear environment loading conditions

Description	Symbol	Chain	Wire (Spiral/Strand)	Riser
Drag normal	C_d	2.8	2.0	1.8
Added inertia	C_{in}	2.0	1.15	1.5

The truncated numerical model was then extrapolated to full depth prototype, the objective was verify the dynamics of the mooring lines and risers through a nonlinear time domain coupled analysis of the FPSO with the complete mooring line and riser systems in full water depth. The results for both the horizontal motion response of the FPSO in the surge direction, the WF motions and the tension responses of the most critical mooring lines and risers for four significant design controlling targets, were studied through separation of the LF and the WF components in the overall motion responses and tensions. The cut-off frequency for the low pass and high pass filtering was chosen at 0.033Hz (30 secs). The motion responses of the FPSO were normalized to the total maximum surge response from the truncated model for LF and maximum heave motion from the truncated model for WF, while the critical values of the mooring line tension and riser tension were normalized to the total maximum tension response of the truncated model.

$$\bar{X} = {}^{X_{WF\ or\ LF}}/_{X_{total}} \tag{3.50}$$

where $\bar{X}$ is the normalized quantity, $X_{WF\ or\ LF}$ the statistic values (WF or LF component) and X_{total} of truncated model (total motion response or total tension response) (Baarholm, 2004).

3.5.1 Collinear 'In-line' case with irregular waves only (FB16)

Table 3.7 shows that the total surge motion response is over-predicted around 26 % by the truncated model compared to the full depth model. Among the total surge motion, the LF motion component is seen over predicted approximately 25 % by the truncated model compared to that of the full depth prototype model. This is due to the increment of the mooring line length increases the drag forces acting as damping in the full depth prototype model.

As can be seen in Table 3.7, the WF motion component is relative small compared to the LF response component for both the truncated and the full depth models as was expected. The total time series responses in the surge and in the spectra response by both the truncated model and the full depth model are illustrated in Figures 3.48 to 3.49.

For heave and pitch motion responses, both the LF and the WF components obtained by the truncated model and the full depth model are reasonably similar, in other words, they do not show significant differences which indicates that dynamics of the mooring lines having less

effect on these motion responses provided that the truncation model being properly designed (Table 3.7).

For the dynamics of the mooring lines, the most loaded line (L-1) was analysed. Differences in dynamic components of LF and WF tension responses were observed between the truncated model and full depth model (Figures 3.50 to 3.52). Specifically, the LF component of the tension response is over predicted approximately 22% by the truncated model compared to the full depth model while the WF component tension predicted by the truncation model is significantly smaller compared to that of the full depth model in a range of frequency from 0.4 to 0.6 rad/s associated to the wave frequency of the incident wave (Figure 3.51).

Table 3.7 Normalized statistics values for Collinear 'In-line' case irregular waves only (FB16)

	Description	FPSO with Mooring lines only					
		Truncated model			Full depth model		
Collinear 'In-Line' irregular waves only		LF	WF	Total	LF	WF	Total
	Surge	0.993	0.116	1.000	0.744	0.071	0.744
	Heave	0.116	0.971	1.000	0.147	0.914	0.978
	Pitch	0.119	1.276	1.276	0.151	1.258	1.298
	L-1	0.974	0.077	1.000	0.799	0.330	1.028

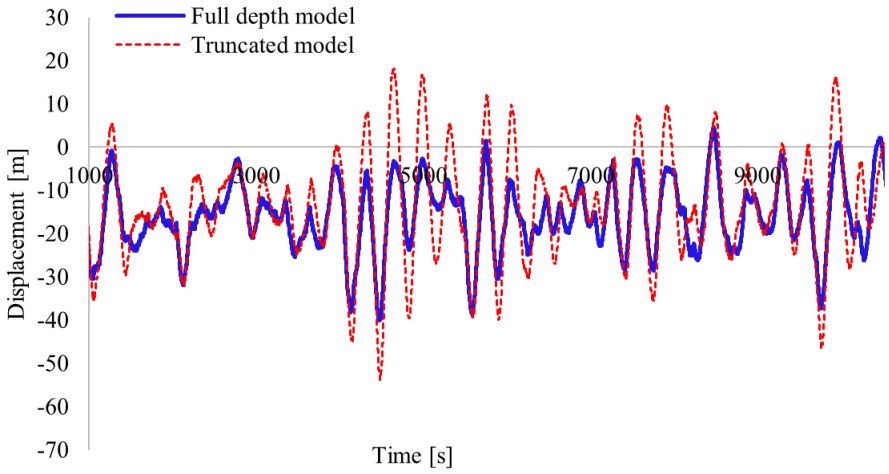

Figure 3.48 Surge motion response of the 'In-line' case (irregular waves only), truncated model vs full depth prototype model, (FB16)

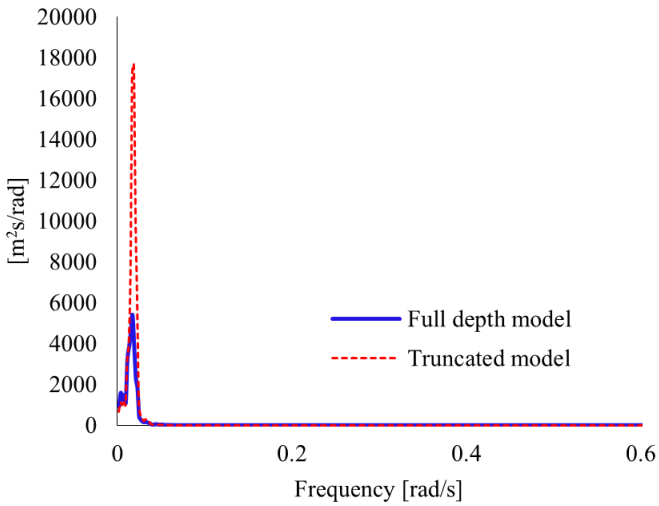

Figure 3.49 Surge motion response spectra of the 'In-line' case (irregular waves only), truncated model vs full depth prototype model, (FB16)

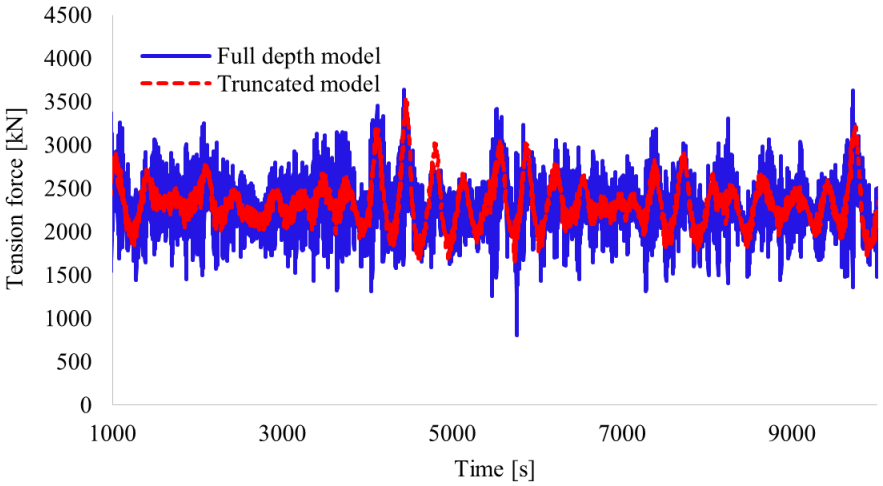

Figure 3.50 Comparison of the tension response for the most loaded mooring line (L-1), truncated model vs full depth model, for the collinear 'In-line' case (FB16)

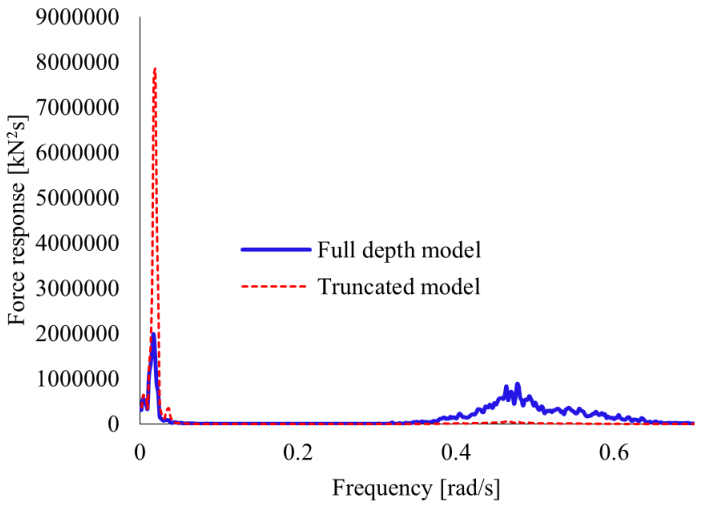

Figure 3.51 Line tension response spectra (L-1) of the 'In-line' case (irregular waves only), truncated model vs full depth prototype model, (FB16)

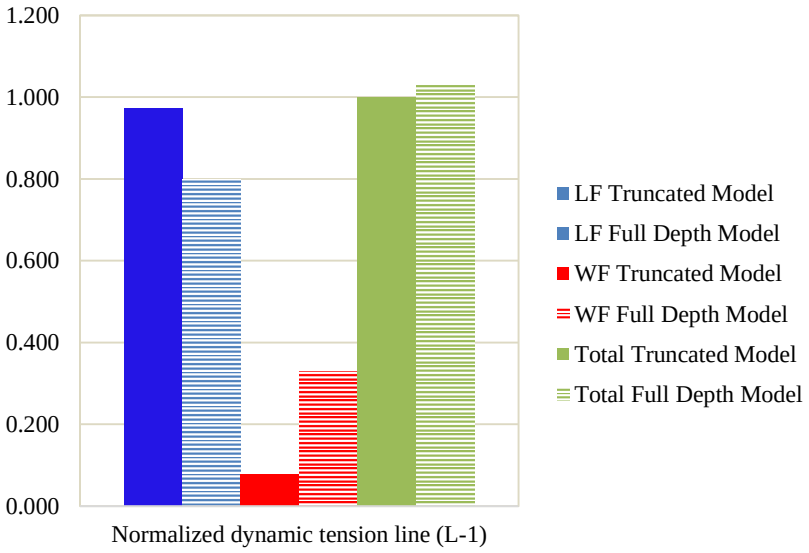

Figure 3.52 Normalized dynamic tension line components of the most loaded mooring line (L-1), for the collinear 'In-line' case (FB16)

3.5.2. Collinear 'In-line' case with irregular waves + current + wind (FB19)

The collinear 'In-line' case with irregular waves, current and wind was studied. The dynamic components of the LF and WF motions in the surge direction predicted by the truncated model and the full depth model were observed to be of the same order of magnitude. For the WF heave and pitch motions, it was also observed that they are only slightly affected

by the dynamics of the lines. In the case of the most loaded mooring line (L-1) the truncated model over predicts the dynamic LF component response (13%) while the dynamic WF component was under-predicted compared to those of the full depth model. As a result the total tension difference (LF+WF combined) of the truncated model is under predicted about 7% compared with that of the full depth model as shown in Table 3.8 and Figures 3.53 to 3.57. It is seen that, by including wind and mainly current load in the analysis, the difference in the dynamics of the mooring lines between the truncated model and full depth model increases compared to the case of the system under the irregular waves only. Furthermore, for the LF surge motion response, the differences between truncated model and full depth model slightly decrease compared to the case of system under irregular waves only.

Table 3.8 Normalized statistics values for Collinear 'In-line' case irregular waves, current and wind (FB19)

Collinear 'In-Line' irregular waves+current+wind	Description	FPSO with Mooring lines only					
		Truncated model			Full depth model		
		LF	WF	Total	LF	WF	Total
	Surge	0.979	0.057	1.000	0.916	0.053	0.916
	Heave	0.136	0.962	1.000	0.081	0.907	0.919
	Pitch	0.165	1.237	1.233	0.119	1.192	1.199
	L-1	0.976	0.066	1.000	0.861	0.311	1.072

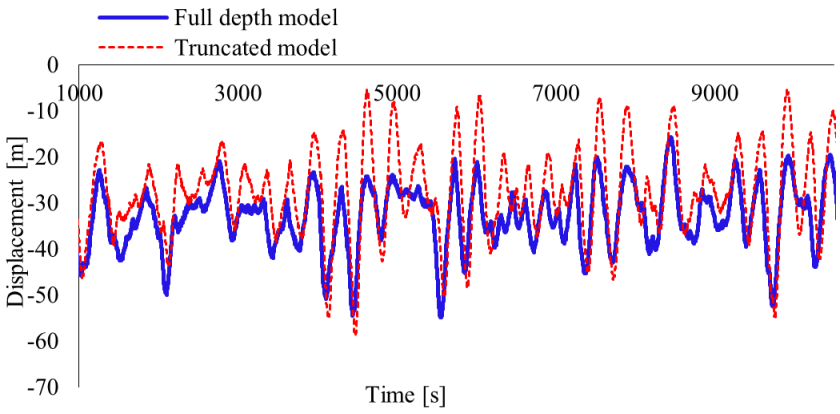

Fig. 3.53 Surge motion response of the 'In-line' case (irregular waves+current+wind), truncated model vs full depth prototype model, (FB19)

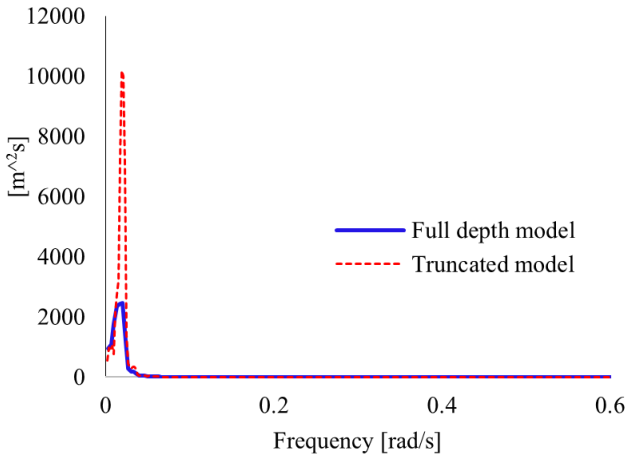

Figure 3.54 Surge motion response spectra of the 'In-line' case (irregular waves+current+wind), truncated model vs full depth prototype model, for the collinear 'In-line' case (FB19)

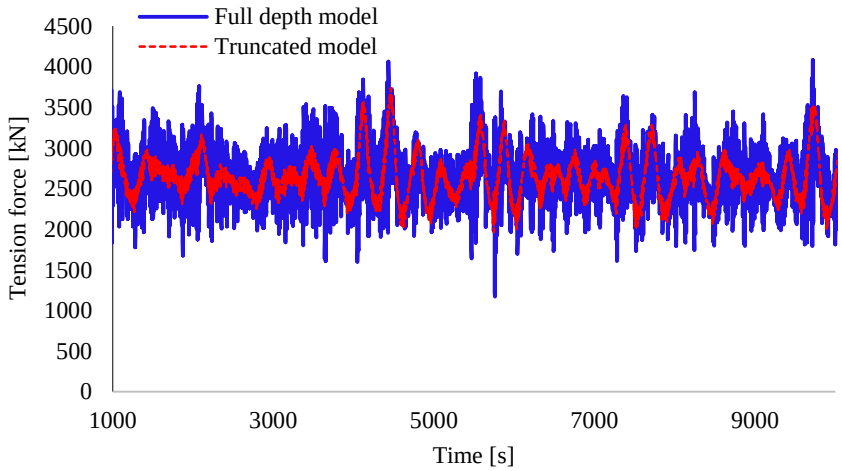

Figure 3.55 Comparison of the tension response for the most loaded mooring line (L-1) truncated model vs full depth prototype model, for the collinear 'In-line' case (FB19)

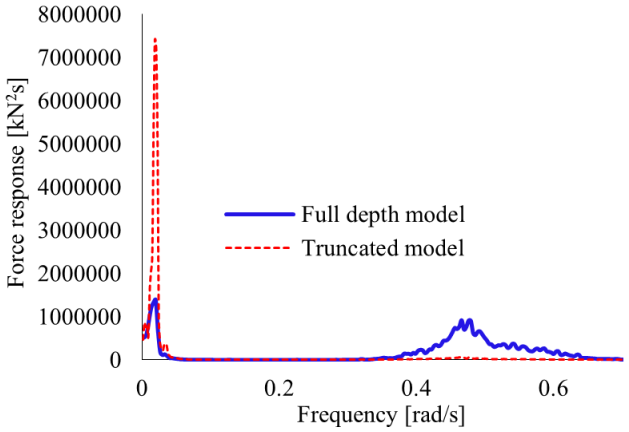

Figure 3.56 Line tension response spectra (L-1) of the 'In-line' case (irregular waves+current+wind), truncated model vs full depth prototype model, (FB19)

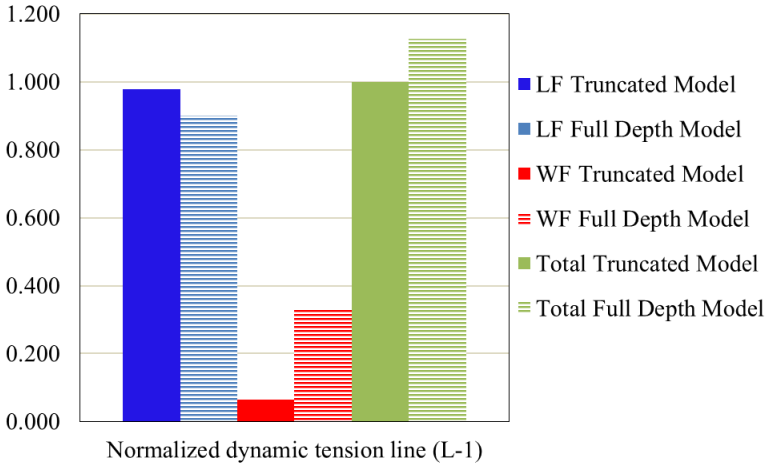

Figure 3.57 Normalized dynamic tension line components of the most loaded mooring line (L-1), fort the collinear 'In-line' case (FB19)

3.5.3 Influence of risers (FC37)

Table 3.9 shows the influence of the risers on the dynamics of the overall system (FC37). Similar to the influence from the mooring system, the WF motion responses in heave and pitch show only slight differences by including the risers in the system. The truncated model and the full depth model show the same tendency in their differences in results as in the other previous cases, since the truncated model under predicts the dynamic WF component in the mooring

line tension while the dynamic LF component is slightly over predicted compared to the full depth model for the most loaded mooring line (L-1). However, the differences of the total dynamic components (LF+WF) of the most loaded mooring line increase resulting from the truncated model under predicting by 7% of the total tension compared to that from the full depth model. For the most loaded riser (R-1), the dynamic LF tension component calculated by the truncated model agrees well with that of the full depth model. However, the truncated model appears to under-predict the dynamic WF tension component compared to the full depth model. The total dynamic tension response of the riser (R-1) is under predicted (17%) by the truncated model compared to that of the full depth model (Figures 3.58 to 3.60).

Table 3.9 Normalized statistics values for Collinear 'In-line' case irregular waves, current and wind, including risers (FC37)

Collinear 'In-Line' irregular waves+current+wind	Description	Risers influences					
		Truncated model			Full depth model		
		LF	WF	Total	LF	WF	Total
	Surge	0.941	0.085	1.000	0.866	0.057	0.866
	Heave	0.108	0.981	1.000	0.123	0.927	0.968
	Pitch	0.119	1.238	1.235	0.139	1.204	1.216
	L-1	0.918	0.091	1.000	0.830	0.333	1.066
	R-1	0.711	0.298	1.000	0.751	0.481	1.174

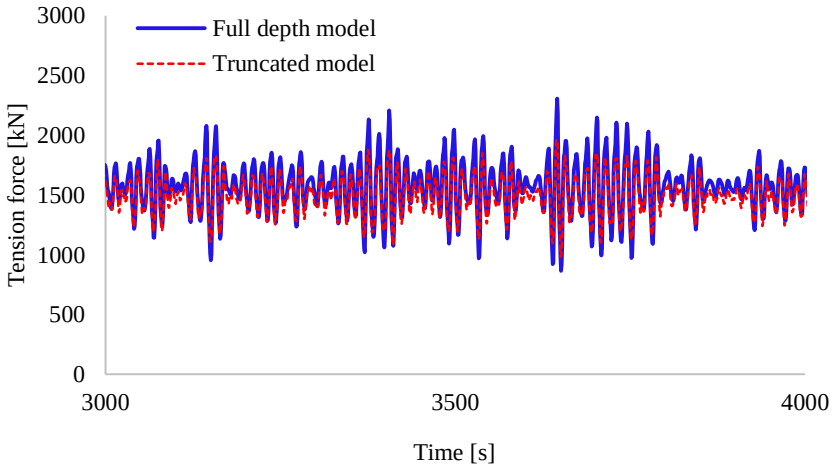

Figure 3.58 Comparison of the tension response for the most loaded riser (R-1) truncated model vs full depth prototype model, for the collinear 'In-line' case, (FC37)

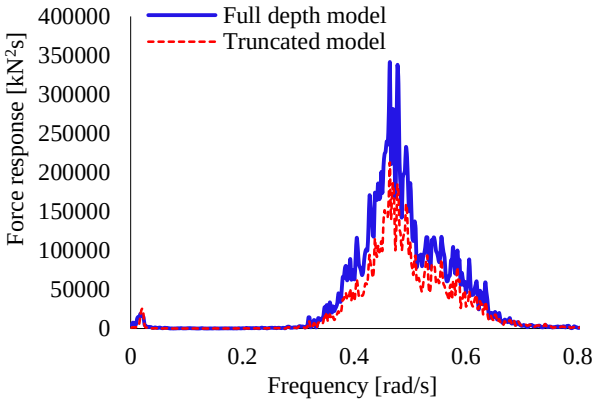

Figure 3.59 Riser tension response spectra (R-1) (irregular waves+current+wind), truncated model vs full depth prototype model, for the collinear 'In-line' case (FC37)

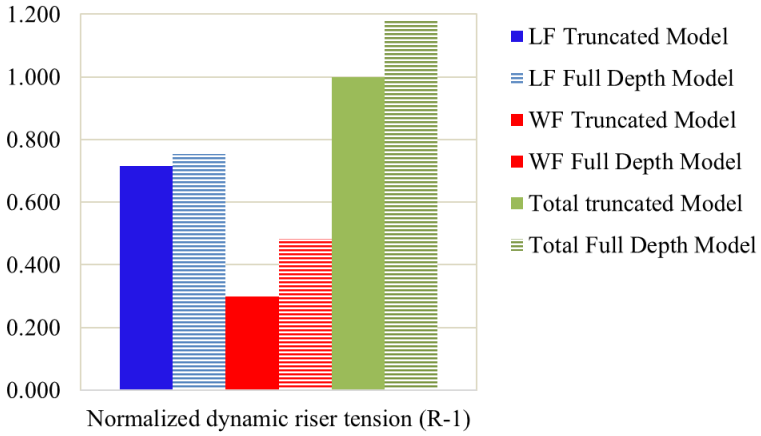

Figure 3.60 Normalized dynamic tension components of the most loaded riser (R-1), for the collinear 'In-line' case, (FC37)

3.5.4 Non-collinear case with irregular waves + current + wind (FC39)

The full system of the FPSO with mooring lines and risers under non-collinear environment was also analysed. The dynamic components of the LF and WF motions in the surge direction are overestimated about 14 % by the truncated model compared to the full depth model. For the WF motions in heave and pitch, the differences appear to be insignificant between the truncated model and full depth model, while the roll motion response predicted by the full depth model is smaller than that of the truncated model. This indicates that the heave and pitch motions are less sensitive to the dynamics of the mooring lines and risers while the dynamics of mooring lines and risers are important to the roll motion of the FPSO (Table 3.10).

Table 3.10 Normalized statistics values for Collinear 'In-line' case irregular waves, current and wind, including risers (FC39)

	Description	FPSO with Mooring lines and risers (FC39)					
		Truncated model			Full depth model		
		LF	WF	Total	LF	WF	Total
Non-collinear Irregular waves+current+wind	Surge	0.999	0.049	1.000	0.863	0.034	0.865
	Sway	0.320	0.080	0.321	0.248	0.037	0.249
	Heave	0.114	0.978	1.000	0.111	0.915	0.915
	Roll	0.173	2.943	2.967	0.166	2.277	2.325
	Pitch	0.054	1.343	1.026	0.055	1.030	1.007
	Yaw	0.346	0.004	0.346	0.316	0.006	0.316
	L-1	0.978	0.091	1.000	0.875	0.372	1.114
	R-1	0.691	0.372	1.000	0.736	0.582	1.248

For the most loaded mooring line (L-1), the truncated model under predicts the total tension force response by 11 % compared that from the full depth model. The main differences are observed in the WF component for the mooring line tension response within the frequency range of 0.4 to 0.6 rad/s (Figures 3.61 to 3.63). In the same way, the most loaded riser (R-1) was also studied. It is seen that there is a reasonably good agreement in the dynamic LF component for the riser. However, for the most important component response (WF), differences in tension responses are more evident indicating that the truncated system needs careful verification (Figures 3.64 to 3.66).

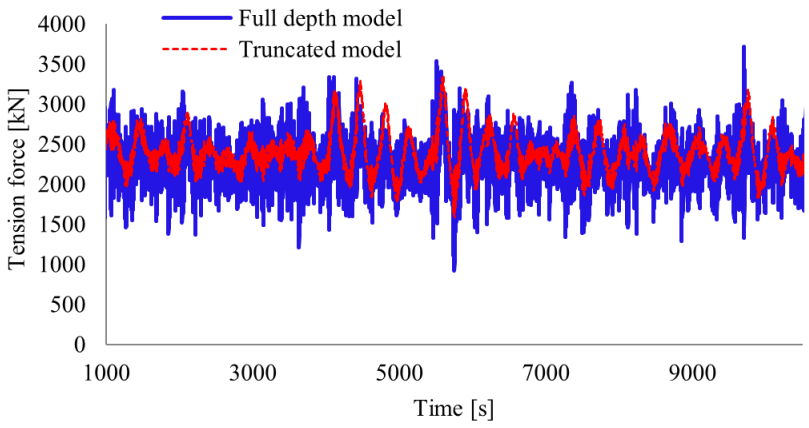

Figure 3.61 Comparison of the tension response for the most loaded mooring line (L-1) truncated model vs full depth prototype model, for the non-collinear case (FC39)

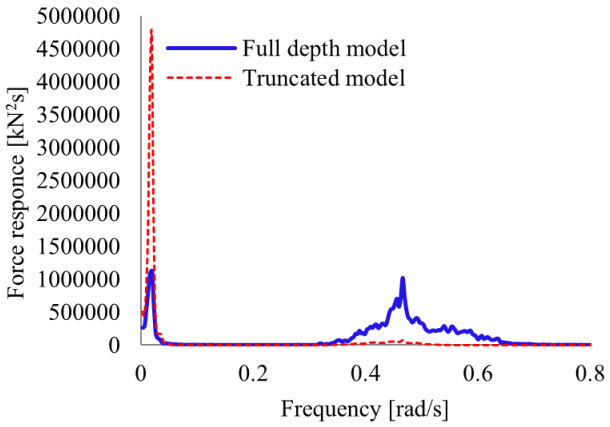

Figure 3.62 Line tension response spectra (L-1) of the 'In-line' case (irregular waves+current+wind), truncated model vs full depth prototype model, for the non-collinear case (FC39)

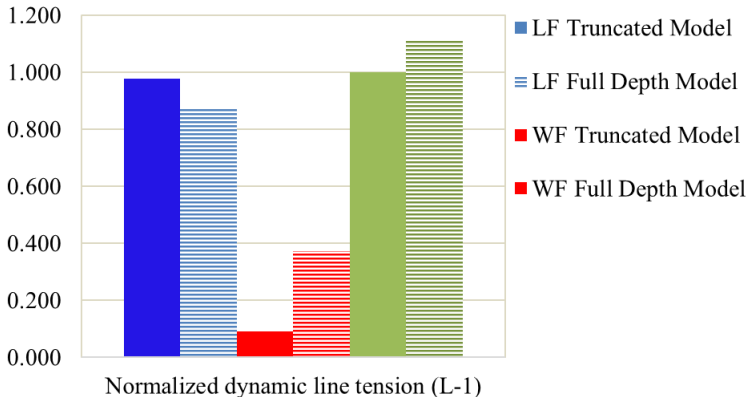

Figure 3.63 Normalized dynamic tension line components of the most loaded mooring line (L-1), for the non-collinear case (FC39)

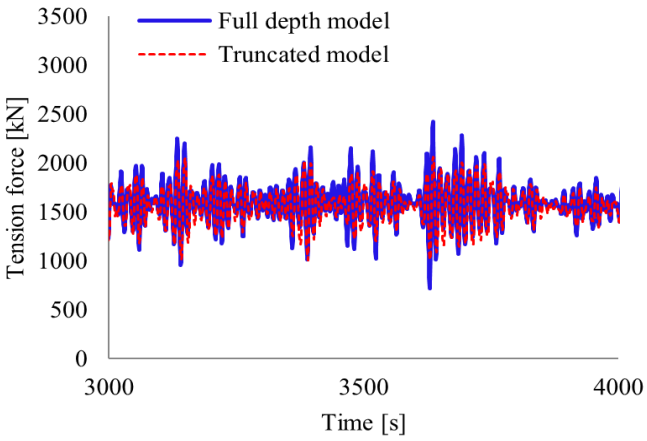

Figure 3.64 Comparison of the tension response for the most loaded riser (R-1) truncated model vs full depth prototype model, for the non-collinear case (FC39)

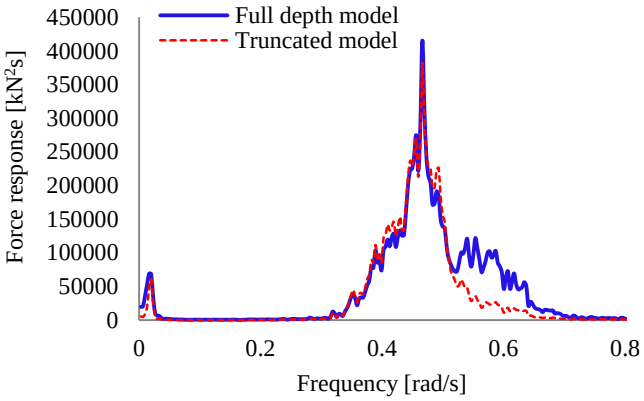

Figure 3.65 Riser tension response spectra (R-1) of the 'In-line' case (irregular waves+current+wind), truncated model vs full depth prototype model, for the non-collinear case (FC39)

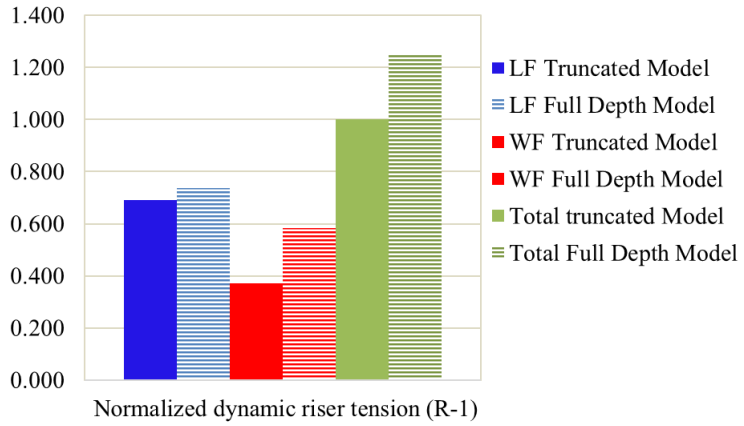

Figure 3.66 Normalized dynamic tension components of the most loaded riser (R-1), for the non-collinear case, for the non-collinear case (FC39)

Finally, it was observed that even though the LF motion response are slightly overestimated (conservative), the WF motions in heave and pitch predicted by the truncated model and the full depth model show, in general, a good agreement for all of the cases analysed. However, the differences can be observed in the dynamic tension response of WF components in the mooring lines and the risers. Baarholm and Palazzo (2004) also reported that the differences were more pronounced in the dynamic WF component for a mooring line system constructed using chain and polyester material components and for a level of the truncation that is higher compared to that used in this study.

The differences in the dynamic WF component are mainly attributed to the non-linear motions related geometry changes in the shape of the mooring lines in a full depth prototype which is difficult to match when the truncated system is designed based on a passive truncated methodology (Stansberg et al., 2002). The changing shape is more pronounced in the catenary mooring line for the full depth model and it is even more sensitive to the relative transverse motion responses occurring mainly from the WF motions of the FPSO. The dynamic WF tension components in the most critical riser (R-1) show better agreement compared to that of the most critical mooring line (L-1) with the full depth model predicting a higher tension in the riser than for that in the truncated model. It is also noted that an arrangement formed of heavier mooring lines and risers may tend to give better results for matching the non-linear geometric behaviour of a typical full depth arrangement, in the same way that a taut mooring line system may attain better results compared with that of a full depth catenary model. The differences in the dynamic WF component of tension responses in the most critical mooring line (L-1) between the truncated model and the full depth model show that the scaled model experimental

test on its own is not sufficiently reliable for designing a semi-taut mooring line system and that a coupled analysis is still necessary a deepwater installation. In addition, Froude's law of similarities is normally applied for the extrapolation of model test results to full scale, and the Reynolds law of similitude is not taken into account so scale effects are not avoided (Chakrabarti, 1998; BMT, 2000).

3.6. Summary

Numerical investigations of an FPSO complete with mooring lines and risers, were carried out in order to study its nonlinear hydrodynamics behaviour. The numerical simulation was based upon a coupled non-linear time domain analysis of the total system. Validation (model to model) experimental and numerical results were carried out and after that an extrapolation to the full depth model was developed for studying the dynamics of the mooring lines and risers. The following conclusions have been drawn and are summarized: The horizontal stiffness properties and the eigen-periods were reproduced well with the numerical simulations. This indicated that the inertia and stiffness properties of the total system were evaluated correctly. In the collinear cases, the influence of the risers was seen to be mainly in the mean motion in the surge direction while for their potential influence on the tension of the mooring lines the effect is relatively small. The WF motion responses of heave and pitch were also observed to be not affected significantly.

On the other hand, the non-collinear environment was identified to be the more critical case for the FPSO motion response and maximum tensions of the mooring lines compared to the collinear environments. The dynamic tension responses of the mooring lines and risers are apparently sensitive to the environment direction (collinear *vs* non-collinear). Newman's approximation was adequate enough to predict accurate the extreme motion responses in both collinear and non-collinear environment conditions but other floater systems may still require the full QTF in order to simulate accurately the LF and WF motion responses. The numerical simulation using the truncated numerical model, in general, agreed well with the experimental results for all cases studied. The LF and WF motion response components of the truncated model showed conservative results, but in general, a reasonable agreement compared with the full depth numerical model.

Furthermore, the truncated numerical model predicts the dynamic LF tension component well, but shows a limitation in its ability to capture the dynamic WF tension component response for the most critical loaded mooring lines and risers. As a result, the passive truncated experimental methodology for mooring lines and risers arrangement has limitations to predict the dynamic tension response of the mooring lines and the risers, in particular the WF tension component, and a coupled analysis verification is needed in order to determine reliable dynamics (LF+WF) of a semi-taut mooring line system and an associated riser system.

Chapter 4

Coupled Effects of Mooring Lines in Deepwater and Ultra-deepwater

4. Introduction

This chapter presents a sensitivity analysis using the validated numerical model (1000 m water depth) as the basis case described in Chapter 3. The main focus is to investigate the coupled effects of the FPSO and the mooring lines in two different water depths and how they affect the extreme motion responses, in terms of the mean, LF and WF motions, of the FPSO and the dynamics of the mooring lines.

A complete integrated system analysis of the FPSO with mooring lines and risers is important for a reliable prediction of the motion responses and estimation of the dynamics of the mooring lines and risers. Chapter 1 described the advantages and disadvantages of both the de-coupled analysis and the coupled analysis and the accuracy and efficiency in the calculations clearly play a major role with both methodologies. In this case study, the FPSO with its mooring lines only is further examined. The two different water depth installations are examined in this research in order to demonstrate the importance of the coupled effects on the FPSO with its mooring lines in two deepwater locations (1000 m and 2000 m water depths). The restoring forces and the viscous damping effects from the mooring lines and the effects of the current load and the wave kinematics on mooring lines are used for evaluating the influences of the coupled effects on the FPSO motions responses and tension response of the mooring lines.

4.1 System description

The numerical model that previously validated in 1000 m water depth (wd), was used as the basis case (Case A). The same overall arrangement of the anchor installation but with an increased spread and keeping the physical property characteristics and configuration of the FPSO with mooring lines is used for establishing the corresponding numerical model for 2000 m water depth (Case B and Case C with buoy) as shown in Figures 4.1.

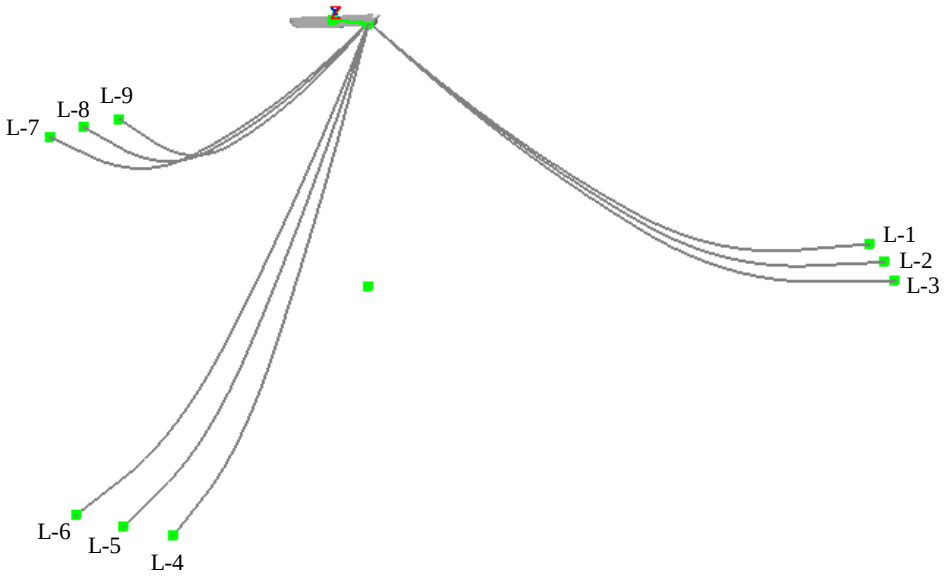

L= mooring line

R= riser

Figure 4.1 FPSO model with mooring line system in 2000 m wd

The Case C with a spherical-buoy on each mooring line which were assumed to be installed to 150 m below the water surface. A parametric study was carried out in order to select the volume of the buoy considering a mass of 1 tonne. The tension of mooring lines and the motion response of the FPSO were analysed for different volumes from 10 m^3 to 75 m^3. As can be seen in Figures 4.2 to 4.4 the advantage of including spherical buoys in the mooring lines is evident that they decrease the tension response in mooring lines while in the motion response for the surge direction an advantage is not perceived. The buoy was installed to be 1 tonne of mass with 45 m^3 in order to produce similar pretension as the basis Case A (2025 kN).

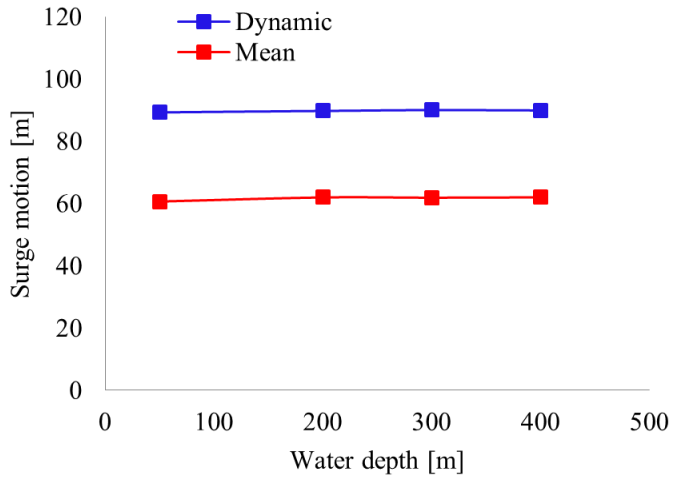

Figure 4.2 Surge motion response of the FPSO model with mooring lines system in 2000 m wd, Case C

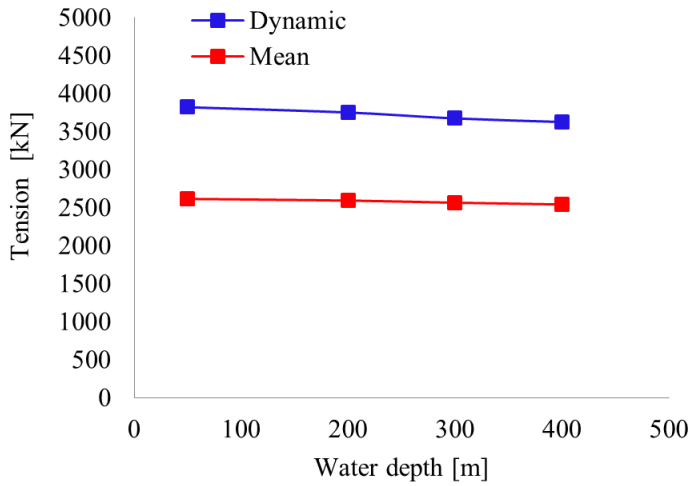

Figure 4.3 Tension response at the fairlead of mooring line (L-1) in 2000 m wd, Case C, varying buoy volume

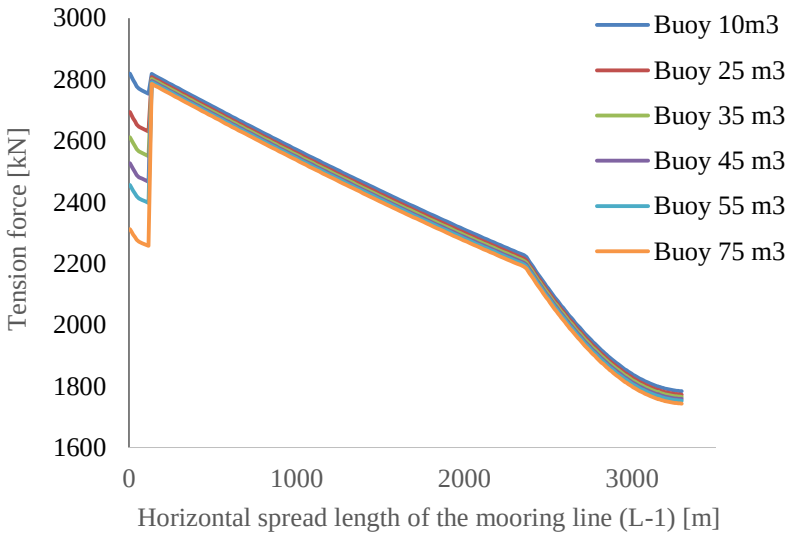

Figure 4.4 Static tension response in the mooring line (L-1) in 2000 m wd, Case C

A semi-taut mechanism was established for all arrangements of the mooring lines. Table 4.1 provides the characteristics of three cases that were studied.

Table 4.1 Mooring line system characteristics

Description	Case A	Case B	Case C with buoy
Water depth installation (m)	1000	2000	2000
Number of mooring lines	9		
Pretension (kN)	2025	2453	2075
Buoy	-	-	443 kN
Total Length of each mooring line (m)	2185	3300	3300
Segment 1: Fairlead chain	R4S Studless		
Length (m)	50	50	50
Diameter (mm)	90	90	90
Mass in water (tonnes/m)	0.146	0.146	0.146
EA (kN)	691740	691740	691740
Breaking strength (kN)	8167	8167	8167
Segment 2: Mid-section	Spiral Strand	Spiral Strand	Spiral Strand
Length (m)	1200	2315	2315
Diameter (mm)	90	90	90
Mass in water (tonnes/m)	0.0336	0.0336	0.0336
EA (kN)	766000	766000	766000
Breaking strength (kN)	7938	7938	7938
Segment 3: Chain ground section	R4S Studless	R4S Studless	R4S Studless
Length (m)	935	935	935
Diameter (mm)	90	90	90
Mass in water (tonnes/m)	0.146	0.146	0.146
EA (kN)	691740	691740	691740
Breaking strength (kN)	8167	8167	8167

Note: In the Case C, the hydrodynamic drag coefficients for the buoys were assumed to be Cd = 0.5 and Ca = 0.1 for drag and added mass coefficients respectively (Yuan et al., 2014).

4.2 Environment loading condition

The same storm condition for a 100-year return period, with a sustained wind velocity at 10 m standard reference height for one hour of 21.95 m/s and the current velocity on the surface 1.44 m/s, were used for evaluating the coupled effects of the mooring lines and risers and the motions responses of the FPSO (see Table 2.7, Chapter 2). The collinear 'In-line' loading case was used in order to evaluate the coupled effects on the mean motion, and LF and WF motions of the FPSO as shown in the Figure 4.5.

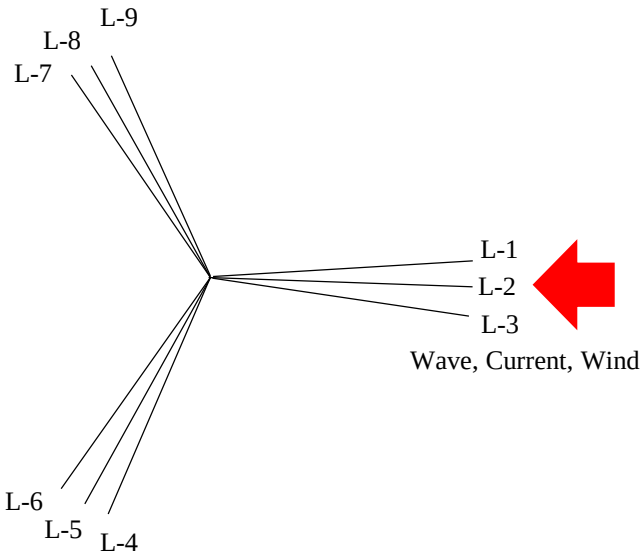

Figure 4.5 Collinear 'In-line' case environment loading

4.3 Restoring forces characteristics of the mooring lines

The static shape characteristic of the mooring lines were set up similar for Case A and Case B. Figure 4.6 shows the static shape characteristics of a representative mooring line (L-1), actually all 9 mooring lines (L-1 to L-9) have the same geometric shape for each of the cases studied. The mooring line system was established to have a semi-taut mechanics condition.

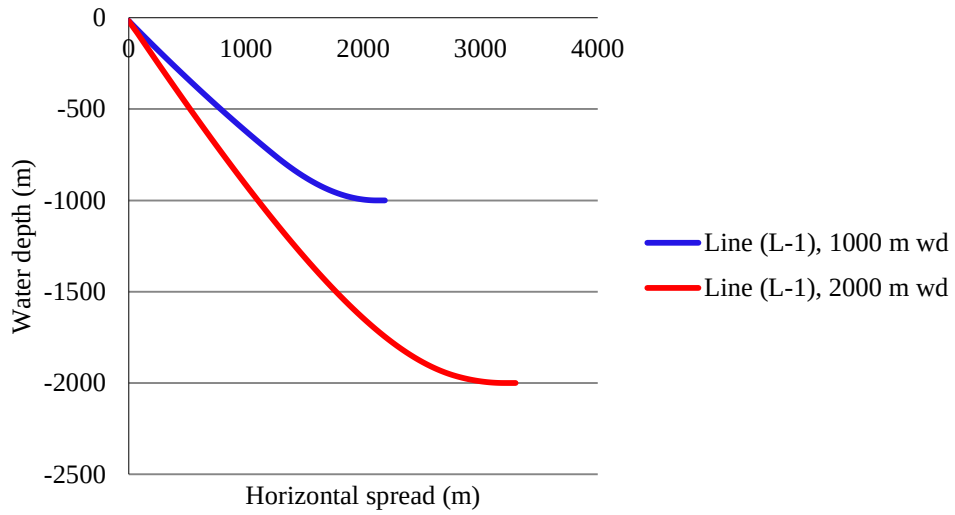

Figure 4.6 Static shape characteristic of the mooring line (L-1)

On the other hand, the motion response of the FPSO in the horizontal plane was mainly kept to be within a maximum offset limit equal to approximately 10 % of the installed water depth (Whichers, 2013). The mooring line system was designed to provide the main source to limit the offset of the FPSO through its horizontal restoring forces. Then, the restoring forces and offsets for the two representative cases were compared in order to analyse the overall effects of the water depth.

The system installed at 1000 m water depth was observed to have the higher restoring force compared with the system installed at 2000 m water depth, and the difference was about two times (Figure 4.7). This may be in partly explained due to that larger water depth and keeping the same properties of the mooring lines and risers such as the submerged mass and axial stiffness in the two cases, thus higher deformation or elongation behaviours are developed in other words creating a more flexible overall system in terms of the restoring force in 2000 m water depth. Further, deeper the water, the angle at which the mooring line connects to the fairlead at the base of the turret tends to be smaller than shallow water which will decrease the horizontal restoring force contribution.

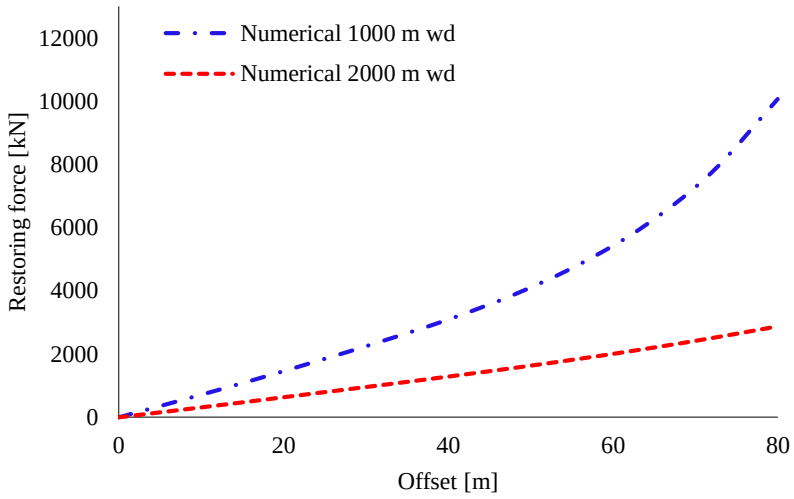

Figure 4.7 Restoring forces vs offsets for the FPSO with mooring lines 1000 m and 2000 m water depth

4.4 Coupled effects in 1000 m (Case A) and 2000 m water depths (Case B)

-FPSO with mooring lines

The coupled effects such as damping from mooring lines and current load contribution on the mooring lines to the motion response of the FPSO were evaluated. The Case A or basis case and Case B defined previously were analysed using coupled and decoupled analysis methods respectively in the following cases studies:

Case 1: Decoupled analysis (including non-linear restoring forces but not including the damping contribution from the mooring lines)

Case 2: Decoupled analysis (including non-linear restoring forces and damping from mooring lines but not including the current load contribution on the mooring lines)

Case 3: Coupled analysis (including non-linear restoring forces, damping from the mooring lines, and the current load contribution on the mooring lines)

The main objective of the cases studies is to quantitatively examine the coupled effects on the motion response of the FPSO and the dynamic response of the mooring lines. The coupled effect of damping of the mooring lines was studied through of the variation of the Cd values for simulating a decoupled analysis. A similar process was applied previously by Wichers (2001) and Tahar and Kim, (2003), for studying the influence of the damping of the mooring

lines. Thus, a non-linear time domain coupled analysis was carried out for evaluating the mean values of motion responses and the total dynamics of the FPSO with mooring lines (WF motion plus LF motion).

-Coupled effects in the Case A (1000 m wd)

As can be seen in Figure 4.8, the contribution of the mooring line damping to the surge response is important for the collinear environment. The maximum difference, in the mean surge motion response calculated without line damping (Case 1, Cd = 0) reaches up to 46 % in comparison with Cd = 3 (for the chain component) and Cd = 2 (for the spiral/strand component) as set for the mooring lines analyses (Case 3) while the differences in the dynamic component are about two times higher in the simulated de-coupled analysis (Case 1) compared to the results of the coupled analysis (Case 3). For the influence of current (Case 3), the mean motion increases 46% compared with the Case 2 (without current) while the influences of the current on the dynamic motion response of the FPSO is thus seen to be insignificant.

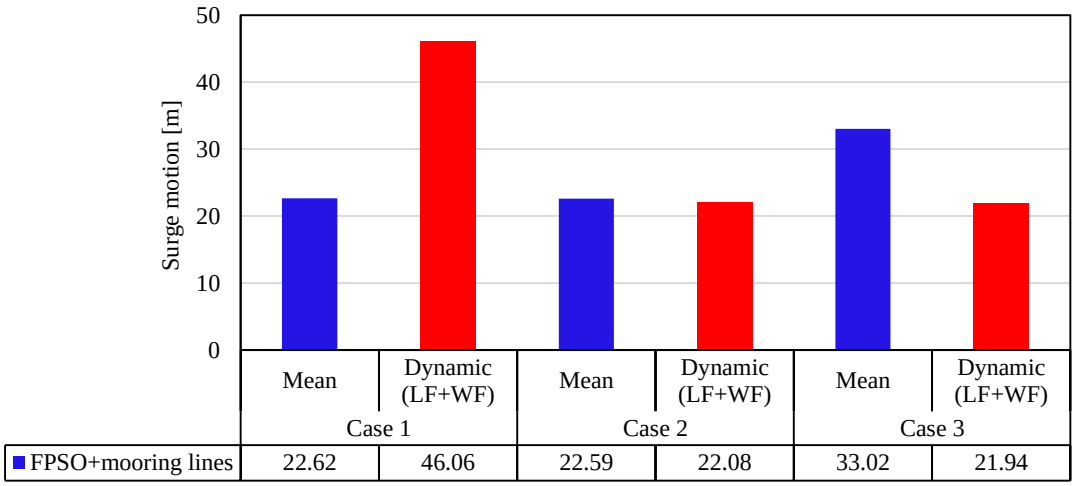

Figure 4.8 Coupled effects affecting the surge motion response, Case A

Furthermore, the coupled effects of the mooring lines on the most important WF motion responses in heave and pitch under collinear 'In-line' environmental condition were also analysed. Figures 4.9 and 4.10 show the spectra responses in heave and pitch motion respectively. It is seen that both the heave and pitch motions are not affected significantly by the damping and current load from the mooring lines.

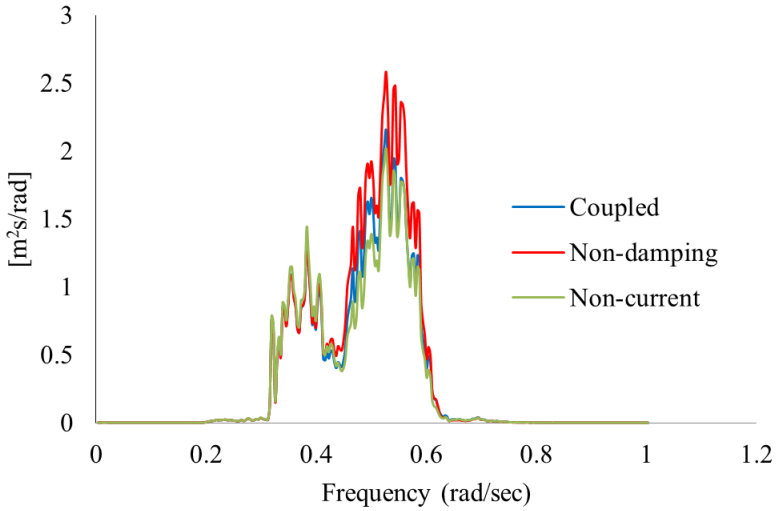

Figure 4.9 Coupled effects from mooring lines affecting heave motion response, Case A

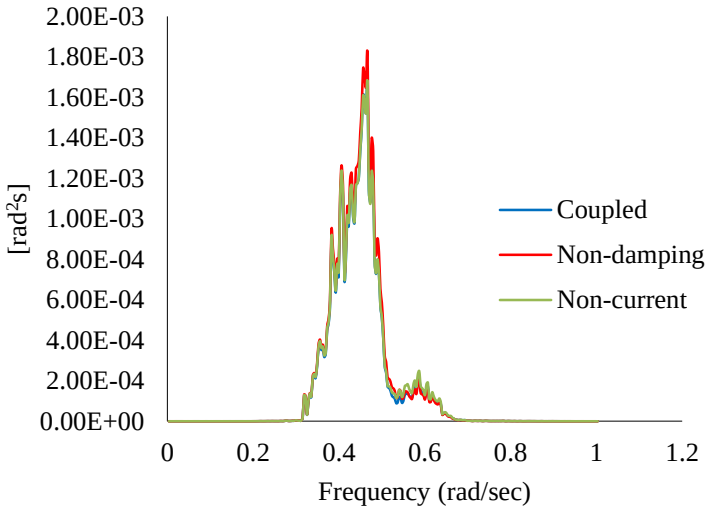

Figure 4.10 Coupled effects from mooring lines affecting pitch motion response, Case A

The coupled effects (damping and current load) on the dynamic response of a representative mooring line (L-1) were also studied. Figure 4.11 shows that the tension in the mooring line (L-1). It is observed that there is a slightly decrease in the mean tension response (Case 1) when damping of the mooring lines is not taken into account compared to the Case 3. However, a significant increase in the dynamic tension of 39% is observed when mooring line damping contribution is excluded.

The current load on the mooring line (L-1) is seen a slight influence on the mean tension response (Case 2, 2420.8 kN vs Case 3, 2654.01 kN) and the influence on the dynamic tension response is also relatively small.

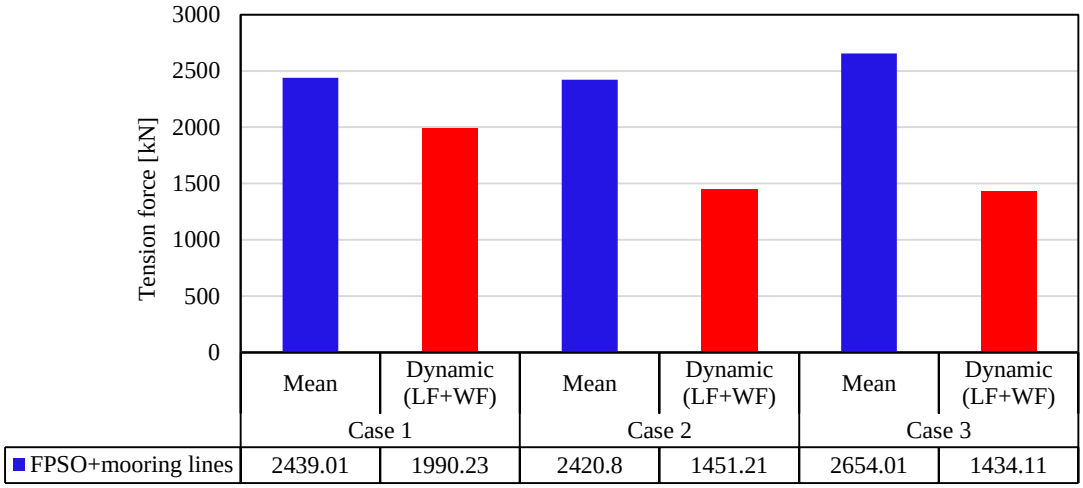

Figure 4.11 Coupled effects affecting the tension response of the mooring line (L-1), Case A

-Coupled effects in ultra-deepwater (Case B, 2000 m wd)

The influences of the mooring lines due damping and current load on the motion response of the FPSO in an ultra-deepwater installation (Case B, 2000 m) was also studied. Differences of 22 % between Case 1 and Case 3 are observed in the mean motion response of the FPSO when damping contribution from mooring lines is not taken into account (Figure 4.12). In the case of the dynamic motion response of the FPSO, the influence of the damping from mooring lines is seen to be significant.

On the other hand, the influence on the motion response of the FPSO due to current load on mooring lines is seen to increase the mean motion response approximately 21% (59.90 m, Case 3) compared to the system without the influence of current load on the mooring lines (49.44 m, Case 2). For the dynamic motion response of the FPSO, the current load on the mooring lines is insignificant.

It is noted that damping contribution from mooring lines tends to significantly affect the dynamic motion response of the FPSO while current load on the mooring lines has influence mainly on the mean motion response of the FPSO.

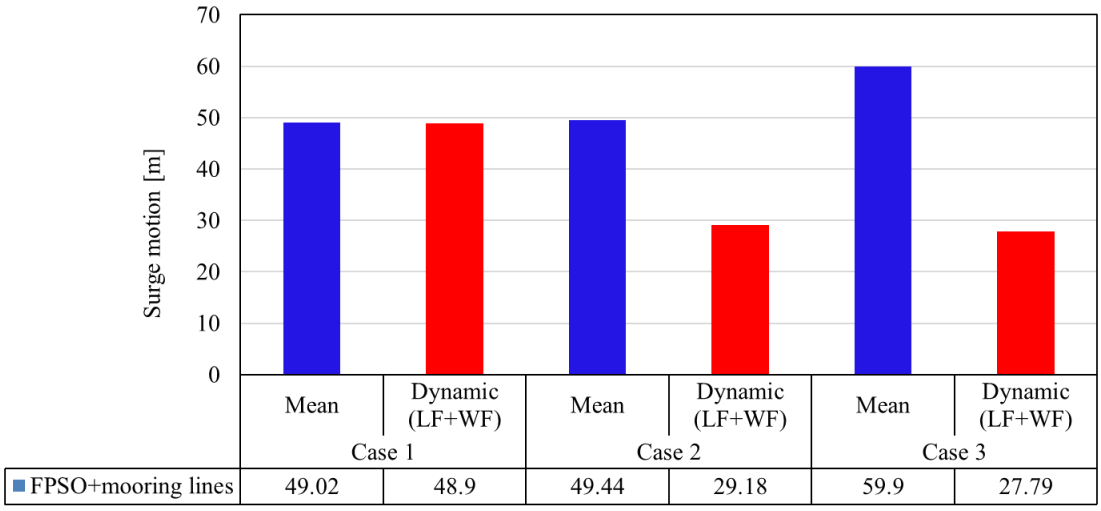

Figure 4.12 Coupled effects affecting the surge motion response, Case B

In the same way as Case A, the WF motions in heave and pitch are observed to be not affected significantly by the coupled effects of the mooring lines for 2000 m wd (Case B) Figures 4.13 and 4.14

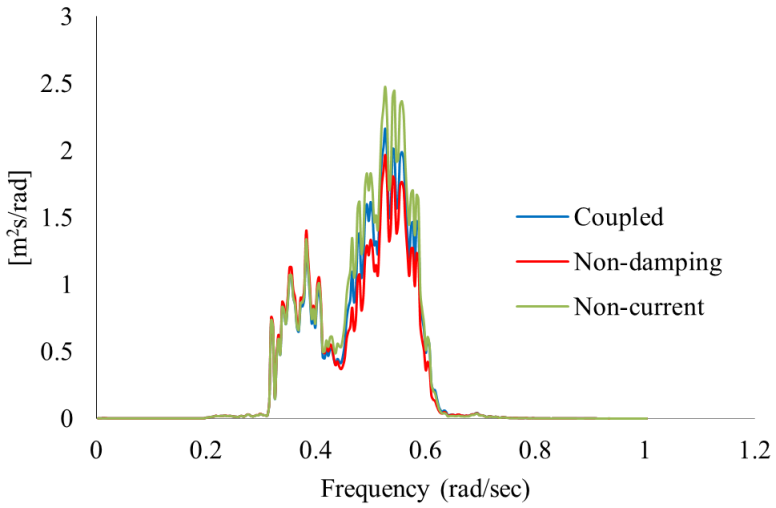

Figure 4.13 Coupled effects from mooring lines affecting heave motion response, Case B

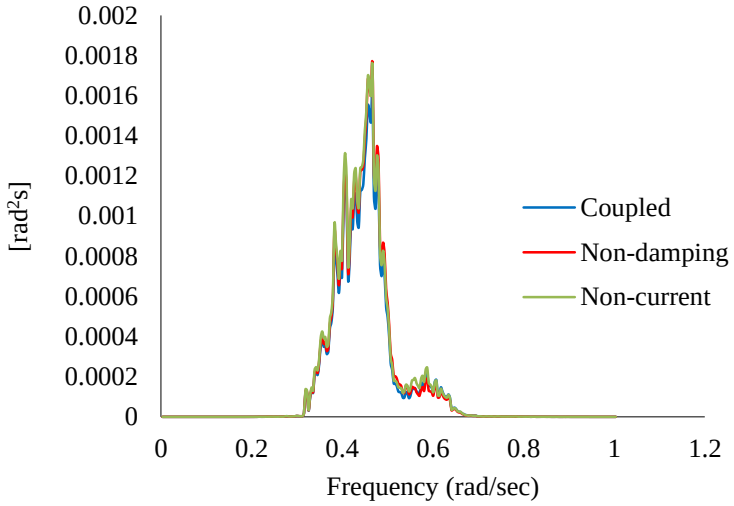

Figure 4.14 Coupled effects from mooring lines affecting pitch motion response, Case B

On the other hand, the mean tension response of the mooring line (L-1) for the Case 1 (without damping) is seen to be slightly lower (3 %) compared to that when the effect of damping is included in the mooring lines (Case 3) (Figure 4.15). For the dynamic tension response of the mooring line (L-1), it is observed that coupled effect from mooring line damping (Case 3) slightly decreases the dynamic tension (compared to Case 1). It is observed that the influences of current load on mooring lines on both the mean tension and dynamic tension response of the mooring line (L-1) are relatively small.

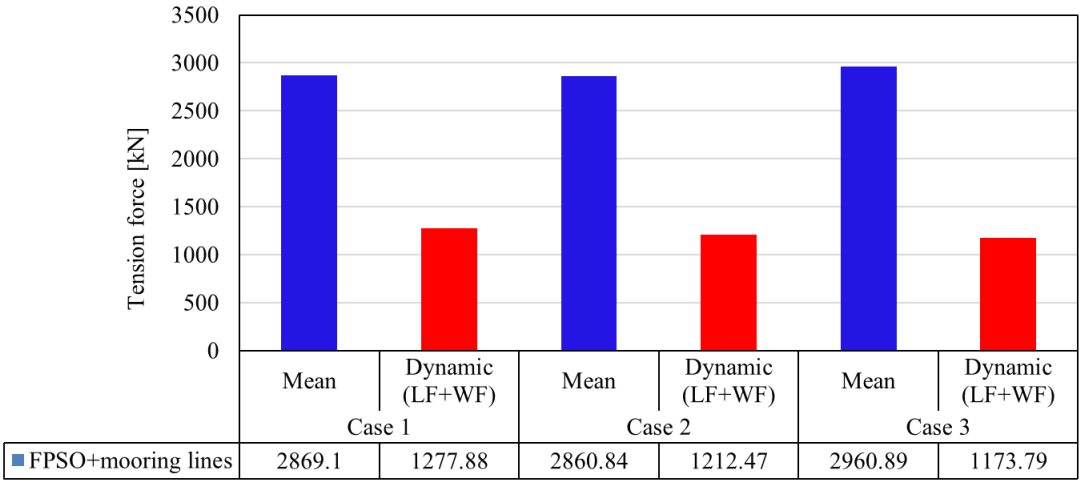

Figure 4.15 Coupled effects affecting the tension response of the mooring line (L-1), Case B

-Coupled analysis Case A vs Case B and Case C

A non-linear time domain coupled analysis was carried out for evaluating the total dynamic response of the FPSO and the mooring lines. The extreme motion response in the surge direction and the dynamics of the mooring lines for the FPSO installed in 1000 m and in 2000 m water depths were evaluated and compared for the system under the collinear 'In-line' condition including irregular waves, wind and current environment loads.

It is observed that the mean motion component in Case A (1000 m wd) is approximately 51% larger than the dynamic response component response. However, for ultra-deepwater installation (Case B, 2000 m and Case C, 2000 m with buoy), the mean motion component response increase considerably (more than two times) than the dynamic motion components. Further, the dynamic factor (Fd) of motion responses in terms of (maximum value - mean value)/standard deviation for Case B and Case C was observed to decrease (Fd = 2.88 and Fd = 2.84, respectively) compared with the Case A (Fd = 3.19) (see Figure 4.16).

The differences of the mean and dynamic motion responses of the system with or without a buoy is seen to be insignificant as the (Fd) is seen to be similar.

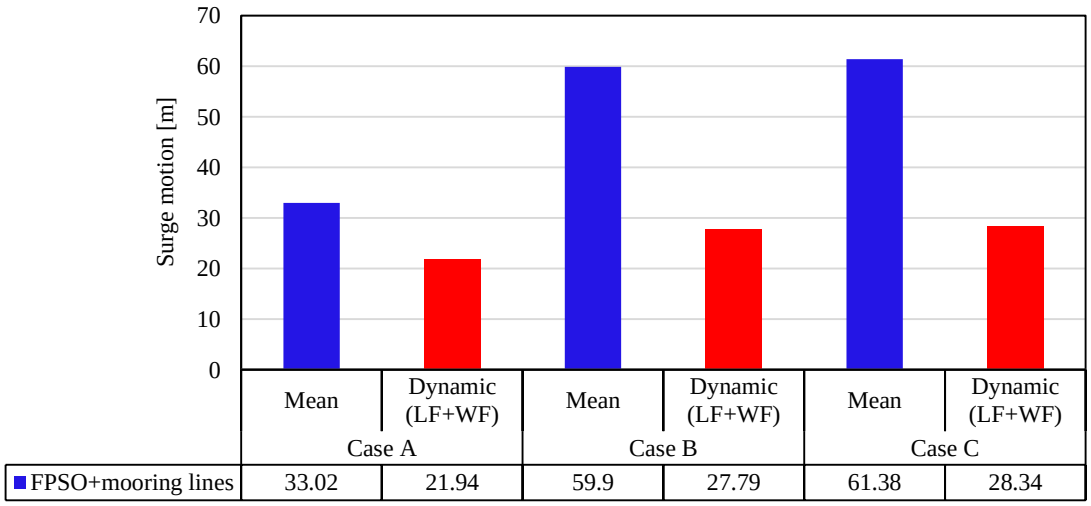

Figure. 4.16 Comparisons of the surge motion response 1000 m vs 2000 m water depth

Similarly, Figure 4.17 shows the tension response of the mooring (L-1) for all three case analysed. It is observed that the mean tension component has the higher tension contribution on the system while the dynamic component is seen to decrease significantly as the water depth increases. The dynamic factor of the tension response of the mooring line (L-1) is observed to

be Fd = 4.12 and Fd = 3.80 for Case A and Case B, respectively. This is mainly due to the damping contribution of the mooring lines that increases as the water depth increases and, as a result, the dynamic factor (Fd) for tension response and LF motion response in the surge direction decreases.

On the other hand, the mean tension force response for Case C is observed to be smaller (2597.94 kN) compared to that of Case B (2960.89 kN). The reason is due to the direct effect of the positive local vertical tension of the buoy of 443 kN in Case C which reduces the line tension. In the dynamic component, however, any differences were not observed since both the hydrodynamic drag coefficient and the inertia coefficient for the buoys were assumed relatively small in the calculation.

As the dynamic component is the major concern owing to the various uncertainties, it is clear that for installations in a greater water depth the uncertainties from the dynamic component for both FPSO motion and tension force responses of the mooring lines decrease and both the mean motion and mean tension will play the major role. The coupled effects that control the dynamics of the mooring lines and risers must be accurately estimated such as their damping contribution. Therefore, a coupled analysis will be essential in order to avoid overestimating the tension response of the mooring line and riser systems.

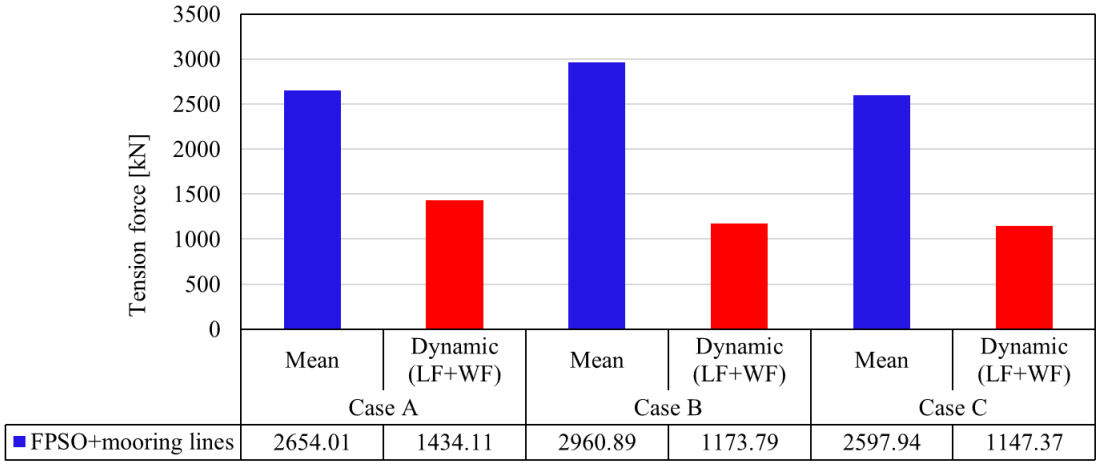

Figure 4.17 Comparisons of the tension force response for the mooring line (L-1) 1000 m vs 2000 m water depth

4.5 Summary

This chapter presents the analyses and results of the restoring forces and damping contributions to the system dynamics for two different water depth mooring line arrangements. The analyses of the mean motion, the WF motion and the LF motion responses for the different arrangements by using both decoupled and coupled analysis are presented. Additionally, the basis case (Case A), established in 1000 m water depth is extended to 2000 m water depth and the associated dynamic components of extreme motions and tension response of the most loaded mooring lines were analysed and discussed.

An important finding is that the dynamics of the mooring lines appear not affect significantly the WF motions in heave and pitch under the collinear 'In-line' environmental condition. Moreover, the dynamics of the mooring lines decrease as the water depth increased, and the mean motion and mean tension is dominant in deepwater and ultra-deepwater installations. By adding the buoys to the mooring system, the mean tension response of the mooring lines decrease while dynamics tension response is not affected significantly. However, the effect of the drag forces on the buoys may be higher near the water surface than in deepwater, thus the effect of the buoy should be investigated on the dependences to water depth and volume.

Chapter 5

Conclusions and Recommendations for Future Work

This research work investigated the extreme motion responses of a typical FPSO and the associated dynamics of its mooring lines and risers in a deepwater installation based on a hybrid passive truncated experimental methodology representing the mooring lines and risers. The experimental results (viscous damping, decay tests, motions in 6 DOF of the FPSO and the tensions in the mooring lines and the risers) are used for a comprehensive numerical study on the hydrodynamic behaviour of the complete coupled system under collinear and non-collinear environmental conditions (irregular waves, current and wind). Frequency domain analysis and coupled time domain analysis are conducted for the complete FPSO with mooring and riser system in deep and ultra-deepwater locations in the GOM.

5.1 Conclusions

5.1.1 Experimental study on the hydrodynamic behaviour of the FPSO with its mooring lines and risers

The experimental study employed the hybrid passive truncated experimental method for representing the behaviour of the mooring lines and risers. The experimental tests were undertaken in an offshore basin with 10 m of water depth at SJTU. The main focus is to study the nonlinear hydrodynamic effects on the FPSO vessel fully coupled with both mooring lines and risers. The FPSO global responses for both the Full and the Ballast Load conditions and the associated dynamics of the mooring lines and risers are studied under both collinear and non-collinear environmental conditions. The experimental model test results lead to the following conclusions:

1. The motion response linear transfer functions (RAOs) were calculated and evaluated for both the Full and the Ballast load conditions.

   i. The motion response of the FPSO for both the Full Load and the Ballast Load conditions are sensitive to the direction of the incident waves. The beam and quartering sea conditions are the critical conditions leading to the maximum roll motion response.

2. The response spectra and statistical values are calculated and evaluated for both the collinear and the non-collinear environmental load conditions for the Full Load and Ballast Load conditions of the FPSO model with mooring lines and risers.

   i. The motion response spectra analysis revealed that the risers have a significant influence on low-frequency damping, particularly in the surge direction, whereas the damping contribution to the wave frequency motion response contributes mainly to the roll motion response.

   ii. In the non-collinear environmental condition, the interaction between the irregular waves and the current significantly increases the steady wave drift force on the FPSO compared to the collinear environment.

   The yaw motion response is identified influence the wave frequency motions in heave, roll, and pitch under the non-collinear environmental condition. Thus the vessel will be more sensitive to the wind, as it presents a great area above the water line.

   iii. Under the collinear environment for the Full Load condition, the ‘In-line’ case results in the most critical mooring line tension, while the ‘Between-lines’ case leads a higher motion response of FPSO.

   iv. The WF motions in heave, roll, and pitch for the Ballast Load condition are found slightly higher than those for the Full Load condition in the non-collinear case.

   v. The highest tensions in the mooring lines are observed in the Ballast Load condition for the non-collinear case due to a higher coupled surge and sway motion response and the less draught of the FPSO. However, the maximum tensions in the risers are observed under the non-collinear environment for the Full Load condition, and these tensions were slightly higher than those in the Ballast Load condition. This indicated that the risers are relatively sensitive to the wave frequency motions.

vi. The interaction between the waves, current and wind under collinear environment increases the mean drift motion response but decreases the slow-drift oscillation of the FPSO compared to the irregular waves only and for which the former behaviour is attributed to the increase of the drift damping on the FPSO.

vii. The interaction of the waves, current and wind under non-collinear environment is more complex which tends to increase the mean drift motion, the drift damping, the damping from mooring lines and the slow-drift oscillation responses on the FPSO compared to the system exposed to irregular waves only.

It is worth noting that some of the above conclusions may be specific to the particular mooring line and riser arrangement selected for this study and may not be applicable to other arrangements.

5.1.2 Numerical investigation on the hydrodynamic behaviour of the FPSO with mooring line and riser system

Numerical investigations are carried out based on potential flow theory for solving the first-order and second-order wave forces on the FPSO hull and the Morison formulation is applied for the slender mooring lines and the risers. The viscous damping contribution of the FPSO is obtained from the experimental decay tests. Numerical models for truncated moorings and risers and a full water depth are developed to study the dynamics of the mooring lines and risers coupled with the FPSO hull using a non-linear time domain coupled analysis. Several conclusions have been drawn:

1. An FPSO with coupled truncated mooring lines and risers was built and validated through experimental results (model to model process)

i. The horizontal stiffness and the eigen-periods are reproduced well by the numerical simulations. This indicates that the inertia and stiffness properties of the entire system are evaluated correctly.

ii. Under the collinear condition, the influence of the risers was found to be mainly in the LF motions in the surge direction while their influence on the tensions in the mooring

lines is relatively small. The WF motion response of the FPSO in heave and pitch are not affected significantly by the risers.

iii. Tension responses of the risers are apparently more sensitive than mooring lines to the (collinear and non-collinear) environmental conditions.

iv. Newman's approximation is adequate to predict the LF motion responses of an FPSO under both collinear and non-collinear environments with reasonable accuracy. However, other floaters may still require the full QTF for accurate prediction of the LF motion responses.

v. The results of the numerical simulation from the truncated moorings and risers model in general agree well with the corresponding experimental results for all cases studied, and therefore can be used to validate the full depth numerical model.

vi. The calibration of the environment, that is mechanically generated inside the offshore basin, such as the waves only and then the waves and the current acting together is essential in order to evaluate accurately the efficiency of the numerical models.

2. The validated truncated numerical model (FPSO with truncated mooring lines and risers) is extrapolated to the full depth prototype water depth and further applied to a case study of FPSO with mooring and riser system in an ultra-deepwater installation.

i. The LF and WF motion responses of the truncated model shows, in general, a good agreement when compared with the responses of the full depth numerical model. Moreover, a good agreement is also observed in the dynamic LF tension components obtained by the truncated numerical model and the full depth numerical model. However, the truncated numerical model shows some limitations in its ability to capture the dynamic response in WF tension component for the most critical loaded mooring lines and riser elements.

ii. It is evident that the passive truncated experimental methodology for the mooring lines and risers is having a limitation in its ability to predict the dynamic component of the

tension response in particular for the WF tension component. Thus a coupled analysis verification is needed in order to determine reliable dynamics (LF+WF) of a semi-taut mooring line system and the associated riser system.

3. The validated full depth model in 1000 m was extrapolated to 2000 m water depth in order to study the dynamics of motion and tension responses of the complete system.

   i. As the dynamic component is the major concern due to the uncertainties, it is found that for ultra-deepwater (2000 m), the dynamic factor for both motion and tension response of the complete system (FPSO with mooring lines and risers) decrease, however the coupled effects that control the mean and LF components increase. Thus a coupled analysis will be essential in order to avoid to overestimate the dynamic components (mean and LF component responses) of the total system. By adding the buoys to the mooring system in ultra-deepwater, the mean tension response of the mooring lines decrease while dynamics tension response is not affected significantly. However, the effect of the drag forces on the buoys may be higher near the water surface, thus the effect of the buoy should be investigated on the dependences to the drag forces, water depth and volume.

5.3 Recommendations for future work

5.3.1 FPSO system

Numerical simulations tools need to continue to be improved even though the first-order and second-order forces of the wave interaction with the structure can be handled and estimates of the mean drift force and the dynamics of the second-order forces can be made with acceptable accuracy. However, the interaction effects of the irregular waves combined with a current is not the same case, since the resulting increase in the mean drift force on structure tends to be underestimated in the present study. Thus, additional research is needed in order to generate a numerical algorithm that can be employed for predicting and handling the nonlinearities present in the wave-current interactions which are more significant under the non-collinear environment. Furthermore, the prediction of the drift damping resulting from the wave-current interaction needs more research, since the conventional programs generally only calculate the drift damping from the effects of the waves only (SIMO-SESAM, 2015). The drift damping from the interactions between the waves and current is essential for an accurate

estimation of the motion response in real environmental conditions at the installation sites of the floating structures.

The non-collinear environmental conditions should be taken into account carefully in the evaluation of the hydrodynamic performance of the FPSO. Wave run-up and, possibly, the green water effects should be investigated as they can be critical issues for the design load displacement condition and the freeboard verification in deepwater locations. The model tests also need to be extended to incorporate regular waves to estimate the mean drift forces and also extend the test program to include irregular waves for moderate and severe sea states representing the extreme hurricane and storm conditions.

The present study used long crested waves that were generated in the basin and the results were used as input data to the numerical model analyses. It will be interesting to verify the behaviour with short crested seas since it can potentially result in the worst case in motion responses when FPSO is in the Ballast Load condition.

As the FPSO with its internal turret is sensitive to the directional effects of non-collinear waves, wind and current combinations, future work considering a long term response analysis should be undertaken in order to obtain a reliable spectrum of design data for fatigue assessments of the total system. Such research effort will also improve the design practice in an efficient selection of the turret location within the hull in order to minimize the LF and WF motion responses and the tensions in the mooring lines and riser systems.

5.3.2 Mooring lines

In this research, the hybrid passive truncated methodology was used for overcoming the physical limitation of the offshore basin. A clear drawback associated with the methodology is identified in the estimation of reliable dynamic response of mooring line and riser system, particularly the WF component dynamic response. Due to the non-linear geometry, it is important to establish algorithms and procedures for the modelling of the mooring lines and risers which can better handle their non-linear geometry behaviour together with the more conventional design parameters such as: the restoring forces, the pretension, submerged weight and axial stiffness. The accurate dynamic estimation of the tension response fluctuations of the mooring lines and risers will be a critical factor in their design for the avoidance of fatigue.

Furthermore, the drag coefficients of the mooring lines and risers and their components should to be studied including the effects of marine growth and how such could influence the accurate estimation of the changes in both drag and the damping of the mooring lines and risers during the required life of the field. Consequently, how such changes may affect the fatigue life of each of these systems and potentially effect the benefits for an extension in the installations service life.

5.3.3 Riser system

The hydrodynamic loads on the steel catenary risers (SCR) due to the vessel motions, imposed wave loads and especially strong currents which can produce the vortex-induced-vibrations (VIV), phenomena which may increase the in-plane and the out-plane response due to drag coefficient amplifications. Both the VIV and drag amplification can adversely affect both the riser's strength and its fatigue life. As a result it can lead to high investment costs, high maintenance costs and affect the reliability of the risers system. This issue is of the great importance for the offshore oil industry and was not attended in the present research. However, the results of this research can be used as an input to further studies leading to reliable design solutions for the SCR with the FPSO system for future oil field exploitation having particular requirements to handle high pressure flows and hydrostatic pressures in deep- and ultra-deepwater locations in the GOM.

List of References

1. API-RP-2SK, 2005. Recommended practice for design and analysis of stationkeeping systems for floating structures: Exploration and production department. API recommended practice 2SK (RP 2SK), 3rd edition, American Petroleum Institute, Washinton, DC.
2. Atlar, M., 1986. Towards the understanding of the staeady tilt phenomenon in semi-submersibles. (Doctoral dissertation, University of Glasgow).
3. Avalos, G. O., Wanderley, J. B., Fernandes, A. C., & Oliveira, A. C., 2014. Roll damping decay of a FPSO with bilge keel. Ocean Engineering, 87, 111-120.
4. Baar, J.J.M., Heyl, C.N. and Rodenbusch, G., 2000. Extreme response of turret moored tankers. 32nd Annual Offshore Technology Conference, Paper OTC-12147-MS, Houston, Texas, Vol. 2, pp. 749-759.
5. Baarholm, R., Fylling, I., Stansberg, C.T. and Oritsland, O., 2006. Model testing of ultra-deepwater floater systems: Truncation and software verification methodology. Proceedings of 25th International Conference on Offshore Mechanics and Arctic Engineering, Paper OMAE2006-92492, Hamburg, Germany, Vol 1, pp. 527-537.
6. Baarholm, R. and Palazzo, F.G., 2004. Hybrid verification of a DICAS moored FPSO, The Fourteenth International Offshore and Polar Engineering Conference, International Society of Offshore and Polar Engineers, May 23-28 , Toulon, France, Paper No. ISOPE-I-04-101.
7. Barltrop, N.D.P., 1998. Floating structures: a guide for design and analysis. vol. 2. The centre for marine and petroleum technology CMPT, Ledbury, England.
8. Barton, C., Heather H., 2015. Deepwater concept selection and record poster. Mustang Engineering Co., Offshore Magazine, Houston, Texas, USA.
9. Beck RF, Cao Y. Lee, TH., 1993. Fully nonlinear water wave computations using the desingularized method. Proc. of 6th International Conferency on Ship Hydrodynamic, 3-20.

10. Beck RF., 1994. Time-domain computation of floating bodies. Applied Ocean research 16: 267-82
11. Bendat, J.S. and Pierson, A.G., 1980. Engineering Application of Cross Corelation and Spectral Analysis. New York.
12. BMT, 2000. Review of model testing requirements for FPSO's. BMT Fluid Mechanics Ltd. -Offshore Technology Report 2000/123, Teddington, United Kingdom.
13. Brown, D. T., & Fang, J., 1996. Hydrodynamic damping contributions for an advanced floating production system design. Marine structures, 9(7), 649-670.
14. Brinati, H.L., Nishimoto, K., Fucatu, C.H., Maseti, I.Q., Fuljahn, M., 1999. The effects of mooring lin damping and wave drift damping on moored tanker dynamics. Offshore Engineering, 1, 11-27.
15. Buchner, B., Wichers, J.E. W., De Wild, J.J., 1999. Features of the State-of-the-art Deepwater Offshore Basin. Offshore Technology Conference. OTC-10814-MS.
16. BW offshore, 2014. Annual report BW Offshore Limited
17. Cao Y., Tahchiev G., 2013. A Study on an active hybrid decomposed mooring system fro model testing in ocean basin for offshore platforms. Proceedings of the ASME, 32th International Conference on Ocean, Offshore and Arctic Engineering, OMAE2013-11471, Nantes, France.
18. Chabaud, V., Steen, S., Skjetne, R., 2013. Real-time hybrid testing for marine structures: Challenges and strategies. Proceedings 32nd International Conference on Ocean, Offshore and Arctic engineering, Nantes, France, OMAE2013-10277.
19. Chakrabarti, S.K., 1987. Hydrodynamics of offshore structures. WIT press.
20. Chakrabarti, S.K., 1994. Offshore structure modeling. Advanced Series on Ocean Engineering, Volume 9, pp. 445-451.

21. Chakrabarti, S.K., 1998. Physical model testing of floating offshore structures. Proceedings of MTS Dynamic Positioning Conference, Houston, USA, pp. 1-33.
22. Chakrabarti, S.K.; 2002. The theory and practice of hydrodynamics and vibration. Advanced series on ocean engineering-Volume 20. World Scientific. Offshore Structures Analysis, Inc. Illinois, USA
23. Chakrabarti, S.K., 2005. Technical editor. Handbook of Offshore Engineering, (2-volume set), chapter 13, Elsevier Publications, Oxford, UK.
24. Chakrabarti, S., 2008. Challenges for a total system analysis on deepwater floating systems, Open Mechanics Journal, 2, pp. 28-46.
25. Chitrapu, AS., Erketin, RC., 1995. Time-domain simulation of large amplitude response of floating platforms. Ocean Engineering; 22-4 367-85
26. Comisión Nacional de Hidrocarburos (CNH), 2010. Factores de Recuperación de Aceite y Gas en México. Comisión Nacional de Hidrocarburos, Available at: http://cnh.gob.mx/_docs/DOCUMENTOTECNICO1FINAL.pdf (Accessed: 29 january 2014).
27. Comisión Nacional de Hidrocarburos (CNH), 2012a. Análisis de Información de las Reservas de Hidrocarburos de México al 1 de enero del 2012. Comisión Nacional de Hidrocarburos,. Available at: http://cnh.gob.mx/_docs/Libro_de_Reservas_CNH_2012.pdf (Accessed: 29 january 2014).
28. Comisión Nacional de Hidrocarburos (CNH), 2012b. Proyecto Área Perdido (Exploración). Available at: http://www.cnh.gob.mx/_docs/Exploracion/20.pdf (Accessed: 20 november 2013).
29. Correa, F. N., Senra, S. F., Jacob, B. P., Masetti, I. Q., & Mourelle, M. M., 2002. Towards the Integration of Analysis and Design of Mooring Systems and Risers: Part II—Studies

on a DICAS System. In ASME 2002 21st International Conference on Offsho*re* Mechanics and Arctic Engineering OMAE2002-28151, pp. 291-298 .

30. De Kat JO, Pauling RJ., 1989. The simulation of ship motions capsizing in severe seas. Transactions of the Society of Naval Arch Marine eng; 97:139-168
31. Dixon, A.G., Greasted, C.A. and Salter, S.H. 1979. Wave Forces on Partially Submerged Cylinders ASCE, Journal of the Waterway, Port, Coastal and Ocean Division.
32. DNV-RP-C205, 2007. Environmental conditions and environmental loads. Recommended practice, Det Norske Veritas, Norway.
33. DNV-RP-F205, 2010. Global performance analysis of deepwater floating structures. Det Norsle veritas, Norway.
34. Faltinsen, O.M., 1990. Wave loads on offshore structures. Annual review of fluid mechanics, 22, pp. 35-56.
35. Faltinsen, O.M., 1994. Wave and current induced motions of floating production systems, Elsevier, Applied Ocean Research, 15, pp. 351-370.
36. Faltinsen, O.M., 1998. Sea loads on ships and offshore structures.Ocean technology series, Cambridge university press.
37. Floating Production Systems report, (FPS), 2000. Assesment of the outlook for FPSO vessels, production semis, TLPs and spars, International Maritime Associates, Inc. Washington, DC USA, 2000.
38. Fylling, I.J., Stansberg, C. T., 2005. Model testing of deepwater floating production systems: Strategy for truncation of moorings and risers. Proceedings of 17th DOT Conference, Vitoria, Brazil, pp. 1-4.
39. Fryer, D., Watts, S. and Evans, M., 2001. Experiments methods for non-linear hydrodynamic response to waves. Proceedings of 20th International Conference on

Offshore Mechanics and Arctic Engineering, Paper OMAE2001/OFT-1251, Rio de Janeiro, Brazil, Vol.1 pp. 57-66.

40. Garrett, D.L. 2005. Coupled analysis of floating production systems, Ocean Engineering, 32(7), pp. 802-816.
41. Hauteclocque, G., Rezende F., Waals, O., Chen, X., 2012. Review of approximations to evaluate second-order low-frequency load. In: ASME 2012, 31st International Conference on Ocean, Offshore and Artic Engineering, Rio de Janeiro, Brazil, pp. 363-371.
42. Haveman C., Jeffrey Parliament J., Sokol J., Swenson J., Timothy Wagner T., 2006. Design of a floating, production, storage and offloading vessel for operation in the South China sea. Texas University Final Report.
43. Hermans, A. J., 1999. Low-frequency second-order wave-drift forces and damping, Journal of Engineering Mathematics, 35, (1-2), pp. 181-198.
44. Heurtier, J. M., Le Buhan, P., Fontaine, E., Le Cunff, C., Biolley, F., & Berhault, C., 2001. Coupled dynamic response of moored FPSO with risers. In The Eleventh International Offshore and Polar Engineering Conference. International Society of Offshore and Polar Engineers, ISOPE-I-01-050, Stanvanger, Norway.
45. Hoerner, S.F., 1965: Fluid-dynamic Drag Own, Washington D.C.
46. Irani, M.B., Johnson R. P. and Ward E. G., 2001. FPSO responses to wind, wave and current loading. Proceedings of 20th International Conference on Offshore Mechanics and Arctic Engineering, Paper OMAE2001/OFT-1023, Rio de Janeiro, Brazil, Vol.1 pp. 57-66.
47. ITTC, 2008. Recommended Procedures and Guidelines, Testing and Extrapolation Methods, Loads and Responses, section 7.5-02-07-03.5, Truncation of Test Models and Integration with Numerical Simulations, Ocean Engineering Committee of 25th ITTC, Fukuoka, Japan.
48. Journee, J.M., Massie, W.W., 2001. Offshore hydrodynamics. Delf University of Technology, 4, 38.

49. Kaplan, P., & Silbert, M. N., 1976. Impact forces on platform horizontal members in the splash zone. In *Offshore Technology Conference*. Offshore Technology Conference, OTC-2497-MS.
50. Kim, CH., 1995. Recent progress in numerical wave tank research: a review. 4th International Conference of the Society of Offshore Polar engineering, Osaka, 9p.
51. Kim, M.M., Tahar, A., Kim, Y.B., 2001, Variability of Spar Motion Analysis against Design Methodologies/Parameters, OMAE2001/OFT-1064.
52. Kim, C.H., 2008. Nonlinear waves and offshore structures, Advanced Series on Ocean Engineering-Volume 27. London: World Scientific.
53. Lee, C.H., Newman, J. N., 1991a. The computation of second-order wave loads by WAMIT, 10th International Conference on Offshore Mechanics & Arctic Engng, Vol 1, pp. Part A, p 113-123
54. Lee, C.H., Newman, J. N., 1991b. First-and second-order wave effects on a submerged spheroid, Journal Ship Research, Vol 35, (Marine Transportation), pp. 183-190.
55. Lee, C.H, Newman, J. N., 2005. Computation of wave effects using the panel method. Numerical Models in Fluid Structure Interaction, 42, 211-251.
56. Lewis, F.M. 1929. The inertia of the water surrounding a vibrating ship, SNAME Trans., vol. 37, pp. 1-20.
57. Longuet-Higgins, M., Cokelet E., 1976 The deformation of steep surface waves on water: 1. a numerical method of computation. Proceedings of Royal Societey of London. A350:1-26
58. Low, Y. M., Langley, R. S., 2006. Time and frequency domain coupled analysis of deepwater floating production systems. Applied Ocean Research, 28(6), pp. 371-385.

59. Low, Y.M., Langley, R. S., 2008. A hybrid time/frequency domain approach for efficient coupled analysis of vessel/mooring/riser dynamics, Ocean Engineering, 35(5), pp. 433-446.

60. Luo, Y., Baudic, S., Poranski, P., Wichers, J., Stansberg, C.T. and Ormberg, H., 2004. Deepstar study on predicting FPSO responses—model tests vs numerical analysis, Offshore Technology Conference, paper OTC 16585, Houston Texas.

61. Ma, S., Duan W.Y., Han, X.L. and Xu L., 2015. Dynamic asynchronous coupled analysis and experimental study for a turret moored FPSO in random seas. Journal of Offshore mechanics and Artic Engineering, Vol. 137/041302.

62. Maruo, H., 1960. On the increase of the resistance of a ship in rough seas. J. Zosen Kiokai, 108, 9, 73-91.

63. Monroy, C., Giorgiutti, Y. and Chen, X.-B., 2012. First and second order wave-current interactions for floating bodies. Proceedings of 31st International Conference on Ocean, Offshore and Arctic Engineering, OMAE2012-83409, Rio de Janeiro Brazil, Vol. 1, pp.373-382.

64. Moxnes, S., Larsen, K., 1998. Ultra small scale model testing of a FPSO ship. Proceedings of the 17th International Offshore Mechanics and Arctic Engineering, OMAE98-0381, Lisbon, Portugal.

65. Newman, J. T., 1967. The drift force and moment on ships in waves. Journal of ship research, 11(1), 51-60.

66. Newman, J.N., 1974. Second-order, slowly-varying forces on vessels in irregular waves. Proc Int Symp DYnm Marine Vehicles Struct Waves, IMechE, London.

67. Newman, J.N., 1977. Marine hydrodynamics. the Massachusetts Institute of Technology, MIT press, USA.

68. Newman, J. N., Lee, C. H., 2002. Boundary-element methods in offshore structure analysis. Journal of Offshore Mechanics and Arctic Engineering, 124(2), 81-89.
69. Newman, J.N., 2004. Progress in wave load computations on offshore structures, 23rd International Conference on Offshore Mechanics and Arctic Engineering, Vancouver, Canada, pp. 20-25.
70. Nutter, T., 2014. Worlwide survey of floating production, storage and offloading (FPSO) units, wood group Mustang, Offshore magazine, Houston, Texas, USA.
71. Qualisys, 2010. Contactless optical tracking motion system Qualisys, Gothenburg, Sweden.
72. ORCAFLEX, 2014. Manual version 9.8a, Orcina Ltd. Daltongate Ulverston Cumbria, UK.
73. OCIMF, 1994. OCIMF prediction of wind and current loads on VLCCs. Witherby and Co. Ltd, London, England.
74. Ormberg, H., Larsen, K., 1998. Coupled analysis of floater motion and mooring dynamics for a turret-moored ship, Applied Ocean Research, 20(1–2), pp. 55-67.
75. Pinkster, J. A., 1975. Low-frequency phenomena associated with vessels moored at sea. Society of Petroleum Engineers Journal, 15(06), 487-494.
76. Pinkster, J. A., Van Oortmerssen, G., 1977. Computation of the first and second-order wave forces on oscillating bodies in regular waves. In Proc. Second Int. conf. Numerical ship hydrodynamics, ed. J. V. Wehausen and N. Salvesen, pp. 136-56, Berkeley: University Extension Publications, University of californis, Berkeley.
77. Pinkster, J.A., 1980. Low frequency second order wave exciting forces on floating structures. TU Delft, Delft University of Technology.
78. RIFLEX-SESAM, 2013. RIFLEX-Theory Manual version 3.6, Marintek, Trondheim, Norway.

79. Sarpkaya, T., 1978. 'Fluid forces on oscillating cylinders', Journal of Waterway, Port, Coastal and Ocean Division, 104(3), pp. 275-290.
80. Sen, D., 2002. Time-domain computation of large amplitude 3D ship motions with forward speed. Ocean Engineering, 29(8), 973-1002.
81. Senra SF., Correa FN., Jacob BP., Mourelle MM., Masetti, IQ., 2002. Towards the integration of analysis design of mooring systems risers, Part I: Studies on a DICAs system. Proceedings of Offshore Mechanics Arctic Engineering Conference; OMAE2002-28151 pp. 291-98.
82. SIMO-SESAM, 2015. SIMO-Theory Manual version 4.4 rev 1, Marintek, Trondheim, Norway.
83. Standing, R. G., 1988. 'Second-order wave spectral methods, mooring forces and lowfrequency response of floating structures', Journal of the Society for Underwater Technology, 14, (4), pp. 2-12.
84. Stansberg, C.T., Hoff, J.R., Hermundstad, E. M., Baarholm, R., 2013. Wave drift froces and responses in current. Proceedings 32nd International Conference on Ocean, Offshore and Arctic engineering, Nantes, France, OMAE2013-11407, pp. V001T01A0771.
85. Stansberg, C.T., Karlsen, S.I., Ward, E.G., Wichers, J.E.W. and Irani, M.B., 2004. Model testing for ultradeep waters, Offshore Technology Conference, paper OTC 16587, Houston Texas.
86. Stansberg, C.T., Ormberg, H. and Oritsland, O., 2002. Challenges in deep water experiments: Hybrid approach, Journal of Offshore Mechanics and Arctic Engineering, 124(2), pp. 90-96.
87. Stansberg, C.T., Øritsland, O. and Kleiven, G., 2000. VERIDEEP: Reliable methods for laboratory verification of mooring and stationkeeping in deep water. Offshore Technology Conference, paper OTC-12087, Houston Texas.

88. Su, Y., Yang, J., Xiao, L. and Chen, G., 2009. Experimental and numerical study on large truncation of deepwater mooring line. Proceedings 28th International Conference on Ocean, Offshore and Arctic Engineering, OMAE2009-79218, Honolulu, Hawaii, USA, pp. 201-212.
89. Tahar, A., Kim, M. H., 2003. Hull/mooring/riser coupled dynamic analysis and sensitivity study of a tanker-based FPSO, Applied Ocean Research, 25(6), pp. 367-382.
90. Tian X., Yang J., Lu H., 2010. Development of data analysis program for offshore engineering hydrodynamic model test. Research and Exploration in Laboratory. Vol 29(6).
91. Waals, O., Van D., Radbound R.T., 2004. Truncation methods for deep water mooring systems for a catenary moored FPSO and a semi taut moored semisubmersible, DOT2004, paper 24-1, New Orleans, USA.
92. WADAM-SESAM, 2014. Frequency domain hydrodynamic analysis of stationary vessels-wadam. Wadam Hydro-D User Manual, DNV Software, 2014.
93. Ward, E.G., Irani, M.B. and Johnson, R.P., 2001. Responses of a tanker-based FPSO to hurricanes. Offshore Technology Conference, paper OTC-3214-MS, Houston, Texas.
94. Wichers, J.E.W., 1988. A simulation model for a single point moored tanker. PhD thesis, TU Deft 243 pp.
95. Wichers, J.E., Qun J.C. 1997. Behaviour of turret moored tankers in combinaded extreme metocean parameters. Offhsore Technology, OTC8272, Houston, Texas.
96. Wichers, J., 2001. Effect of coupling of mooring lines and risers on the design values for a turret moored FPSO in deep water of the Gulf of Mexico. International Offshore and Polar Engineering Conference, ISOPE-I-01-304, Stavanger, Norway, 2001.
97. Wichers, J., 2013. Guide to single point moorings, Wmooring.inc. Houston, Texas, USA.
98. Xiong, L., Lu, H., Yang, J., Zhao W., 2015. Motion response of a moored barge in shallow water, Ocean Engineering, 97, pp. 201-217.

99. Zhao, R. and Faltinsen, O.M., 1989. Interaction between current, waves and marine structures. 5th International Conference on Ship Hydrodynamics Hiroshima, pp. 513-27.

100. Zheng, Z. S., Kim, W. J., 2010. Numerical investigation of vortex shedding and vortex-induced vibration for flexible riser models. International Journal of Naval Architecture and Ocean Engineering, 2(2), 112-118.

101. Yuan, Z. M., Incecik, A., & Ji, C., 2014. Numerical study on a hybrid mooring system with clump weights and buoys. Ocean Engineering, 88, 1-11.

Appendix A

Mooring lines design

A.1 Mooring line design

Assumptions:

- Design service life: 25 years
- 1000 m water depth (wd)
- 100 year return period of storm and hurricane environment loading
- Semi-taut catenary mooring lines
- 9 mooring lines: Chain RK4S stud-less type and wire spiral Strand Xtreme
- Lengths of the chain section in fairlead – bottom: 50-935 m respectively
- Length of wire spiral strand section: 1200 m
- No friction with soil is considered
- No Corrosion and marine growth
- Vessel in Full Load condition

Table A.1 Tension criteria (Factor of Safety), applicable for permanent and MODU moorings (API-RP-2SK-2005)

Condition	Analysis Method	Tension Limit (% Breaking Strength)	Factor of Safety
Intact	Quasi-Static	50	2
Intact	Dynamic	60	1.67
Damaged	Quasi-Static	70	1.43
Damaged	Dynamic	80	1.25
Transient	Quasi-Static	85	1.18
Transient	Dynamic	95	1.05

Table A.2 Offset limits, (Wichers, 2013)

Conditions	Rigid Riser
Intact	10 % WD
Damaged	12% WD

Table A.3 Environment loading condition for design

Description	Unit	Storm	Hurricane
Waves			
Hs	m	9.67	8.56
Tp	s	13.28	12.81
Wave spectrum	Jonswap (γ=2.3)		
Wave direction	deg	180^0	180^0
Wind speed (1-hr)		21.95	23.23
Wind spectrum	API RP 2A-WSD		
Wind direction	deg	0^0 and 60^0 relative to waves	
Current profile			
Surface	m/s	1.44	1.60
Current direction	deg	0^0 and 90^0 relatives to waves	

Sensitivity analysis of the mooring lines (small length variations)

	Basis case	
Fairlead section:	50	m
Mid-Section:	1200	m
Bottom Section:	935	m
Base Case	**2185**	**m**
	Case 1	
Fairlead section:	50	m
Mid-Section:	1205	m
Bottom Section:	940	m
	2195	**m**
	Case 2	
Fairlead section:	50	m
Mid-Section:	1210	m
Bottom Section:	945	m
	2205	**m**
	Case 3	
Fairlead section:	50	m
Mid-Section:	1230	m
Bottom Section:	980	m
	2260	**m**

-Influence of the different mooring lines lengths:

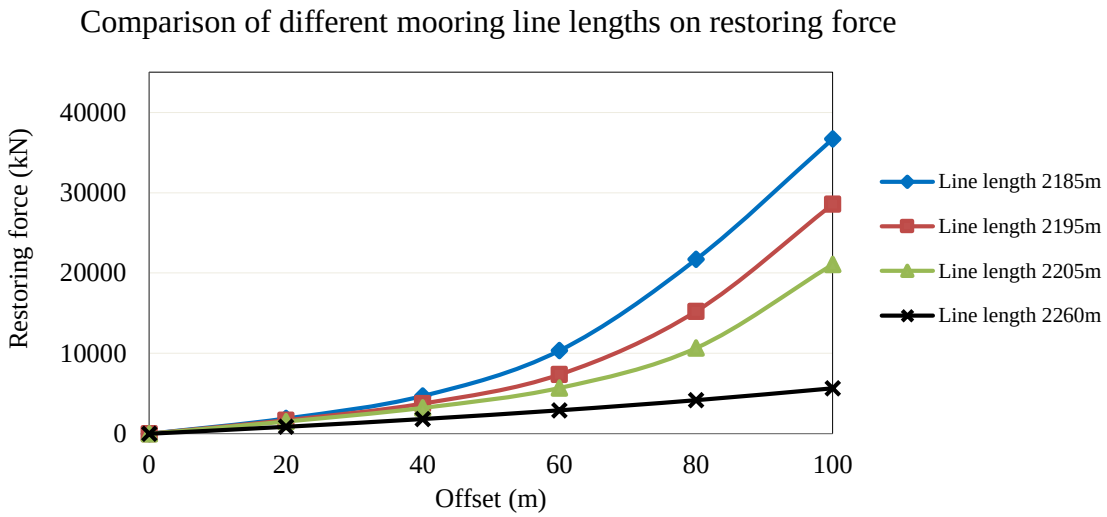

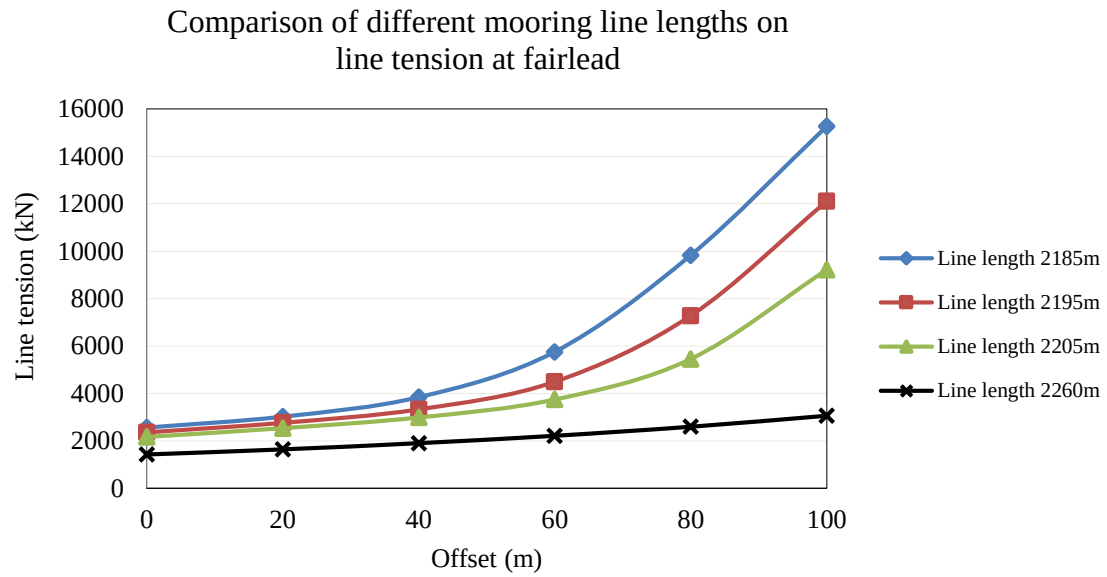

Comments:

The influence of the mooring length plays a significant role in the restoring force and pretension and tension of the lines. The basis case study considers a length of the mooring line = 2185 m

-Influences of different diameters

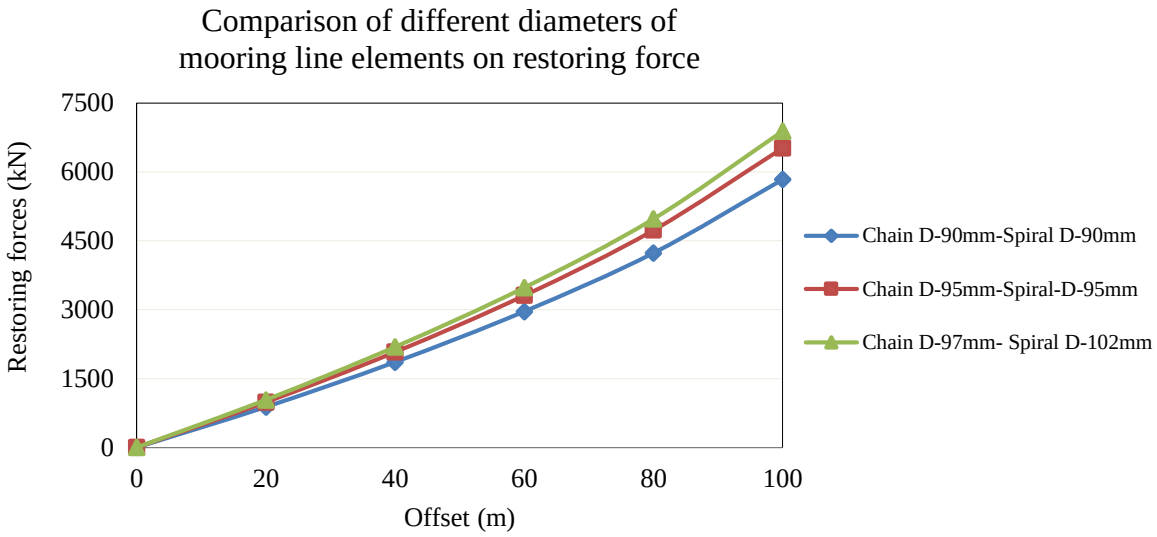

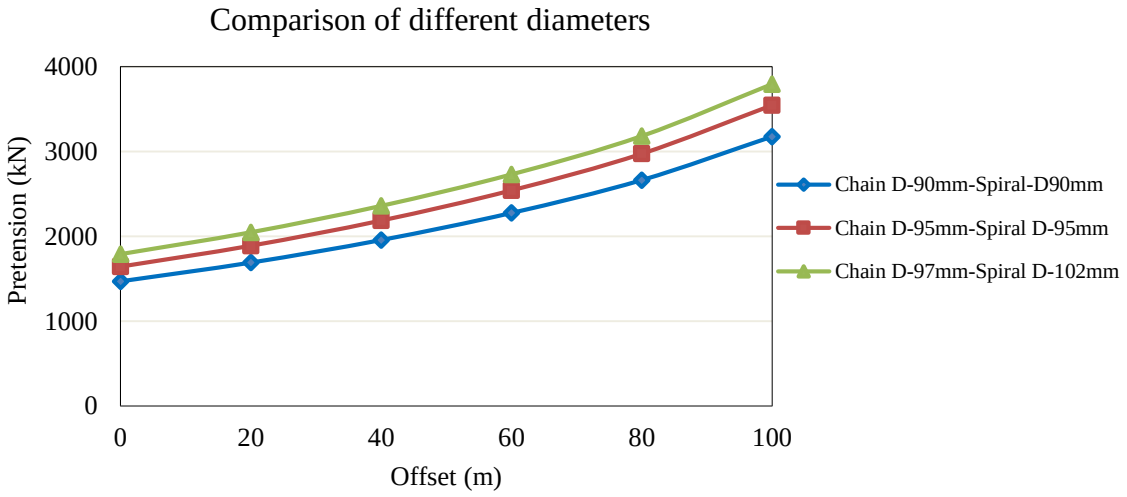

Comments:

The influence of different diameters, reflecting the line weight, for restoring forces and pretension is minimal, however the major influence is given in respect to the breaking strength of the lines. The diameter is selected with respect to the tension criteria (Factor of safety), applicable for both permanent and MODU moorings (API-RP-2SK-2005).

-Influences of different anchor locations

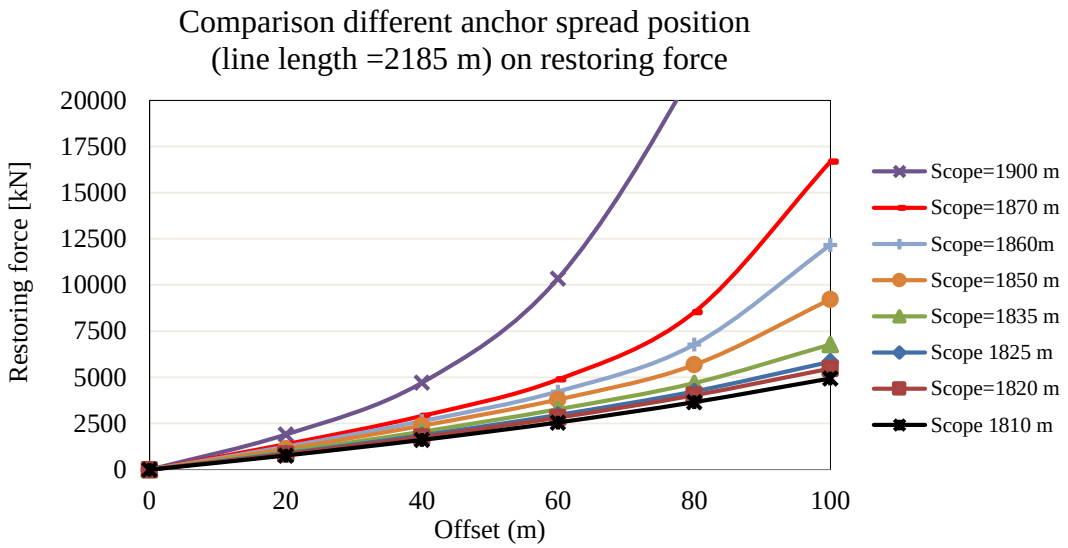

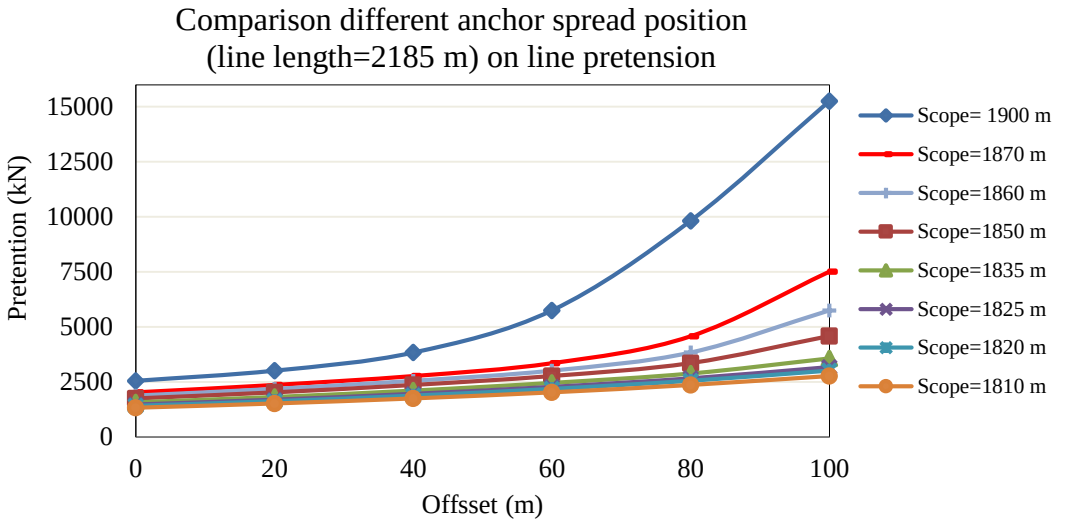

Comments:

The anchor positioning has a significant role in the pretension and restoring forces.

The arrangement with a horizontal spread length of mooring lines = 1870 m and Pretension= 2025 kN were selected to be used in the mooring line configuration

A.4 Results for the arrangement 3x3 = 9 mooring lines under storm loading condition

Only mooring lines Turret 30 m aft LPP (10%Lpp) Full Loading Condition, anchor spread position 1.87 times water depth (3 hrs Time simulation)									
Intact Condition									
Configuration	**Case**	**Environment loading**	**Condition**	**Analysis Method**	**Maximum tension (kN)**	**SF**	**API SF**	**Maximum Offsset (m)**	**API Maximum offset (m)**
9 lines	Case 1: In line	Storm Collinear (180^0)	Intact	Static	2496.11	3.18	2	26.61	100
9 liines	Case1: In line	Storm Collinear (180^0)	Intact	Dynamic	3883.80	2.04	1.67	51.45	100
9 lines	Case 2: Between lines	Storm Collinear (0^0)	Intact	Static	2272.45	3.49	2	30.89	100
9 liines	Case2: Between lines	Storm Collinear (0^0)	Intact	Dynamic	3528.43	2.25	1.67	68.64	100
9 lines	Case 3: Non-collinear	Storm Collinear (Wave=$180^{0,}$ Wind=$60^{0,}$ Current= 90^0)	Intact	Static	2369.46	3.35	2	25.04	100
9 liines	Case3: Non-collinear	Storm Collinear (Wave=$180^{0,}$ Wind=$60^{0,}$ Current= 90^0)	Intact	Dynamic	3789.00	2.10	1.67	48.14	100
Damage Condition									
9 lines	Case 1: In line	Storm Collinear (180^0)	Damage	Static	3262.22	2.43	1.43	57.03	100
9 liines	Case1: In line	Storm Collinear (180^0)	Damage	Dynamic	5202.16	1.53	1.25	77.38	100
9 lines	Case2: Between lines	Storm Collinear (180^0)	Damage	Static	2852.93	2.78	1.43	47.67	100
9 lines	Case2: Between lines	Storm Collinear (180^0)	Damage	Dynamic	4272.72	1.86	1.25	88.39	100
9 lines	Case 3: Non-collinear	Storm Collinear (Wave=$180^{0,}$ Wind=$60^{0,}$ Current= 90^0)	Damage	Static	3008.87	2.64	1.43	48.07	100
9 liines	Case3: Non-collinear	(Wave=$180^{0,}$ Wind=$60^{0,}$ Current= 90^0)	Damage	Dynamic	5134.71	1.55	1.25	79.44	100

A.5 Results for the arrangement 3x3 = 9 mooring lines under hurricane loading condition

Only mooring lines Turret 30 m aft LPP (10%Lpp) Full Loading Condition, anchor spread position 1.87 times water depth (3 hrs Time simulation)									
Intact Condition									
Configuration	**Case**	**Environment loading**	**Condition**	**Analysis Method**	**Maximum tension (kN)**	**SF**	**API SF**	**Maximum Offsset (m)**	**API Maximum offset (m)**
9 lines	Case 1: In line	Hurricane Collinear (180^0)	Intact	Static	2473.36	3.21	2	24.99	100
9 liines	Case1: In line	Hurricane Collinear (180^0)	Intact	Dynamic	3633.09	2.18	1.67	41.78	100
9 lines	Case 2: Between lines	Hurricane Collinear (0^0)	Intact	Static	2264.19	3.51	2	-28.79	100
9 liines	Case2: Between lines	Hurricane Collinear (0^0)	Intact	Dynamic	3322.13	2.39	1.67	-56.21	100
9 lines	Case 3: Non-collinear	(Wave=$180^{0,}$ Wind=$60^{0,}$ Current= 90^0)	Intact	Static	2310.8	3.44	2	-22.7	100
9 liines	Case3: Non-collinear	Hurricane Collinear (Wave=$180^{0,}$ Wind=$60^{0,}$ Current= 90^0)	Intact	Dynamic	3315.53	2.39	1.67	-46.22	100
Damage Condition									
9 lines	Case 1: In line	Hurricane Collinear (180^0)	Damage	Static	3153.96	2.52	1.43	-53.87	100
9 liines	Case1: In line	Hurricane Collinear (180^0)	Damage	Dynamic	4546.15	1.75	1.25	-69.95	100
9 lines	Case2: Between lines	Hurricane Collinear (180^0)	Damage	Static	2833.09	2.80	1.43	44.89	100
9 lines	Case2: Between lines	Hurricane Collinear (180^0)	Damage	Dynamic	3955.09	2.01	1.25	71.86	100
9 lines	Case 3: Non-collinear	Hurricane Collinear (Wave=$180^{0,}$ Wind=$60^{0,}$ Current= 90^0)	Damage	Static	2915.4	2.72	1.43	-44.93	100
9 liines	Case3: Non-collinear	Hurricane Collinear (Wave=$180^{0,}$ Wind=$60^{0,}$ Current= 90^0)	Damage	Dynamic	4042.49	1.96	1.25	-65.16	100

Note: The most loaded line is used in the analysis:

- Collinear 'In-line' and Non-collinear case: (L-2)
- Between lines condition: (L-7)

Comments:

The simple configuration of 3x3 mooring lines is enough for keeping the safety factor and offsets limits according to API-RP-2SK (2005) and Wichers (2013). Additionally, the storm environment condition is identified to be the most severe loading condition compared with hurricane condition on system in the specific location. Thus the storm environmental loading condition is selected to be used in the experimental model tests.

Appendix B

Wind and current coefficients

B.1 Wind areas on the FPSO

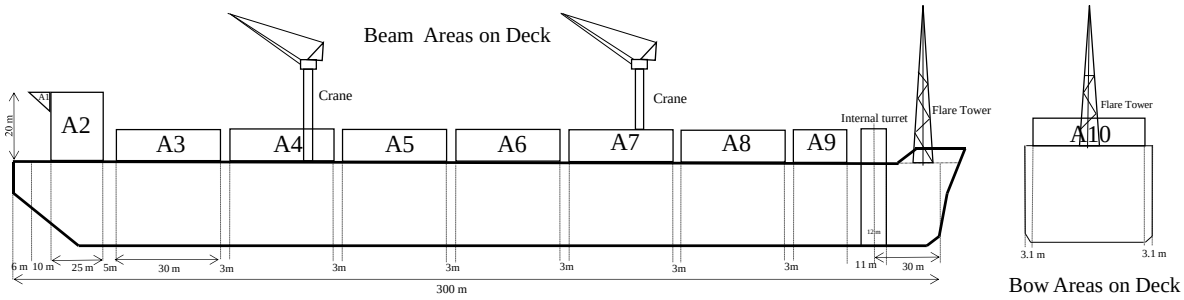

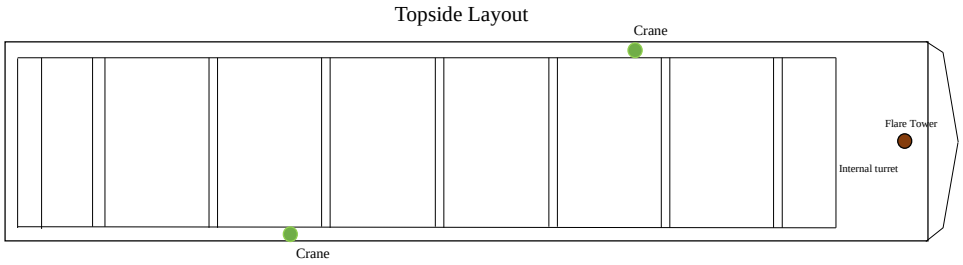

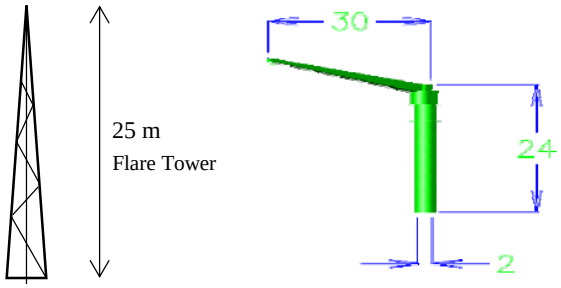

Table B.1 Wind areas on the FPSO vessel (Haveman et al., 2006)

Area	Length (m)	Width (m)	Height (m)	Beam Areas on Deck (m^2)
A1	10	40	5	25
A2	25	40	20	500
A3	30	40	9	270
A4	30	40	9	270
A5	30	40	9	270

A6	30	40	9	270
A7	30	40	9	270
A8	30	40	9	270
A9	15	40	9	135
Hull	300	-	9.7	2910

Table B.2 Wind areas on the FPSO vessel (Haveman et al., 2006).

Area	Width (m)	Height (m)	Bow Area on Deck (m^2)
A10	40	20	800
Hull	46.20	9.7	448
Flare tower	4	25	100 approximate
Crane	4	25	100 (2 cranes)

Full Load Area:

Wind area bow (A_T): 1448 m^2

Wind area beam (A_L) m^2: 5190 m^2

Table B.3 Wind coefficients on the FPSO vessel (OCIMF, 1994)

Full Load Condition					
Surge Heading	C_{xw}	Sway Heading	C_{yw}	Yaw Heading	C_{xyw}
0	0.75	0.00	0.00	0.00	0.00
20	0.73	20.00	0.28	20.00	-0.11
22.5	0.72	22.50	0.30	22.50	-0.13
40	0.53	40.00	0.55	40.00	-0.16
45	0.45	45.00	0.60	45.00	-0.17
60	0.29	60.00	0.68	60.00	-0.16
67.5	0.23	67.50	0.70	67.50	-0.16
80	0.14	80.00	0.72	80.00	-0.13
90	0.05	90.00	0.73	90.00	-0.12
100	-0.05	100.00	0.70	100.00	-0.11
112.5	-0.23	112.50	0.68	112.50	-0.09
120	-0.33	120.00	0.64	120.00	-0.08
135	-0.58	135.00	0.50	135.00	-0.06
140	-0.62	140.00	0.43	140.00	-0.05
157.5	-0.80	157.50	0.23	157.50	-0.02
160	-0.83	160.00	0.19	160.00	-0.02
180	-0.96	180.00	0.00	180.00	0.00

Table B.4 Current coefficients on the FPSO (OCIMF, 1994)

Full Load condition					
Surge Heading	C_{Xc}	Sway Heading	C_{Yc}	Yaw Heading	C_{XYc}
0	0.04	0	0.00	0	-0.01
20	0.03	20	0.15	20	-0.06
40	0.00	40	0.35	40	-0.08
60	-0.03	60	0.50	60	-0.08
80	-0.01	80	0.60	80	-0.03
100	0.03	100	0.58	100	0.01
120	0.04	120	0.50	120	0.08
140	-0.01	140	0.35	140	0.09
160	-0.03	160	0.15	160	0.06
180	-0.04	180	0.00	180	0.00

Appendix C

Experimental decay tests

C.1 FPSO with mooring lines, Full Load condition

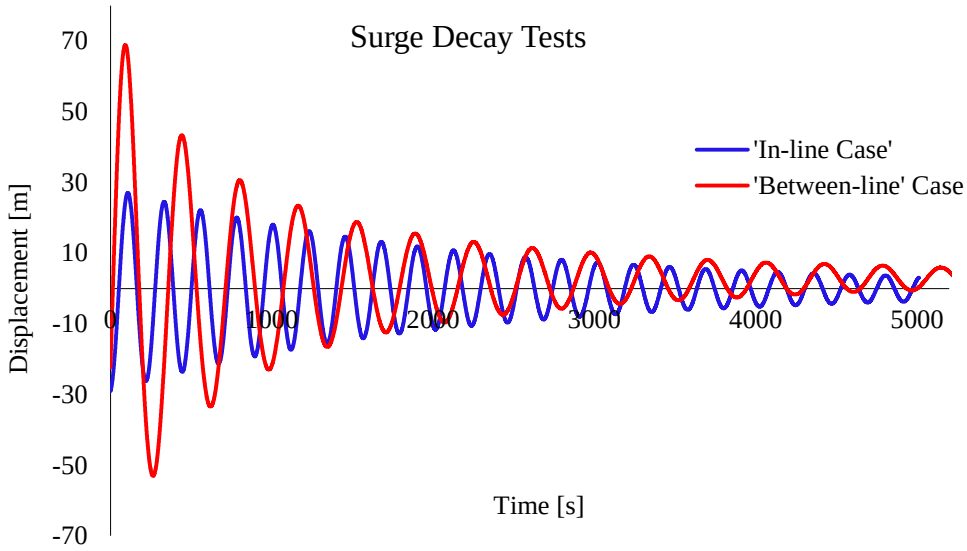

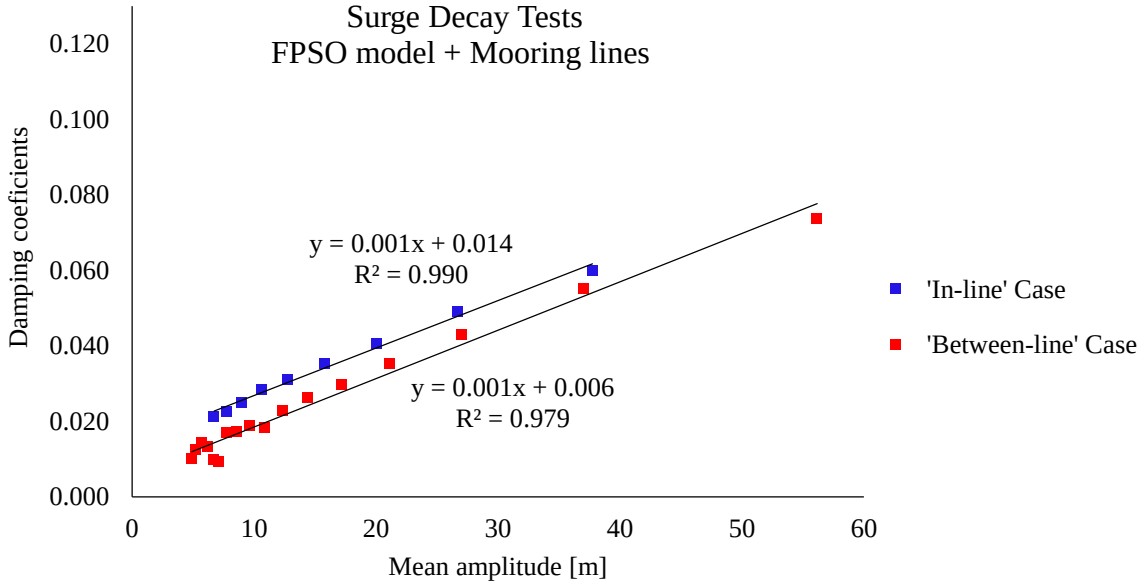

C.2 FPSO with mooring lines and risers, Full Load condition

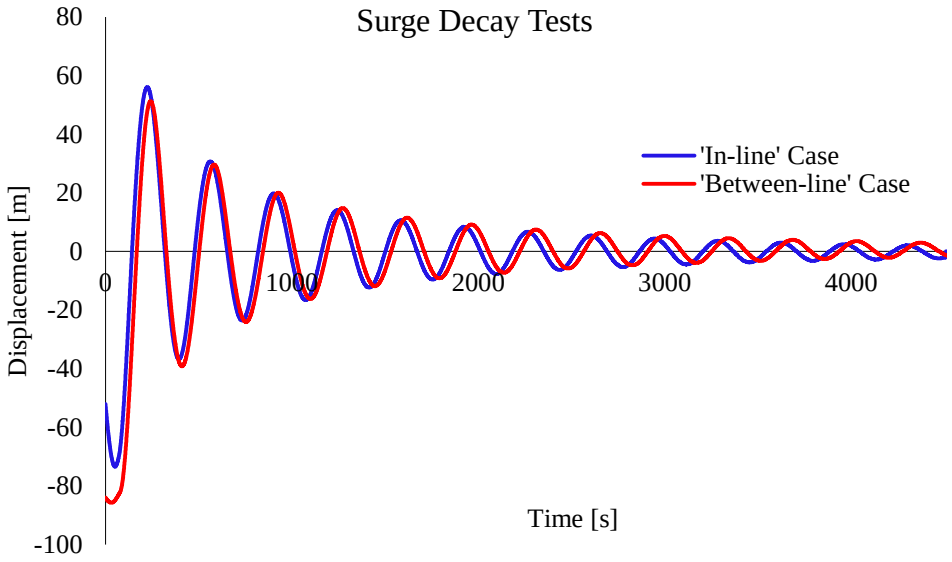

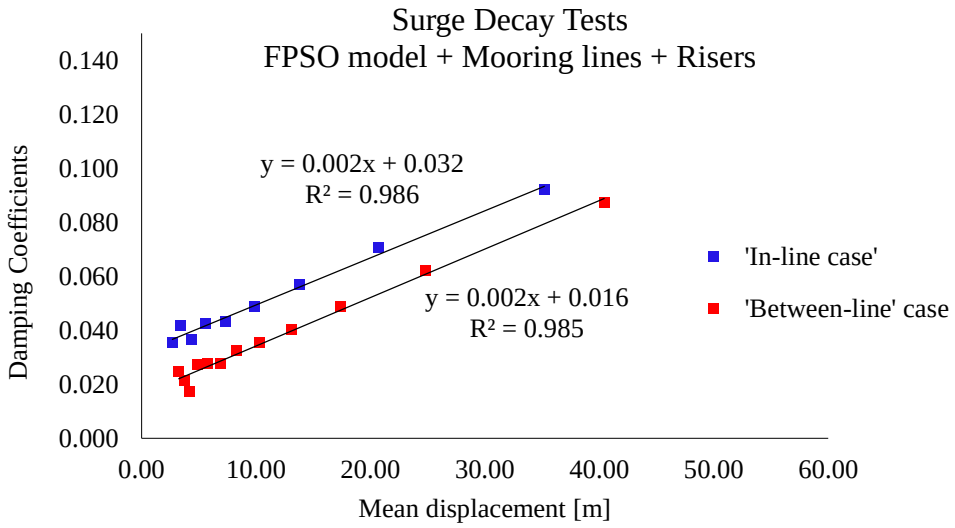

C.3 FPSO Full Load condition

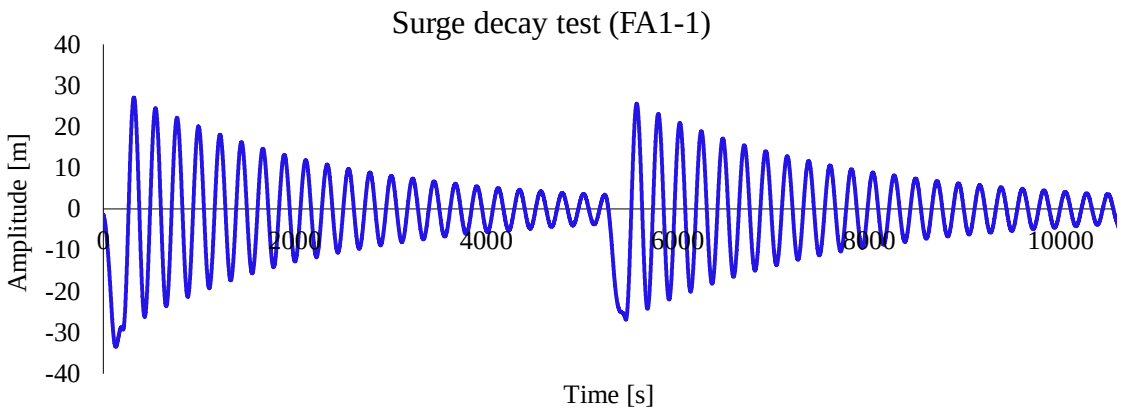

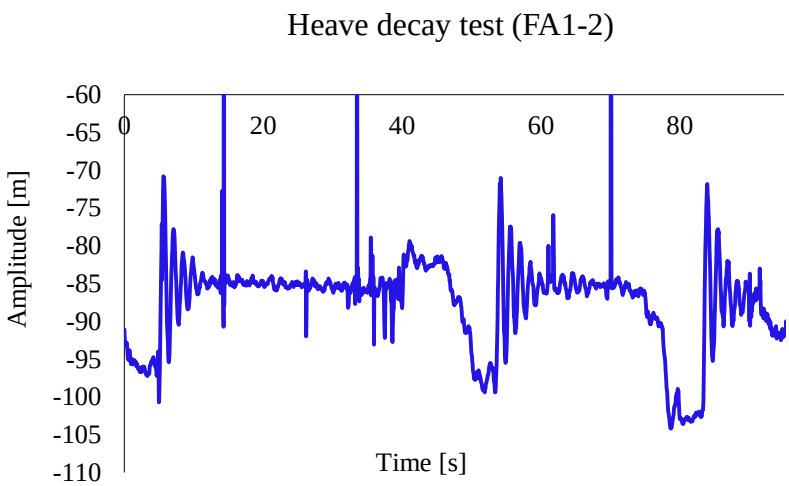

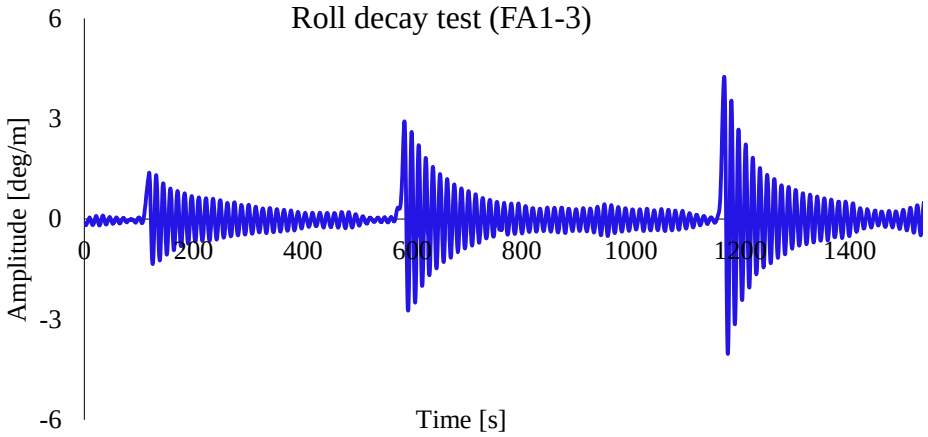

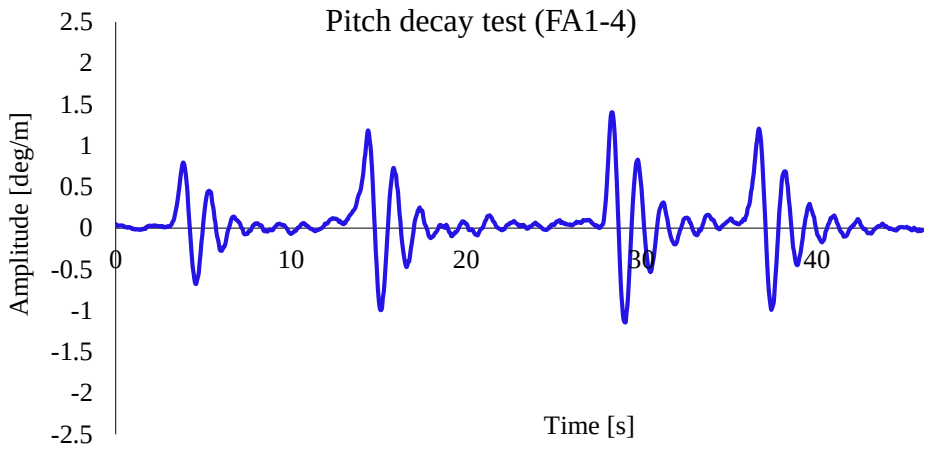
Pitch decay test (FA1-4)
Amplitude [deg/m]
2.5
2
1.5
1
0.5
0
-0.5
-1
-1.5
-2
-2.5
0
10
20
30
40
Time [s]

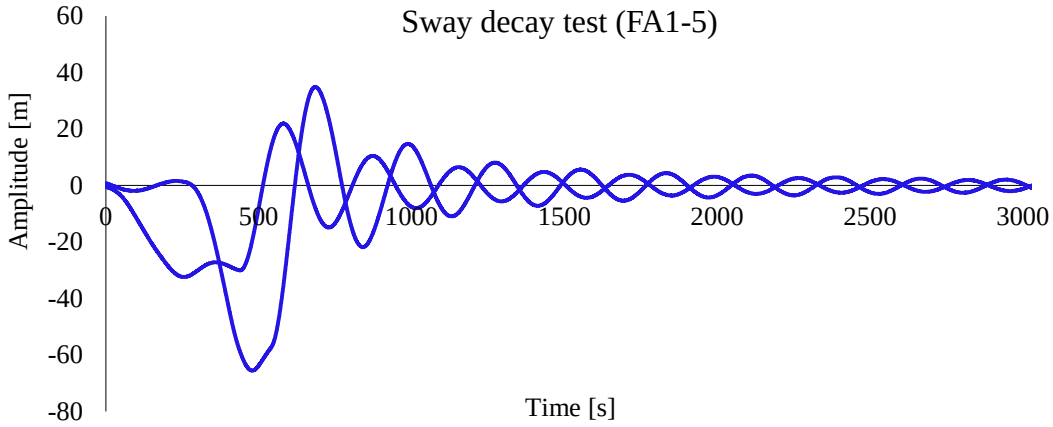
Sway decay test (FA1-5)
Amplitude [m]
60
40
20
0
-20
-40
-60
-80
0
500
1000
1500
2000
2500
3000
Time [s]

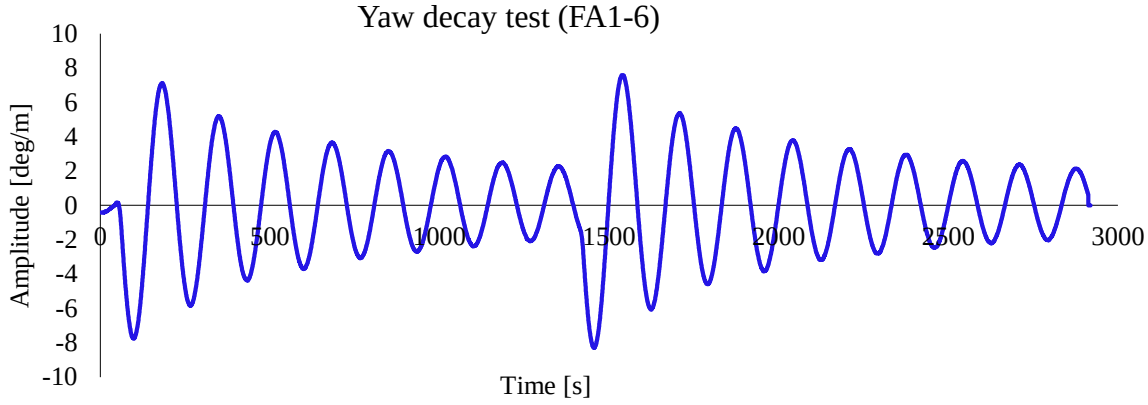
Yaw decay test (FA1-6)
Amplitude [deg/m]
10
8
6
4
2
0
-2
-4
-6
-8
-10
0
500
1000
1500
2000
2500
3000
Time [s]

C.4 FPSO Ballast Load condition

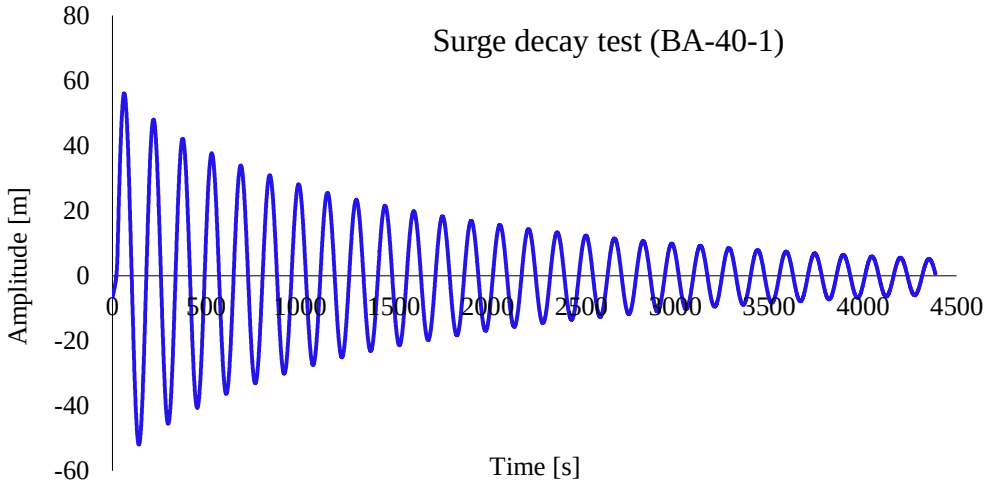

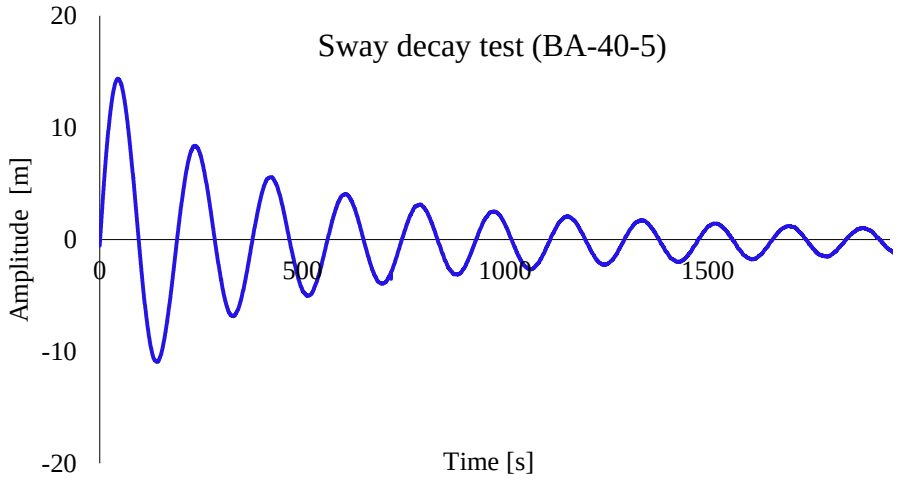

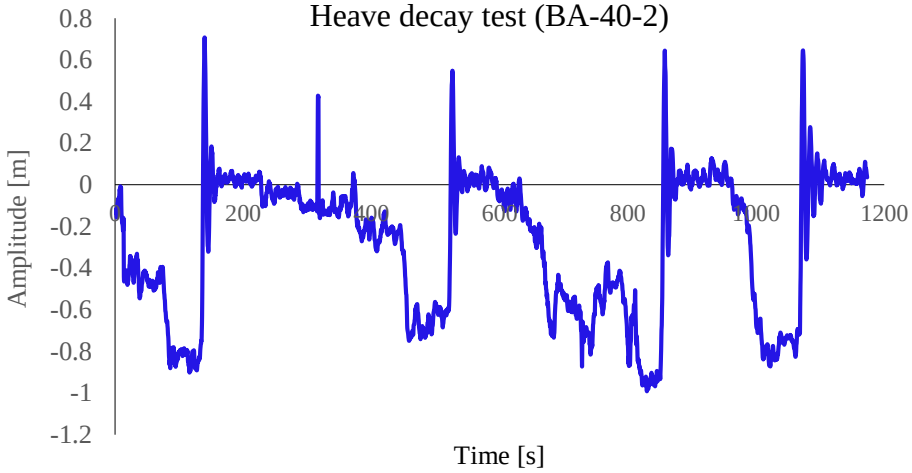
Heave decay test (BA-40-2)
Amplitude [m]
Time [s]
0.8
0.6
0.4
0.2
0
-0.2
-0.4
-0.6
-0.8
-1
-1.2
0
200
400
600
800
1000
1200

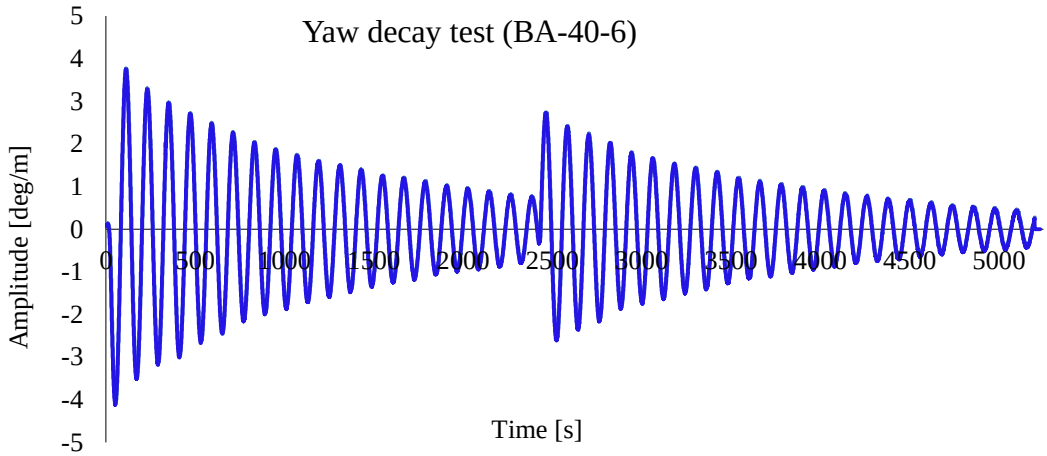
Yaw decay test (BA-40-6)
Amplitude [deg/m]
Time [s]
5
4
3
2
1
0
-1
-2
-3
-4
-5
0
500
1000
1500
2000
2500
3000
3500
4000
4500
5000

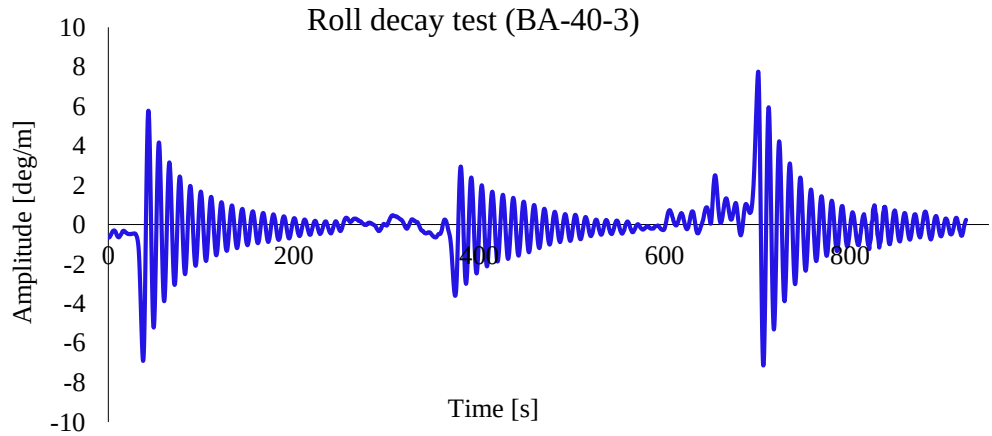
Roll decay test (BA-40-3)
Amplitude [deg/m]
Time [s]
10
8
6
4
2
0
-2
-4
-6
-8
-10
0
200
400
600
800

Appendix D

Experimental time series results

D.1 Full Load condition

-Collinear 'In-line' condition of irregular waves-current-wind (FB-19)

-System FPSO and mooring lines

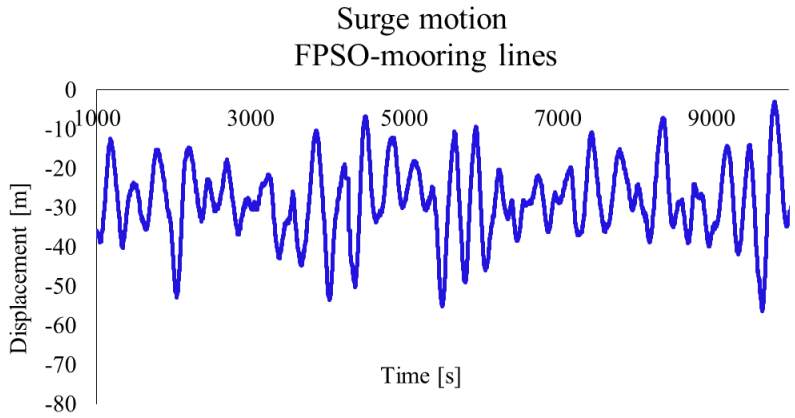

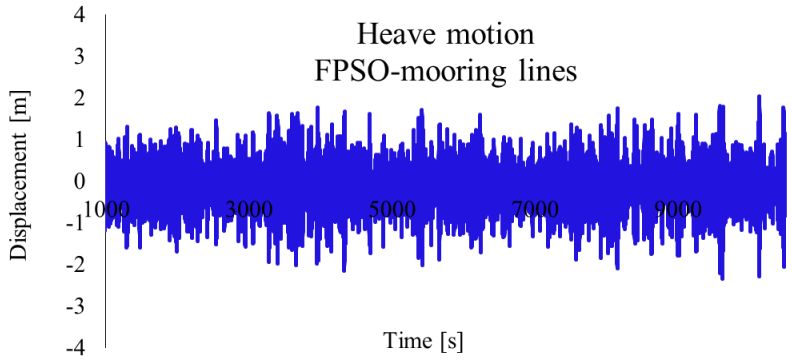

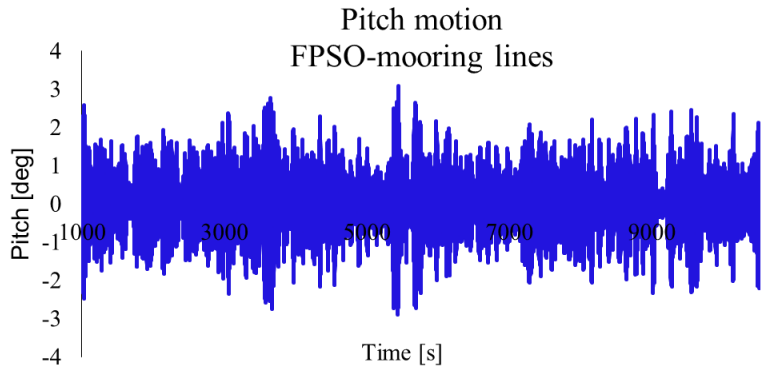
Pitch motion
FPSO-mooring lines
Pitch [deg]
4
3
2
1
0
-1
-2
-3
-4
1000
3000
5000
7000
9000
Time [s]

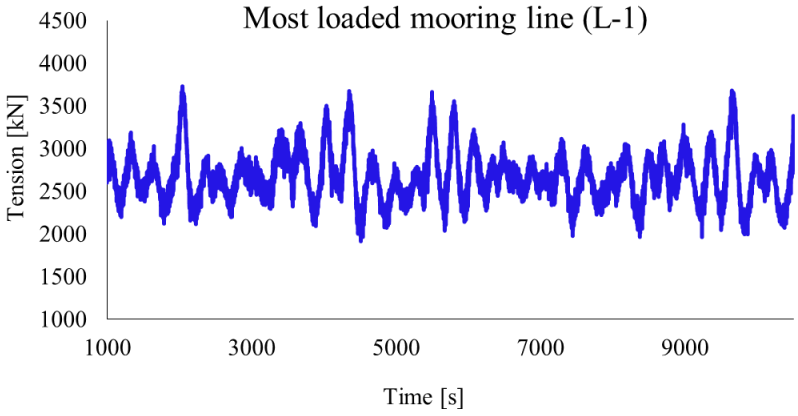
Most loaded mooring line (L-1)
Tension [kN]
4500
4000
3500
3000
2500
2000
1500
1000
1000
3000
5000
7000
9000
Time [s]

-Collinear 'Between-lines' condition of irregular waves-current-wind (FB-20)

-System FPSO and mooring lines

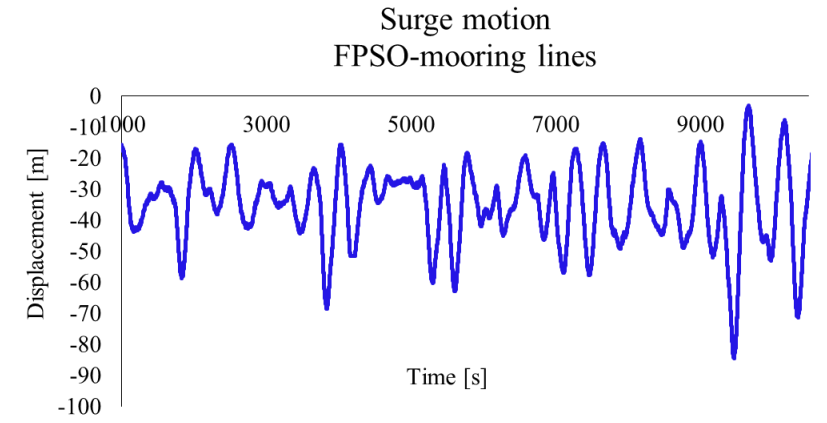

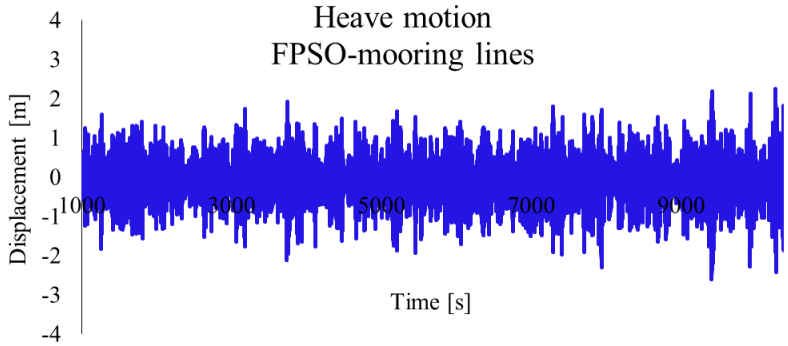

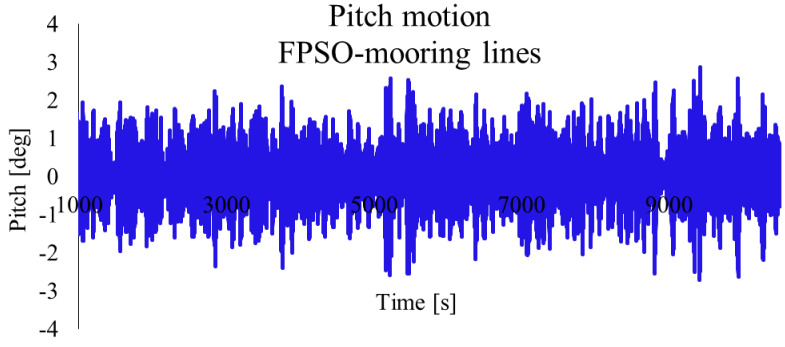

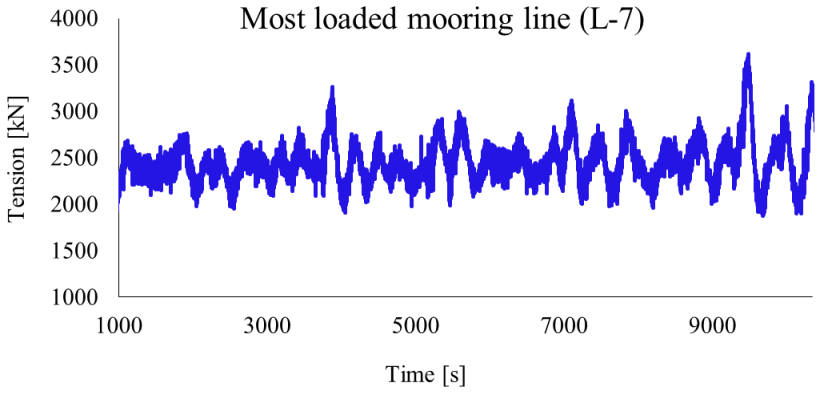

-Non-collinear condition of irregular waves-current-wind (FB-21)

-System FPSO and mooring lines

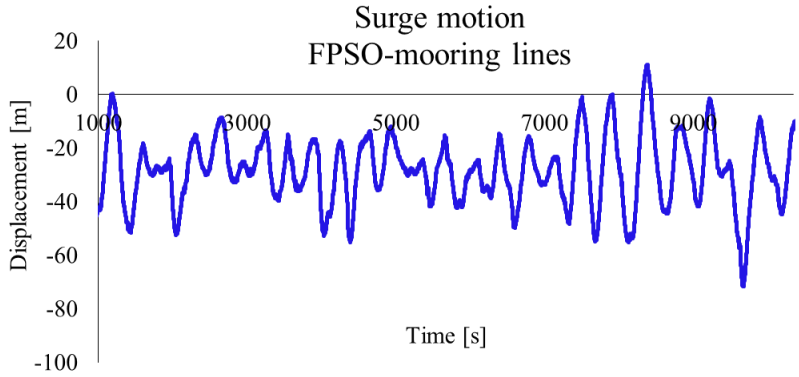

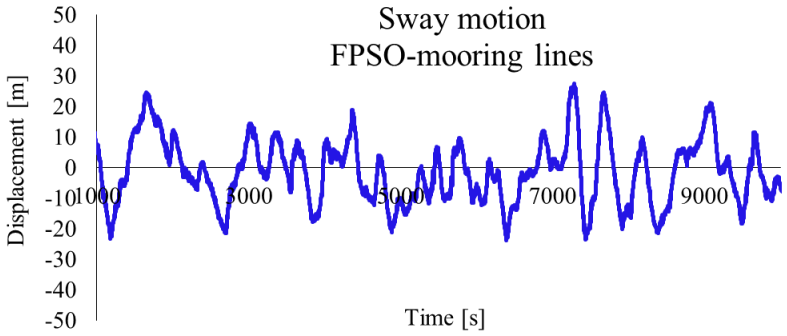

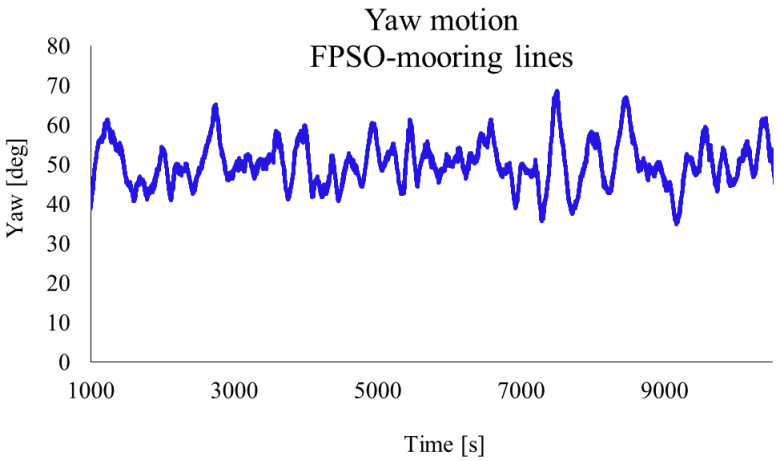

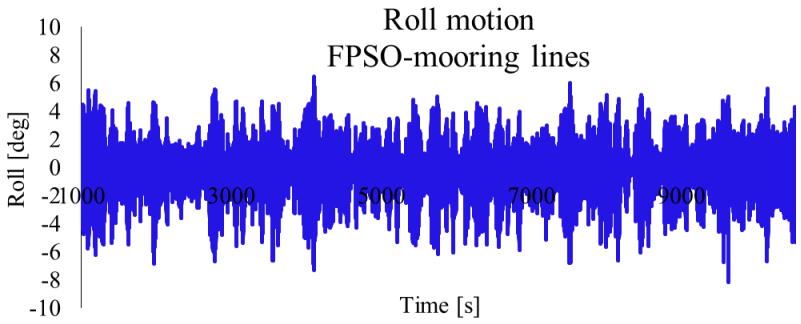
Roll motion
FPSO-mooring lines
Roll [deg]
10
8
6
4
2
0
-2
-4
-6
-8
-10
1000
3000
5000
7000
9000
Time [s]

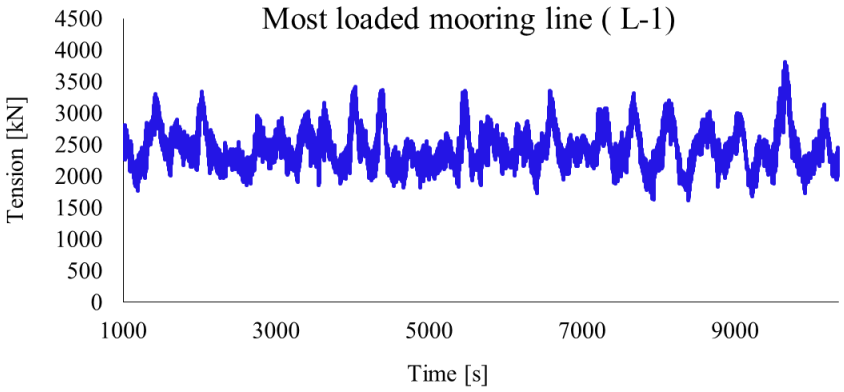
Most loaded mooring line (L-1)
Tension [kN]
4500
4000
3500
3000
2500
2000
1500
1000
500
0
1000
3000
5000
7000
9000
Time [s]

-Collinear 'In-line' condition of irregular waves-current-wind (FC-37)

-System FPSO with mooring lines and risers

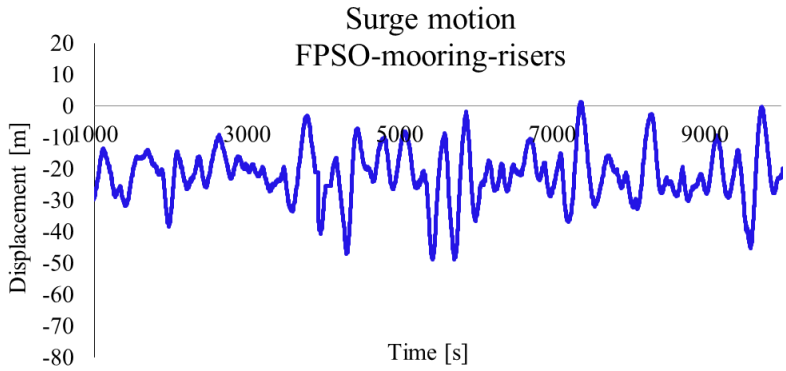

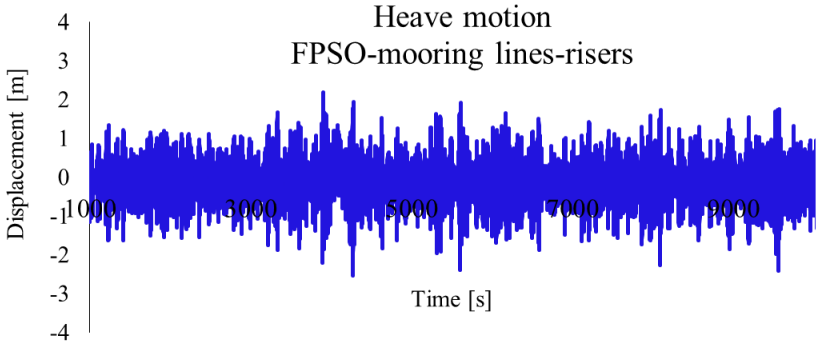

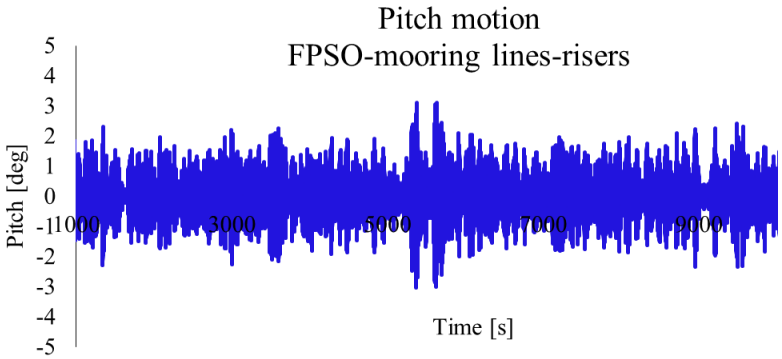

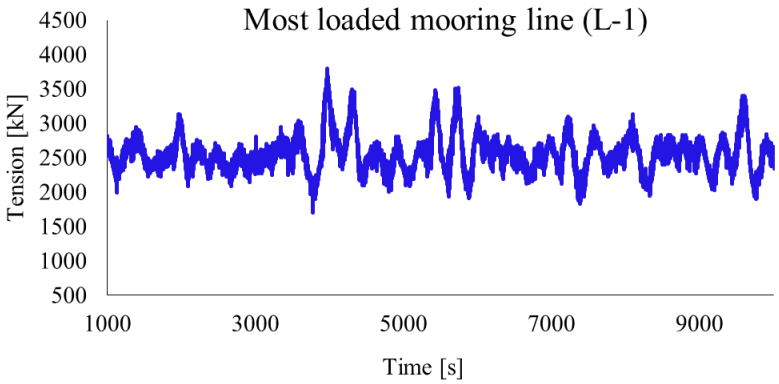
Most loaded mooring line (L-1)
Tension [kN]
4500
4000
3500
3000
2500
2000
1500
1000
500
1000
3000
5000
7000
9000
Time [s]

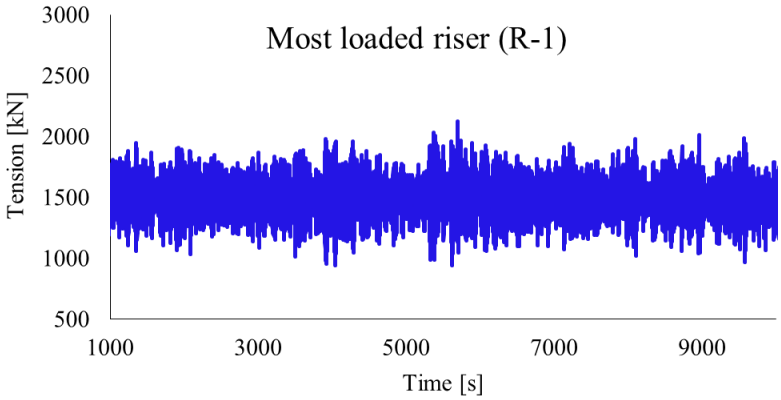
Most loaded riser (R-1)
Tension [kN]
3000
2500
2000
1500
1000
500
1000
3000
5000
7000
9000
Time [s]

-Collinear 'Between-lines' condition of irregular waves-current-wind (FC-38)

-System FPSO with mooring lines and risers

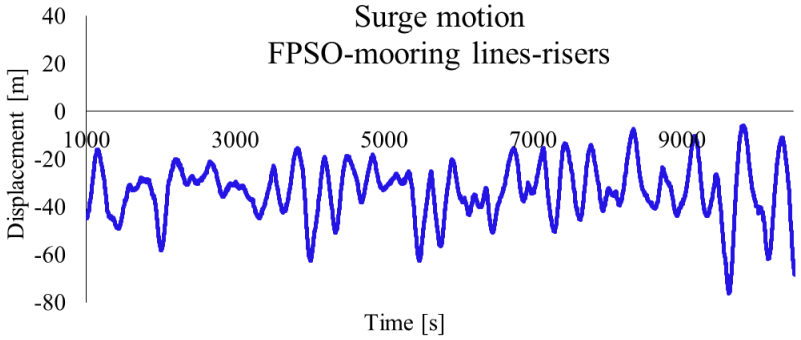

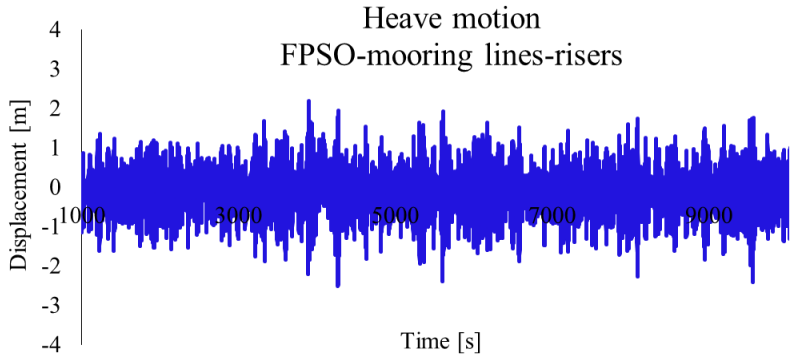

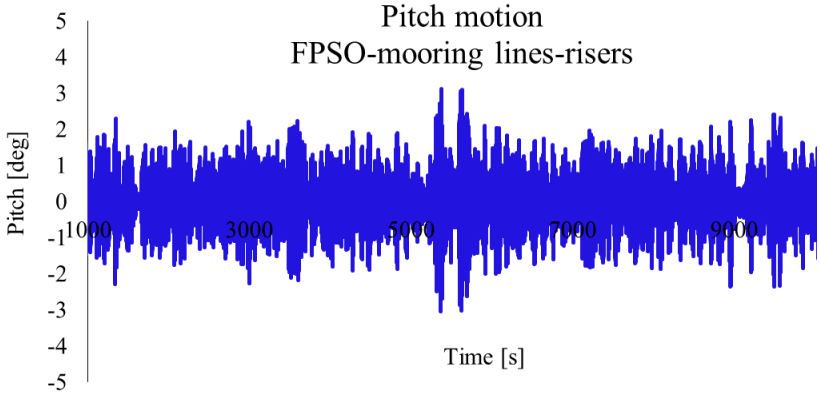

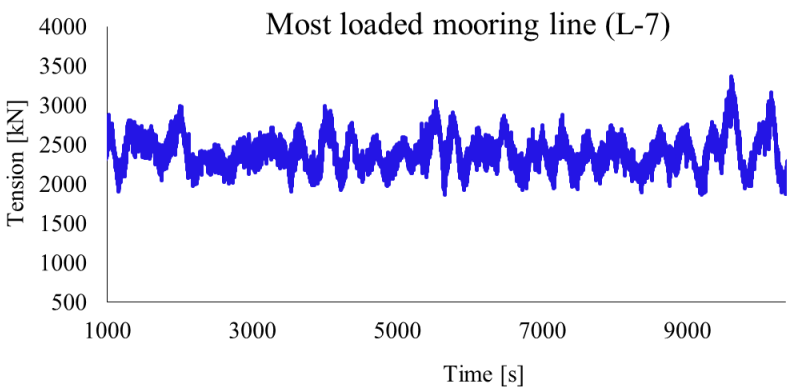
Most loaded mooring line (L-7)
Tension [kN]
4000
3500
3000
2500
2000
1500
1000
500
1000
3000
5000
7000
9000
Time [s]

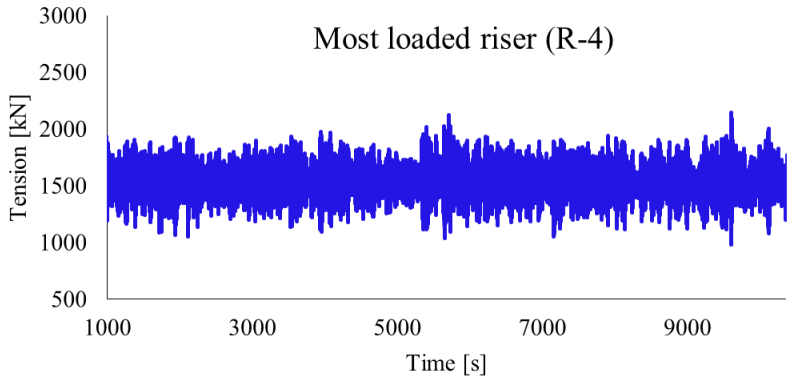
Most loaded riser (R-4)
Tension [kN]
3000
2500
2000
1500
1000
500
1000
3000
5000
7000
9000
Time [s]

-Non-collinear condition of irregular waves-current-wind (FC-39)

-System FPSO with mooring lines and risers

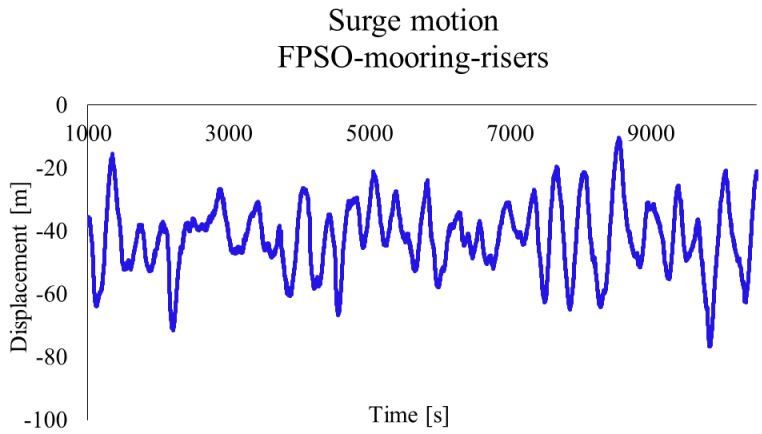

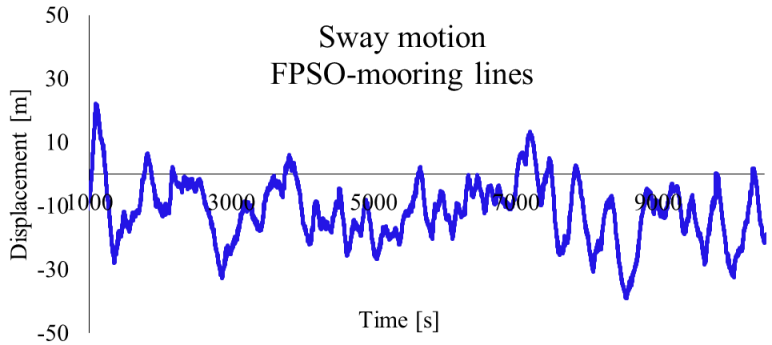

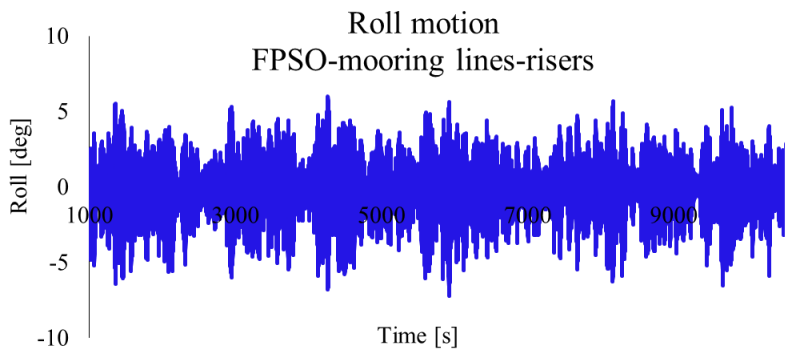

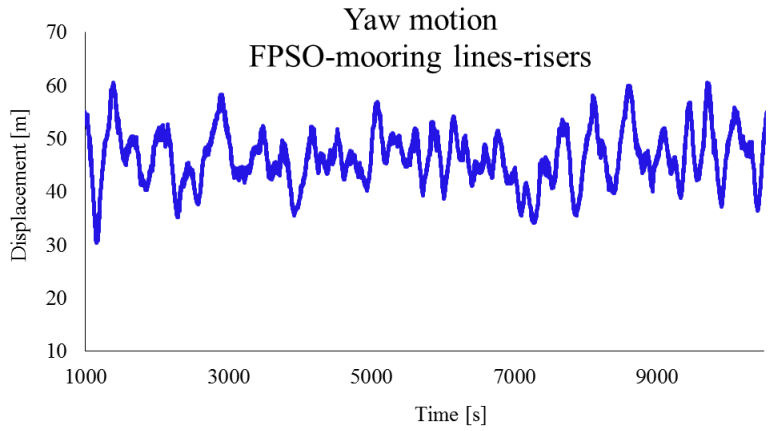
Yaw motion
FPSO-mooring lines-risers
Displacement [m]
70
60
50
40
30
20
10
1000
3000
5000
7000
9000
Time [s]

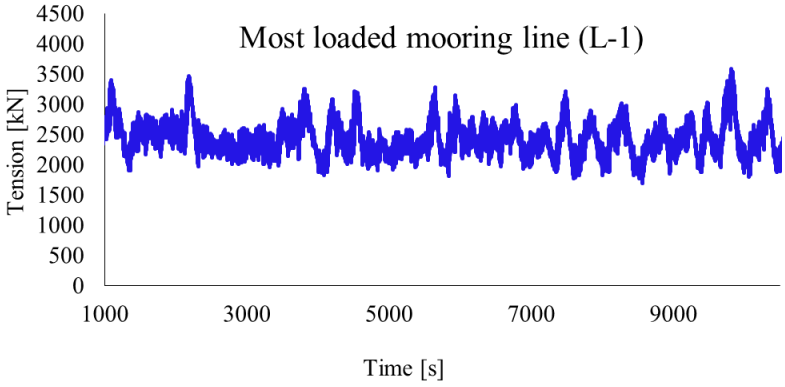
Most loaded mooring line (L-1)
Tension [kN]
4500
4000
3500
3000
2500
2000
1500
1000
500
0
1000
3000
5000
7000
9000
Time [s]

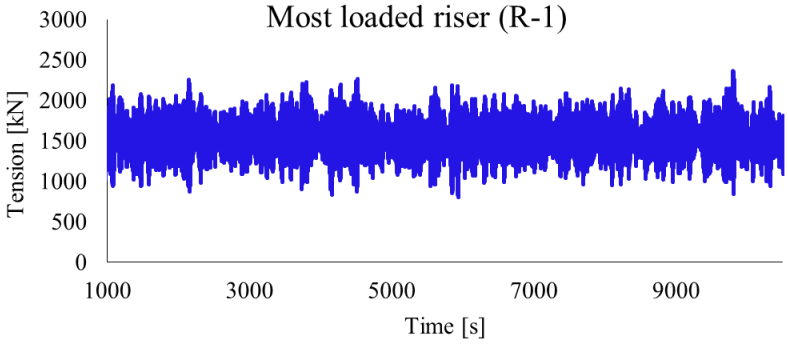
Most loaded riser (R-1)
Tension [kN]
3000
2500
2000
1500
1000
500
0
1000
3000
5000
7000
9000
Time [s]

Appendix E

Hydrodynamic coefficients: FPSO in Full Load condition

E.1: Drift damping

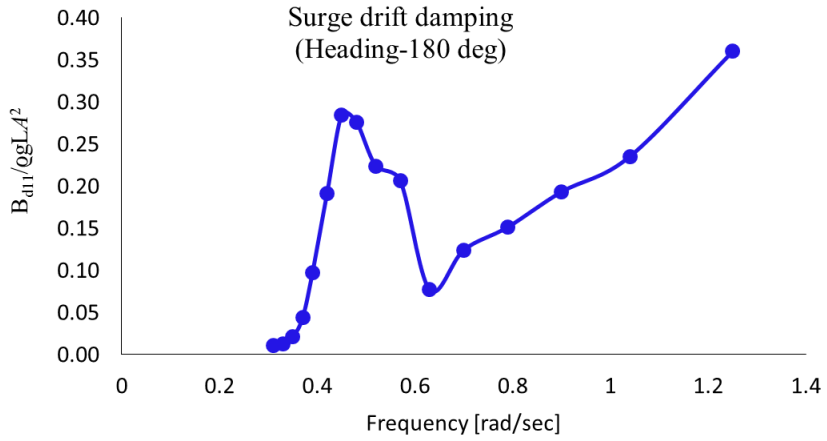

Figure E.1.1 Surge drift damping of the FPSO hull

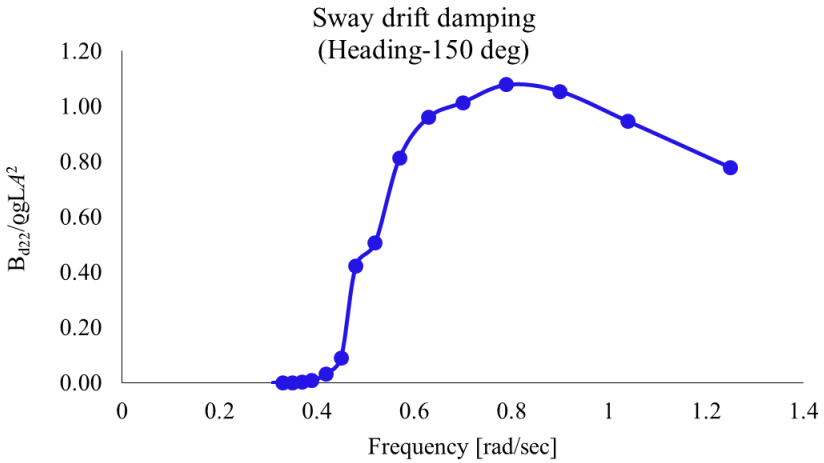

Figure E.1.2 Sway drift damping of the FPSO hull

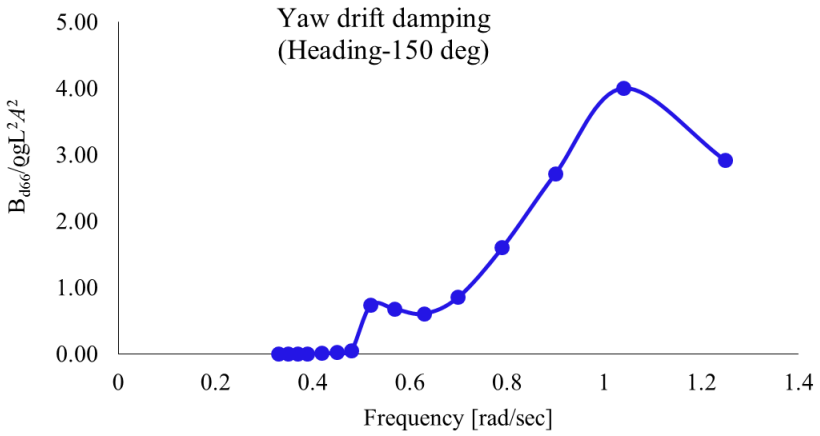

Figure E.1.3 Yaw drift damping of the FPSO hull

E.2: Radiation damping

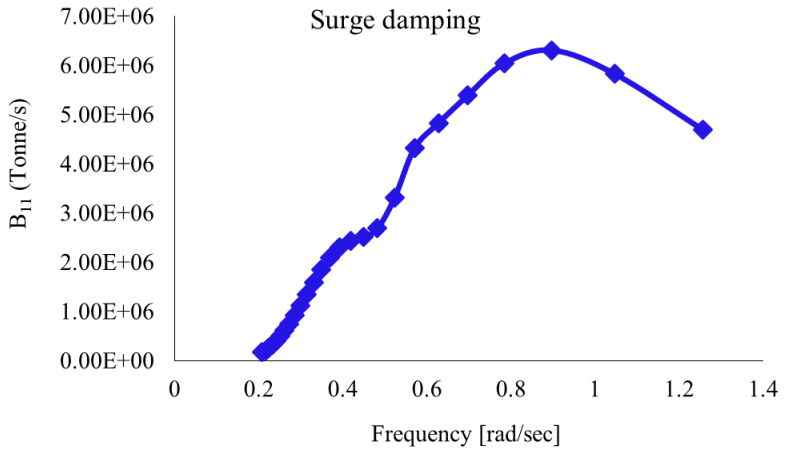

Figure E.2.1 Surge radiation damping of the FPSO hull

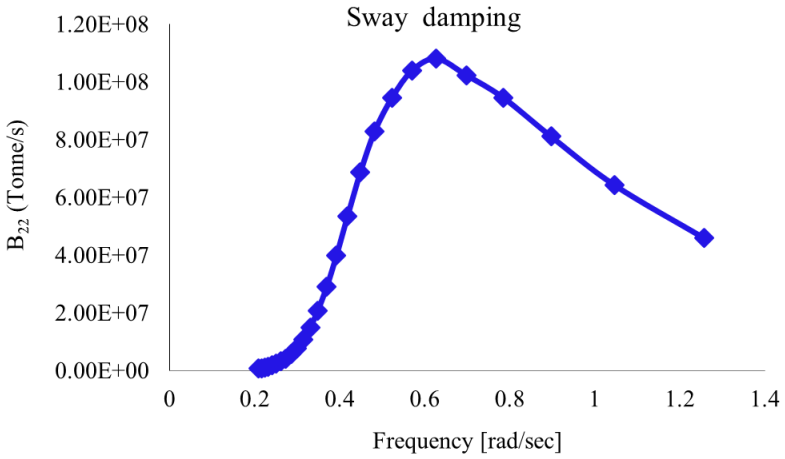

Figure E.2.2 Sway radiation damping of the FPSO hull

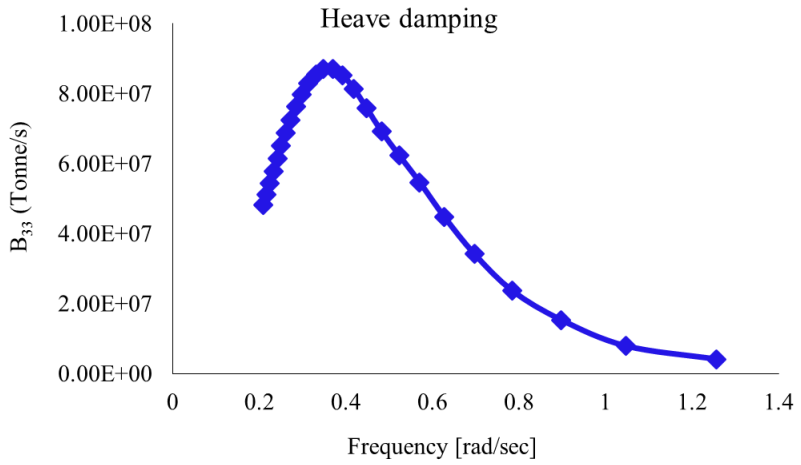

Figure E.2.3 Heave radiation damping of the FPSO hull

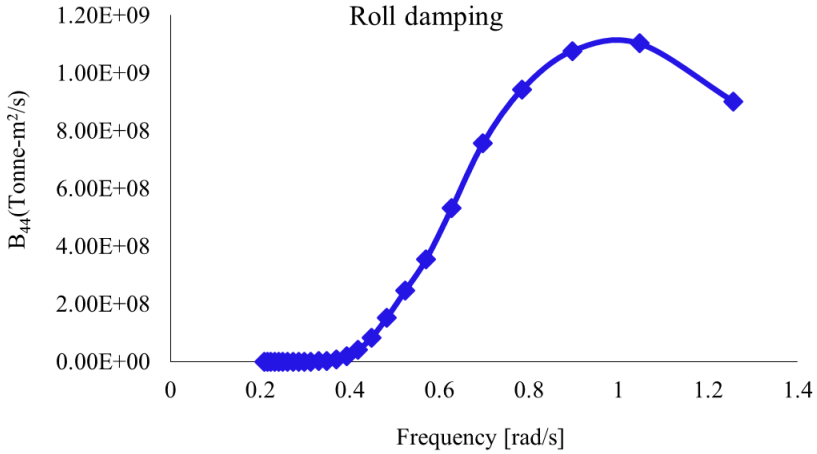

Figure E.2.4 Roll radiation damping of the FPSO hull

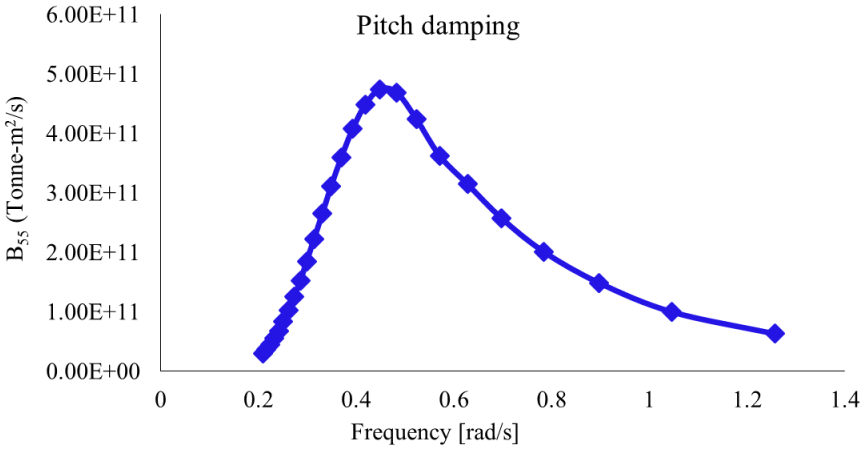

Figure E.2.5 Pitch radiation damping of the FPSO hull

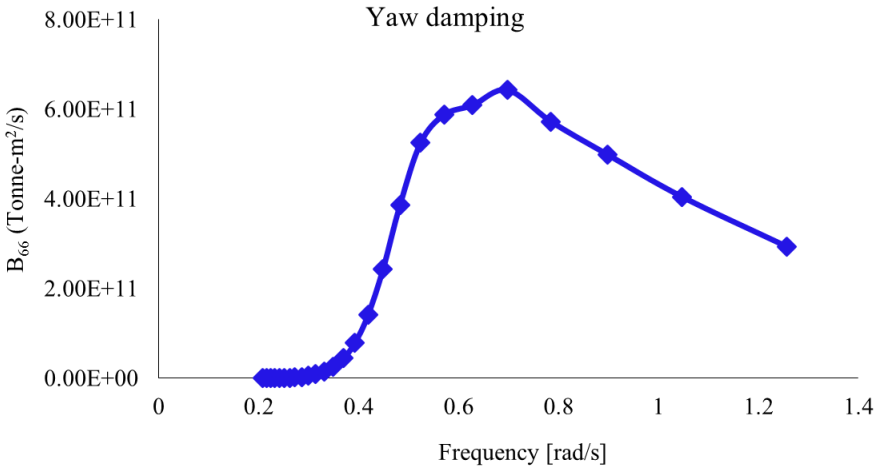

Figure E.2.6 Yaw radiation damping of the FPSO hull

E.3: Added mass

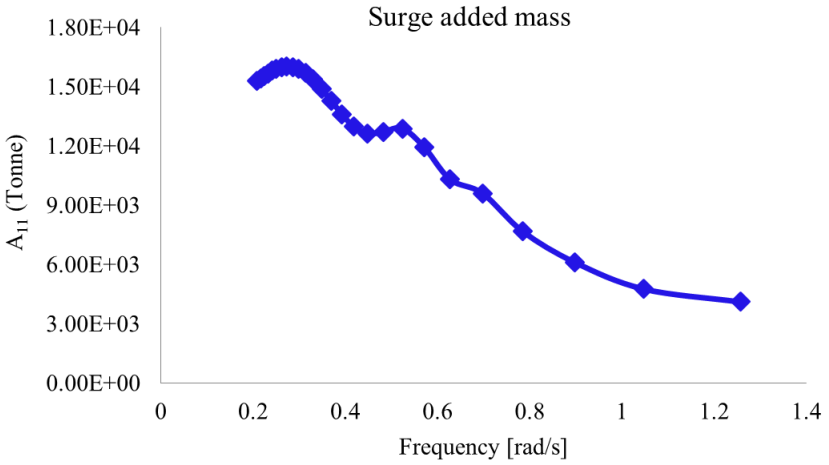

Figure E.3.1 Surge added mass of the FPSO hull

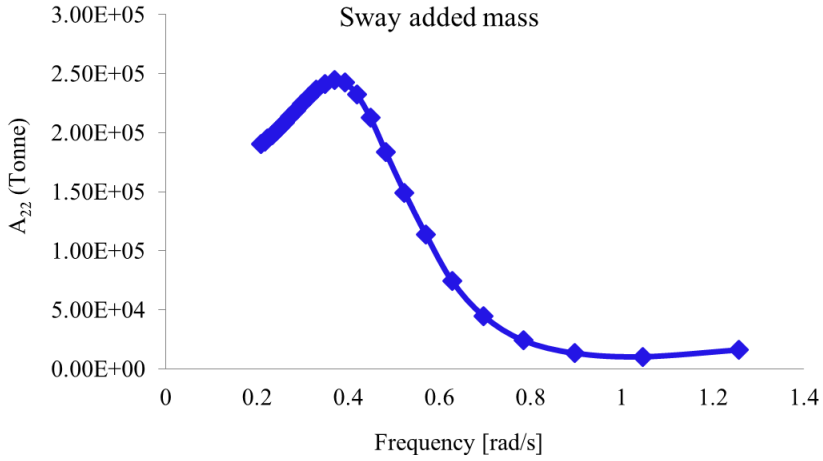

Figure E.3.2 Sway added mass of the FPSO hull

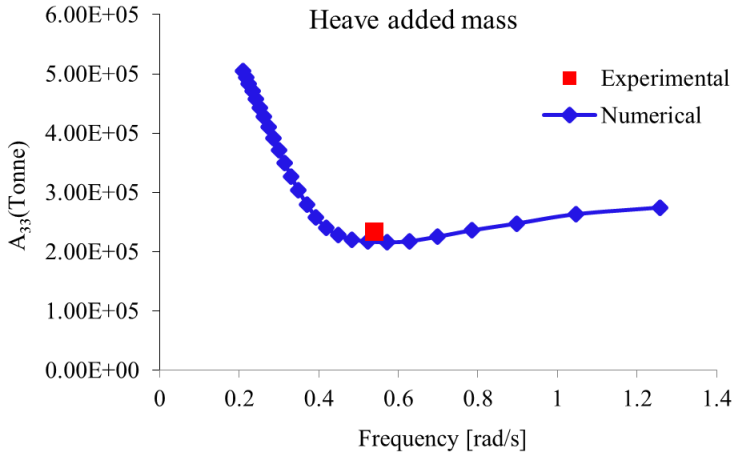

Figure E.3.3 Heave added mass of the FPSO hull

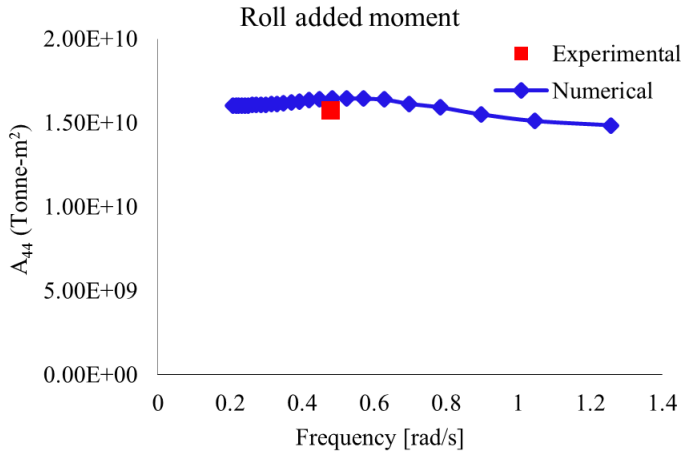

Figure E.3.4 Roll added moment of the FPSO hull

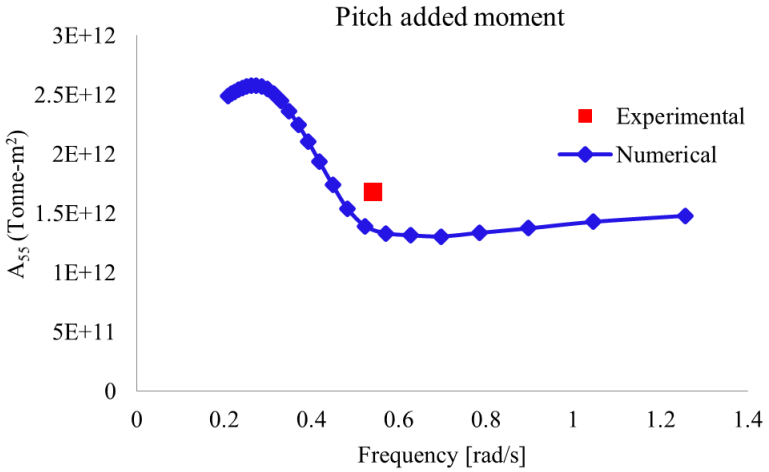

Figure E.3.5 Pitch added moment of the FPSO hull

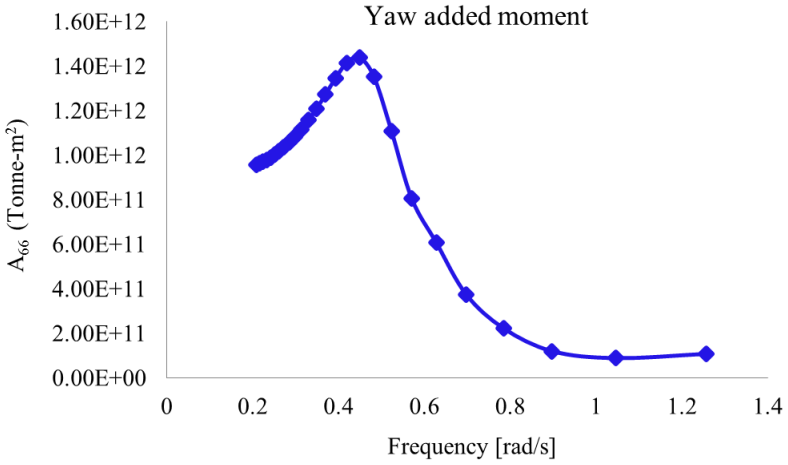

Figure E.3.6 Yaw added moment of the FPSO hull

E.4: Mean wave drift forces/moments

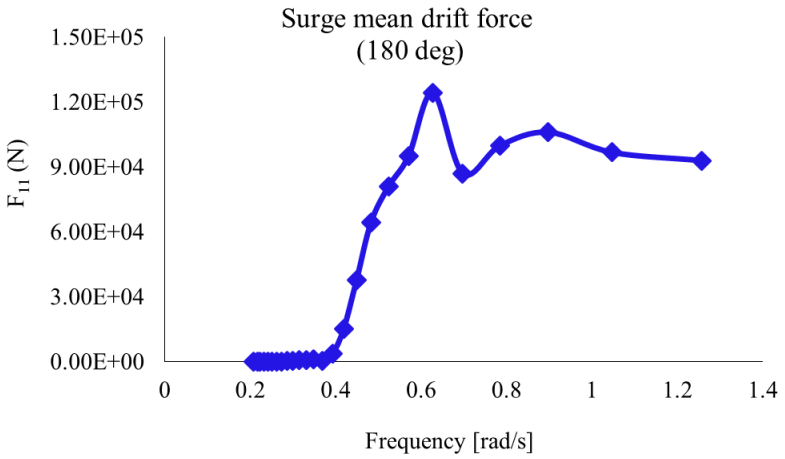

Figure E.4.1 Surge drift force of the FPSO hull

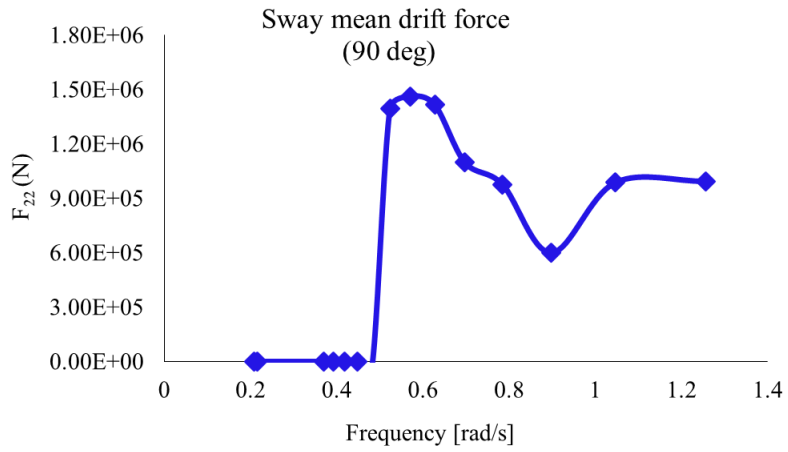

Figure E.4.2 Sway drift force of the FPSO hull

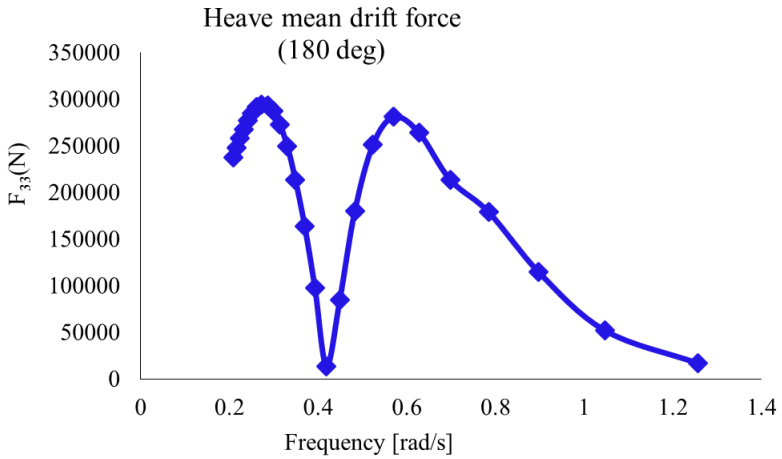

Figure E.4.3 Heave drift force of the FPSO hull

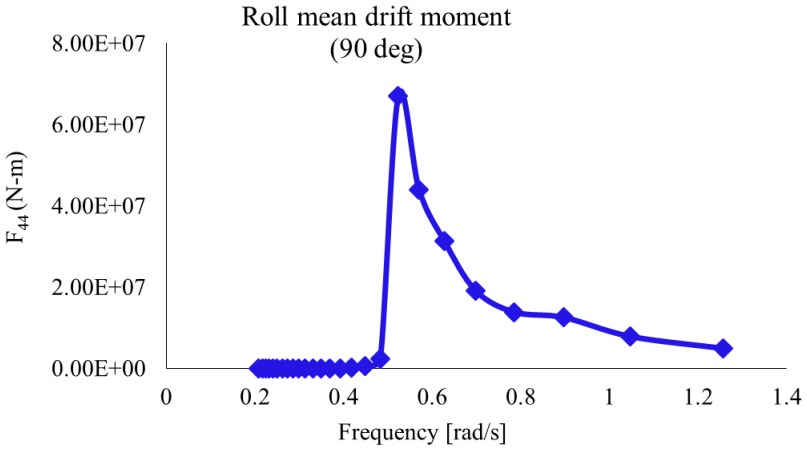

Figure E.4.4 Roll drift moment of the FPSO hull

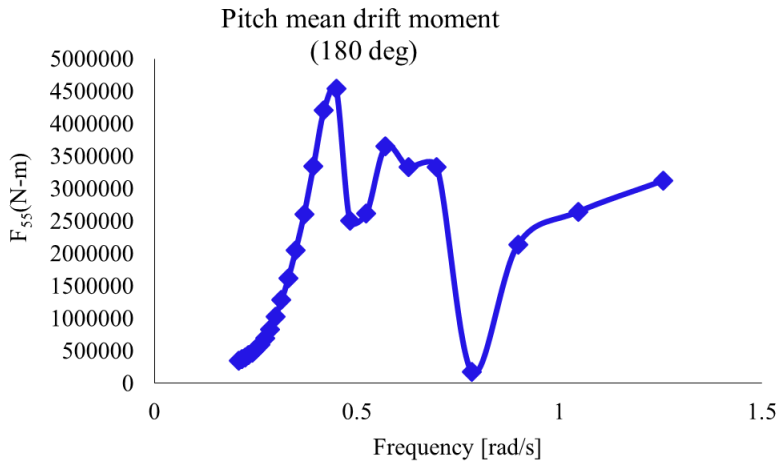

Figure E.4.5 Pitch drift moment of the FPSO hull

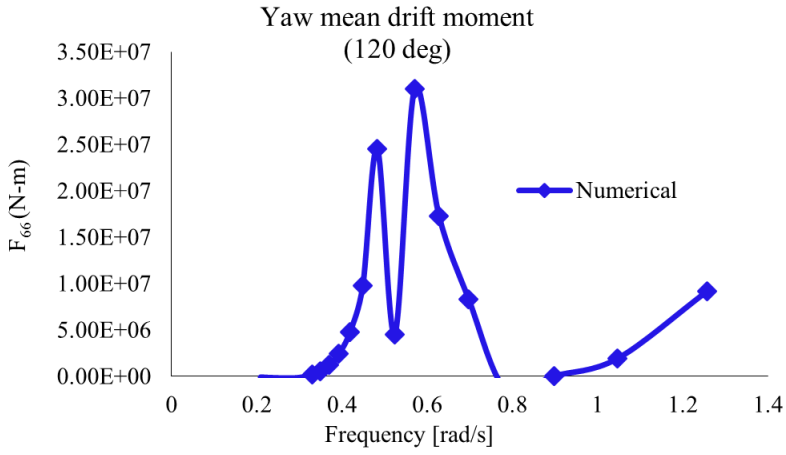

Figure E.4.6 Yaw drift moment of the FPSO hull